AN INVESTIGATION INTO HIGH-LOAD SFI EGR BOOSTED OPERATION FOR DOWNSIZED GTDI ENGINE WITH VALVE-OVERLAP REDUCTION

A Thesis submitted for the degree of

Doctor of Philosophy

by

Ray Shimura

Department of Mechanical, Aerospace and Civil Engineering

College of Engineering, Design and Physical Sciences

Brunel University London

July 2020

Abstract

Downsized gasoline turbocharged direct injection (GTDI) engines deliver superior fuel economy by operating the engine at higher loads but become prone to knocking combustion at boosted operations, which requires the application of knock mitigation strategies, such as the retarded spark timing, with a negative impact on the engine performance and efficiency. Furthermore, the use of wide valve-overlaps to maximise positive scavenging by elevated intake pressure at low and medium engine speeds leads to greater tailpipe NO_x emissions. In light of increased use of Real Driving Emissions (RDE) test where higher load operations are far more prominent, there is a strong need to further explore the approaches to improve engine efficiency and lower harmful emissions at knock limited operations. This project investigates the use of stratified flame ignition (SFI) combustion with exhaust gas recirculation (EGR) on a downsized GTDI engine. EGR dilution is added to control the knocking combustion to replace the traditional knock mitigation strategies. The subsequent combustion is further improved by stratified fuel injection and uprated ignition system. The valve-overlap duration is shortened to avoid the air short-circuiting and hence reduced tailpipe NOx emission through greater conversion efficiency of the 3-way catalyst, but with trade-off with lower volumetric efficiency and knock onset. The novelty of the study is identified as the combination and optimisation of these strategies to improve operational efficiency and reduce harmful tailpipe emissions at knock limited loads.

The results showed that the EGR dilution lowered knock tendency and high energy (HE) ignition accelerated the combustion and recovered stability exclusively at boosted operations. Split injection strategy showed fuel consumption benefit at very limited cases, and most cases led to the loss of efficiency from slower less efficient combustion. Through computational fluid dynamics (CFD) analysis, this was found to be caused by the unfavourable mixture preparation of the multi-hole injectors due to high spray penetration and insufficient mixture preparation time. However, the combined use of EGR dilution and reduced valve-overlap improved mixture preparation due to increased charge temperatures and induced turbulence. Indicated specific fuel consumption (ISFC) improvements of 4.8% and 5.2% were achieved at 13.7bar and 16.4bar Net_IMEP at 2000rpm, respectively. The reduction of valve-overlap also improved the combustion efficiency and reduced emissions of tailpipe NO_x and particulates due to eliminated short-circuit air and enhanced turbulence for faster mixture preparation. Hence, a synergy between valve-overlap reduction, split injection, and EGR dilution was found, and the proposed strategy successfully lowered fuel consumption and harmful emissions from this combined synergy effect.

Keywords: SI engine; Direct injection; SFI; external-EGR; valve overlap; Knock mitigation; Downsizing; High load operation;

Acknowledgements

This work would not have been possible without the financial, and technical support of the Ford Motor Corporation University Research Program. I would especially like to thank the technical staffs of Ford Motor Company Helmut Ruhland, Keizer Tufail, Shane Keithly, Roland Stark, Georg Louven who supported this project. And thank you for providing the necessary pieces of equipment for the use of this project.

My utmost respect goes to my principal supervisor Professor Hua Zhao, who gave me the opportunity of this PhD project along with the insightful guidance for the past 4 years.

I would like to thank Dr Xinyan Wang for his invaluable technical contribution to the research. The help received not only improved the quality of the project but also taught me greatly.

My thanks also go to the academic staffs of Brunel University, Mechanical and Aerospace Engineering Dr Apostolos Pesyridis, Dr Jun Xia and Dr Lionel Ganippa who were very generous with their time to guide me through the journey with their expert knowledge. All your support gave me great assurance in the direction of the research.

I would like to thank the lab technical members Andrew Selway, Eamon Wyse, Minal Shah for the works of impeccable standards of work performed around the lab. All my tests went smoothly, owed to the quality of test rig and great safety standards that were practised.

The same goes to William Schkzamian and Michael Lateo of the electronics department who were more than accommodating to help me with the electronics problem-solving. A lot of the success around the lab work is owed to your collective expert knowledge.

I would also like to thank Thomas Jefferson who at short notice accepted to proofread this thesis. The inputs really improved the quality of the work.

I must extend the thanks to my fellow researchers and office pals, especially Megvian Juknevshaft who tolerated myriads of my technical questions and distracting banters. It made my time at Brunel University truly joyful.

And I cannot end my acknowledgement without mentioning the vital supporters of my life. To my girlfriend, family, friends, and housemates who supported me along the course of the PhD. Thank you very much, you all provided me with endless happiness.

Table of Contents

List of Figures

List of Tables

Nomenclature

Abbreviations

AFR	Air Fuel Ratio
AI	Analogue Input
API	Application Programming Interface
aTDC	After Top Dead Centre
BDC	Bottom Dead Centre
BEV	Battery Electric Vehicle
BMEP	Brake Mean Effective Pressure
BSFC	Brake Specific Fuel Consumption
CA10	Crank position at 10% Mass Fraction Burnt
CA50	Crank position at 50% Mass Fraction Burnt
CA90	Crank position at 90% Mass Fraction Burnt
CAD	Crank Angle Degree
CAI	Compression Auto Ignition
CFD	Computational Fluid Dynamics
CoV	Coefficient of Variation
CR	Compression Ratio
DAQ	Data Acquisition Device
DI	Direct Injector
ECR	Effective Compression Ratio
ECU	Engine Control Unit
EGR	Exhaust Gas Recirculation
EIVC	Early Intake Valve Closing
EOI2	End of Second Injection
ER	Equivalence Ratio
EU	European Union
EVC	Exhaust Valve Closing
EVO	Exhaust Valve Opening
FCV	Fuel Cell Vehicle
FMEP	Friction Mean Effective Pressure
GHG	Green House Gas
GTDI	Gasoline Turbo Direct Injection
HCCI	Homogeneous Charge Compression Ignition
HEV	Hybrid Electric Vehicle

HFET	Highway Fuel Economy Test Cycle
HP	High Pressure
HRR	Heat Release Rate
ICE	Internal Combustion Engine
IMEP	Indicated Mean Effective Pressure
IR	Infra-Red
IS[Gas]	Indicated Specific Emissions
IVC	Inlet Valve Closing
IVO	Inlet Valve Opening
KLSA	Knock Limited Spark Advance
LIVC	Late Inlet Valve Closing
LNT	Lean NO_x Trap
LP	Low Pressure
LSHL	Low-Speed High-Load
LSPI	Low-Speed Pre-Ignition
MAF	Mass Air Flow
MAP	Manifold Air Pressure
MBT	Mean spark advance for Best Torque
MEP	Mean Effective Pressure
MFB	Mass Fraction Burnt
MFR	Mass Flow Rate
MON	Motor Octane Number
NA	Naturally Aspirated
NDIR	Nondispersive Infra-Red
NVO	Negative Valve-Overlap
P_{drop}	Pressure Drop
PEMS	Portable Emissions Measurement System
PFI	Port Fuel Injector
PFR	Primary Reference Fuels
PHEV	Plug-in Hybrid Electric Vehicles
PM	Particulate Matter
Pmax	Max Pressure
PN	Particulate Number
PPC	Partially Premixed Combustion
PSU	Power Supply Unit
RANS	Reynolds-Averaged Navier-Stoke

RDE	Real Driving Emissions
RH	Relative Humidity
RON	Research Octane Number
RPM	Revolutions Per Minute
SFI	Stratified Fuel Injection
SI	Spark Ignition
SIDI	Spark Ignition Direct Injection
SOI	Start of Injection
ST	Spark Timing
STD	Standard
TC	Turbocharger
TDC	Top Dead Centre
TKE	Turbulent Kinetic Energy
TWC	Three Way Catalyst
UEGO	Universal Exhaust Gas Oxygen
UI	User Interface
ULG	Unleaded Gasoline
VOC	Volatile Organic Compound
WLTP	Worldwide Harmonised Light Vehicle Test Procedure
WOT	Wide Open Throttle

Chemical abbreviations

CO	Carbon Monoxide
CO_2	Carbon Dioxide
O_2	Oxygen
NO_x	Nitrogen oxides
THC	Total Hydrocarbon

Chapter 1 Introduction

1.1 Preface

There is an enormous demand for transport worldwide, and this demand is also growing. A significant portion of this demand is catered by road transport. However, there is an ongoing environmental concern caused by emissions of GHG and harmful gases, of which road transport contributes significantly. With climate change causing environmental disasters around the world, and harmful emissions causing atrocious levels of health issues leading to premature deaths, pressure is applied to responsible sectors to respond with advancements which reduce these emissions. Combined with the uncertainty of fuel resource availability, road transport powertrains such as IC engines are always under development for efficiency and clean-burning technology.

Alternative powertrain vehicles such as Battery Electric Vehicles (BEVs) and Fuel Cell Vehicles (FCVs) are under rapid development, increasing in selection, versatility, and market share. However, such alternative powertrains are not yet suitable for mass adoption due to primarily their cost and infrastructure for charging and hydrogen supply. In the next few decades, most vehicles will have electrified IC engines as their main power source.

IC engine improvements are always underway, and there are many opportunities for improvement. For example, advanced combustion techniques such as Homogeneous Charge Compression Ignition (HCCI) are known to improve emissions and efficiency drastically but limited to part-load operation due to the onset of knock.

Recent success to achieve efficiency and emissions benefits have mostly been achieved by the rise of downsized GTDI engines in gasoline vehicles. However, fuel costly measures are implemented to reduce knock tendencies at boosted high load operations. Furthermore, the use of the large valve overlap to extend the torque limit at Low Speed High Load (LSHL) is found to cause higher tailpipe NO_x emissions, which is under scrutiny with updated emission regulations that tests boosted high-load operations more frequently.

This project undertakes the test and analysis of Stratified Flame Ignition- Exhaust Gas Recirculation (SFI EGR) combustion with valve-overlap reduction on a downsized GTDI engine at boosted high-load operation. SFI EGR is a combustion strategy that aims to improve high-load operation efficiency. The strategy employs a second late injection to create an ignitable mixture around the plug electrodes while higher levels of EGR dilution minimizing the knocking combustion. Finally, the valve-valve overlap is reduced to improve the combustion efficiency and to significantly reduce the tailpipe NOx emissions by avoiding the air short-circuiting.

The combined use of these techniques has the potential to reduce fuel consumption during the boosted high load operation and further reduce harmful tailpipe NO_x emissions.

1.2 Research objectives

This research aims to investigate the combustion and engine control technologies to improve the efficiency and lower harmful tailpipe emissions of a downsized GTDI engine at LSHL boosted operation. Operation demands in LSHL regions are frequent in downsized engines due to their characteristics of the performance. However, due to the strategies to lower knock tendencies, the efficiency and emission at LSHL boosted operation range are compromised. Hence, there is an opportunity to improve efficiency by exploring alternative methods to lower knock tendency. Through mostly engine experiments supported by in-cylinder studies using CFD, the specific objectives of the PhD project are: -

- To evaluate the ability of external EGR to improve the efficiency of the engine at high load conditions
- To investigate the effectiveness of ignition enhancement techniques to recover the combustion speeds and ignitability lost by external EGR dilution presence
    - Ignition energy effects with varying degree of EGR dilution
    - Split injection fuel stratification with presence of 10% external EGR dilution
- To explore the effects of valve phasing and overlap reduction during LSHL boosted operation
- To identify the combined effects and synergies of SFI EGR (external EGR dilution, split injection), and valve-overlap reduction for improved engine efficiency and lower NO_x emissions

1.3 Thesis outline

The thesis is structured into four main sections across seven chapters, starting with the introductory chapter that contains the introduction, objective, and the structure of the thesis. The technical chapters span across five chapters as seen in Figure 1-1, first starting with the literature review that covers the pre-requisite and up-to-date knowledge of the strategies used by the SI gasoline engine, these are: - EGR dilution, split injection, and advanced valve profile implementation.

Chapter 3 details the experimental rig and engine. The chapter contains information on the engine used with the modifications performed, instrumentation and control, analysis method used, and finally commissioning of the engine testbed.

Chapters 5, 6 and 7 present the test results and analysis. The engine tests were carried out to study one variable-sweep with detail before progressing to the next, but only carrying over the necessary factors to minimise the complexity. By testing many strategies, an optimised approach was taken to progress the project.

The first result chapter (Chapter 4) focuses on the EGR dilution response at boosted load and the effectiveness of advanced ignition system. Chapter 5 assesses the split injection strategy with a high-resolution sweep with EGR dilution. Finally, Chapter 6 covers the final objective over two studies which test the use of varying the inlet and exhaust valve phasing. Here, the first tests take place to understand the interaction with EGR dilution with various valve phasing combinations, and the following test focuses on the reduced symmetrical valve-overlap at boosted loads with EGR and split injection to report the interaction of the strategies with synergy effects.

Chapter 7 summarises the results from each chapter to report on the emission and fuel efficiency gains and the notable effects observed to achieve these improvements. The final remark gives the verdict on the effectivity of the proposed strategy and lists the recommended works that arose from the project.

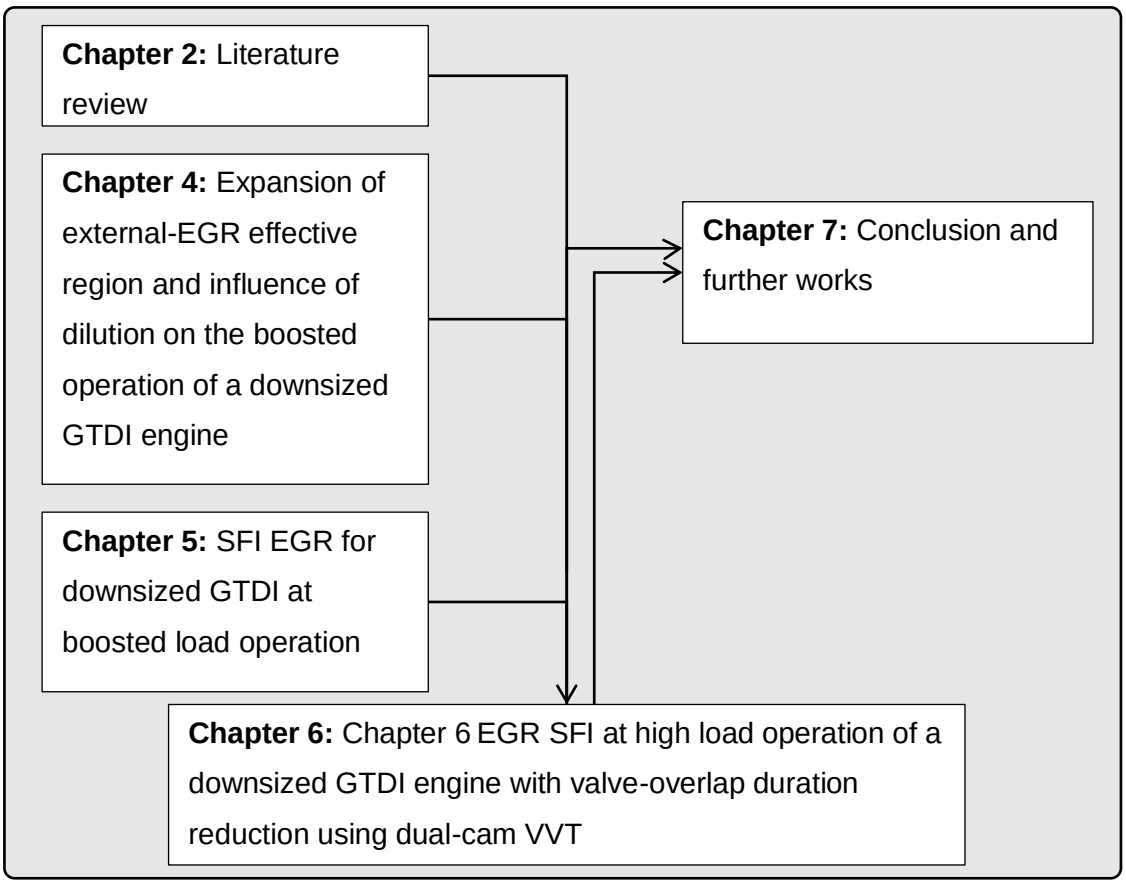

Figure 1-1 Chapter interaction diagram

Chapter 2 Literature review

2.1 Introduction

In this chapter, the fundamentals and pre-requisite knowledge, and the up-to-date knowledge of the employed strategies are reviewed in detail. The aim is to understand the current state of research, clarify the demand for such a study, and to identify the contribution of this project.

The literature review is structured with four parts: 1) the demand for lower emission transport 2) pre-requisite knowledge of the project 3) updated literature review of the adopted strategies 4) justification and novelty of such a project. The first section notes the demand for transport with higher efficiency and lower emissions. The second part is basic but supporting contents of the review, doing so by laying the foundation of the required knowledge. The third part focuses on the specific strategies of diluted SI combustion, enhanced ignition systems, advanced valve timing and actuation, and fuel/air mixture preparation, before finally concluding the literature review and positioning the knowledge that this project aims to provide.

The topics covered here are designed to prepare the reader to a full understanding of the significance of this study and facilitate the reader to understand the main results of this thesis.

2.2 The direction of the automotive market

It is important to understand the current and future trend of technological demand for powertrains, considering the demand for higher efficiency engines in the future. This sub-section discusses the review of future demand based upon the study of fuel reserve concern, customer demand of future powertrain, lifetime emissions of cars, which all have an effect towards corporate research and determine the IC engines of the future.

2.2.1 The importance of transport

The global motor vehicle sales numbers are on an increase year on year. The data from the automotive trade association, OICA, shows an increase of motor vehicles rise from 66M in 2005 to a peak of 96M in 2017[1]. Many forecasted sales to continue rising [2], but the fall in vehicle sales was seen since 2017 across many countries due to the rise in global environmental concerns. The sales trend is plotted in Figure 2-1. The increase in world population and demand for personal/fleet contributed to the growth in sales, but the prominent drop in sales is down to the decline in car ownership from the rising popularity of

car share schemes and environmental concerns by prospective buyers, yet it is important to note that the demand for logistics has not declined.

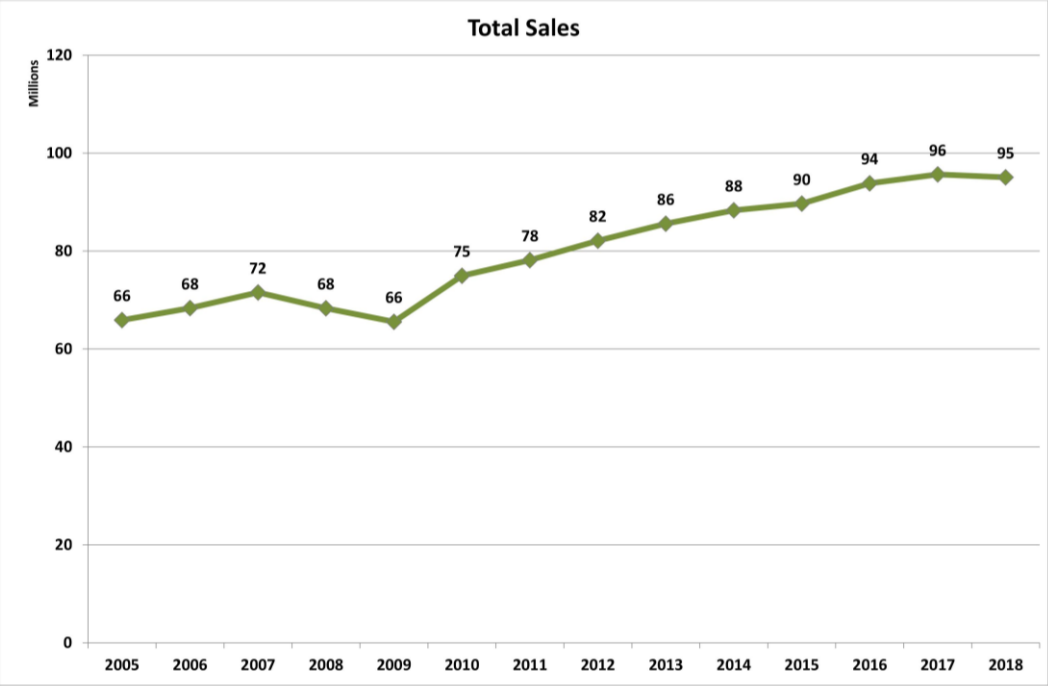

Figure 2-1 World motor vehicles sales statistic ranging from 2005 to 2018. Count includes sales of Passenger car and Commercial vehicle sales. Original source: [1]

2.2.2 Challenges of future transport: air pollution and GHG emissions

Air pollution and climate change are two of the biggest environmental concerns faced around the world. Global warming is accelerated by artificial heat capacity increase due to excessive release of GHG into the atmosphere. The predicted changes to the global climate has a catastrophic knock-on effect on the habitat. These studies have forced many countries to reprioritise their policies for future survival [3, 4]. The concern of air pollution arises from the direct health effects of those exposed to the atmospheric air with high levels of harmful gases and/or particles. Premature deaths are strongly linked to local air quality that leads to health issues such as heart disease, respiratory disease, and strokes. The transport emission includes respiratory sensitive gases such as NO_x and particulates. Transport emissions from internal combustion engine were estimated to have caused 361,000 premature deaths from PM2.5 and ozone worldwide in 2010 [5]. The same study also reports premature death linked to transport emissions in 2015, all are linked to the high concentration of traffic in urban environments where diesel vehicle accounted for half the offending emissions. Annenberg *et al.* [6, 7] from the ICCT notes the impact of excess diesel NO_x emissions to be responsible for 107600 premature deaths worldwide and offers a

recommended NO_x emission controls standard that when implemented is predicted to avert 174000 premature death.

The Paris agreement is a global initiative to limit global warming to well below 2°C of the pre-industrial period to limit the dangerous consequences caused by climate change. Restrictions are put in place for the transport sector which lowers the possible GHG emissions of newly registered cars. In 2016 the transport sector contributed 27% of Europe's GHG emissions, of which 72.1% is by road transport, further of which 43.7% are from light-duty vehicles. This means the light-duty vehicle are responsible for around 12% of total CO_2 emissions in the EU [8]. The EU has set targets for CO_2 emission for new light-duty vehicle due to the large impact it will have on the environment. The targets and historical data is as seen in Figure 2-2 originally published by the ICCT in 2019 [8]. A target set of 130g/km by 2015 was achieved much earlier than planned, and a new target was set of 95g/km of CO_2 emissions for the year 2021. The trend is however on an increasing trend due to the absence of target before 2020, thus as of 2018, a continues CO_2 reduction of 7.6 g/km per year is required to meet the 2021 CO_2 emission target. The emission values are measured in a set test cycle of tailpipe CO_2 emissions, and the binding CO_2 targets are specific to each manufacturer based on the average mass of their vehicles. There are other incentives set by the EU regulators such as a penalty scheme for excess emission, eco-innovation based target alleviation, super credits, and more. All these schemes help achieve the overall CO_2 output reduction through means that cannot be demonstrated on the current test protocol.

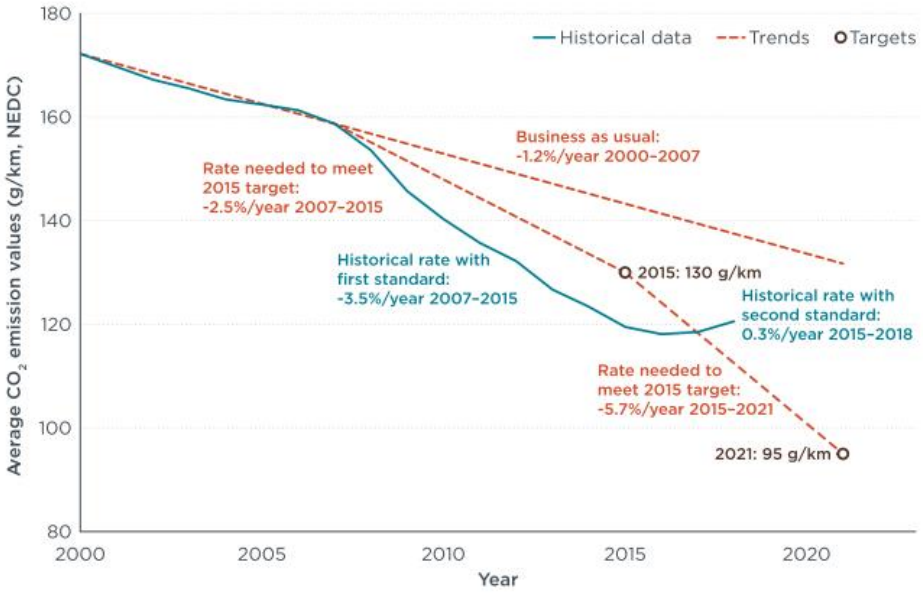

Figure 2-2 EU fleet average CO_2 emission and target, the orange line represents the required trend to meet set reduction targets for 2015 and 2021. Original source: [8]

Europe now has a target to cut GHG emissions by 40% below 1990 levels by 2030. This is expected to have a knock-on effect on the CO_2 targets with more stringent targets that require heavy hybridisation or zero-emission vehicles to take a major portion of the manufacturers fleet.

For road transport vehicles, local legislations of emission limits are another factor that drives the powertrain development directions and targets. Depending on the country or region, new models undergo emission tests under a specific test procedure set. For Europe, emission tests are carried out in laboratory conditions under the 'New European Driving Cycle' (NEDC) and 'Worldwide Harmonised Light Vehicle Test Procedure' (WLTP) is designed to test emissions with a better match to on-road conditions. The WLTP certification also takes place on the public road with the 'Real Driving Emissions' (RDE) test, where a vehicle fitted with Portable Emissions Measurement System (PEMS) is driven under a set guideline to monitor real emissions of NO_x and PN [9]. Such a test is considered a complement to the traditional drive cycle emissions test, where fair reproducible laboratory conditions enable comparisons. The RDE test was started in 2017 but had come into full force in 2020.

The major difference between the NEDC and WLTP test cycles are the longer cycle time extension from 20 to 30 minutes, longer travelled distance, from 11km to 23.25km, as well as increased average and maximum speeds. The dynamic conditions in the operating range can also be seen by the comparisons of speed vs time charts in Figure 2-3. This simulates powertrain load conditions of much faster and aggressive driving patterns, meaning the emissions of the wider operating range can be tested. Further testing with RDE also ensures full vehicle driving conditions (with NO_x and particulate emission) into consideration such as altitude, wind and traffic but it is also these uncertainties that bring concerns to the accuracy of the results. The differences in operating range of the engine load and speed can be seen in a visualised map on Figure 2-4. As shown in the figure, higher load operations are far more prominent with speeds reaching regions never achieved by other drive cycle tests.

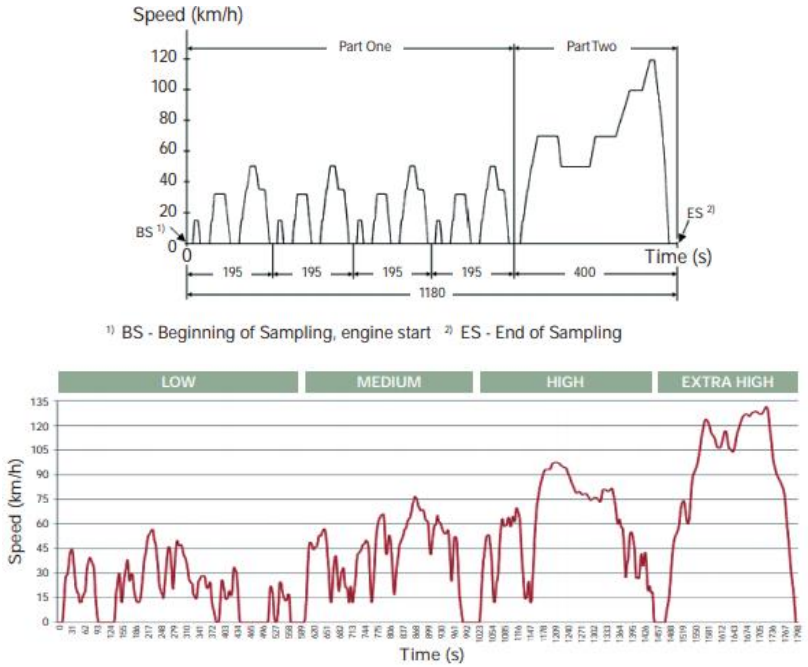

Figure 2-3 Comparison of the drive cycles, top NEDC, bottom WLTP. Original source [10]

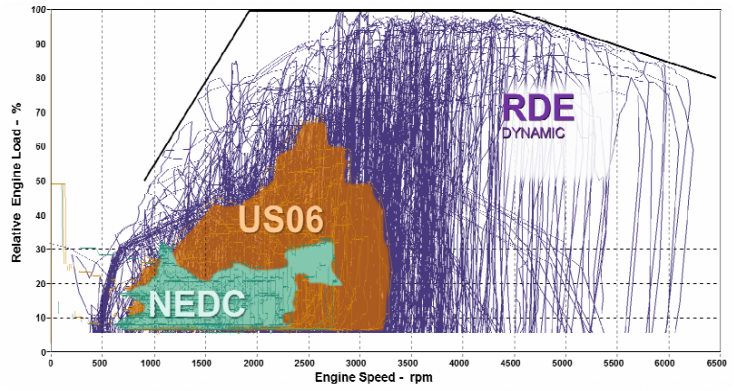

Figure 2-4 Comparison of drive cycle range between NEDC, US06 and RDE. RDE dynamic range covers a much wider speed and load. Original source [11]

A timeline for harmful gas emission limits for Europe is as seen in Table 2-1. The first limit was introduced in 1992 with the first compulsory fitment of an exhaust after-treatment system. Further limits were then updated and/or introduced that car manufactures responded with updated technology to comply. With the introduction of gasoline direct injection (GDI) engines, a particulate emission limit was introduced as concerns grew with additional particulate emissions which were already causing issues with emissions from existing diesel IC engines. The ICCT reports that improvements to the fuel injection timing or addition of a particulate filter in the exhaust after-treatment may be required to comply with these figures [12].

Table 2-1 Euro emission limit for gasoline engine (PN emissions only apply to GDI engines), g/km

Tier	Active	CO	THC	NMHC	NO_x	PM	PN/count
Euro 1	July 1992	2.72					
Euro 2	Jan 1996	2.2					
Euro 3	Jan 2000	2.3	0.2		0.15		
Euro 4	Jan 2005	1.0	0.1		0.08		
Euro 5a	Sept 2009	1.0	0.1	0.068	0.06	0.005	
Euro 5b	Sept 2011	1.0	0.1	0.068	0.06	0.0045	
Euro 6b	Sept 2014	1.0	0.1	0.068	0.06	0.0045	6×10^{12}
Euro 6c	-	1.0	0.1	0.068	0.06	0.0045	6×10^{11}
Euro 6d	Jan 2020	1.0	0.1	0.068	0.06	0.0045	6×10^{11}

While the review focused on the efforts of the EU countries, emission limit targets are updated for all markets of the world. The plan and timeline are as seen in Figure 2-5, frequent updates of rules and restrictions can be seen to lower transport-related emissions of GHG and harmful gases.

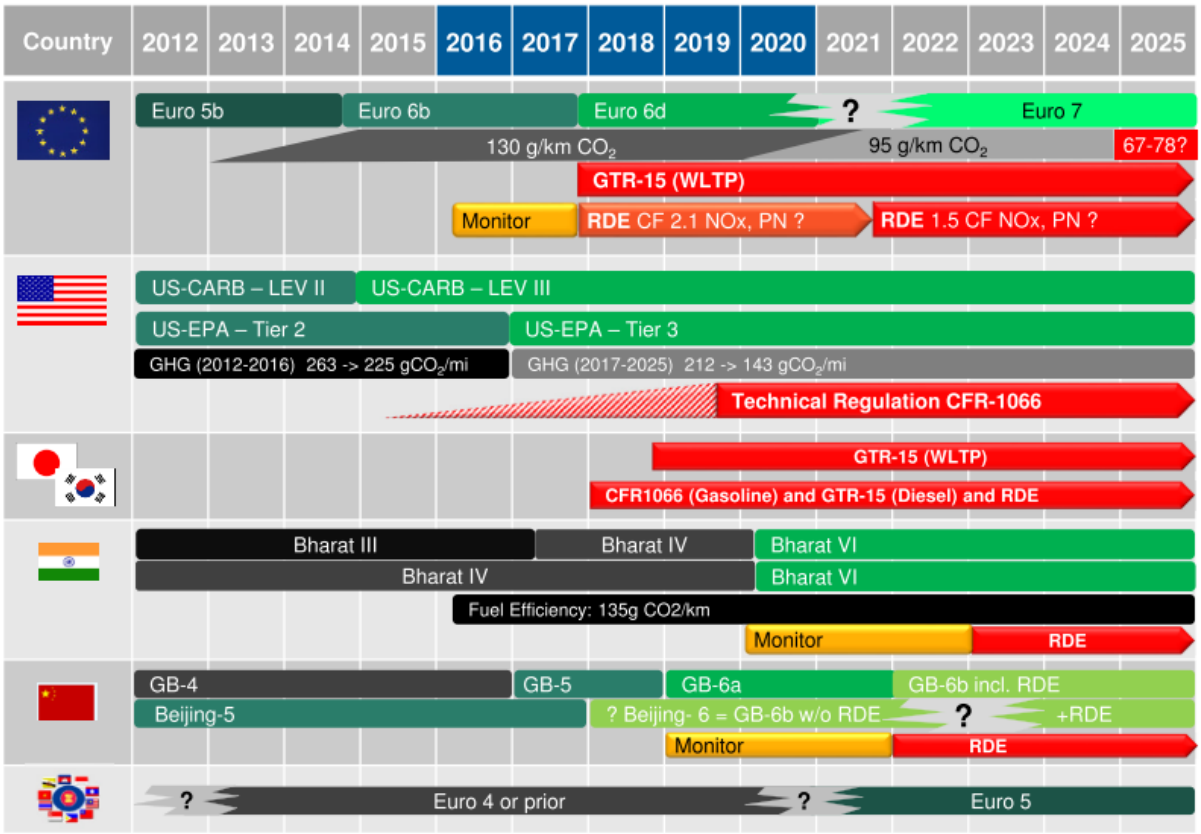

Figure 2-5 Emission limit timeline for different major automotive markets. All have frequent updates in the limits and test procedures, especially with the rise of RDE test protocols. Original source [11].

There is a continual interest in the development of IC engines, especially for lowering of harmful emissions and improving the thermal efficiency of the engine. But there are many ways to achieve this. Fuel consumption and emissions reduction with prospective engine technology are reviewed in [13]. The high-level list as shown in Figure 2-6 shows that the IC engine has much to offer with advancements in engineering technology.

Engine Technology	CO_2 Reduction	Challenges, Implications for Emissions	Status
Baseline: GDI, turbo, stoich.	0	PN	Implemented
Atkinson cycle (+ VVT)	3 - 5%	Reduction in peak power, torque	Implemented
Adv. start-stop	2 - 5%	Consumer acceptance PN at re-start?	Implemented
Dyn. cyl. deac. + Mild Hybrid or Miller	10 - 15%	Noise, vibration	Adv. Eng.
Lean-burn GDI	10 - 20%	LT NOx and PN	Implemented
Variable CR	10%	Reduced emissions	Implemented
Spark assisted GCI	12 - 15% (a)		Implemented
Water Injection	5 - 10%	Low exh. T, low NOx, high HC	Adv. Eng.
Homog. Lean	15 - 20%	Low NOx, HC, but particulates	Development
Dedicated EGR	15 - 20%	Stability at high dilution HC traps needed	Adv. Eng.
RCCI*	20-30%	Operating load range, LT HC+CO	Adv. Eng.
2-stroke opp. piston Diesel	25-35%	Conventional DPF + SCR	Adv. Eng.
GDCI*	15 - 25%	Low NOx, soot. Low ex. T (High HC, pre-turbo cat.)	Adv. Eng.

Figure 2-6 A summary of major IC engine technologies, CO_2 emission reduction potential, and status of implementation. Original source [13]

Due to differences in possession of intellectual properties, visions and targeted market, the direction of research to achieve the same goal can differ greatly. Powertrain researchers are looking for new/improved solutions, for cleaner mobility that meets or exceeds the demands set out by the consumer and regional governing body.

The logistical demand is growing, and transport offers the solution. With advancements in technology, there is a bigger selection in powertrain than ever. The potential demand for IC integrated powertrain are predicted to remain high for into the far future [14–17]. With the

ever-tightening emissions regulations and a high number of units to be added to the fleet, advancements of IC powertrains are highly sought.

2.2.3 Summary

There is an ongoing crisis related to air quality and global warming, and at the same time, there is an ever-growing demand for logistics and transport with a growing number of vehicles. It is evident that the two trends do not complement. It is therefore important to improve the powertrain technology to lower fuel consumption and reduce emissions of harmful species such as NO_x and particulates.

It is of strong interest for governments to regulate the emissions of road transport vehicles, as they are major contributors of both GHG and offenders of local air quality, both of which affect the current and future quality of life. This leads to the ever-tightening restrictions of emissions targets faced by the vehicle manufacturers, which also affects the ownership cost of vehicles due to increased count of control and exhaust after-treatment components.

Technological advancements have improved the IC engines efficiency and emissions, and more improvements are still in the pipeline. This factor drive the demand for such a project that improves the efficiency of SI combustion engines, and such a demand is predicted to remain for years to come.

To conclude, there is a strong demand for transport that is ever-growing, yet to cater for this demand with current technologies will contribute to negative environmental consequences. While regional legislations and taxing solutions are constantly updated to accelerate the research, research projects that look at improving fuel efficiency and emission reduction such as this one cater for a very important demand.

2.3 Fundamentals of the research topic

The pre-requisite but crucial knowledge of IC engines are reviewed in this section. This includes the core theory of the SI engine working process, SI engine efficiency, SI engine emissions, and the significance of the stoichiometric operation.

2.3.1 Operations of a four-stroke SI engine

The basic mechanisms of the four-stroke ignition engines will be reviewed along with the fundamentals of thermodynamics that determine the thermal efficiency of the engine. The section starts with the thermodynamics of IC engines followed by an explanation of the four-stroke ignition combustion cycle with all events explained. The fundamentals of a real operating efficiency and emissions are then reviewed to end the section.

2.3.1.1 SI operation combustion and the 4-stroke cycle

The idea of the four-stroke automotive engine used today was first patented in 1862 by a French engineer Alphonse Beau de Rochas. Such patent was first used when Nikolaus Otto successfully implemented the cycle in 1876. Here on, the term Otto cycle was coined for the heat cycle [18]. Otto cycle IC engines were further suited to be mounted on rolling platforms as an automotive powertrain.

Such an engine converts localised heat energy into rotational motion utilising the natural thermodynamic effects. The cyclic gas expansion and compression process is used with heat transfers, and the levels of Compression Ratio (CR) and gas properties such as ratios of specific heat determines the maximum attainable thermal efficiency based on the fundamental knowledge of heat engines as commonly outlined in publication [19].

A four-stroke engine comprises of a combustion chamber with a piston that slides within the bore, the piston is attached to the crank via a connecting-rod to the crankshaft that rotates as the piston reciprocates along the bore. Valves open and close to allow the flow of gases to and from the combustion chamber. The four strokes of the piston along the bore performs the four processes induction, compression, expansion (power) and exhaust.

Within this process, induced turbulence and flows are found to result in faster flame propagation and fuel/air mixing, though work to encourage these high intensity flows often results in inlet flow restrictions which hinder the performance [20, 21].

The combustion process is performed only on the trapped mixture, this refers to the mixture that is present in the combustion chamber when the inlet closes. The ratio and amount of air and fuel determine the overall combustion equivalence ratio, the full effects of the emissions, combustion intensity and speeds are fully documented in numerous studies and publications [19, 22–25].

Furthermore, the influences of throttling and boosting upon the trapped mass and the subsequent combustion are well documented in [19, 26]. Additionally, if the IVC occurs at any point other than Bottom Dead Centre of the piston (BDC), the cylinder volume will be at an arbitrary volume lower than the maximum, thus the volume of trapped air is less which equates to mass also, this technique is termed Atkinson or Miller cycle, and is an alternative method to controlling inlet air to reduce throttling requirements [27].

Fuel is added to the mix through a Port Fuel Injector (PFI) or a Direct Injector (DI) system. The differences between the two are detailed in numerous publications [19, 28]. A certain fuel concentration distribution can be achieved by late or split injection events with internal flow manipulation [29], novel fuel mixing strategies are discussed in sections 2.4.3 and 2.4.4.

The combustion phasing is a strategic placement of burn phase along the cyclic piston motion that is controlled by the Spark Timing (ST). Mean spark advance for Best Torque (MBT) typically lines up with 50% mass fraction burn position (CA50) at 10CAD aTDC (Crank Angle Degrees after Top Dead Centre) and CA_P_{max} (crank angle location of max in-cylinder pressure) at about 15CAD aTDC [19]. Combustion phasing and indications of optimal phasing for different strategies are discussed in many works including one from Ma *et al*. [30] who performed a zero-dimensional study to find the significant detrimental effect on cyclic variability.

Towards the end of the expansion process, the exhaust valve would open. The increased levels of in-cylinder pressure will be released down to the exhaust port pressure, this effectively ends the positive work of the piston due to expansion. The piston switches direction towards TDC to exhaust the combustion products. As the piston approaches TDC, the exhaust valve begins the closing process and the inlet valves start to open which initiates the valve-overlap, but the degree of this overlap is entirely dependent on the valve settings. Furthermore, the desired outcomes of the valve-overlap depend on the strategy and will be discussed further in section 2.4.3.

Losses are all forms of energy that leave the engine other than by crankshaft work. An example of an energy distribution chart of a car is as seen in Figure 2-7, the chart represents the typical inefficiencies of an IC engine where most energy used is lost as heat and operational losses (such as friction and pumping loss), typically with a thermal efficiency around 20% as seen in this case.

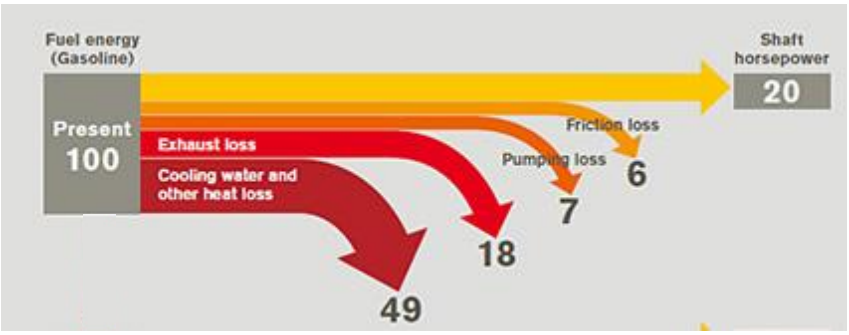

Figure 2-7 Energy distribution of an IC engine in operation against the fuel energy input. Original source: [31]

SI engines are well-known for their pumping losses at part-load operation. This comes from the piston to work against the low inlet pressures during the inlet cycle. Pumping losses are larger on engines with higher swept volume operating at part load due to the increased need to restrict the inlet air. Advanced engines aim to lower this inefficiency through a selection of

options such as, downsizing, early/late IVC, air dilution with inert gas which is all found to be effective [32–34].

SI engines also suffer from knocking combustions at high load which are overcome by late combustion phasing, as the strategic placement of heat released is phased later in the downstroke of the piston, there is also a combustion phasing loss that results [35].

2.3.1.2 Emissions of SI combustion

Discussed here are the combustion products found in the exhaust system. These are the GHG, harmful gases and particulates.

The emissions of a SI combustion change at different ST, load, speed and air/fuel ratio [26]. The formation of common SI combustion emissions (NO_x, CO, THC) is noted comprehensively by Haywood [19].

Particulate Matter (PM) is the quantity of solid and liquid particulates that are suspended in the air. It is quantified in terms of total mass and count sometimes assorted by their size.

PM emissions are found in combustion products of IC engines, but the quantities of formed particulates vary greatly depending on the type and air/fuel mixing strategy of the engine; for example, GDI engines produce more PM than PFI types due to the way the mixtures is prepared [36].

Most of the particulates are either volatile particles that settle at either liquid or solids and are products of partial combustion of fuels and lubricants. The organic carbon particles are formed by flame quenching near the wall, crevice volume, absorption of fuel into oils or defective combustion such as partial burns and misfires [19]. Most of which are processed by the TWC if fitted.

Raza *et al*. [37] explains the carbon particle formation to come from a complex mix of chemical and physical processes. Pyrolysis occurs without oxygen at high temperatures to dehydrate the fuel molecules to become the soot precursors, the growth of these precursors with interaction with species forms the nucleation particles [37]. From here, post-combustion processes take place which promotes further growth and agglomeration takes place to form the larger particles with a total particle size ranging from 5 to 100nm in size.

Thus, the process of a solid formation of carbon comes from presents of unevaporated fuel during combustion and are best controlled by optimising for best evaporation opportunities. The details particulate formation and control are reviewed in section 2.4.5.

2.3.2 SI engines at high load operation and the shortfalls

The use of throttling produces higher pumping loss at lower load conditions. The thermal efficiency benefits of using higher intake pressures were evident at high load. Where higher efficiency engines are in demand, engines have started to implement strategic use of higher load operation. This section reviews the use of high-pressure operation including the shortfalls to better understand the advancement and issues of current efficient engine technologies.

2.3.2.1 Irregular combustions; Knocking, partial burns and misfire

There are several types of irregular combustions in SI combustion engines. Failed propagation of charge results in partial burns and misfires, but SI engines also encounter issues when the end-gas ignites ahead of propagating flame front. This section details these knock phenomena that occur in engine operations and its classification.

Knocking combustion is an unwanted engine combustion event when end-gas detonates ahead of the flame front propagation. This can occur if the reactivity of the end-gas meets a certain condition limit. The knock event results as a sudden increase of in-cylinder pressure due to the sudden heat addition from auto-ignition flame sights, a shock wave is also generated by the auto-ignition which travels back and forth within the cylinder as it bounces off the walls [19]. These occur as a result of increased blow-by or localised heat build-up [19, 38].

Due to the trigger mechanisms of knock, the most severe cases are often found in higher Mean Effective Pressure (MEP) ranges with lower engine speeds where more time is available for detonation to start and propagate. Knock can be caused by one of two possible mechanisms 1) autoignition, and 2) pre-ignition. The reactivity threshold of fuels, ST, and trapped mixture properties affect the knock tendency greatly, these factors are well documented across multiple publications [19, 26, 39, 40].

Pre-ignition is the detonation of charge by means other than the engines ignition system. The source of ignition in these cases are hot spots (such as plug electrodes and valves), auto-ignition of lower knock limit elements (lubricants) [41], and combustion remnants such as dislodged carbon deposits [42]. The offending elements ignite the charge before the spark ignited event, which triggers an early heat release possibly nearer to TDC where pressures are high, and volume is limited. This gives the possibility to cases of extremely intense knock termed differently by many as ‘super knock, ‘mega knock’ or Low Speed Pre Ignition (LSPI) [43–46]. And also, for this reason, the implementation of regular knock mitigation techniques such as spark retardation is not deemed to be effective [38].

As suggested by the name of LSPI, the more severe cases of pre-ignition that turn to super knocks/LSPI occur at lower engine speeds as the time available for the reaction to initiate exceeds the autoignition delay time [47].

The classification of super knock or LSPI to differentiate from regular post ignition auto-ignition knock is different for many. Zahdeh *et al*. [47] from the General Motor Company published their research into pre-ignition occurrences in boosted SI engines and determined cycles with max pressure above 105 bars as pre-ignition. Haenel *et al*. [48] from FEV Inc. consider 2 detection criteria where the severity of peak-to-peak pressure oscillations was analysed. The study also reported pressure far beyond the calibration limit of the pressure transducer (250bar) which indicates the degree of impact.

With such high pressures, the engine damage is imminent in high-pressure operations. It is important that knock and pre-ignition cases are kept to a minimum throughout the life of the engine. But with greater demand for higher engine efficiency by using high-pressure operations, it is vital to carry on the knocking and pre-ignition research to mitigate their impact. A review of knocking combustion performed by Wang *et al*. [38] in 2015 recorded 339 publications on this field alone, and the range of investigation varies from detection methods, simulation, optical diagnostics, theoretical study, engine optimisation and fuel properties and additives.

On the contrary to auto ignition and pre-ignition is the occurrence of misfires and partial burns. Details on occurrences and their effects are well studied and noted in common publications [19].

2.3.2.2 Downsizing and GTDI strategy

The combined use of downsizing and GTDI is already successfully implemented as a light-duty vehicle engine especially in European markets, and it has contributed towards the fleet CO_2 emission targets. This section details the benefits and synergies of the two strategies, along with the methods to lower the most prevalent shortfall, knocking combustion.

The smaller swept volume encourages the use of wider throttle opening during regular road resistance conditions which is also where the best efficiency of the engine lies. The loss in peak power is recovered by the strategic use of forced induction. Figure 2-8 shows a typical Brake Mean Specific Consumption (BSFC) map of a 2l NA engine and a downsized TC engine of equivalent power specification. The best BSFC island is expanded and is more under use with a downsized TC engine due to the use of higher MEP conditions for typical road load.

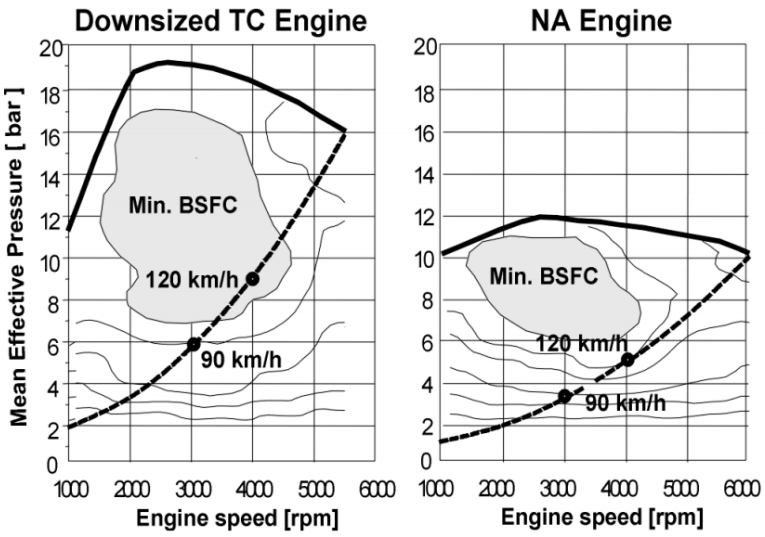

Figure 2-8 A typical best BSFC island in an IS engine operating map, a comparison with the downsized TC engine with a typical driving load to represent the benefits of downsizing. Original source: [53]

However, the use of higher MEPs and addition of TC components add cost and weaknesses to the strategy by increasing knock tendency. Furthermore, there is a need to regulate exhaust temperatures due to TC component protection. As seen in Figure 2-9, the best efficiency island sits above the throttled range where pumping loss dominates the causes for inefficiency. However, with lower speeds on high loads (LSHL), knocking combustion is very prominent that the ignition is heavily delayed, losing the gained efficiency by downsizing. In the high-power output region, exhaust temperatures are often lowered by over fuelling to protect the TC components, leading to lower fuel efficiency.

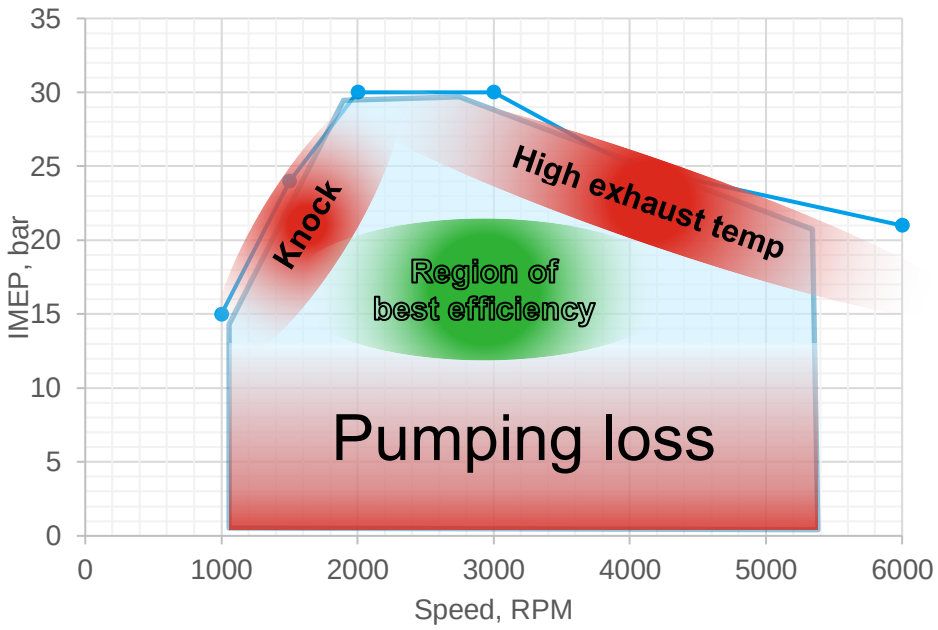

Figure 2-9 Notable strategies required to manage a downsized TC engine; issues of high MEP operation localise the area of best efficiency to a limited range

The benefits of DI system over PFI systems can be summarised by [54–56]. The injection can be timed after the Exhaust Valve Closing (EVC) which disables the possibility of fresh charge short-circuiting; thus, combustion efficiency is considerably improved. There is also a possibility of lessened fuel loss to wall attachment as the spray is directly targeting the cylinder centre where combustion takes place. But this is highly depending on the success of injection strategies employed [57–60].

The highlight of the DI system comes when it is combined with the downsized TC operation at high loads to make full use of the charge cooling effect offered by the evaporation of fuel. A study in 2012 highlights such an effect for knock mitigation effects in a SI combustion, where additional anti knock effects equivalent of up to 18 octane numbers were confirmed by direct injection using E85 fuel. The effect was greater with increased ethanol content due to the increased injection quantity [61, 62].

Further review relating to advanced stratified/late/ and split injection strategies will be detailed under section 1.4.4.

On the downside of DI systems, the implementation comes at a cost due to the requirement of a high-pressure pump, HP-fuel rail, and HP DI. The successful application can be offset by the efficiency and environmental gains, which in most case is also encouraged by the vehicle economy targets. Furthermore, and as discussed previously, the shortened mixture preparation time is suspected to increase the harmful particulates emission. The review of

particulate emission with employed relevant strategies (including direct injection) will be carried out in section 2.4.5.

2.4 Novel SI combustion strategies

As mentioned in a previous section (Section 2.2), there is a strong demand for lower emission transport, but these are achievable only with successful implementation which requires advancements in technology. Discussed in this section are the literature reviews for novel SI combustion strategies. These are defined to be the combustion strategies that are yet to be commonly implemented in the market or limited to success in controlled or lab environments. These strategies are also related to the topics involved in the current project, which covers mixture dilution, advanced ignition systems, novel valve train system and uses, and mixture preparation with SFI. As an addition, the review will also focus on the resulting GHG and harmful emission with the use of these advanced combustion methods, due to the high relevance to the project.

2.4.1 Diluted SI combustion

Diluted combustion is the intentional use of diluent to change the combustion property. Two common diluents in consideration are excess air (with lean operation) and combustion products (such as EGR dilution) due to the abundance of availability during operation and relative ease of implementation to market. Improved fuel economies are reported for both diluents but at different implementation and emission costs. This subsection details the literature review for the use of such a strategy.

2.4.1.1 Lean mixture combustion

Lean mixtures are achieved by simply allowing more air to enter the cylinder, doing so at part load decreases the need for throttling. Controlled lean mixtures improve engine efficiency. Furthermore, successful combustions of very diluted mixtures can drastically improve thermal efficiency through lowered combustion temperatures and thus less heat loss [19].

The pursuit of engine efficiency by operating with lean mixtures has been implemented by several manufacturers [63, 64]. These strategies use lean mixtures to attain the best thermal efficiency and reduce pumping loss. Toyota first showcased their lean burn technology in 1976. The consequential tendency for misfire due to lean operation was overcome with the use of turbulent mixing chambers [64], and the engine reported superior fuel efficiency at the time. Since then, the introduction of more stringent emission limits had deterred manufacturers from pursuing such strategies as the lean operation had led to large NO_x emissions. However, BMW started a production run of the N43 engine which ran SI

combustion in a dynamic AFR between 12 to 30 depending on the load and speed. A paper from Chambon *et al*. [63] reported fuel efficiency improvements of up to 14.6% based on HFET drive cycle. While the engine was proven for its efficiency benefits, the technology was not without the expensive after-treatment devices to remove the NO_x emissions. In addition, these devices also required a specific drive style and engine management protocol to operate correctly.

Further boosting with lean operation conditions were explored by some researchers as a way of extending the benefits at higher loads. Ratnak *et al*. [24] tested the lean-boost combustion in an experimental engine, the engine performed with thermal efficiency up to 43.56% at lambda=1.3 but reported further boosting led to the requirement of ignition delay that lowered efficiency. Stokes *et al*. [65] report a 9.2% improvement in fuel consumption in city drive cycle conditions at lambda=1.4 with higher Brake Mean Effective Pressure (BMEP) ranges (8bar +).

The efficiency improvements of lean operation are thus proven, but the resulting tailpipe NO_x emissions is a major hurdle to overcome. The use of advanced exhaust after-treatment such as the Lean NO_x Trap (LNT) system is under consideration but as a major cost and complicated strategy setback. While the technologies are available with a few success cases, such a technology has not been made available on a large scale.

2.4.1.2 Exhaust Gas Recirculation

The reactivity of a charge mixture can be lowered by altering the gas composition. Exhaust gases contain higher concentrations in CO_2 which has desirable properties and are in abundance with an operating engine, making it a suitable diluent for knock mitigation. The reuse of combustion products can improve engine operation by four possible strategies: -

1. Reduction of throttling (thus pumping loss) at part load operation
2. By replacing over-fuelling to lower exhaust gas temperatures
3. Lower knock tendency of the mixture to unlock phasing advancements at Knock Limited Spark Advance (KLSA) conditions to optimise combustion
4. Decrease combustion temperature and thus decrease NO_x emissions and heat transfer loss

This review focuses on the third and fourth benefits, especially as knock tendency and NO_x reduction are of the key benefits when considering the LSHL operation of a downsized engine.

There are several types of EGR systems present, each with their own advantages and disadvantages. Figure 2-10 shows the main different classifications of how EGR dilution can be achieved in an engine set up. Residual gas refers to the use of combustion products that

remain in the cylinder for the following cycle, it can be intentionally trapped by the valves with the use of short or negative valve-overlap (NVO). Providing the IV is open, early EVC forces combustion products into the intake port which increases the trapped fraction of residual gas. External EGR requires the application of pipework from the exhaust pipe to the inlet pipe with a flow controlling valve. The positive pressure difference present between the two sides create a natural tendency of flow. This is further split into two classifications in a TC engine. The difference is the origin of exhaust gas (pre or post-TC), which also determines where the EGR gas is reintroduced (pre or post compressor). Unlike the residual gas trapping, the external-EGR requires additional pipework with a mixer valve. These cases perform better with EGR cooler systems but for different reasons, HP variants may suffer from increased knocking from increased inlet temps from high dilution, whereas LP varies will result in lower compressor efficiency of the TC, hence the importance of the EGR cooler is pronounced [66].

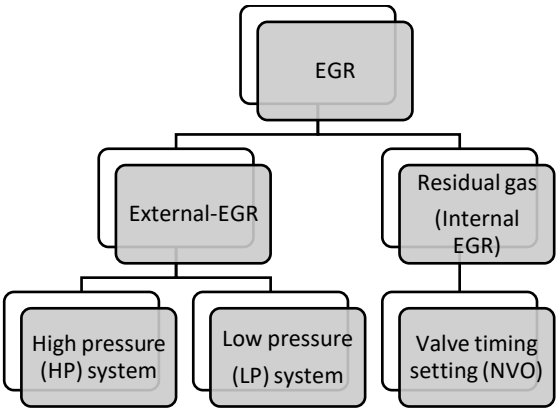

Figure 2-10 Possible implementation map for EGR combustion strategies

Experimental trials report internal EGR to have the least knocking combustion mitigation capability due to the higher contents of reactants and higher temperature of the mixture. Besides, the internal EGR strategy relies on a valve timing system [67]. Internal EGR is most often tested with positive valve-overlap in throttled loads to lower pumping loss, thermal efficiency improvements are reported [68, 69].

HP-EGR takes the shorter path than an LP-EGR system and operates with a much better transient response [66, 70]. However, as the exhaust mass is taken away from the TC inlet, this method leads to a loss of peak power with increased dilution. It is also harder to implement sub-systems to cool or ‘clean’ the gases which is a disadvantage to mitigate knock. However, THCs in the exhaust can be combusted to increase combustion efficiency [71].

LP-EGR system offers the use of post-TWC exhaust. Further cooling of the gas would further reduce the reactivity of the charge mixture [72, 73]. As a downside, the long pathway of EGR to the inlet has a big transient operation disadvantage, especially as response time is very important at dynamic operations. Many studies, as a result, focus on the use of HP-EGR systems with gas cleaners or LP-EGR systems with greater responses to enable the use of these techniques.

The benefits of treated EGR diluent is noted by a study performed by Francqueville *et al*. [73] who conclude that the presence of NO reduced the knock mitigation effects of the EGR, based on a series of tests performed on a single-cylinder engine using different diluent gas. Further review performed by Parsons *et al*. [74] shows the success of post-TWC EGR to lower knock tendency at high loads based on 4 results where catalysed EGR shows greater benefits.

The benefits of EGR was compared against lean boosting by Ratnak *et al* [24]. Better performance gains were seen with EGR dilution at higher loads where lean boosting failed to emulate due to the lack of knock mitigation capability. The paper reports a maximum indicated thermal efficiency of 45.9% at MAP=1.5bar using external-EGR dilution, which is an increase of 2.4% from lean boosting at 1.3bar MAP with equivalent excess air to EGR dilution ratio.

The use of EGR at high load conditions has been reported by several other papers. Terry *et al*. [75] report a BSFC improvement of ~10% at 2000RPM and 18bar BMEP, using up to 20% of EGR dilution. On the contrary, James *et al*. [76] reported reduced effectiveness of EGR at high loads in boosted engines. The tests showed an increase in knock tendency with the use of pre-TWC exhaust gas which may have a higher reactivity.

Further cooling of EGR gas prior to reintroduction has enabled the compressor performance to remain effective at high demands. Alger *et al*. [75] carried out a study on the topic to find significant aid to the operation of a downsized TC engine. The study further notes the importance of keeping the temperature above a certain threshold to prevent condensation of water vapour which will cause impact damage to the compressor fins.

The benefits of EGR at high load comes from the lowered reactivity of mixture which mitigates the end-gas auto-ignition. Francqueville *et al*. [73] also report on the root benefit comes from the heat sink effect of increased Cp with combustion products.

A comparison of LP-EGR and internal EGR was performed by Guillaume *et al*. [72] at loads between 6-10bar Net_IMEP. The study concludes the success of LP-EGR to lower fuel consumption at higher loads, where internal EGR increased the knock tendency resulting in

an increase of fuel consumption. The results strongly favoured the use of LP-EGR where knock was present.

Emission effects were dominated by EGR dilution in many ways. The change to the combustion speed and temperature meant that formation of NO_x, CO and THC differed to that of regular combustion. One of the earlier reports of EGR at high loads with pre-TWC emission comes from Alger *et al*. [77] in 2008. Using a 1.6l PSA engine modified with both HP and LP EGR system, a wide range of load and speed was tested for EGR effectivity towards performance and emissions. At 2000RPM with 14 and 18 bar BMEP, EGR dilution lowered NO_x and CO while increasing THC emissions. At high power operation (4000RPM and higher) the comparison to 0% EGR condition was influenced greatly by eliminating the enrichment that was required for component protection reasons. This had seemingly made the NO_x increase and THC and CO decrease in comparison as with the EGR dilution where the AFR was reverted to stoichiometry. The ability to run full stoichiometric operation to lower exhaust temperatures through enrichment or lean operation was found to be one of the advantages of EGR operation. A similar study was performed by Shen *et al*. [66] at 2000 RPM with mid and WOT conditions. In particular, the HP-EGR system was tested at 5000RPM and WOT conditions for comparison against enrichment conditions. The general finding for pre-TWC emissions showed a reduction in CO and NO_x which was due to the lowered flame temperature and the reduction of dissociation of CO_2. The increased concentration of THC emission is reported mainly due to the increased combustion duration from increased inert gas fraction and lowered in-cylinder temperatures. Similar findings were also reported by papers that experimentally studied the use of EGR at high loads [71, 78, 79].

There are a few reports concerning the combined use of internal EGR at higher loads. Bourhis *et al*. [72] tested the combination of external EGR and RGF at 10bar Net_IMEP to report efficiency improvement with external-EGR, but the onset of knock with increased RGF due to increased reactivity of the mixture. Internal EGR was increased by NVO. Francquiville *et al*. [73] also reports similar work but uses both PVO and NVO with external EGR dilution at high-loads. Here, efficiency benefits were seen with both cases, as the external EGR dilution was increased, but the emissions varied due to the increased reactivity of the mixture with NVO and increased combustion products. Overall, no positive outcomes are reported from the use of high RGF at high loads due to increased reactivity, where knock limited operation restricts engine optimisation.

2.4.2 Enhanced ignition systems

The initiation of a SI combustion can have a large impact on the combustion process. It has an important role in producing a stable flame kernel that develops into bulk combustion. Each consecutive ignition to produce the flame kernel must be similar in size and intensity to ensure the same combustion takes place every cycle. Such stability in combustion enables a tighter control combustion phasing which can be closer to optimal crank location and improve the efficiency of the engine. Increase in the size and intensity of the initial flame kernel leads to a faster bulk burn which can significantly reduce the onset of knock [80]. Furthermore, the enhanced ignition can improve the success rate of initiating combustion in very diluted mixtures [81]. In summary, the ignition system is a key component of a SI engine, for its potential to create stable combustion for hard flame kernel creation conditions and further improve engine performance.

In almost all automotive engines, an electrical spark ignites a combustion. A rapid discharge creates a small high temperature plasma across a pair of electrodes that ignites the mixture. The plasma (or spark) is a resulting electrical discharge across an ionised gas between the plug electrodes. The ionisation and tunnelling of the gas happen as the electric field strength exceeds the breakdown voltage of the gas. Properties like composition and velocity of gas between the electrodes can affect the required breakdown voltage which also changes the spark intensity [82, 83].

Discussed in this subsection is the latest studies into uprated ignition systems to improve the ignitability of diluted mixtures. Discussions of in-cylinder flow conditions and the use of stratified/split injections will be discussed in a later section of the review.

A review highlighting the ignitability of diluted mixtures and use of High Energy (HE) ignition systems was first published in 1997 by Dale *et al*. [84]. From these times (and earlier), the potential of diluted mixtures to improve engine efficiency has been recognised along with the concerns mounting on the reliance on ignition performance. The focus of the study was the use of multiple spark plugs, jet igniters and multiple discharge events.

Recent developments of ignition considers the use of smarter spark creations through integration with microcontrollers. One example from Delphi reveals an alternating current ignition system along with the first experimental findings as a demonstrator published by Piock *et al*. [83]. The experimental result is not the highlight of the study but shows good improvement in a full range of stratified injection cases to advance combustion and lower combustion stability. However, these were performed at part load and efficiency details were not published.

Another paper looks at the use of multi-electrode pole spark plugs to ignite very lean mixtures (λ=1.84) at part load. This lean limit was extended from λ=1.6 with a single pole ignition system. The resulting combustion led to increased thermal efficiency and lowered NO_x emission from the successful ignition of a lean mixture. Advancements in initial combustion speeds (SOI to CA5) were seen using the uprated spark plug but advancements in CA50 were not seen. The tested load was limited by the unavailability to further dilute the mixture [85].

Novel ignition systems have been studied extensively for their promising application benefits. Turbulent Jet Ignition (TJI) and corona discharge are just two of many examples. These systems are also referred to as distributed ignition, creating a much larger field of ignition in the cylinder compared to a single line of plasma seen in a typical spark plug. This larger stretched ignition site creates bulk combustion much faster than an equivalent SI system. A plasma system was used with lean and EGR diluted mixtures in a test performed by Sevik *et al*. [86]. The authors used a low-energy transient plasma at various settings, resulting in delivery of energy varying between 131mJ to 525mJ depending on the pulse count. The results are compared against a conventional spark plug which discharges 75mJ of spark energy. The study confirms the use of increased discharge energy with a plasma system improves combustion stability of diluted mixtures. But the initial flame speeds were also improved, and the bulk combustion speeds were slower compared to conventional SI combustion. The EGRs dilution limit was improved by 5% using the novel ignition system.

The use of distributed ignition systems has unlocked dilution limits to lower combustion temperature and increase operating efficiency. But a similar study using electrical sparks was seen by a series of studies performed by Iida *et al*. [87]. The lab aims to achieve 50% efficiency through successful combustion of “super lean” mixtures with a high energy super stretched spark plasmas and high tumble. Interestingly, the study performed with increased ignition energy has resulted in slower end combustion which reflects well to previous reviews from other studies [88]. The authors here consider the faster initial burns lead to radiating velocity of charge away from the epicentre of combustion, leading to slower end-burns.

Summarising the literature review on the topic, the benefits of improved ignition comes from a larger and more powerful ignition flame kernel. The resulting fast combustion can lead to mitigation of knock or successfully stabilised combustion of very lean (or diluted) mixtures. Most studies concentrate on the optimisation of ignition systems to stabilise or improve ignition of lean mixtures to lower combustion temperature. Conventional spark plug had limitations due to the small ignition point but the use of increased energy and multiple or high-frequency strikes have been found to improve stability of difficult conditions, but most

tests were focused on the use of dilution at lower loads which opened questions for responses at high load and low speed where knocking combustion is present. Another interesting point to note was the positive impact of the uprated ignition towards initial burn speeds that slowed down the end of combustion compared to the reference conventional ignition system.

2.4.3 Valve event timing and valve-overlap strategies

Synchronised valves allow four-stroke SI engines to cycle working gas through the combustion process. The importance of a well-executed intake and exhaust stroke is important for the operation of the SI-engine, but due to mechanical restrictions, the requirement from inlet and exhaust valve operations are not performed at ideal conditions. New valve-train systems are constantly under development to allow for greater versatility of valve control that can cater for a wide range of SI operation with greater performance and lower emissions.

Discussed in this section is the review of the use of valve timing system for LSHL operation and investigation into recent valve timing related research.

The use of Variable Valve Actuation (VVA) gives the engine a dynamic operation region by having an adjustable gas exchange strategy for different engine operating points. A classification of some of the basic strategies for VVA is as follows: -

- Variable Valve Timing (VVT)
  Control of valve profile offset with respect to the crank angle position. Often realised with an angle position phaser between the driven medium and camshaft.
- Variable Valve Lift (VVL)
  Valve lift modulation often achieved through the motorised kinematic device. Restricting breathing from either exhaust or inlet for load control to lower pumping loss. Often combined to shorten the valve opening duration to achieve a miller cycle operation or overlap control.

2.4.3.1 Positive valve-overlap

Adjustable valve timing strategy has been a necessity for successful downsizing GTDi due to the ability to unlock of very wide operation range, it has also unlocked the availability of adjustable positive valve-overlap. Positive valve-overlap refers to the strategic opening of both Intake Valve (IV) and Exhaust Valve (EV) simultaneously at the end of the exhaust stroke and beginning of intake stroke. With a dynamic pressure difference caused by the flow inertia, the gas exchange of the clearance volume is realised. This flow of gas has

several advantages but are also associated with losses in a complex and dynamic interaction. These are summarised as the following points[89–91]:-

1. Increase volumetric efficiency
2. Cooling of the cylinder and exhaust gas
3. Enrichment of trapped mixture (with short-circuit)
4. Increased TC flow rate optimisation

At boosted operations, an increase in volumetric efficiency is the primary target of valve-overlap. TC 3-cylinder engines are suited for this strategy due to the greater pressure's gradients between the inlet and exhaust ports created at high load, this is due to the absence of pulse interference between the cylinders [92]. This recovers the performance cap and decreases the mixture reactivity which is extremely important and for a downsized TC engine [91, 93].

DI system has enabled positive-scavenging without the release of unburnt fuel, and also enable trapped enrichment that can lower knock tendency [62]. The effects of valve timing to lower knock tendency are noted by several studies. Tests performed on a 30bar BMEP engine performed by Martin *et al*. [89] notes the successful knock mitigation from the use of enrichment of in-cylinder mixture resulting from fresh air short-circuiting. Furthermore, there are similar studies that report the synergy of lambda=1 operation with high IMEP using TC [94–96], to name a few studies. In addition, the use of wide valve-overlap and thus high short-circuit air has also enabled the expansion of torque limit.

Recent simulation work performed by Zhuang *et al*. [97] also confirms the mixture cooling effect with the wide valve-overlap, providing averaged temperature drop of up to 40.9% in the simulation-based tests. The study also confirms the wide valve-overlap to successfully remove the majority of the carbon particulates and residuals to unlock the engine peak performance.

Enrichment of trapped mass is associated with loss in combustion efficiency, meaning this is a trade-off between knock mitigation and combustion efficiency. Engines such as the Ford Ecoboost 1l engine has implemented a lambda map regions with a lean setting to adjust the in-cylinder condition towards stoichiometric [98].

The use of wide valve-overlap and high boosting causes surges of fresh air to short-circuit, leading to a measurement error in exhaust oxygen content by the lambda sensor. This has been proven to operate the engine in overall lean conditions, and trigger tailpipe emission of NO_x due to lowered TWC efficiency [28, 99, 100].

2.4.3.2 IVC timing impacts to engine operation

Early or late IVC operation leads to lower Effective Compression Ratio (ECR) from the shorter piston stroke with closed valves. It is referred to as the Miller cycle and is implemented as a part of the knock mitigation study.

The use of novel CamInCam® system developed by MAHLE powertrain was used to implement LIVC at part and high load operation (including boosted region) by Taylor *et al*. [101]. The study performed at 10bar Net_IMEP showed steady improvement of efficiency with later IVC due to the lowered ECR which was defined as the ratio of volume at physical IVC to clearance volume. Extra tests carried out at 15bar IMEP (boosted load) showed the elevated levels of turbo-compression required from LIVC lowers the effective inlet charge temperature to effectively advance the combustion, however, these were not fully realised due to the increased ratios of hot residual gases. During this work, the IVO timing was also shifted, but the subsequent effect towards volumetric efficiency, short-circuit and in-cylinder enrichment were not discussed.

The use of EIVC with variable lift actuation to lower peak compression pressures and thus lower knock tendency is seen by a study performed by Wang *et al.* [102]. Here, a 1.6 litre PSA engine was used to compare the use of external-EGR and EIVC, the idea being lowered ECR and thus controlled peak pressures. The conclusion showed the ineffectiveness of EIVC to lower knock, whereas external EGR was able to smoothly advance the combustion phasing. The combined use of both external and internal EGR was also reported but with very limited results due to the limited amounts of external EGR usable at reduced lift. Highlighted here was the overall effect of EIVC, while ECRs were successfully lowered, the charge motion had reduced which slowed the combustion and increased the onset of knock.

An engine with variable valve lift and phasing was tested for early and late IVC at a very wide range of high load engine operating points (14-21bar BMEP and 1500 -5000RPM) [103]. While some LSHL cases were not tested due to the inability of the TC to provide further boosting, a peak efficiency benefit of 20% was seen at 3000RPM through knock mitigation with LIVC. EIVC had not performed in the same way according to the study. Implementation of such a cycle into a down speeding engine has also been documented from Dongfeng Motor Corporation [104].

An established Toyota SI-engine boasts the use of later IVC with optimised hydraulic lash adjusters. The resulting Atkinson cycle can improve engine efficiency at low loads. The paper extends the report by mentioning the increased losses in combustion due to lowered tumble intensity as seen by the included comparison chart in Figure 2-11 [105].

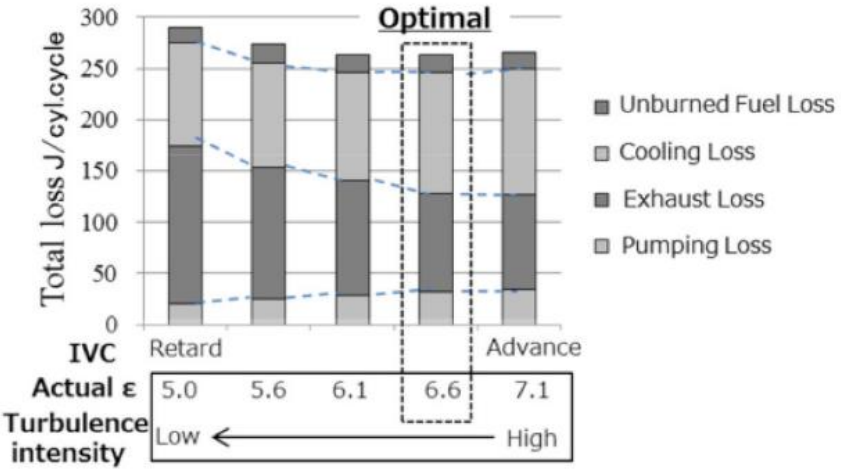

Figure 2-11 trade-offs between later IVC and loss of tumble in the 2017 Toyota in-line 4 engine. Original source: [105]

Inlet port and valve topology are very important for inlet flow tumble production and thus the creation of faster combustion properties[20, 106–108]. But with the rising use of adjustable valve event timing, the impact of the customised characteristic of IVC timing (and valve lift) on internal flow motion has been gathering interest in recent years. A paper by Wheeler *et al*. [109] from AVL powertrain engineering Inc. published the results of increased EGR tolerance of a GTDI engine using high tumble flow. The tumble was varied with a new head geometry, which increased the tumble from 1.93 to 2.4 to create a faster initial flame development from the increased kinetics at TDC condition, the effect was further backed up by Computational Fluid Dynamics (CFD) analysis.

Wang *et al*. [110] studied the impact of intake maximum valve lift (with the same duration) upon the swirl and tumble motion. The conclusion notes that higher valve lift produces greater vertical flows which turn to big scale tumble flow. But when it comes to kinetic energy, lower valve lifts created greater results due to the higher velocities involved in the intake process. With the example engine used, this did not result in a greater tumble. While the works of Wang *et al.* did not cover the impact towards combustion speeds, Myung *et al*. [111] found the effect of extra tumble to reduce combustion speeds. The extra tumble was created by port masking rather than valve lift. The results were also found to have an effect upon the emissions, lowering THC emissions from extra mixing and increasing NO_x from faster combustion. The testing was performed at low load conditions which may have amplified the tumble effects in comparison to higher load conditions. Nonetheless, the use of inlet valve manipulation can be found to have some impact on the combustion through flow control.

2.4.3.3 NVO and strategic combustion with residual gas

Another common research topic of valve timing is the use of NVO for the purposeful trapping of residual exhaust gas. Like external exhaust gases, the combustion products carry higher concentrations of inert gas from the combustion. But due to the higher temperatures and other species of gas from incomplete burns, increased residual fractions can lower engine performance at higher loads [92].

Residual gases are often tested for their uses in raising mixture reactivity to promote Combustion Auto Ignition (CAI) combustion but the use is limited to part-load operation due to the onset of harmful autoignition at higher pressure demands [72, 112].

At lower loads, the use of very wide NVO can dilute the mixture thus reducing the need for throttling and pumping loss. But such a gain requires a versatile and wide actuation range of the cam. Rodriguez *et al*. [69] studied the potential of wide NVO (up to 80CAD) to trap significant amounts of residual gases at throttled loads. The team succeeded in reducing pumping loss by up to 60%. However, due to the very early EVC requirements, losses were reported on the work output due to earlier EVO.

Through the use of variable cam profiles, Doornbos *et al*. [33] were able to dilute the charge with residual gases to compare the use of residual gas dilution with lean combustion for efficiency gains and emission reduction at partial loads of a GDI engine. This was performed at throttled loads and knocking combustion was not an issue, but the versatility of cam phasers to create lean or residual diluted mixtures were demonstrated with some efficiency gains at this point. Other cases of using valve phasers for residual gas reintroduction are noted by other studies with various goals [72, 113].

2.4.3.4 Summary of variable valve event strategies

Valve timing and lift can change the cylinders breathing properties, but this also depends heavily on the engines operating condition as this effect the pressures behind the cylinders. The desired strategy is often limited by the chosen valve train where the complexity of the engine seemingly increases with a form of control. The strategies are chosen for the pursuit of volumetric efficiency, combustion efficiency, combustion or ignitability of diluted mixture or reduction of pumping loss. But the achievability of this also depends on many other factors of the engine.

It appears there is a trend towards fully variable valve train where the duration, phasing and lift would be controllable. But the evident increase in cost and engine complexity may keep such a system hard to employ in a light domestic vehicle. For now, the use of existing valve train such as VVT/VVL still holds a promising future through use with innovative strategies such as the one seen in the review.

The review spells major losses associated with valve-overlap removal where the hot residual gases will remain in the cylinder. However, the late IVC with the use of VVT and increased use of boosting with TC may recover some combustion speed from altered tumble at the high-load operation region.

2.4.4 Mixture preparation control

The injection system adds fuel in a concentrated manner, it is then down to the flow fields (including turbulence) and fuel evaporation to form a mixture prior to combustion. The fuel injection strategy and thus the air-fuel mixing is discussed in this section.

DI systems are becoming mainstream to help meet emissions and efficiency targets. But doing so has also introduced a new possibility, due to the availability of late injections after IVC which was not available with traditional PFI systems. With later injections as well as multiple injection strategies now available, the variables for mixture preparation had become highly customisable.

Two types of injectors are available for DI systems: - piezo injectors and solenoid injectors. The two differs in the fuel actuation/valving design which ultimately changes spray pattern. The piezo type has a single hole that is closed with a cone nozzle that when opened creates a hollow conical spray curtain. Solenoid types are further exposed to the chamber through a hole that is targeted with a direction, it is often referred to as the multi-hole nozzle. The difference of spray characteristic is evident in the Mie scattering image as shown in Figure 2-12. The penetration length is less on a piezo type with finer atomisation characteristics due to the dispersed nature of the fuel, however, multi-hole systems have the advantage of unit cost and directional control which can be optimised for mixing in specific setups. Stratified and multiple injections can be achieved on both types of injectors, but a review into this broad subject by Fansler *et al*. [29] highlights the unsuitability of the multi-hole system to open and close in quick successions due to their ballistic opening mechanics.

There are little studies that directly compare the performance of the two injector types. One such case was performed by Smith *et al*. [114]. The study used two single-cylinder engines to compare performance impacts of the injector types, both engines were optimised for better stratification based on the injectors spray pattern, but the conclusion was showed little difference between the two that note suitability towards a stratified system.

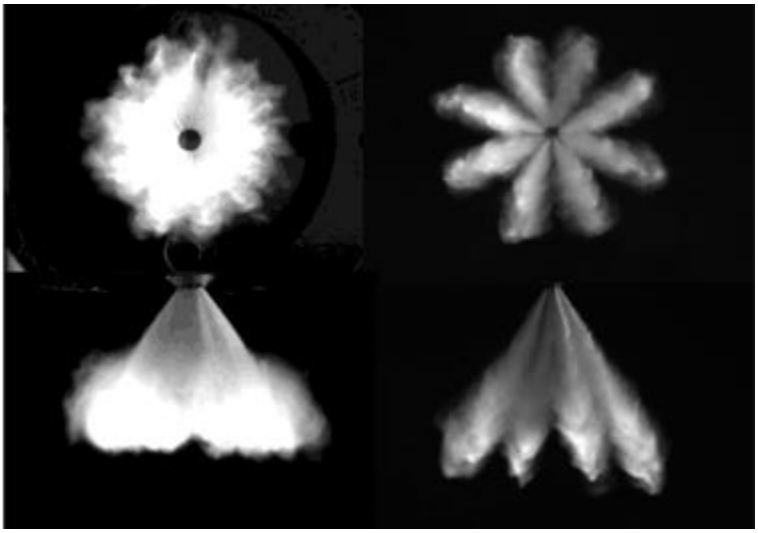

Figure 2-12 Mie scattering image of a Piezo injector spray and a multi-hole injector spray. Original source:[114]

Use of multiple direct injections of the gasoline engine for SI will be reviewed and discussed in this section. The purpose of such a strategy is focused on creating a region of concentration towards the ignition centre of the cylinder surrounded by a lean mixture near the walls to enhance the combustion and lower THC emissions. A similar technique called partially premixed combustion (PPC) employed to aid compression ignition of reactive fuels will not be reviewed [115], rather, the focus of this review is on knock limited propagating SI combustions at high load.

2.4.4.1 Spray guided SIDI combustion

The use of direct injection is popular due to the benefits outlined in sections 2.3.2.1. The ability of late injection opens possibilities for late and multiple injections to stratify the fuel-rich mixture for increased combustion speed with diluted mixtures. However, a successful implementation is not without the shortfalls of stratification to be overcome with optimisation of various factors.

The difficulty of the challenge was first reported by Ricardo in 1922, but the source of problematic optimisation of having a repeatable and consistent stratification and thus combustion can be found in the paper published by Drake *et al*. [116] in 2005. The study notes the difficulty of successfully optimising a SIDI prepared mixture. The CFD backed experimental work showed the required ignitable mixture around the electrode to be at lambda=0.9-1.6, with a flow velocity of 14-16m/s. Conditions out of this range resulted in the combustion of significant instability, due to reliance on shorter mixing and ‘correct’ in-cylinder flow for the mixture preparation to take place. Achievement of specific conditions was found to be challenging, especially in diluted mixtures where successful combustion relied on a successful stratification.

Successful stratification results in efficiency or performance benefits due to the extension of lean or dilution limit from localised combustible (stratified) fuel towards the centre and between the plug electrodes. The stratification in these combustions is extremely important to be able to ignite the mixture and further allow for propagation of the flame kernel to the bulk mixture. In 2015, Fansler *et al*. [29] reviewed the instability associated with diluted SIDI mixture preparation and ignition. The extensive review notes the improvements made towards the development of stratified charge combustion stability and recent research findings from optical observations of various spray guided systems. One conclusion defined the source of instability to three possible reasons which all relate to the development of spark induced flame kernel production to bulk combustion mechanism. The extensive review continues to difference between piezo and multi-hope injectors and effects with a late injection for improvements to the combustion. Again, the overall conclusion is the difficulty of optimising a spray guided combustion to achieve stable combustion, especially with diluted mixtures. An interesting observation noted was the mechanism for misfires, through the review of all optical studies performed, the ignition had not failed in the process of creating a flame kernel, rather all cases of misfires happened as a failure of the flame kernel to propagate to the bulk mixture.

Park *et al*. [117] tested on a single-cylinder direct injection experiment engine with optical access with lean conditions up to lambda=3. Using late injection to sustain stratified relatively rich condition around the plug electrodes, the overall lean combustion was sustained at 2.8bars IMEP at 2000RPM. One variable of condition was injection pressure of a piezo type DI. Best efficiency was found at the highest injection pressure of 200bars with a lean condition (lambda=3). The injection position was moved later with leaner combustions to regain a combustible condition, the leaner conditions successfully reduced the ISFC values to 255g/kWh at lambda=3 from 275g/kWh at lambda=1. With lower injection pressures, the delay of injection timing to account for leaner mixtures resulted in worse combustion properties due to the insufficient mixing process taking place, which has also resulted in a sooty inefficient burn. As an extended experiment, Park *et al* test with up to 20% EGR dilution which led to worse efficiencies due to fluctuations in burn properties. The authors did not delve deep in the EGR dilution results. But single late injection was not found to perform well with EGR dilution over excess air condition.

Another study also considered the use of single injection events to achieve successful stratification for lean combustion. Oh *et al*. [118] tested lean stratified operation with a single-cylinder spray guided direct injection engine with optical access. The test performed at 1200rpm with fixed injection duration at low load conditions. The importance of a well-timed

injection timing was highlighted, noting issues with over mixing and under mixing on either side, which was visually identified as a part of the work.

2.4.4.2 Spray guided SFI and multi injection strategy for combustion improvements

The previous section (Section 2.4.4.1) reviewed the challenges and findings of single injection stratification under diluted conditions. This section looks at the studies that focus on the effort of stratification with multiple injections. The single injection case highlighted an issue of late injection that led to the underprepared mixture prior to ignition. In comparison, the split injection event aims to lower the ratio of fuel that is underprepared. Thus, a possibility for partially premixed combustion can take place with a single point ignition. Such use of targeted fuel concentration through injection techniques is termed the SFI strategy.

Split injection for SFI increases the variables of operation with injection split ratio and timing. Some papers consider the use of 3 or more injections. But the increased complexity also brings a range of benefits.

One major reason to adopt multiple injections is to reduce fuel penetration, compared to continual single injections. This is not to be mistaken with the SFI strategy which aims to manipulate mixture distribution. In such a strategy, multiple injections are closely coupled together while the flow carries disperse the fuel. Doing so can minimise the piston wetting from shortened travel length of the spray, and thus increase combustion efficiency from increased mixing properties.

The main benefits of SFI to extend lean limits to achieve greater efficiencies are seen in a study from Park *et al*. and Oh *et al*. [119, 120]. Park and the team performed experimental work on a single-cylinder engine at 4 bar IMEP @ 3000RPM to achieve an excess air ratio of up to lambda=2. This is extended from lambda=1.2 with single intake injection. The paper noted sweeps at different injection pressures to note the favourability of higher injection pressure with piezo DIs for efficiency (as noted by ISFC), combustion stability, and emissions. Some findings were reported in the use of different strategies such as weighted split ratio and 3 injections per cycle to find that weighted late injection led to unfavourable conditions, especially for soot output. Oh *et al*. performed their work on a similar single-cylinder experimental engine with optical access. Tests were performed at 1200RPM with a fixed fuel flow rate of 11mg/cycle but with WOT. The resulting excess air ratio was around lambda=2.74 [120]. The combustion properties of split injection cases were compared against a single late injection case with changes in excess air ratio. The use of split injection was found to retain and improve these conditions from well-timed SFI condition. Further comparison of high-speed imaging verifies the lesser extent of luminous soot producing flame with later split injection as opposed to a late single injection.

The same strategy is found to work with EGR diluted combustion thus stoichiometric combustion can be retained. Such work was carried out experimentally by Feng *et al* and published in 2018 [121]. Work was carried out at 1400RPM with a fixed rate fuel flow of 2kg/h on a 1.4l 4-cylinder GDI engine. Up to 30% of EGR dilution was tested at this throttled load, and analysis of in-cylinder pressure revealed the ability of successful SFI to advance the combustion speeds at highly diluted loads. When it came to efficiency improvements, the 9:1 split ratio was found to improve efficiency over the single injection case with 20% EGR. The split ratio of 8:2 was found to have little benefit. The increase in late injection amount led to decrease of combustion efficiency from the late mixing. Hence a regulated portion was needed to create a good stratification to ignite a fast-burning flame kernel.

Another paper published the results of using experiment backed simulation to optimise a split injection strategy to a motorcycle engine under development. The test was performed at high speeds (5000RPM and 7500RPM) but at mixed loads of 13bar and 3 bar BMEP with different operating excess air ratio. The 1D to 3D CFD coupled simulation work revealed the inability of split injection to have a benefit at high speed high load operation due to the worsened condition of the combustion. But at the lower speed and loads, there was an optimisable range of improvement in recovering lean combustion losses [122]. The work performed here was entirely at 50:50 split which has limited the improvements from late injection due to the comparatively large weighting on the late injection compared to other studies. Costa *et al*. [123] revisited the use of 50:50 split injection at slower speeds (2000RPM) and presented the findings in 2016. The work highlighted lower emission from split injection cycles at higher loads (8bar BMEP). An experimental optical engine was used with 3D simulation. The results showed greater heat release at very limited ranges of late injection position and ignition advance that proves an optimisable benefit of the strategy at higher loads. But the most optimised late injection position was found to be just after IVC which is earlier than most other cases found. This is thought to be an effect limited by the larger late injection quantity that requires adequate mixing.

Successful SFI conditions to increase combustibility of diluted mixture is proven through experimental and simulation approaches at lower to mid loads. In all of these cases, the efficiency increase was due to the reduced use of throttling and burning a diluted mixture. A more in-depth look into the mechanism of the split injection combustion is published by Merola *et al* [124]. Digital imaging of the split injection combustions are analysed for lean combustion with 4 injection cases, of which 3 are split injections of different late injection positions. The data analysis of the combustion image taken on a bottom up optical piston shows the big influence split injection has on the flame propagation shape, tumble, and speed. Through this work, Merola *et al* concluded optimised split injection to have a faster

flame development and propagation at bulk combustion with greater repeatability, but with difficulty to achieve successful cases.

Several papers published findings of successful knock suppression on a stoichiometric high load operation using split injections. The main benefit being the continued use of TWC while allowing for better phasing of combustion. Yunlong *et al*. [125] reported a successful reduction of knocking intensity with split injection as the late injection ratio was increased, while the power output was affected negatively. The losses made by split late injection outweighed the loss due to ignition retarding that it should have eliminated. Costa *et al*. [126] also studied split injection under knocking conditions to analyse the mechanism of the behaviour with optical access. The experimental engine with an operating condition (1500RPM and 1.3bar inlet pressure) was run with semi-consistent knocking condition with single injection as well as split injection mode for comparison. Through visual combustion data obtained from the optical engine, the plotted knock onset location across 80 consecutive cycles as seen in Figure 2-13. An evident change in knock characteristic can be observed which the authors put down to changes in combustion distribution leading to lower wall temperature distribution through 3D CFD simulation. The paper concludes the effect of split injection to have a significant effect on the combustion with changes extending to wall temperatures, verifying the positive impact of split injection to lower knock tendency and cycle-to-cycle stability. A similar discovery that published split injection to lower occurrence rates of very high-intensity knock or ‘super-knock’ was published by Meng *et al*. [127] in 2016. The very brief paper concluded on similar remarks but without the presence of 3D CFD data. The paper found that the occurrence of ‘super knocks’ was eliminated with retarded late injection timings.

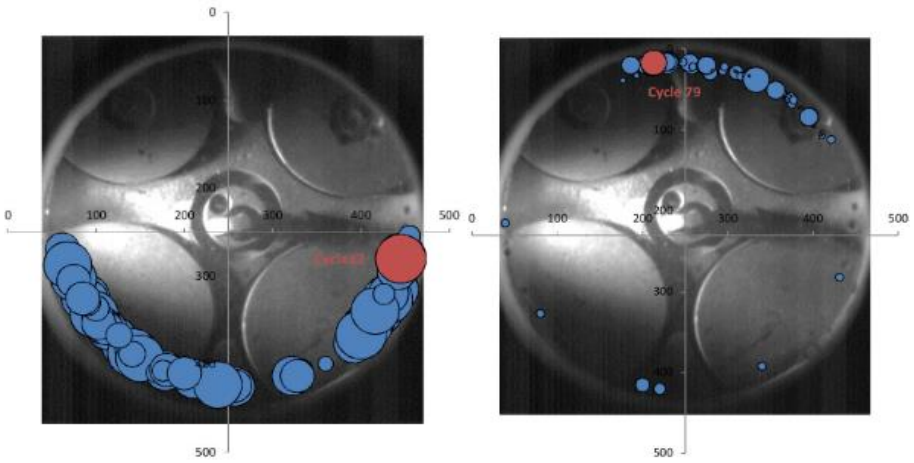

Figure 2-13 Spatial distribution of knock onset location. Left: single injection; Right: split injection. Original source: [126]

Finally, study into split injection with different fuels was found with an interesting conclusion. Pereira *et al*. [128] performed experiments with a range of fuels from gasoline blends to alcohols. The study focused on the spray development in a motored optical engine at varying engine conditions. The very thorough study with injection property comparison draws a conclusion on the sensitivity of injection properties and coolant temperatures with the following points: -

- Early injection timings can lead to impingement of fuel plume on the inlet valve that deflects up into the inlet side
- Higher load operation does not lead to longer injection plumes due to the increased intensity of bulk flow tumble motion that deflected these spray structures
- Splitting fuel injection events early in the intake stroke helped achieve earlier overall stoichiometry from improved fuel evaporation
- The effect of inlet condition and injection strategy also took place on the spark formation. The main reason was the change in flow field around and between the spark electrodes which at some conditions varied wildly between cycles
- Late injection closer to ST with spray guided systems can influence the local flow field to manipulate a cyclically stable flow during ST. It was also found that there is a preferred flame development direction for every combustion condition

A range of studies were reviewed with the use of split injection, most of which reported successful SFI effects from positive concentration control. However, a common occurrence noticed throughout these studies was the dominant portions of result that deteriorated the combustion conditions. Such cases are reported to be due to the use of late injection timings which under-prepares the droplets for combustion, alternatively, unfavourable mixture conditions were made by either an overly rich or lean mixture at the ignition site at the moment of ignition. Depending on the study, this is seen as an increase in smoke output, reduced fuel efficiency, or combustion stability. Additionally, some success reports also document prominent decrease in combustion efficiency or stability. This concludes the strategy to have very mixed reports, but some success cases can be expected once several conditions are fulfilled.

2.4.5 Particulates emission

Noted here is the review of particulates emissions related to use of EGR and split injection strategies on a SI-GDI engine.

A review of PN emission performed by Raza *et al*. [37] covers the topic of direct injection mixture preparation effects and types of particulates. The conclusion is broad due to the large topics covered, but the main points cover the favourability of fully atomised and

evaporated fuels for lower PN counts, particularly of accumulation mode particles which comprise of carbonaceous particles and smaller particles (<50nm) which are mainly known to be condensates of Volatile Organic Compounds (VOC) [129]. However, publications reporting the elemental structure of these particles suggest that nucleation mode particles also contain solid cores, though these take place on diesel engine emissions [130]. The review performed by Reza also comments on the impact of many engine strategies such as boosting, split injection and EGR, concluding that they all affect the PN count and that some can be a trade-off with other harmful emissions or efficiencies. One common conclusion was always the combustion of underprepared mixture, enrichment, improper burn, and impingement leads to the production of particles including a higher fraction of agglomerates.

The effect of ST on PN and PM depends on the combustion condition, where at non-knock limited loads, the MBT is known to produce the most particulates. Earlier ignition leads to longer combustion duration which offers longer time for particulate oxidation and retarding the ignition from MBT leads to hotter exhaust gas conditions which encourages more post-flame oxidation [37]. And so, for that reason, the advancement of ignition in knock limited conditions are reported with an increase in particulate emissions [131]. While there was no literature that focuses on the ST effects on GDI particulate emissions. A paper published in 2007 by Price *et al*. [132] found that earlier ignition created a much higher concentration of nucleation mode particles in combustion that took place with MAP=0.8 bar lambda=1. And Qin *et al*. [133] provided similar results but on a much lower load of 2bar BMEP at 2000RPM. Neither of these cases included knock limited loads.

For the impact of fuel equivalence ratio on particulate formation, as found by a few papers, fuel enriched combustion leads to an increase in particulate emissions. Experiments performed by Price *et al* varied the lambda from 0.8 to 1.2 at 1500RPM at inlet manifold pressure at 0.8bars. It was clear between all the fuels tested that the fuel enrichment of lambda=0.8 resulted in the highest emission of PM, especially for the accumulation mode particles. With unleaded gasoline, the nucleation mode particulates increased, and accumulation mode decreased under excess air conditions. The reason for this was not clearly noted, but it is understood that the excess air condition increased the combustion uncertainty that may have led to increase in VOC emissions, a trend that was not seen with ethanol-blended fuels. AFR effects on PN was also performed by He *et al*. [36]. The team used two conditions (1000RPM 3bar, 1500RPM 13bar with unleaded gasoline) with AFR between 14.5 and 13.4 where stoichiometric AFR =14.6. Again, enrichment led to increased accumulation mode PN and lower nucleation mode PN.

Boosting is suggested to increase PN emissions of smaller particles due to combustions with higher pressure conditions, but related studies have also reported a reduction of these PN numbers with increased exhausting temperatures due to extended post-combustion oxidation process with increased exhaust back pressures with increased boost demand [134–136]

With regards to EGR at high load operations, lowered particulate counts were reported with experimental tests [78]. And in particular, hotter inlet conditions with hot EGR dilution led to even better control of particulate formation, however at the expense of losing compressor efficiency and increased knock tendency [137]. The reason for the drop, in this case, was the increased mixing and evaporation performance from hotter conditions. In one paper [71], a very big drop in particulate emission was seen due to the reference high load condition combusting a rich mixture (for exhaust temperature control). The use of EGR lowered these exhaust temperatures which alleviated the need for the enrichment, reverting to stoichiometric mixture improved the combustion which drastically lowered the particulates.

A study performed by Longfei *et al*. [138] reported a strong link of residual gas fraction due to valve timing change to control particulate emissions. Greater RGF from decreased valve-overlap at high loads led to drops in particulate numbers. The authors confirmed with simulation results of the increased evaporation effects due to hotter in-cylinder conditions which led to greater evaporation.

Engine operating temperature as seen by coolant temperatures were also found to be sensitive towards particulate emission. Two studies are found on the topic and both reports great reduction in particulates. Longfei *et al*. [138] also reported a factor of increase of 2 to 6 by particulate mass when the coolant temperature was reduced from 90°C to 20°C using unleaded gasoline. Sun *et al*. [139] performed tests at idle condition with change in coolant temperature to find that hotter operating conditions create less PM and PN even at idling condition, again from warmer conditions that encourage mixing without condensation at the walls. The same study also tested common start-up strategies such as enrichment, and several injection position and pressure to conclude that enrichment and lower injection pressure increased particulate counts due to fuel-rich combustion and undermixing. As a part of the analysis of the results, it was found that the successful lowering of accumulation mode PN led to increasing of nucleation mode PN. This was hypothesised as the very small condensate droplets were left to suspend in the gas without merging with a larger carbonaceous particle due to the decreased concentration of these particulates.

Injection property was found to be another important property towards engine particulates emission. He *et al*. [36] performed tests on a single-cylinder engine to correlate injection to

particulates emission. Tests were carried out using E0 and E20 blended fuel on a wall guided engine with loads going up to 14.4bar Net_IMEP. Through comparison of E0 and E20 fuels, the authors reported a higher level of particulate with greater ethanol content, while the cause was due to impingement that occurred at higher loads (stressing that this was a wall guided engine). Ethanol has a higher heat of vaporisation than gasoline that led to this result. It was also noted that the lower calorific content of ethanol had resulted in longer injection durations that extended the injection plume length in the cylinder, creating an even worse condition for pool fires to occur. The analysis of the controlled tests with varying injection properties reveals the detrimental impact of fuel impingement of fuel on the walls with increased levels of particulates and lowered combustion efficiency. The fuel injection pressure was found to be higher but with a threshold where further increase led to no improvements in PN [36, 140].

Two experimental studies on split injection reports successful reduction of PN, however, the focus of the study was on optimisation for reduction of particulates emission. The use of early successive split injection improved the mixing while shortening the plume travel which reduced piston wetting. He *et al*. reported lowest levels of PN emission with split injection in comparison to two single injection cases performed at different timings, summarising with a 50% reduction of PN emission with split injection at high loads where improved mixing conditions were achieved [140, 141]. However, the timing of the split injection is still important for the impact towards PN emission as shown by some late injection results that result in impingement and unmixed burns. A study by Merola *et al*. [142] shows increasing levels of exhaust gas opacity as the split injection timings are retarded towards TDC.

2.5 Summary

2.5.1 Summary of literature review

A comprehensive literature review is performed in this chapter to provide basic knowledge and landscape to the research topics to be studied in this project.

The automotive market is analysed first to highlight the continuous demand for clean and efficient gasoline engines to further reduce environmental pollution from GHG and harmful gas. To meet the stringent restrictions on the limits of emission to better address the health and environmental issues, new combustion strategies are therefore required to comply with these needs.

The fundamentals of the four-stroke gasoline SI combustion engines were then discussed to provide basic knowledge in terms of the thermodynamic cycle, SI engine operations, efficiencies, and emissions.

In particular, the downsized GTDI engine was reviewed to understand its potential for efficiency improvement. On the other hand, the related irregular combustion of downsized SI engine, including the knocking combustion, miss fire and partial burn, are also discussed.

Through the review, an environmental crisis caused by fossil fuel is identified. Transport emissions of GHG and harmful gases are found to cause devastating consequences. The need for logistics and transportation is also reviewed, and the need for continued reliance on IC engines to cater for this demand is very clear. Current IC engines are found to operate with inefficiencies and harmful emissions. However, much potential to reduce emissions and fuel consumption through further technological advancements are identified.

Based on new emission test protocols, the downsized GTDI engines with the current strategies maybe emitting offending levels of tailpipe NO_x. It is also understood that the strategies which are employed to mitigate knocking combustion have a negative impact on efficiencies at boosted high load operations. Strategies that can alleviate these issues were considered by reviewing their literature. These are: -

- EGR to lower knock tendency through thermal and chemical effects.
- Valve-overlap optimisation for reduced short-circuit air, to lower tailpipe NO_x and improve combustion efficiency.
- Uprated ignition system and split injection to recover ignition instability losses and improve combustion speeds.

The learnings of the literature review have been used as the tools to plan, execute and understand the results of experimental tests performed.

2.5.2 The identified novelty of the project

As summarised in the literature review, each or small sub-combinations of these strategies were proven to be effective in improving the engine's emissions or efficiency, but the combined effect of these strategies on the engine fuel consumption and emissions are not clear. Additionally, the review has also identified the scarcity of study focusing on the use of reduced-valve-overlap at high-load operations due to the evident onset of knock. Therefore, a thorough exploration of valve-phasing at high load with EGR dilution and ignition improvement methods yields valuable information to potentially improve the boosted high-load operation of a downsized GTDI engine. Most importantly, this project aims to explore and perform a comprehensive study of the combined synergy among these strategies to further improve the GTDI engine efficiency and reduce their emissions.

Chapter 3 Methodology

3.1 Introduction

All experiments were performed on a Ford EcoBoost 1l engine installed on a testbed. The running parameters of the engine with split injection and EGR strategies could then be compared with reference conditions to evaluate the effectiveness of the strategy. This section details the experimental setup, control methodology, data processing for the analysis, and CFD simulation setup of a downsized GTDI engine.

The measurement and accuracy requirements were identified and implemented to the test rig based on the literature review and planned tests. These are in-cylinder pressure, brake power, inlet and exhaust conditions including the important gas compositions, fuel consumption, and engine operation condition monitoring including controls. The measurements were further verified and tested to omit possibilities of errors and measurement bias. This section notes the setup in detail for all measurements systems and CFD models used, including calibration and validation.

3.2 Overview of the experimental setup

A Ford EcoBoost 1l engine was modified with an external EGR system and instrumentation for data collection. Figure 3-1 shows the block diagram of the experimental setup. On the diagram, the passing elements and interconnections are divided into colours. Yellow elements represent electrical power. The orange colour is used to represent the data movement, for example, signal handling blocks and connections. Green blocks and lines represent the connection and user inputs of cooling water control and interconnections. Red lines represent the connection of exhaust gas sample from the engine to the three gas analysers.

The user interface for the experiments includes six devices, consisting of three computers, two gate valves for controlling cooling water flow, and a key-operated power relay. This is where the test conductor controls all the engine running parameters and dynamometer speed, as well as monitoring and recording test data. Critical condition monitoring and safety controls are also made through the interface. The two water valves are manually operated by the lab user during the test to control the inlet air and EGR gas temperatures. Besides, a third water valve is present inside the test cell, which is controlled automatically to regulate the engines coolant return. More details of the coolant water system can be found later in the chapter. The engine power supply, as well as the starter motor, is controlled by a key-operated switch.

The three computers have been used for engine control and data acquisition and monitoring. The ‘dyno PC’ communicates with the dyno controller and is used to control the dynamometer parameters, such as speed, and monitor dynamometer conditions. The ‘Yantec PC’ is used for engine data acquisition by running in-cylinder pressure analysis software (‘Yantec’), Horiba Gas analyser and a DMC500 fast particle analyser. The final computer, ‘Vision5.1 + Datalogger PC’ runs the two most critical software for engine operation and data recording. Vision 5.1 software communicates directly with the PROtroniC programmable ECU via a CANbus Kvaser adapter and allows the user to control all major engine variables on the fly. The data logger software that runs in parallel is built based on LabView and receives data from the data acquisition (DAQ) systems and Vision5.1 (ECU UI) to process the data and record them for later analysis.

The test cell is a closed room where electricals, waters, ambient air, and fuels enter and leave in a controlled manner, ensuring safety and workable environment for the test conductor that remotely controls from a safe area during the engine tests. Inside of the cell is the devices that must be in proximity of the engine and dynamometer. These are typically made to withstand the warmer environments of the test cell. The blocks for the engine, starter motor, inlet system, EGR system and ECU are separated in the chart but should be considered as a singular device but with separate external influences. The DAQ systems are placed in proximity for reduction of cabling to reduce the electronic noise influences and ease of cable management. These devices are connected to the data recording PCs by a shielded high-speed USB cable.

Each of the systems is explained in more detail in later sections of this chapter, starting with the engine setup and ECU control methods, moving on to data logger and instrumentation devices, then auxiliary devices such as the emissions analysers. The data processing methods will be detailed in each of the instrumentation sections.

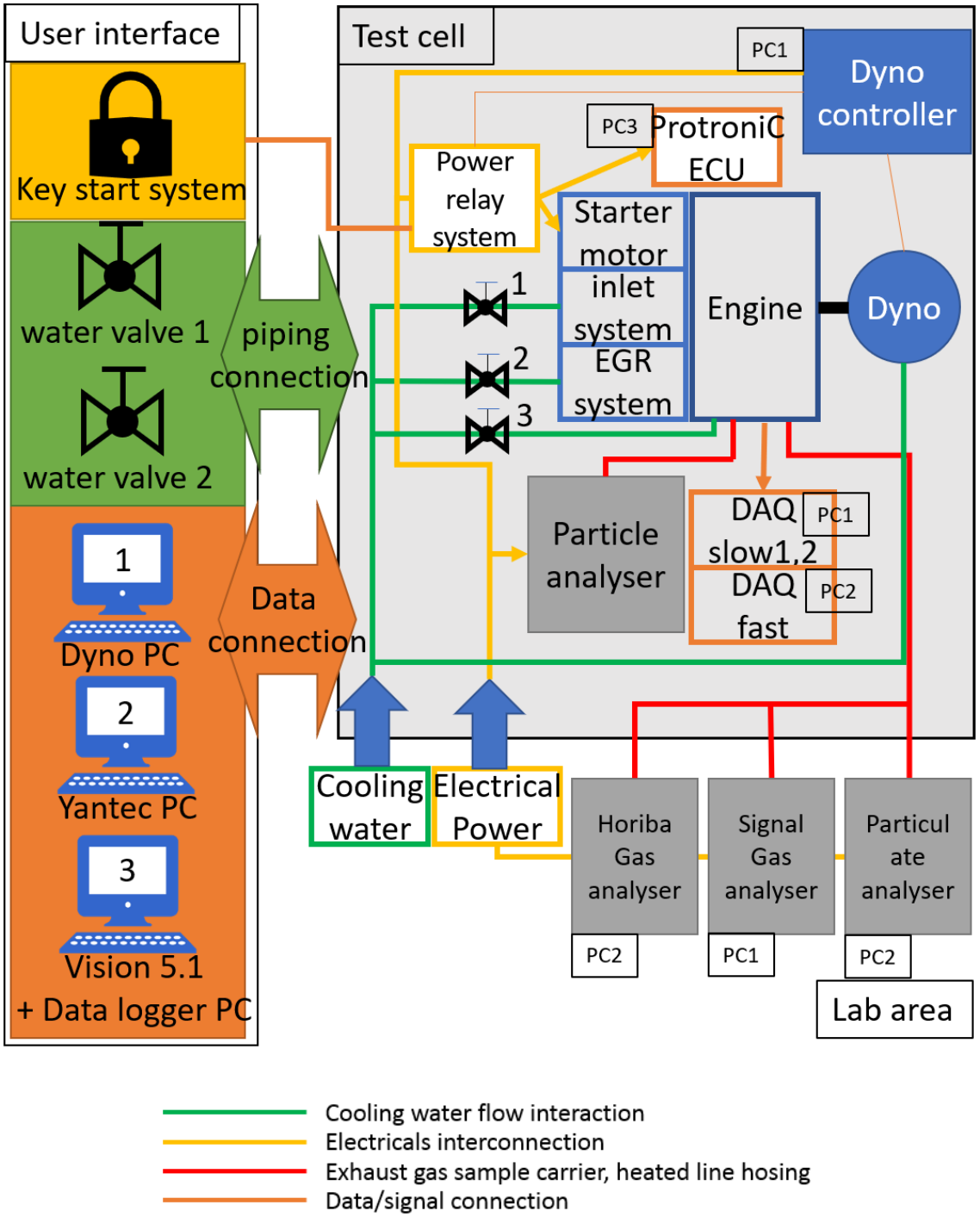

Figure 3-1 Block diagram of the user interface and major components of the test rig.

3.2.1 Engine specifications

Table 3-1 outlines the details of the downsized Ford EcoBoost 1l engine used for the experimental studies. It is a commercially successful downsized GTDI engine which has been in production since 2012. Notable features of the 3-cylinder downsized engine boast a high-efficiency operation in a small package to deliver the power requirements of even D segment cars.

Table 3-1 properties of the Ford 1.0L EcoBoost Fox Engine

Cylinder formation	Inline 3
Displacement volume (per cylinder), cc	333
Bore, mm	71.9
Stroke, mm	82.0
Connection rod length, mm	137
Compression ratio	10
Number of valves per cylinder	4
Valve gear	DOHC twin independent variable cam
Valve control	Inlet VVT / exhaust VVT
Intake valve opening duration	228CAD
Exhaust valve opening duration	228CAD
Injection system	direct injection, 6-hole injector, up to 150 bar injection pressure
Emission control and level	Euro 5, TWC with pre and post UEGO sensor
Turbocharger	Continental low inertia
Lubrication system	Variable displacement oil pump
Cooling	Split flow cooling system, two thermostats

The programmable ECU was flashed with an engine control program which determined the operating strategy of the engine. All default control strategies found in basic ECUs such as cold start and idling strategies were also loaded but deactivated during the tests to ensure no further influences altered the operation of the engine. All control parameters come with a manual toggle and value set for customisable engine operation parameters.

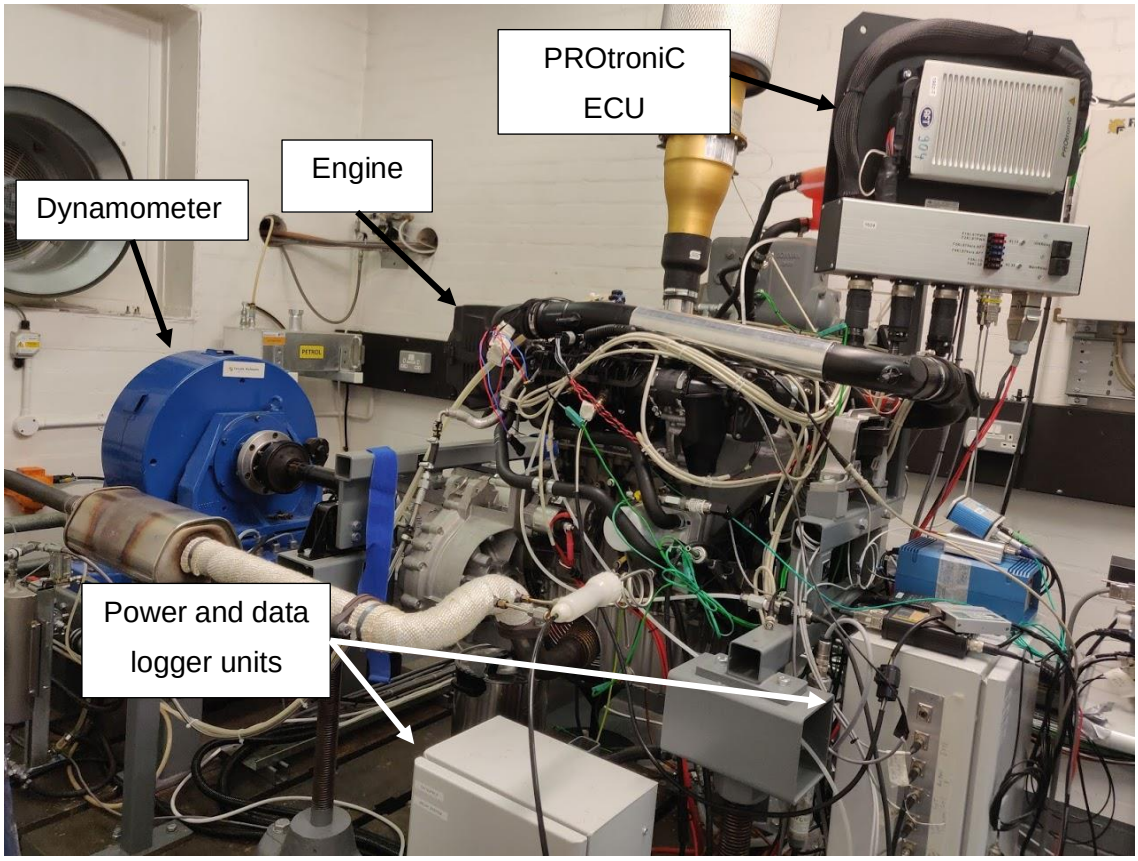

Figure 3-2 Experimental engine with full instrumentation, the key elements are annotated

3.2.2 Gas path: inlet, exhaust and EGR system

The schematic of the gas flow is as visualised in Figure 3-3. The inlet and exhaust piping, including the standard filter air box, were configured to replicate a car setup to achieve real flow restriction and thus the same dynamic pressure conditions. Modifications were made to the standard inlet and exhaust system to accommodate a customised cooled EGR system. An additional inlet flow restrictor and EGR mixer valve were added to intake pipe before the compressor system, and the exhaust gas for recirculation is collected after the TWC by welding a tube to the TWC unit as seen in Figure 3-3. The exhaust gas recirculation system contains an EGR cooler which is a gas to water heat exchanger with a dedicated coolant loop to regulate the coolant temperature as well as the EGR temperature. The dedicated loop was installed to reduce thermal stress to the EGR cooler by allowing for a high flowrate of temperature-regulated coolant as opposed to the regulating flow of cold coolant.

The two valves that control the EGR flow rate are controlled by the user through Vision 5.1 software where the ECU provides a PWM signal which corresponds to the valve opening fraction. The EGR dilution rate is measured by the Horiba gas analyser where the user has full manual control of the EGR valve opening for dilution rate control. The additional inlet flow restrictor here will remain fully open by default unless required.

The impact of the droplet condensation on the compressor fins were prevented by the implementation of several measures;1) Stainless steel pipework that carries the EGR was thermally insulated to prevent condensation forming on the walls 2) cooled EGR temperatures below 60 ºC were prohibited from testing. The user controls the EGR temperature using a water gate valve for cooling and a heater switch. The latter is used to increase the temperature, which is only to be used in warm-up situations.

The full working gas system with the EGR system is shown in the schematic diagram Figure 3-3.

It is also important to note that the EGR loop was not optimised for transient operation, hence the response time for EGR dilution rate was not ideal. Therefore, conclusions regarding the response time of external EGR dilution effect was omitted.

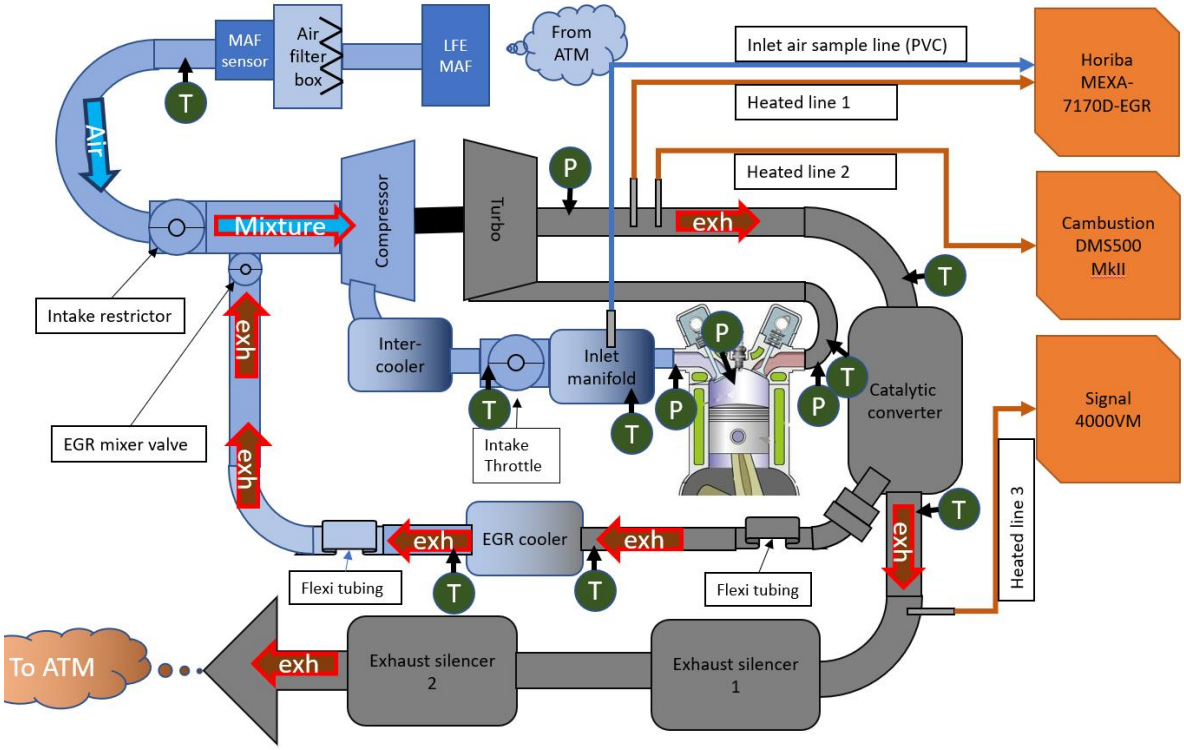

Figure 3-3 Working gas path schematic of the engine with gas analyser units/pressure transducer points/ thermocouple points

3.2.3 Variable valve timing

A standard VVT system is used in the Ford 1.0L GTDI engine along with the standard camshaft and valve setup. The valve lift profile and timing change are as detailed in the graph of Figure 3-4. The fitted system is a dual overhead camshaft valve train, and the timing sprocket is mounted to both camshafts with actuated shift phasor in between. The lift profile is the same for both inlet and exhaust valves, the opening duration is 228CAD, and the maximum lift is 8.26mm with a symmetrical profile. At phase shift position of 0CAD, the

valve-overlap is at -5CAD in the inlet stroke. As the phase is shifted the valve-overlap is increased, and both the inlet and exhaust phasors would progress into a wider overlap, such that the exhaust valve profile is delayed, and inlet valve profile is advanced.

Each camshaft has a position sensor that feedbacks relative phasor position to the ECU for the validation of the camshaft phase position and its consistency during the tests.

The ECU takes the phasor position '0' as the minimum angle reached during the operation. Once the ECU loses power, the '0' position needs to be reset. Thus, during the tests, the engine was started with a valve phasor position of '0' to calibrate the phasor position on start-up.

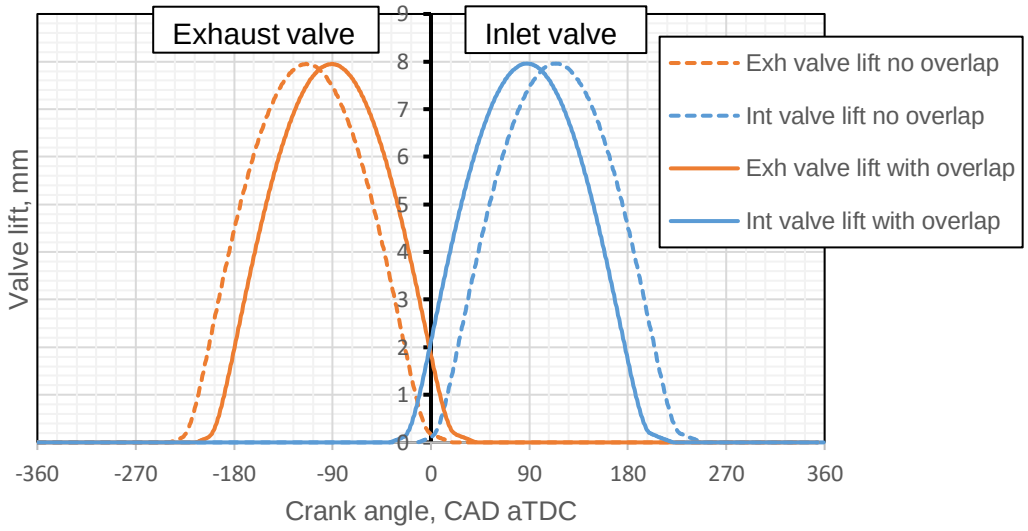

Figure 3-4 Valve lift profile at two settings. *Solid line*: with total 53CAD of valve overlap *Dotted line*: no valve overlap setting

3.2.4 Fuel delivery system

The fuel line schematic is as seen in diagram Figure 3-5 with a DI HP fuel injector system. The fuel is measured by an Endress+Hauser Coriolis type mass flow meter (shown in Figure 3-6, model: Promass 83A02, DN2 1/12") before entering the engine assembly. The fuel injection pressure sensor is installed on the fuel rail to be read by the ECU. The HP side of the fuel system does not have a feedback loop system; thus, the single mass flow sensor can accurately meter the engine fuel consumption.

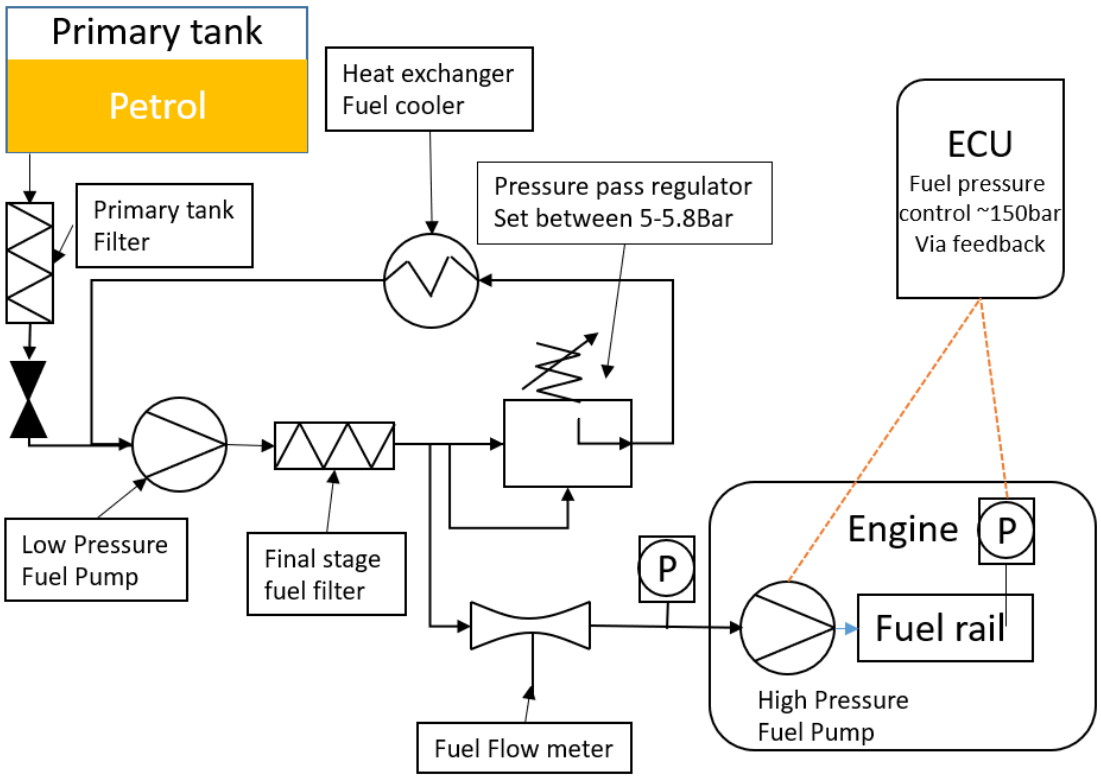

Figure 3-5 Schematic diagram of the fuelling system

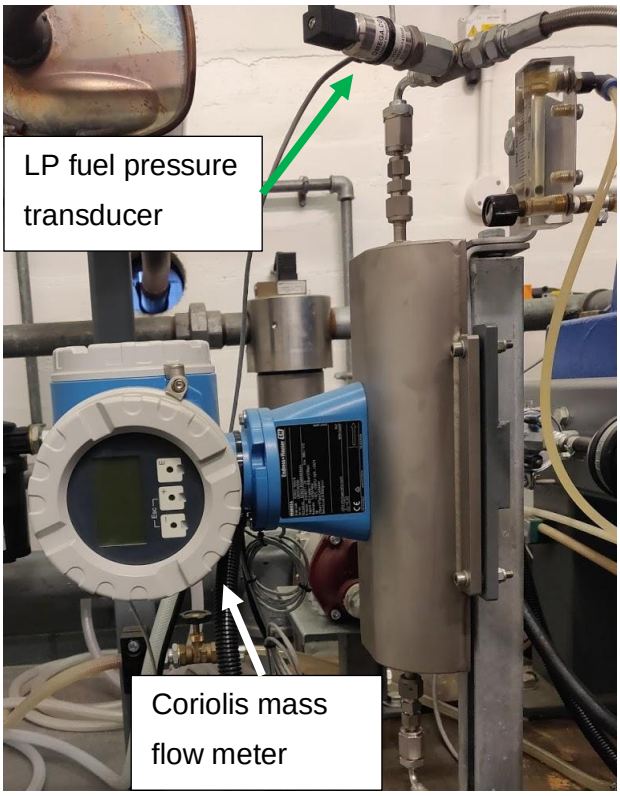

Figure 3-6 Coriolis mass flow meter with an LP fuel feed pressure transducer

The measurable range and the maximum measurement error of the Coriolis mass flow meter are dependent on the tube thickness of the measuring element. For this test, a 1/12” pipe was chosen, which yields the measurement error characteristic as seen in Figure 3-7. The

measurable range starts around 1kg/hr to an undefined limit where the tube thickness starts to act as a flow restriction.

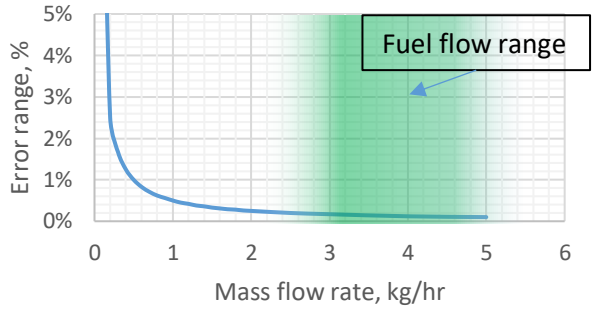

Figure 3-7 Mass flow meter, maximum measurement error based on gasoline flow measurement, overlaid with expected fuel flow range during tests

Two fuels are used during this project: 1) pump grade unleaded gasoline fuel and 2) experiment grade gasoline fuel. Initial engine tests were performed using pump grade unleaded fuel, where comparisons were made using a single batch of pump grade fuel to ensure the fuel grade did not differ. Experiment grade fuel was used for longer test campaigns where tight control of fuel blend and property is required. The fuel properties are as seen in Table 3-2. Data for UK pump fuel was referred from the EN225 E5 fuel specification for the UK market. The calorific value of both fuels was measured via bomb calorimeter compliant with IP12 with hydrogen content measured via ASTM D5291 compliant method. Full analysis values of E10 fuel is found in appendix section 1.

Table 3-2 Specification of the fuel used in this study

	Experiment grade E10	**Pump grade E5** [143]
Research octane number	95	Min 95
Motor Octane number	85.8	-
Ethanol Content, %vol	9.8	Up to 5
Density, kg/l	0.7461	-
Calorific value (net), KJ/kg	41420	42380
Stoichiometric	13.92	-
H/C Ratio	1.889	-
O/C Ratio	0.033	-

3.2.5 Cooling system

The schematic of the cooling system is as seen in Figure 3-1, a single inlet of cooling water feed is branched into three separate cooling systems, each with their control methods to maintain the experimental rig.

A more detailed schematic of the cooling system for the engine and EGR can be found in Figure 3-8. For the inlet air, the post compressor mixture of air and EGR is cooled down

using an air to water heat exchanger system. The building-supplied cooling water is passed through the heat exchangers. The user regulates the water flow through the heat exchanger to control the inlet air temperature.

The extracted hot EGR was cooled by before being introduced to the inlet air. This was performed using an EGR gas-to-coolant heat exchanger. Due to the temperature differences within the unit, a high flowrate of warm coolant was required during the operation of the engine with EGR. To accommodate this requirement, a system as seen in Figure 3-8, was constructed. The coolant was actively fed through the system using an electric coolant pump powered by a separate 12V Power Supply Unit (PSU), the temperature of EGR at the introduction point in the intake pipe was monitored by the user, and the coolant temperature was regulated using either cooling water or heater (in case of warm-up). Thus, an EGR coolant-to-water heat exchanger (as seen in Figure 3-9) was placed in the EGR coolant loop. During normal operation with EGR dilution, the user controls the flow of cooling water using a ball valve which regulates the cooling water flow rate through the water to water heat exchanger. This cools down the coolant used to lower the temperature of the EGR whilst maintaining a high flow rate of coolant.

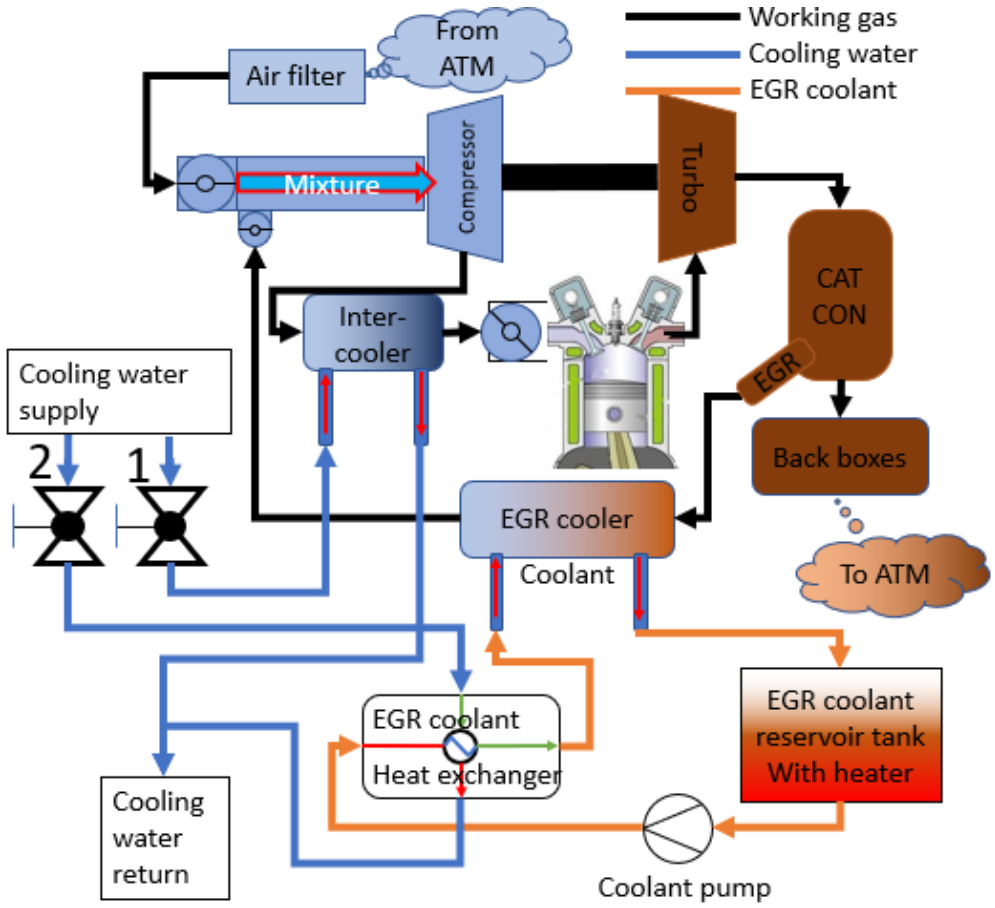

Figure 3-8 Temperature control system schematic for the engine inlet air and EGR system

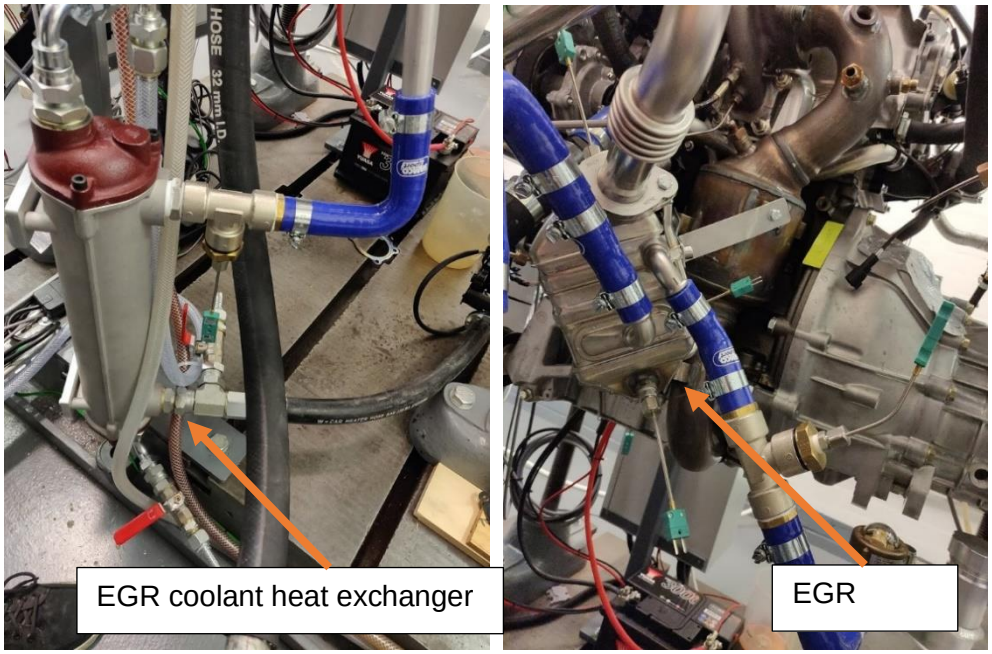

Figure 3-9 Installed EGR coolant heat exchanger and EGR cooler in engine setup

A schematic diagram of the full engine cooling water pathway is, as seen in Figure 3-10.

The coolant used in all loops for the engine cooling is a virgin monoethylene glycol with OAT corrosion inhibitor diluted with water in 50/50 mixture, as per requirement by Ford motor company engineering material specifications [144].

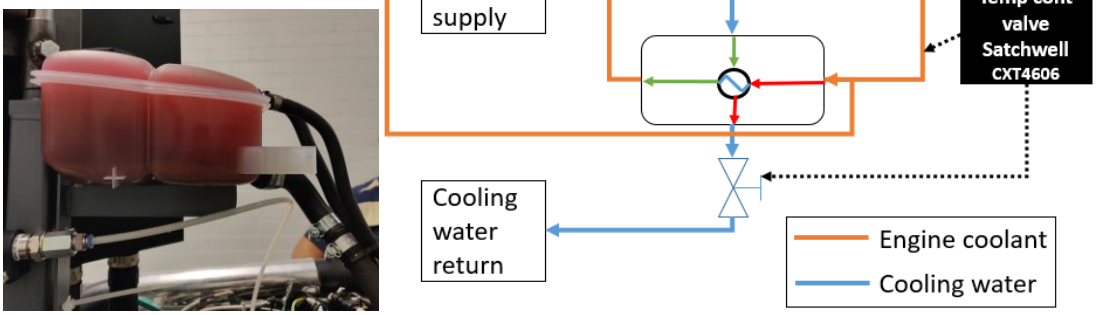

Figure 3-10 coolant and cooling water pathway for engine cooling with the degas system

3.2.6 Dynamometer

The engine and dynamometer were operated at a fixed speed. This was performed by a Froude Hoffman AG150 eddy current dynamometer (shown in Figure 3-11) coupled directly to the engine's crankshaft through a coupling shaft and damper. A Froude Hofmann Texcel V12 system was used to control the dynamometer manually throughout the test.

Figure 3-11 Froude Hoffman AG150 Eddy current dynamometer

3.3 Instrumentation, data logging, and post-processing analysis

Instrumentations were installed to the experiment engine for engine condition monitoring and data logging for subsequent data analysis. The list excludes instrumentation not directly related to the engine such as the manometer for atmospheric pressure reading and dynamometer bearing temperatures sensor for dyno condition monitoring.

The data logging system can be divided into sections depending on the function. **Sensors or analysers** interface the measured medium to the data logger network. The condition of the desired property is converted into electrical signals. **Data acquisition (DAQ)** is a device that converts the signal from the sensors to computer data, ready to be processed digitally, the quality and speed and which the DAQ converts the analogue signal is defined by the sampling frequency and resolution in bits. The **PC** is connected to the DAQ via a data link such as a USB/Ethernet port, and software is used to process and display/save the data according to the set instructions.

Table 3-3 shows the list of DAQs used, one ECU and three National Instruments (NI) DAQs, were used to measure the data. Furthermore, four software was used to collect data simultaneously.

Table 3-3 list of data acquisition devices installed for data logging

ID	Model	Device properties
ECU	PROtroniC	Pre-configured by ford
Fast DAQ	NI USB-6353	32 AI (16-Bit, 1.25 MS/s)
Slow DAQ CH1	NI USB-6211	16 AI (16-Bit, 250 kS/s)
Slow DAQ CH2	NI USB-6218	Isolated 32AI (16-Bit,250 kS/s)

Figure 3-12 is a diagram that shows the relation of DAQ system to PC interconnection with the software that operates the data processing and logging, furthermore the emissions analysers connections are indicated. All sensors are logged via a software interfaced by a DAQ, but 2 exceptions exist: -

1. Particulate analyser data is transferred directly to the laptop via a dedicated data link, a provided software is used to process, display, and save the data due to the complexity of the data sets.
2. The measured emission data from Horiba MEXA is transferred directly to Yantec software on PC2 where it is displayed and logged.

The emissions data measured by the Signal 4000VM is recorded via the normal approach, where the analyser outputs an analogue voltage signal that is read by the PC in LabView interfaced via the DAQ.

The engine health monitoring and data collection environment were generated in a LabView software environment. Data is collected from the DAQ slow CH 1+2 and Vision5.1. The Vision5.1 is an ECU calibration software with a highly customisable environment, the software interfaces with the ECU and any changes to the engine control are made through this software UI, but data was not recorded using the software, rather a MATLAB code in LabVIEW was used to extract data from Vision 5.1 using the ‘Vision API’, which is a software-to-software communication protocol.

During the tests, static point measurements were taken once desired experimental conditions were reached. The Yantec software and LabView were manually triggered by the lab user to record 30 seconds of slow CH/ECU data and 300 cycles of Fast CH data which includes the in-cylinder pressure data. The sampling frequency for the slow CH is 50Hz, while the software refreshes the averaged results at 2Hz, which is also the recording

frequency during the tests. Full list of instrumentation (sensors/analysers) the DAQ interconnectivity and software used are found in the instrumentation list, appendix section 2.

For every test point, three files were created and then collated through post-processing to create a full data set for comparison and analysis.

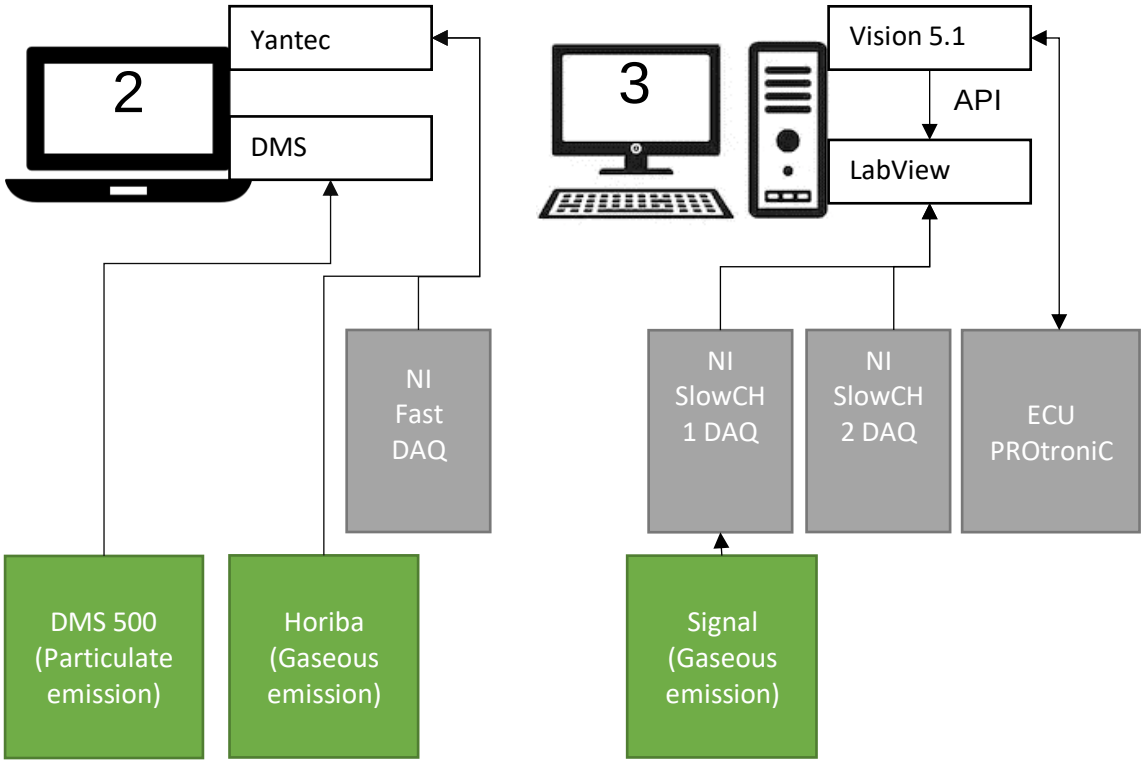

Figure 3-12 Data collection hardware configuration, two of the gas analysers bypass the DAQ as they have direct data link with the recording programs, green blocks=gas analysers, grey blocks=DAQ systems

3.3.1 Transient combustion analyser

An in-house transient combustion analyser “Yantec software” is used to measure and analyse the in-cylinder data during the tests.

Combustion analysis is performed based on the in-cylinder pressure signals against the crank angle encoder signal. As the piezoelectric transducers used to measure the in-cylinder pressure measures the short-term variation in pressure with a constant discharge rate, the measured value is always offset and tends towards zero over time. Therefore, the measured in-cylinder pressure needs to be readjusted based on the reference pressure for every cycle, which is called pegging. For this test, an absolute inlet pressure sensor was fitted close to the intake ports of the measured cylinder. The transient combustion analyser was then set-up to ‘peg’ the absolute pressure value at the inlet port as the in-cylinder pressure at crank angle position of BDC_{intake}. Subsequent pressure signal for in-cylinder pressure then represents the accurate values until the next cycle begins with a new pegged value.

3.3.2 Calculation of engine parameters

Combined with the basic engine specification is as shown in Table 3-1, the Yantec software calculates the common engine operational Mean Effective Pressures (MEP), Specific Fuel Consumptions (SFC), and Power figures according to methods detailed in [19].

The ECR of the engine during operation varies due to changes in boosting and valve timing. The ECR was calculated as seen in Equation 3-1.

$$ECR = \frac{V_{IVC,\ effective}}{V_{clearance}} \qquad \textbf{Equation 3-1}$$

Where the $V_{IVC,\ effective}$ is the cylinder volume when the effective IVC takes place, which is defined as the volume within the cylinder when the MAP equals in-cylinder pressure during the compression stroke.

The stability of combustion was calculated from the deviation factor of the Net IMEP value from the average among 300 consecutive cycles. The equation for the term of Coefficient of Variation (CoV) for Net IMEP was calculated using Equation 3-2.

$$CoV_{IMEP}(\%) = \frac{IMEP_{std}}{IMEP_{avg}} \times 100\% \qquad \textbf{Equation 3-2}$$

Where $IMEP_{std}$ is the standard deviation value and $IMEP_{avg}$ is the mean average value of 300 consecutive cycles of Net_IMEP value.

The addition of heat to a confined volume causes a defined rise in pressure. By considering an open system where no mass exchange takes place, the total chemical energy in the system, δQ_{ch} is transferred to four avenues with consideration to the first law of thermodynamics as adapted from [19] as seen in Equation 3-3.

$$\delta Q_{ch} = dU_s + \delta W + \delta Q_{ht} + \sum h_i dm_i \qquad \textbf{Equation 3-3}$$

Where dU_s is the actual sensible heat energy that is added to the equation due to required change in energy composition, δW is the work transferred by the piston, δQ_{ht} is the heat transfer to the walls of the cylinder, and the term $h_i dm_i$ represents the mass flux travel that is considered as energy loss due to crevice volume flame quenching during combustion. The crevice volume is mainly illustrated as the space between piston skirting within the cylinder in Heywood [19], and the mass flux is dynamic and highly dependent on the combustion characteristics.

The derivations of the equations for heat release calculation from PV values have been documented extensively on traditional publication [19, 26]. The equation used to calculate the heat release is as seen in Equation 3-4.

$$\frac{dQ_n}{d\theta} = \frac{\gamma}{\gamma - 1} P \frac{dV}{d\theta} + \frac{\gamma}{\gamma - 1} V \frac{dP}{d\theta}$$ **Equation 3-4**

The derivation is made possible through several generalizations, which are:

- Considers a single temperature zone with the use of ideal gas law
- The term δQ_{ch} that represents the total chemical energy within the system, is simplified to dQ_n, which considers only the heat addition that results to pressure rise. This incorporates the inefficiency of heat releases such as crevice loss, heat transfer and composition change
- The equation is considered in crank angle basis for considering the pressure comparison. The instantaneous volume, V within the cylinder is calculated by the cylinder geometry as seen in Equation 3-5, the change in volume, dV and pressure difference against calculated volume change, $d\theta$ returns the instantaneous heat input, dQ_n responsible for the pressure rise dp

$$V = V_{clearance} \frac{1}{2}(CR + 1)\left\{\frac{2L}{S} + 1 - cos\theta - \left[\left(\frac{2L}{S}\right)^2 - sin^2\theta\right]^{\frac{1}{2}}\right\}$$ **Equation 3-5**

Where CR is the compression ratio, L is the length between the two pivot centres of a connecting rod, and S is the pistons stroke length.

The crank angle resolution $d\theta$ is determined as the resolution of the installed crank encoder of 1/2 CAD. Furthermore, the calculated heat release was used for comparison purpose between the cases tested within this project, rendering the absolute heat release value to be less important. Hence the γ will remain a constant of 1.33 throughout the analysis.

Subsequently, the results array of HRR, $dQ_n/d\theta$ will be further processed by accumulating the values, the start of combustion is defined as the final crank angle location with minimum HRR and end of combustion as the first dip of HRR to pre-combustion levels. The accumulated heat release, $\sum Q_n$will also be normalized to MFB=100% for further definition of the crank angle location of MFB of 10%, 50% and 90% from the normalized MFB curve, the combustion duration will be further defined as the crank angle duration between MFB of 10% and 90%.

3.3.3 Exhaust emission measurements

A total of three exhaust gas analysis devices were used through the testing period.

The concentration of common exhaust gas species was measured for the gas samples extracted between the TC and the catalytic converter.

3.3.3.1 The gas analysers

The Horiba MEXA7170D-EGR measures several gaseous emission concentrations through a series of measuring devices. The details of the units are listed in Table 3-4.

Table 3-4 List of measurement devices housed in the Horiba MEXA7170D-EGR

Unit	Measured	Measured range	Errors
AIA-722	CO	0-12 vol%	
AIA-722	CO_2	0-20 vol%	± 2.0% of the calibration point
CLA-720MA	NO_x	0-10k ppm	
MPA-720	O_2	0-25 vol%	
FIA-725A	THC	0-50k ppm	

The concentration of CO and CO_2 in the sample gas was measured by a non-dispersive infrared (NDIR) detection method where the Infra-Red (IR) emitted by a lamp passes through a sample, and the absorption rate of the specific wavelength band corresponds to the concentration of different gas species.

Measurement of O_2 concentration was performed through a magnetic pressure type O_2 analyser. Such a system applies a magnetic field to the gas cell, where the O_2 contained in the gas sample experiences a force according to the magnetic field, making use of the paramagnetism of O_2 atoms. The force is measured to find the O_2 concentration within the sample gas.

For THC, the concentration was measured through a flame ionization method. This method first burns the sample gas in a hydrogen pilot flame which emits an ion current that is measured to represent the THC contents.

NO_x concentration was measured via chemiluminescent analysis (CLA). This measures the chemiluminescent emissions of the process ($NO+O_3 \rightarrow NO_2^*$, $NO_2^* \rightarrow NO_2$-hv and O_2). For measurements of NO_x (which includes NO and NO_2), the gas sample is processed for the NO_2 to react with C by ($NO_2+C \rightarrow NO+CO$), which then partakes in the CLA measurement. The Signal 4000VM NO_x analyser used for the tailpipe NO_x measurements also employs the same method of measurement. This analyser was used for the final test where valve-overlap was varied. The basic specifications of measurements are as seen in Table 3-5.

Table 3-5 Measurement features of the Signal 4000VM

Unit	Measured	Measured range	Accuracy
Signal 4000VM	NO_x (tailpipe)	0-10000ppm	±1 % range or ±0.2 ppm

Figure 3-13 Horiba MEXA7170D-EGR and Signal group gas analyser unit

The Cambustion DMS500 was connected to the same sample gas extraction point as the Horiba 7170D-EGR but with a separate heated line. The heated line is a specially made unit with a sample gas dilution point at the extraction point. Hence there is always a flow of either diluted sample or zero gas travelling down the heated line during the operation of the unit.

The presence of particles was detected via an array of electrometer detectors pictured in Figure 3-15. The charged particles were transported by a sheathed flow where larger particles carry charge to further detector rings. Hence the carried charge at each corresponding electrometer detector ring indicates the count and size of particle included in the sample gas. The sample gas was diluted in 2 stages prior to reaching the detector, where the dilution rate was determined during the tests to ensure sample gas-particle concentration to be within the measurable range of detectors. The DMS500 MkII unit is as pictured in Figure 3-14, and the main features are detailed in Table 3-6.

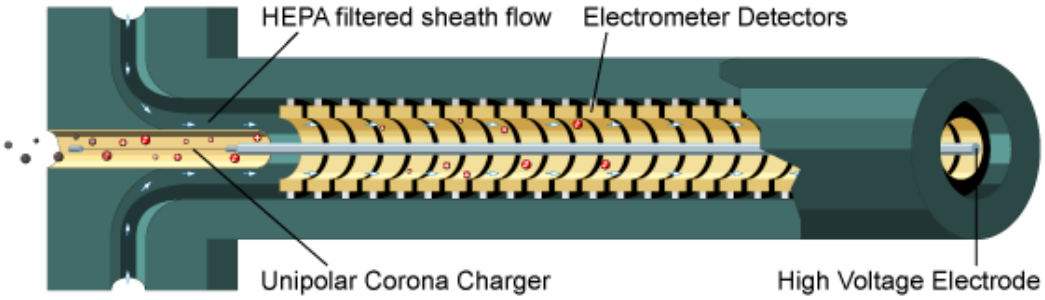

Figure 3-14 the detection principle of particles in sample gas using the DMS500 mkII. Original source: [145]

Figure 3-15 Cambustion DMS500 MkII fast particle analyser

Table 3-6 Main features of a Cambustion DMS500 MkII

Feature	value
Sampling frequency	Up to 10Hz
Repeatability	±1%
Linearity	±1%
Sensitivity	1.0 × 103(dN/dlogDp /cc)
Particulate size range	5 nm – 1 μm
Concentration range	0-10000ppm

3.3.3.2 Pre-TWC emissions and tailpipe NO_x post-processing

The gas volume concentration data recorded by the Horiba MEXA7170D-EGR were converted to indicated specific emissions in the post-processing. Additionally, the tailpipe NO_x emission concentration was measured using the Signal 4000VM gas analyser. The

processing of emissions data was performed in accordance with UN/ECE regulation where dry based concentration measurements are converted to a wet base to account for the water content of ambient air and fuel [146]. The indicated specific emission for CO, NO_x and THC are calculated using equations Equation 3-6 to Equation 3-8.

$$ISCO = \frac{u_{co}[CO]k_w\dot{m}_{exh}}{P_i} \quad \textbf{Equation 3-6}$$

$$ISNO_X = \frac{u_{NO_X}[NO_X]k_w\dot{m}_{exh}}{P_i} \quad \textbf{Equation 3-7}$$

$$ISTHC = \frac{u_{THC}[THC]\dot{m}_{exh}}{P_i} \quad \textbf{Equation 3-8}$$

Where u_{co}, u_{NOx}, u_{THC} are the respective molar mass fractions of each gas, the input value of emission are in units of ppm, k_w is the dry to wet correlation factor as detailed in [146], and P_i is the indicated power of the engine. $\dot{m}_{exhaust}$ is the total mass flow rate of exhaust gas calculated by Equation 3-9, and $\dot{m}_{humid\ air}$ is defined as the combination of dry air and humidity as noted in Equation 3-10.

$$\dot{m}_{exhaust} = \dot{m}_{humid\ air} + \dot{m}_{fuel} \quad \textbf{Equation 3-9}$$

$$\dot{m}_{humid\ air} = \dot{m}_{dry\ air} + \dot{m}_{humidity} \quad \textbf{Equation 3-10}$$

The following set of equations were used to quantify the $\dot{m}_{dry\ air}$ and $\dot{m}_{humidity}$. The estimation of water flowrate is based on the properties of ambient air that is calculated by the saturation pressure (SP) that is estimated by a polynomial best fit suggested by [147].

$$\begin{aligned} SP = {} & 604.8346 + 45.9058(T_a - 273.15) \\ & + 1.2444(T_a - 273.15)^2 \\ & + 0.03522481(T_a - 273.15)^3 \\ & + 0.00009322061(T_a - 273.15)^4 \\ & + 0.000004181281(T_a - 273.15)^5 \end{aligned} \quad \textbf{Equation 3-11}$$

$$H_a = \frac{6.211\ RH\ SP}{p_a - \frac{(RH\ SP)}{100}} \quad \textbf{Equation 3-12}$$

$$\dot{m}_{dry\ air} = \frac{\dot{m}_{humid\ air}}{1 + H_a} \quad \textbf{Equation 3-13}$$

$$\dot{m}_{humidity} = \dot{m}_{dry\ air}H_a \quad \textbf{Equation 3-14}$$

Where T_a, RH, p_a is the temperature, relative humidity, and pressure of the ambient air, and the H_a is the mass of water in the air. Table 3-7 lists the values for the molar mass fraction that was referred for indicated specific emission calculation.

Table 3-7 molar mass fraction of common gases found in gasoline engine combustion products [146]

Gas species(i)	u_i(Gasoline)
CO	0.000966
NO_x	0.001587
THC	0.00499

And finally, the dry-to-wet correction factor, k_w was calculated using Equation 3-15, where k_f is calculated by Equation 3-16.

$$k_w = 1.008\left[1 - \frac{1.2442H_t + 111.19W_{ALF}\left(\frac{\dot{m}_{fuel}}{\dot{m}_{dry\ air}}\right)}{773.4 + 1.2442H_t + 1000\left(\frac{\dot{m}_{fuel}}{\dot{m}_{dry\ air}}\right)k_f}\right] \quad \textbf{Equation 3-15}$$

$$k_f = 0.055594W_{ALF} + 0.0070046W_{EPS} \quad \textbf{Equation 3-16}$$

Where W_{ALF} and W_{EPS} are the hydrogen and O_2 contents of the fuel which were obtained by lab analysis. H_t refers to the total humidity factor where the water content of fuel was combined with the air humidity factor with Equation 3-17 and Equation 3-18.

$$H_t = H_a + H_f \quad \textbf{Equation 3-17}$$

$$H_f = \frac{\dot{m}_{water}}{\dot{m}_{dry\ air}} \quad \textbf{Equation 3-18}$$

The combustion efficiency, defined as the concentration of incomplete burn species left in the exhaust gas, was calculated from the pre-TWC emission values. The $\dot{m}_{co}$ and $\dot{m}_{THC}$ was then calculated for the heat release potential by multiplication with its respective LCV. CO has an LCV of 10.1Mj/Kg while the THC is assumed to be the same as the used fuel. The comparison against the total energy delivered by the injected fuel results in the combustion efficiency, η_c as defined in Equation 3-19

$$\eta_c = 1 - \frac{\dot{m}_{co}LCV_{CO} + \dot{m}_{THC}LCV_{THC}}{\dot{m}_{fuel}LCV_{fuel}} \quad \textbf{Equation 3-19}$$

3.3.3.3 EGR dilution rate calculation

The EGR dilution rate was measured by the Horiba MEXA by comparison of the CO_2 concentration of ambient air, inlet manifold air, and exhaust gas using Equation 3-20.

$$\%Total\ charge = \frac{CO2_{int} - CO2_{bkg}}{CO2_{exh} - CO2_{bkg}} \times 100 \quad \textbf{Equation 3-20}$$

Where $CO2_{int}$ is the CO_2 concentration at the intake manifold, $CO2_{exh}$ is at the exhaust gas, and $CO2_{bkg}$ is at the ambient air that the engine takes in. This ratio is termed the total charge, and it represents the total EGR gas percentage present in the intake gas.

3.3.3.4 AFR calculation

The absolute lambda of the exhaust sample was given by the Horiba gas analyser based on the gas sample readings. The method used to calculate the lambda and thus AFR is based

on the Brettschneider/Spindt method where the total mole balance is calculated through the measured values of CO_2, CO, and THC. The moles of water in the sample required to calculate the lambda was assumed with an equilibrium of a reaction that partially converts $CO_2+H_2 \rightarrow CO+H_2O$ with a set equilibrium order [148].

3.3.4 Knock intensity calculation

The raw cylinder pressure was processed via a comparator of moving average, which acts as a high-pass filter to the original signal. The equation used was as seen in Equation 3-21

$$KI = \frac{\sum_{n-5}^{n+5} P}{21} \qquad \textbf{Equation 3-21}$$

With a measuring resolution of 1/2CAD, every measured point of in-cylinder pressure was compared against the average of the 20 surrounding pressure measurements. Any sudden rises in pressure are indicated as a spike seen in the example plot in Figure 3-16. This is termed as the high pass filtered signal, and the maximum value recorded is defined as the knock intensity of the cycle. Any combustion cycle that exhibits a KI higher than 1.6 was classified as knocking combustion.

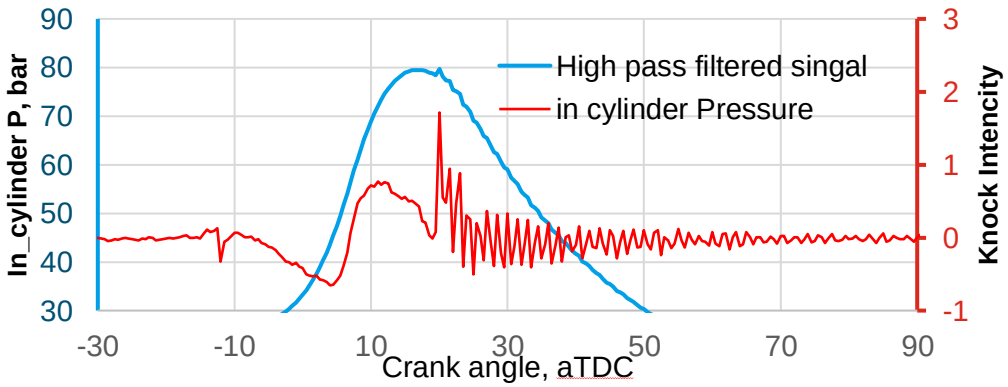

Figure 3-16 Example of knock classified combustion, where in-cylinder pressure and high pass filter signal are overlaid

3.4 Engine control

As a summary of the engine control, a full list of the manually operated control parameter is as detailed in Table 3-8. All the listed parameters were controlled through the ECU.

Table 3-8 List of manually operated ECU based engine control parameters and their value range

Control	Range	Unit
Throttle valve position	0-100	% Duty cycle
TC wastegate position	0-100	% Duty cycle
Injection pressure	0-150	bar
Ignition angle	-50 - 20	CAD aTDC
Inlet valve phaser	0-45	CAD
Exhaust valve phaser	0-45	CAD
Variable Oil Pressure	0-100	% Duty cycle
EGR mixer valve position	0-100	% Duty cycle
Lambda setpoint	0-2	-
Start of First Injection (SOI1)	-320 - -299	CAD aTDC (of combustion)
End of Second Injection (EOI2)	-250 - 50	CAD aTDC (of combustion)
Split ratio for first injection	0-1	(x100) %

The ECU instrumentation is marked in the schematic diagram (Figure 3-1) and summarised in Table 3-9. All instrumentation except the inlet manifold O2 sensor and MAF sensor are standard engine OEM sensors. The MAF sensor was fitted to replace the MAP sensor due to compatibility with faster AFR estimation using a higher fraction of EGR dilution. The engine was also fitted with an O2 sensor on the inlet manifold as a precautionary measure, where any sudden loss in EGR dilution will result in ignition cut off to prevent engine damage.

The variable oil pressure setting was set to 100% throughout the tests to ensure full oil pressure conditions were sustained. This ensured the engine was sufficiently cooled and lubricated during operation. However, this led to relatively higher readings of frictional loss due to extra work input. Hence the values presented in the project should not be taken as absolute performance values for the production engine in a real car scenario.

Table 3-9 List of ECU instrumentation

Device	Measuring
MAF sensor	Inlet air mass flow rate
IAT sensor	Inlet air temperature
MAP sensor	Inlet manifold pressure
Throttle position (feedback)	Actual throttle valve position
Crank angle sensor	Relative crank position
Inlet valve phaser sensor	Inlet cam phaser position
Exhaust valve phaser sensor	Exhaust cam phaser position
Lambda sensor (pre-TWC)	Exhaust lambda
Temperature sensor for the lambda sensor	Lambda sensor temperature
Injection pressure	HP fuel rail pressure
Inlet air Oxygen sensor	EGR rate estimate

3.4.1 Load control of the engine

The current study focused on the higher loads of a downsized GTDI engine, and almost all concerned test points took place at the boosted conditions. These loads were achieved by manually operating the inlet throttle to fully open position and controlling the TC wastegate closure for more load. Figure 3-17 illustrates the schematic of the inlet and TC configuration for the engine. The wastegate defaulted to the fully open position which directs the bulk of exhaust energy to bypass the TC. Closing the wastegate forces the exhaust pressure to spool the TC, which also spins the compressor fins for higher inlet pressures. As the engine speed and lambda were set as a constant, the fuel injection amount was adjusted proportionally to the increased MFR of intake air for a higher load output of the engine.

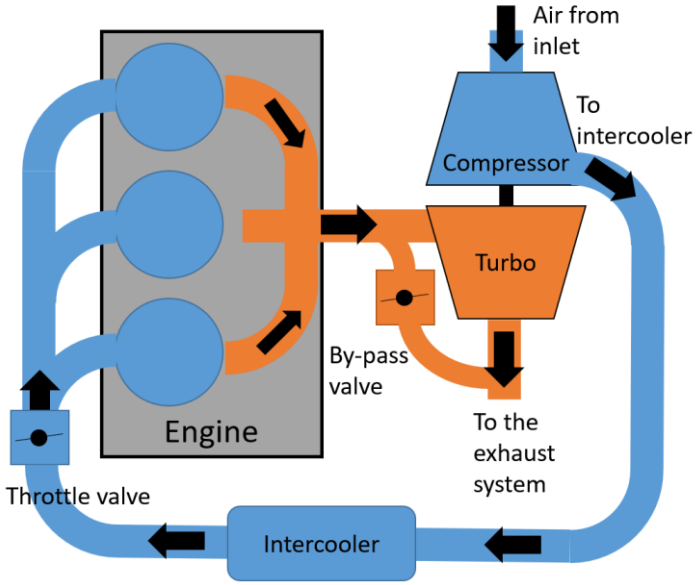

Figure 3-17 piping diagram of TC set up with a bypass valve for load control. Closing the bypass valve increases the exhaust pressure for the TC to increase the compressor speed

The load was either monitored by the BMEP reading on the dynamometer or the IMEP reading calculated from the in-cylinder pressure trace. Slow transient shifts of load were expected as thermodynamic equilibrium are reached between the engine and cooling components during the engine warm-up stage before the testing. Results were only to be taken once this equilibrium was confirmed.

3.4.2 EGR dilution rate control

An external cooled LP-EGR system, as shown in Figure 3-3, was used for the tests with EGR dilutions. The EGR mixer valve position was controlled to achieve the desired dilution rate. A consequential drop in operating load was compensated by further closure of the TC wastegate. This was repeated until the engine load, and EGR dilution rate was within a desired tolerance of the targets. Any slow-acting transitional effects were trimmed by small adjustments to these settings.

The EGR dilution rate was measured by the Horiba Mexa7170D-EGR gas analyser by comparison of CO_2 concentration between the inlet and the exhaust gas. For this, an additional PVC pipe was drawn from the inlet manifold to the secondary CO2 concentration sensor on the gas analyser.

3.4.3 Fuel injection control

Injection duration (and thus fuel amount) was primarily controlled via a lambda feedback loop based on the lambda at specified set point. In this study, the stoichiometric condition was used throughout the tests. Therefore, the lambda control was set to ‘manual’ which turned off any transition correction and strategic lambda-map based set point.

The single injection strategy was used for the baseline engine. Therefore, a programmed control strategy was used to enable split injections. The calculated total injection duration was split based on the split ratio specified by the user, and timed based on the start of injection for the first injection (SOI1) and end of second injection (EOI2). Referring to the second injection by the end of injection clarifies the minimum mixing duration (EOI2 to ST).

The injection timing, as well as the SI, was implemented and controlled through the ECU timer based on crank angle sensors. The factory fitted sensors were used in this study. Specifically, a crank trigger wheel (52 teeth) and two camshaft position sensors were used to determine the event timings to the closest degree via interpolation.

3.5 Commissioning and validation

Initial analysis was performed for the engine and instrumentation before initiating the results collection. The engine underwent a break-in process to stabilize the frictional losses, while

instrumentations were also maintained and calibrated before performing results validation. The process and action are unique to each equipment, but the process is important to ensure the analysis of results are the result of the controlled variables and not due to false readings.

3.5.1 Engine break-in procedure

As the engine came directly from the factory, the engine was prepared as per recommendation by the supplier. This was done by subjecting the engine to varying speeds and loads while monitoring the FMEP value measured by the in-cylinder pressure throughout the process. The monitored FMEP value against engine operation hour count is as seen in Figure 3-18. The frictional losses of the engine are reduced as it approaches the 35-hour mark due to the successful bedding in of friction surfaces. Subsequently, the FMEP value is settled as wear surface condition stabilises. As shown in Figure 3-18, the pass condition was determined as the stability of the FMEP values to be within 0.1bar of each other. A target value of FMEP was not specified as this was sensitive to the engine's instrumentation set up. Instead, the stability and repeatability of the parameter were deemed to be important.

The engine was commissioned for testing once the stability in measurements was observed at 40 hours of operation. Beyond this point, only the 20Nm test point was monitored as a part of the start-up daily test procedure. The number of operational hours of the engine starts at 10 hours as the engine had been run without appropriate instrumentation prior to the start of monitoring.

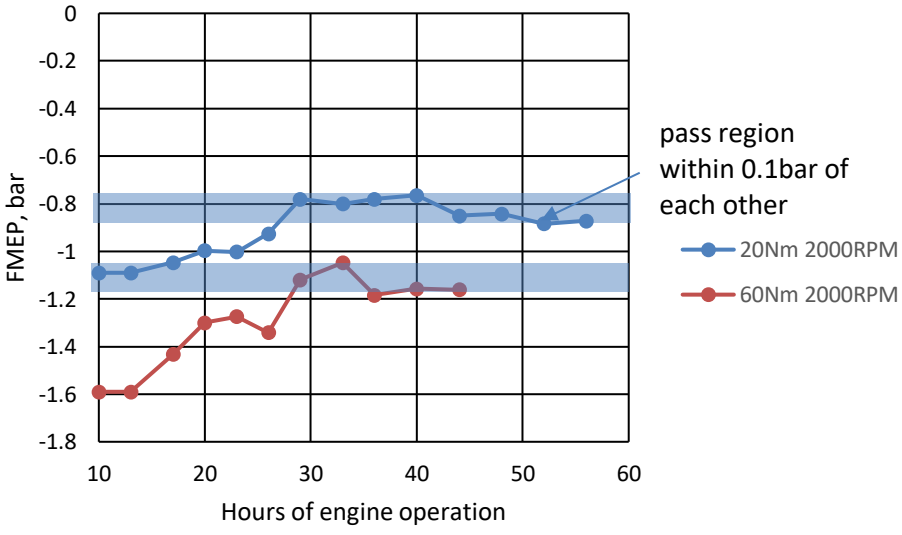

Figure 3-18 FMEP values against hours of engine operation during the break-in procedure

3.5.2 Exhaust gas analyser measurement validation

The Horiba MEXA7170D-EGR exhaust gas analyser was periodically calibrated and serviced by Horiba service engineers. The calibration was also kept up to date. The unit is calibrated using zero and span gas for all gas species tested. And finally, the AFR was checked to match the fuel specification as a part of the start-up check.

For the validation of the tailpipe NO_x concentration measurement, the gas analyser used (Signal group 4000VM) was serviced and calibrated by the manufacturer. The unit was also calibrated and checked with a span and zero gas, which also validates the accuracy of the unit.

The particulate filters' first diluter was cleaned periodically (according to the hours used), and the electrometer detector was cleaned prior to the start of the test campaign. Before and during the tests, an 'auto zero' was performed every hour, and 'zero gas' of specified dryness was circulated in-between measurements.

3.5.3 Validation of engine subsystem operation

3.5.3.1 Cam phaser and valve timing validation

The inlet and exhaust valve positions were controlled and adjusted by the ECU. The valve event timings were validated by monitoring the intake and exhaust cam position signals. The wiring was spliced and read by the fast channel DAQ. The reference event signals are as seen in Figure 3-19, while the measured intake valve signal is seen in Figure 3-20. The measured signal is an average of 300 cycles where the IVO set-point is set to -26CAD aTDC, hence in comparison to the 0CAD phasing referencing, there is a -26CAD phase shift, as intended.

The validation was made for every 5 CAD phase increments for both inlet and exhaust cam phasers. As no errors were seen, the ECU was found to control the phasers accurately and according to the user intended phases.

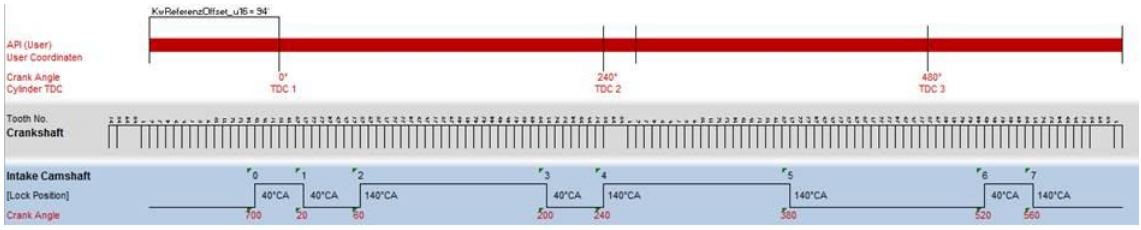

Figure 3-19 Intake camshaft phase position reference at lock position (0CAD phasing)

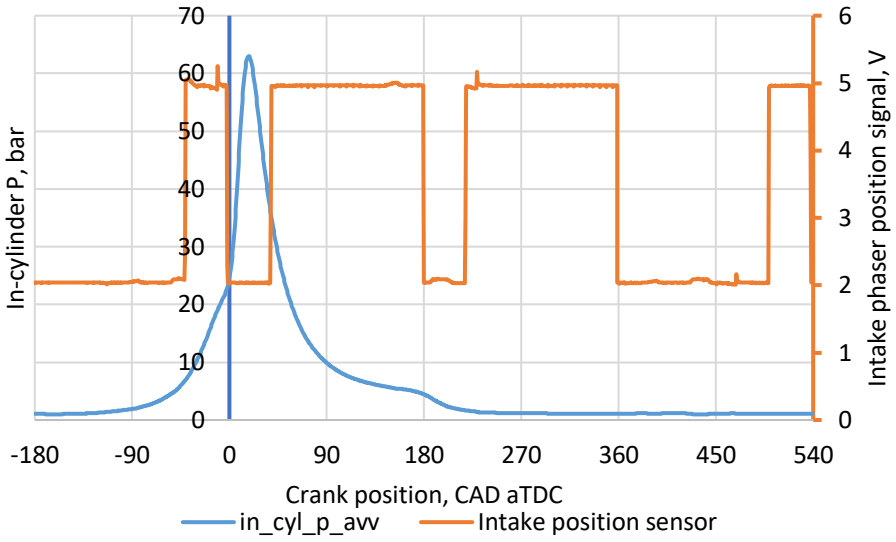

Figure 3-20 Intake cam phaser position signal, in-cylinder pressure signal added for reference, phaser offset =-26CAD

3.5.3.2 Injection timing

The injection timing and duration were set via the ECU based on the parameters of split injection ratio and timing of injections. The occurrences of injections were validated by analysing the injection signal with a current clamp where the signals were recorded by the fast DAQ channel.

Figure 3-21 shows the injection signal for a split injection case. The injection strategy here is for an 80:20 split ratio with SOI1= -299 CAD aTDC and EOI2=-150 CAD aTDC. The signal shows two distinctive injection peaks at the correct locations. The duration, as seen by the crank angle, also indicates an accurate split ratio setting (35 and 8 CAD of opening with 0.5CAD measurement resolution).

Injection signals were checked on the transient combustion analyser for confirmation of timing for the full variable range (-299 to -50 CAD aTDC) to ensure the accuracy of injection timing.

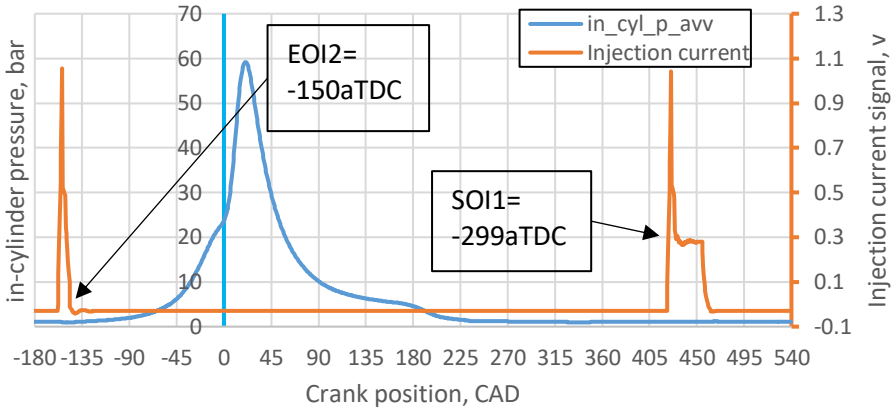

Figure 3-21 Injection signal monitored via a current clamp. Example shows split injection with 80:20 split where SOI1=-299 and EOI2=-150 CAD aTDC

3.5.3.3 Ignition system

An ignition of equal discharge energy was required as a part of the tests performed in this project. The ECU adopts a control method that considers the voltage to adjust the charge duration of the coil. Hence variations in power supply voltage did not affect the discharge energy of the coil.

Two variations of ignition systems were prepared for use with this engine. They were termed the standard (STD) and high-energy (HE) ignition system where the standard ignition system refers to the OEM factory fitted Ecoboost ignition system.

The HE ignition system with a 120mJ discharge required a modification to the map according to the charge characteristic, as seen in Figure 3-22. At 12V, a dwell duration of 6ms was found to produce 120mJ of discharge energy.

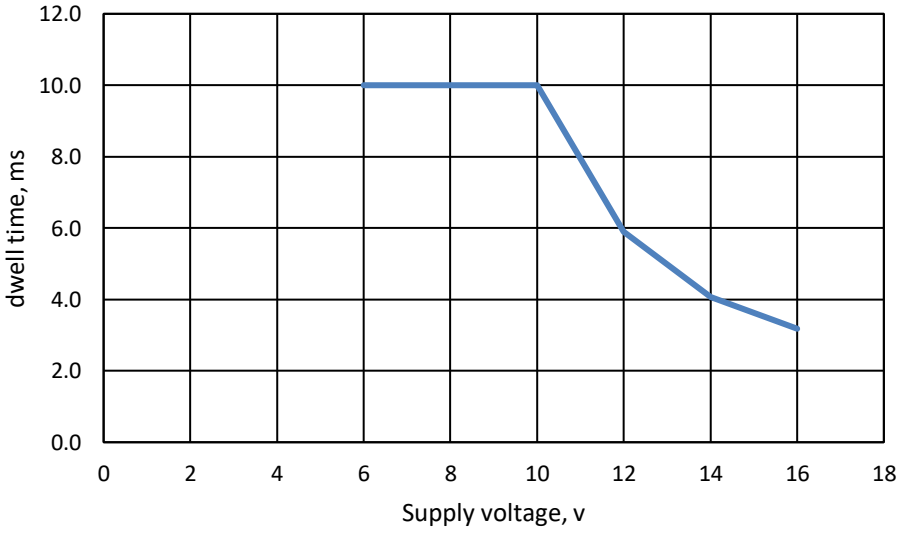

Figure 3-22 HE ignition system dwell time and supply voltage characteristic to achieve 120mJ ignition energy

The ignition energy was further confirmed using an oscilloscope and high voltage (1000V) Zener diode chain, and a 2Ω load resistor. A signal generator was used to control the dwell signal, and an adjustable PSU provided specific power voltage. A picture in Figure 3-23 shows the set up used to verify the discharge energy.

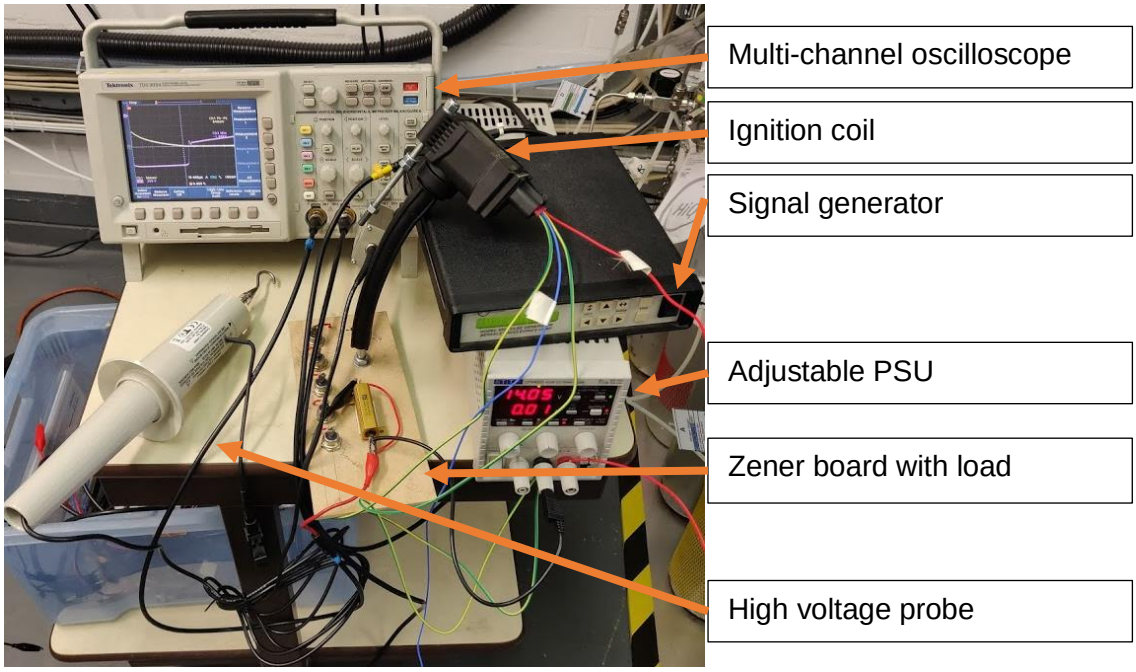

Figure 3-23 Ignition coil discharge energy verification set up, 1000V Zener diode emulated a spark discharge while a load resistor was used to measure the charge.

Supports and connectors were made accordingly with adaptors for secure fitment of the HE ignition system. Figure 3-24 shows the fitment method used. An extended mount was implemented to secure the larger ignition coil while an adaptor cable was made for electrical connections. Finally, a current clamp was used to verify the ignition signal given by the ECU for timing and dwell duration validation.

A torque wrench was used to tighten the spark plugs to the correct torque rating, and care was taken to avoid any contact with the electrodes. The electrode angle was also noted, and any spark plugs with electrode pointing in the exhaust valve positions were omitted due to potential impact towards flame kernel development.

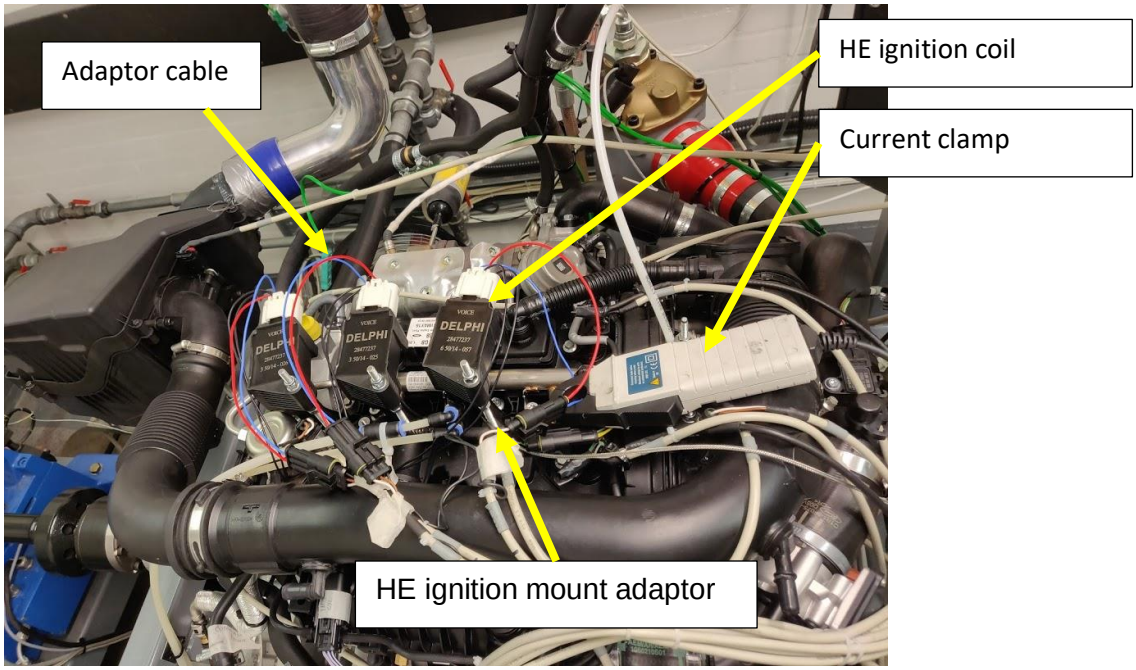

Figure 3-24 HE ignition system installed on the experiment engine with adaptive components. Current clamp for timing and dwell validation

3.5.3.4 Pressure transducers, type K thermocouples

All pressure transducers were purchased as new, thus were calibrated by manufacturer.

The thermocouples used were all type-K (Alumel/Chromel) category. The temperature range depends on the outer protective material. All used thermocouples were validated at ambient temperature and with hot water where the temperature readings were compared against the reading of a calibrated type-K thermocouple reader.

3.5.3.5 Dynamometer

The torque and speed, as measured by the dynamometer, were calibrated professionally. Furthermore, the torque of the dynamometer was checked periodically using a set of hanging calibrated weights and a calibration arm. The measured dynamometer speed was constantly cross-checked with the ECU measured speed as the engine crankshaft is directly coupled to the dynamometer.

3.6 3D CFD Simulation setup

This section details the setup and validation of the 3D CFD simulation cases. Several test cases were further analysed for in-cylinder fuel distribution, spray and flow interaction and short-circuit condition. The steps taken to ensure accurate simulation cases were performed are noted.

3.6.1 Numerical models

Simulations were performed with Star-CD software from CD-adapco. The Reynolds-Averaged Navier-Stokes (RANS) approach was applied with RNG k-ε turbulence model. The RANS simulations have been widely used in engine spray [149] and combustion simulations [150] due to the good trade-off between accuracy and computational costs. The heat transfer was implemented through the general form of the enthalpy conservation equation for the fluid mixture. The Angelberger wall function was used for the simulation of the wall heat transfer.

In order to model the fuel spray from the multi-hole injector, the initial droplet size distribution was determined by Rosin-Rammler equations. The O' Rourke model and Bai model were used to consider the inter-droplet collision and wall impingement, respectively. To predict the gasoline spray droplet breakup process, the Reitz Diwakar model was applied and validated.

3.6.2 Spray validation

The spray model was calibrated before moving to the engine simulations. The comparison between experimental measurement and validated CFD results are shown in Figure 3-25 and Figure 3-26. Both the spray tip penetration and spray plumes show good agreement between experimental measurements and CFD simulations. Therefore, the validated spray models were applied in the subsequent engine in-cylinder simulations.

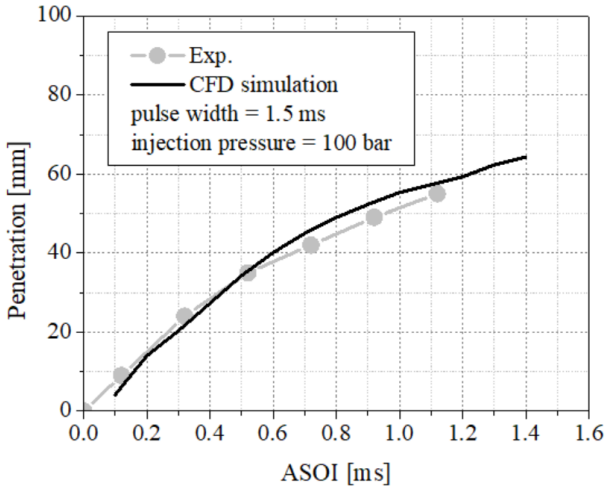

Figure 3-25 Comparison of the spray tip penetration between experimental measurement and CFD simulation

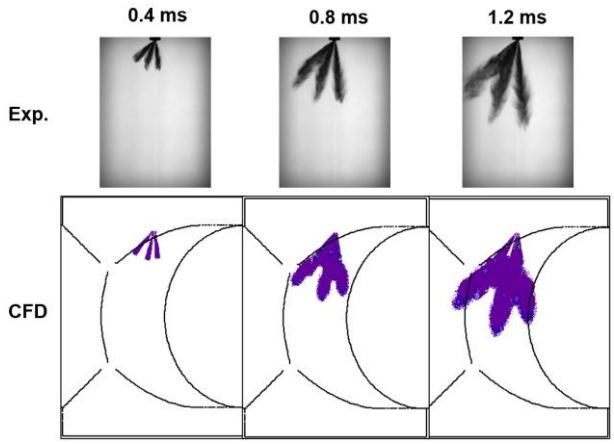

Figure 3-26 Comparison of the spray plumes between experimental measurement and CFD simulations

3.6.3 Mesh sensitivity study

Engine mesh sensitivity study was performed to ensure the simulation results are independent on the mesh size. Three simulation meshes were generated with average grid size at 0.6 mm, 0.75 mm, and 1 mm. It should be noted that for all three meshes the grid size was refined to 0.5 mm for the cells around spark plug and injector tip. The used mesh is presented in Figure 3-27.

The simulation results show that the three meshes agree very well during the intake/exhaust and compression strokes and show limited difference during the expansion stroke due to more sensitivity of the combustion to mesh size. In particular, the mesh size of 0.75 mm showed only slightly higher peak pressure (~1.9%) than the fine mesh (0.6 mm). therefore, the mesh with 0.75 mm was selected for the simulations in this study. Plot comparisons are seen in Figure 3-28.

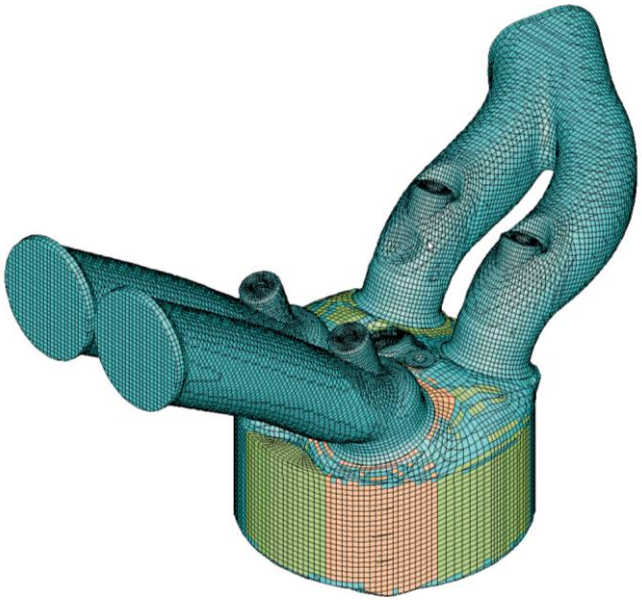

Figure 3-27 Moving mesh used for engine simulations

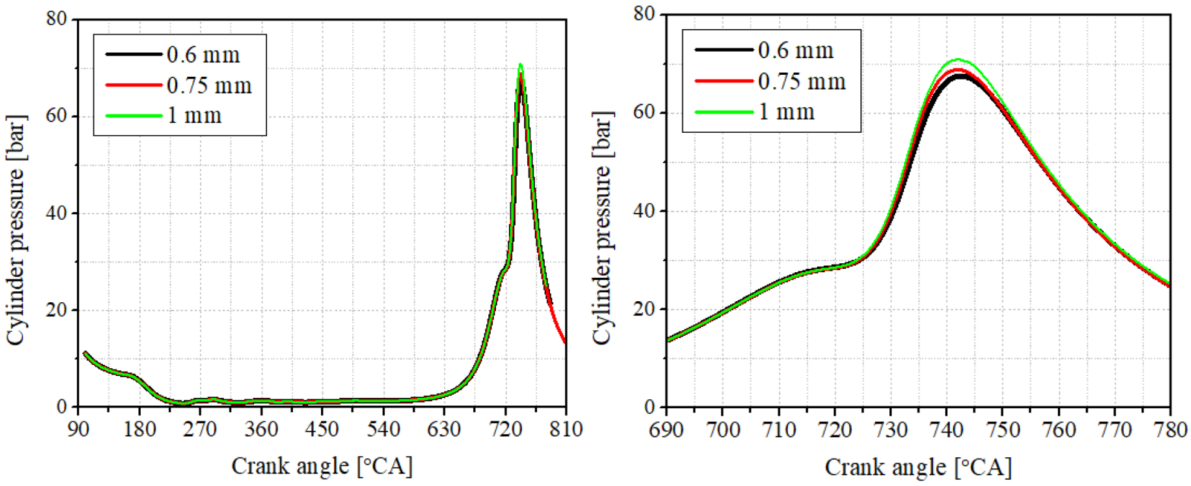

Figure 3-28 left, Impact of grid side on simulation results. Right, impact of grid side on simulation results (plot enlarged around combustion TDC)

3.6.4 Engine simulation validation

The CFD simulation results were compared against the experimental data to ensure the CFD results are valid for further analysis. The following figure shows the results for the scavenging study (Run15 at 16.4 bar without EGR). The CFD results show good agreement with experimental data during the exhaust, intake, and compression stroke (before TDC). As the combustion process is not involved in this simulation study, the combustion model was not calibrated, therefore producing discrepancy against experimental data. But this will not affect the analysis on the scavenging, fuel injection and mixture formation which were focused on this study.

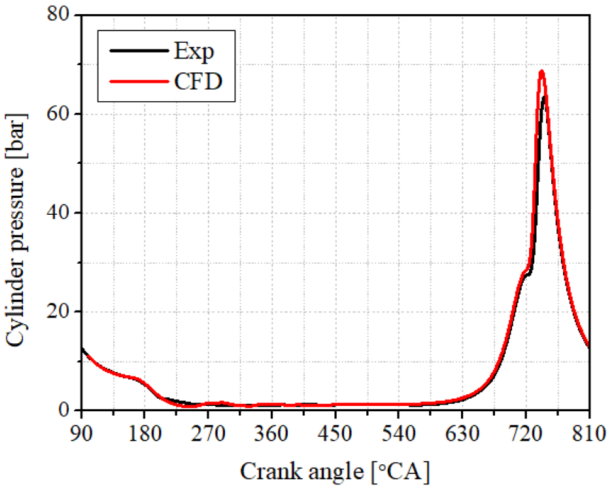

Figure 3-29 Comparison of the CFD results with the corresponding experimental data

3.6.5 Initial and boundary conditions

The engine experimental data and one-dimensional (1D) simulations with Ricardo WAVE were used to provide realistic engine initial and boundary conditions for CFD simulations. Therefore, the simulations at different operating conditions will use different initial and boundary conditions to reflect the experimental setup. Table 3-10, as an example, shows the initial and boundary conditions of the CFD simulations for the scavenging process study.

Table 3-10 Initial and boundary conditions of the CFD simulation

Initial conditions @ 100 ºCA ATDC	
Cylinder temperature	1669 K
Cylinder pressure	11.2 bar
Intake temperature	301 K
Intake pressure	1.36 bar
Exhaust temperature	769 K
Exhaust pressure	1.3 bar
Boundary conditions	
Cylinder head temperature	460 K
Piston top temperature	480 K
Cylinder liner temperature	460 K

The initial mixture components in the cylinder and exhaust ports at 100 CA ATDC are burned gases comprising CO2, H2O and N2. The mixture components in the intake ports and inlet boundary are air (O2 and N2) and burned gas (CO2, H2O and N2) if including external EGR. The CFD simulations were performed from 100 to 720 CAD ATDC, which

covers the whole period of the scavenging, injection, and mixing process. The combustion process was not modelled in this work.

3.7 Summary

The full details of the experimental rig, including the engine used to study the effects of split injection, valve phasing, and EGR dilution are provided in this chapter. All necessary instrumentation, engine life support, safety, and control systems were installed to ensure all the variables could be achieved and recorded for later analysis. Furthermore, the methodologies for the post-processing are discussed in detail. The equipment settings employed are also defined with their explanations.

The instrumentation installed can obtain the results to analyse necessary combined synergy effects of EGR dilution, split injection, valve overlap reduction accurately. Most importantly, the requirements in accuracy and consistency of the results obtainable from the tests are verified through commissioning and validation. Thus, the completed test rig can run the planned tests accurately and safely.

Finally, the 3D CFD simulation models and validation are detailed to ensure accuracy and credibility for further analysis along with experimental results.

The loads and other variable figures as well as experimental procedures are to be defined in each of the results chapters as this varies with the tests performed.

Chapter 4 Expansion of external-EGR effective region and influence of dilution on the boosted operation of a downsized GTDI engine

4.1 Introduction

As detailed in the literature review, the use of EGR for the downsized engine has been tested previously by OEMs engine constructors and academics. The novelty of the results presented in this chapter comes from the combined use of HE ignition system with EGR dilution at boosted loads of the Ford EcoBoost 1litre downsized GTDI engine. The chapter starts by detailing the efficiency benefits of EGR and high energy ignition in combination at boosted loads to verify the dilution effects to lower knock mitigation at KLSA points (also noted as the boosted load). The later sections will focus on other engine parameters. As a complete chapter, the efficiency gains and mechanism are the focus of discussion. The pre-TWC emissions are also presented and discussed.

4.2 Test condition

The engine operating parameters chosen at the testing points are shown in Table 4-1 and Table 4-2. Using E5 pump grade 95RON fuel, 13.7bar Net_IMEP at 2000rpm is achieved at the wide-open throttle (WOT) with no boost. The highest load tested is at 18.9bar Net_IMEP for the engines stock TCs ability to run up to 30% EGR dilution. A total of 3 loads with equal load spacing were chosen for a distributed characteristic understanding of EGR and ignition effects on the engines boosted load. The test points were chosen for their severely knock limited spark timing conditions. 2000RPM represents a low speed condition with higher torque limits to unlock the EGR dilution limit while sustaining the same selected loads. The engine speed was not a variable in this study as the focus of the study was on the interaction of different strategies at knock limited loads, however the engine speed of 2000RPM is representative of a low speed condition due to the ample torque limit available and knock tendency of the resulting combustion.

Table 4-1 static test condition separated by load

Net_IMEP, bar	13.7	16.4	18.9
ST, aTDC	-11.5 (KLSA)	-6.6 (KLSA)	-1.6 (KLSA)
IVO position, aTDC	-26	-27	-24
EVC position, aTDC	27	24	20
Injection pressure, bar	120	128	135

Table 4-2 Global test conditions

Lambda setting	Exhaust UEGO setting=1 (stoichiometric)
Engine speed, RPM	2000
Fuel	Single batch gasoline pump E5 min RON=95
Start of injection 1, CAD aTDC	-299
EGR reintroduction temp, C	60

The EGR dilution rate is controlled by the opening of the EGR mixer valve. As the recirculated exhaust gas is produced by the pressure difference between the engine exhaust and the compressor inlet. The resulting dilution rate is a product of pressure difference generated by engine running condition and controls of EGR valve throttling.

At all three loads without EGR, the spark advance is knock-limited. However, in the case of 13.7bar Net_IMEP, the introduction of EGR has enabled the MBT spark advance to be achieved without experiencing knocking combustion as to be discussed later.

EGR dilution tested starts at 10% with 5 % increments. The EGR dilution limit is determined by one of the three following conditions that first occurred: -

1. Combustion stability as seen by CoV of Net_IMEP > 2%
2. Engine operation with further EGR leads to worsened efficiency
3. TC efficiency limit

The two ignition systems tested was termed ‘Standard’ (STD) and ‘High energy’ (HE). Standard is defined as the default ignition coil system typically installed in the Ford EcoBoost 1 litre engine with an iridium spark plug of default electrode gap of 0.7mm, the discharge energy is 75mJ. The high energy system has a typical single coil energy discharge of 120mJ where the same spark plug electrode gap is increased to 0.9mm. Figure 4-1 shows the

images of the two spark plugs prepared for each respective test. The coil charge time was automatically calculated by the ECU based on the power supply voltage to hold a controlled discharge energy amount.

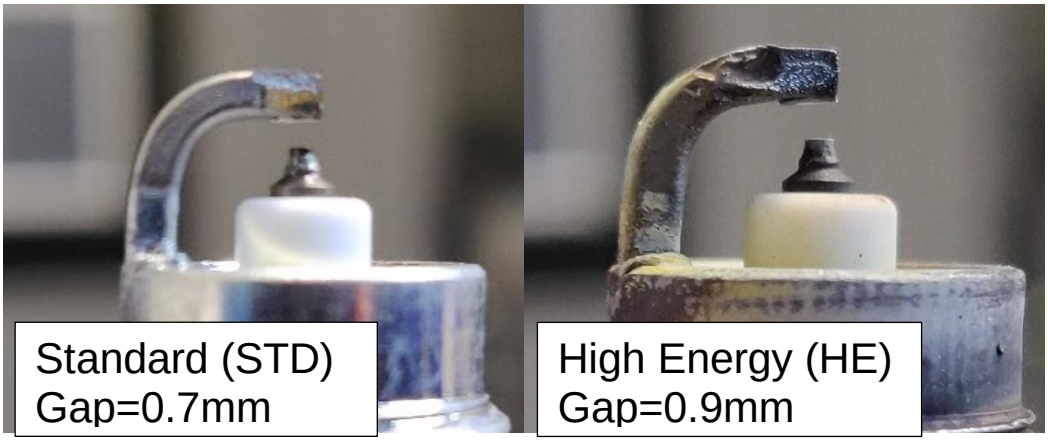

Figure 4-1 Electrode gap setting. Left, STD setting (75mJ) with 0.7mm gap. Right, HE setting(120mJ) with 0.9mm gap

4.3 Results and discussion

The tested cases of different EGR dilution rates and loads are as seen in **Error! Reference source not found.**, along with the defined EGR dilution limits listed in Table 4-3 based on the full test results of the investigation. The maximum EGR dilution rate tested is 33% at 16.4bar Net_IMEP using the standard ignition system. The combustion stability limit is exceeded with the highest load tested (18.9bar Net_IMEP).

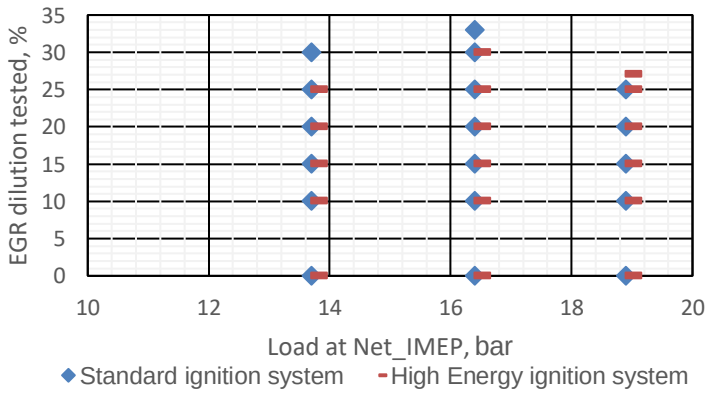

Figure 4-2 Tested points represented by engine load in Net_IMEP and EGR dilution, split by standard and high energy ignition system.

Table 4-3 EGR dilution limits as highlighted by test results

Load Net_IMEP, bar	Ignition type	Limit type	Max EGR dilution tested, %
	STD	SFC decline	30
13.7	HE	SFC decline	25
16.4	STD	SFC decline	30

	HE	SFC decline	33
	STD	Instability	25
18.9	HE	Instability	27

Some exceptions are made in the EGR dilution limits. For example, despite the decline in efficiency after just 15% in the 13.7bar Net_IMEP case, the test is performed to the full range to study the reasons for the decline and characteristics. Also, at 18.9bar Net_IMEP with standard ignition, the test is continued after the combustion instability limit was reached. The test was stopped at higher dilution rates when a sudden rise in instability was observed. More details will be given in the results section.

4.3.1 Effect of EGR on heat release and combustion processes

The positions of CA50 and ignition advancement are as seen in Figure 4-3. For all the loads and ignition systems tested, the combustion phasing, as indicated by CA50, is advanced with the use of external EGR dilution. At the 13.7bar Net_IMEP, the ST is retarded from MBT due to knocking combustion. As the EGR dilution is increased beyond 10%, the MBT can be achieved without knocking combustion, resulting in nearly constant combustion phasing of the target CA50 position (7CAD aTDC).

At the other two higher load operations, the ST advance is limited by the occurrence of knocking combustion. In particular, the higher boosting required for the 18.9bar Net_IMEP case has caused a highly retarded ignition (-1.6 aTDC) to avoid knocking combustion, resulting in very late combustion in the expansion stroke. With the introduction of EGR, the KLSA with the EGR dilution rate indicates a successful knock mitigation effect of the cooled EGR dilution.

The use of HE ignition does not affect the KLSA; however, it leads to more advanced CA50 position for the 16.4bar and 18.9bar Net_IMEP cases. This suggests the HE ignition system can produce fast combustion with lowered knock tendencies at these loads. In the case of 13.7bar Net_IMEP operation, the HE energy appears to have the opposite effect, which cannot be easily explained.

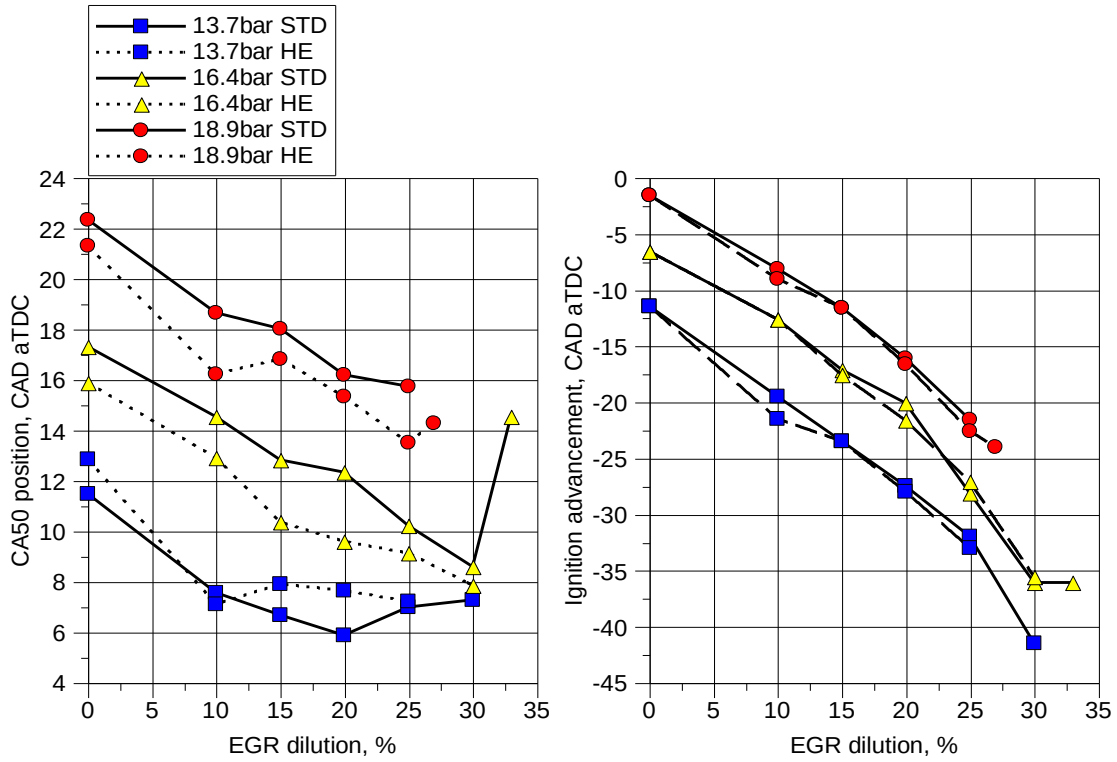

Figure 4-3 CA50 and ignition advancement position with EGR dilution and ignition energy changes

Figure 4-4, Figure 4-5, and Figure 4-6 show the corresponding heat release rate curves. In general, as EGR dilution is added, the heat release takes place earlier due to the earlier KLSA, also decreasing in intensity as it spreads wider over time. The use of HE ignition lowers the peak HRR. These effects appear to be pronounced throughout the EGR dilution range tested. At 13.7bar Net_IMEP where HE ignition does not bring benefits, the HRR is also lowered but appears to be phased later than the STD ignition cases.

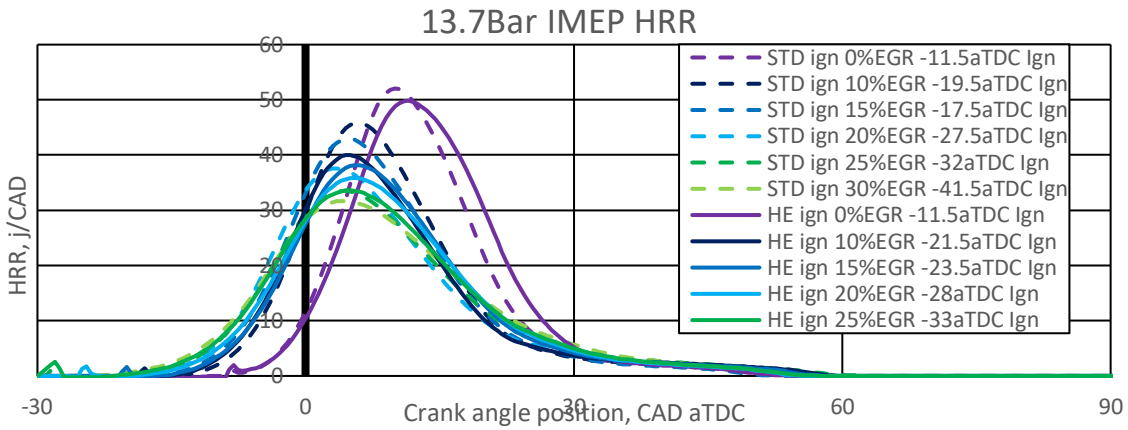

Figure 4-4 HRR graph with EGR dilution for 13.7bar Net_IMEP

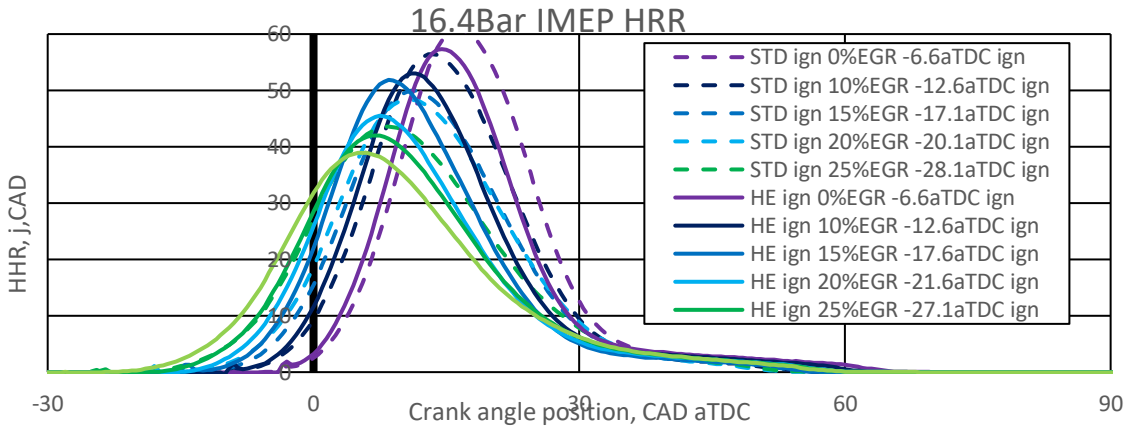

Figure 4-5 HRR graph with EGR dilution for 16.4bar Net_IMEP

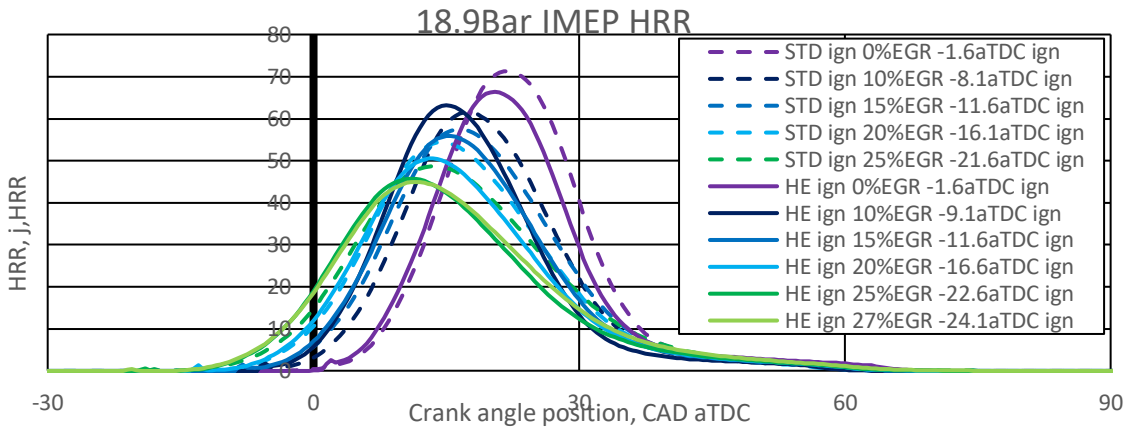

Figure 4-6 HRR graph with EGR dilution for 18.9bar Net_IMEP

Further quantitative analysis of the heat release characteristics and combustion processes are carried out by the results shown in Figure 4-7, which compares the changes in the different stages of combustion brought about by the HE ignition at different EGR rates. Positive percentages here indicate a faster burn in comparison to the STD ignition combustion. At 16.4bar and 18.9bar Net_IMEP operations, the HE ignition shortens the flame kernel development stage (ST-CA10), and early-stage combustion (CA10-CA50) durations are faster (shorter). The higher ignition energy has a greater impact on the initiation of flame kernel development than the early stage combustion duration. However,

the CA50-CA90 durations are extended with the HE ignition which is an onset of rapid expansion during the initial burn, taking effect on the end gas region to cause a slow end-burn near walls, similar results are recorded with similar studies [151].

In the case of the 13.7bar Net_IMEP operation, the HE ignition seems to slow down the initial flame kernel development and the early flame propagation speed due to the lower pressure and temperature conditions.

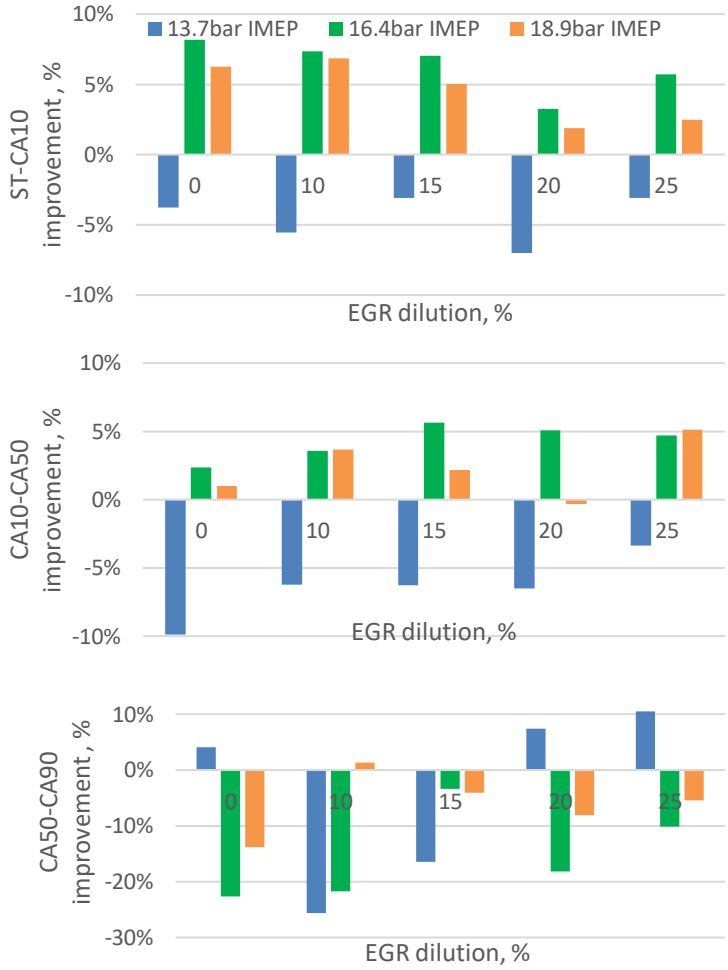

Figure 4-7 Segmented burn duration comparison of, ST-CA10, CA10-CA50, CA50-CA90 between standard and HE ignition. A negative value indicates an accelerated burn.

Figure 4-8 shows combustion remains stable in all but the 18.9bar Net_IMEP with high EGR. The HE ignition improves the combustion stability at 16.4 bar and 18.9bar Net_IMEP cases. At 18.9bar Net_IMEP, the improvement of combustion stability by the HE ignition extends the EGR dilution limit from 15% to 27%. However, at 13.7bar Net_IMEP, the HE ignition has little effect on the combustion stability because of the already very low CoV=1.0%. The gains associated with the HE ignition is displayed as a bar graph in Figure 4-9. Overall, it seems the greater power discharge has allowed for a hotter more stable spark discharge across the

gas mixture which has allowed for a bigger successful flame kernel to be formed at greater boosted loads.

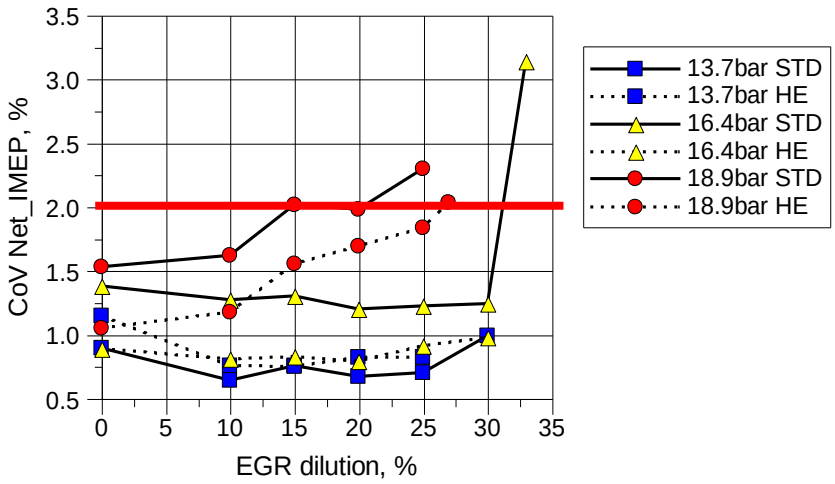

Figure 4-8 CoV Net_IMEP at tested points with STD and HE ignition system

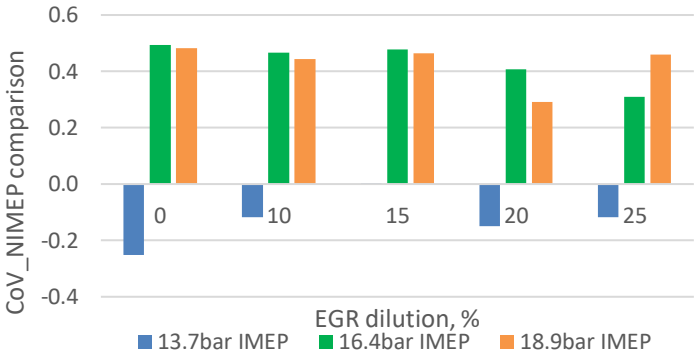

Figure 4-9 Stability gain achieved by HE ignition over standard ignition system for EGR dilution between 0% and 25%, a positive value indicates combustion stability gain

The above results have demonstrated that the cooled external EGR is effective in suppressing knocking combustion and advancing KLSA which tends to suffer from the ignition difficulties as well as combustion speed degradation.

The HE ignition can improve flame development when the same ST is applied as the standard ignition system at the higher load conditions. This can be explained by a larger hotter plasma in the wider gap with high discharge voltage and energy.

There are several possible reasons the same is not seen at 13.7bar Net_IMEP case, 1) lower boosting requirements leading to less response of the hotter plasma to make a successful kernel 2) earlier ST where in-cylinder conditions are less severe leading to nullify the effects of hotter larger plasma 3) Enriched trapped mass from boosting makes a suitable condition for HE ignition response

It appears the HE ignition system has good suitability that overcomes the shortfalls of high EGR dilution where lower NO_x emissions and high efficiency of boosted operation lies, but the suitability is limited to the higher load and boost conditions. The use of HE discharge energy across a wider gap has successfully improved the combustion by increasing burn speeds without the onset of knock and made a stable ignition kernel source which is vital to high dilution combustion.

At the 18.9bar Net_IMEP condition, the increased instability from increased dilution had reached the set limit (CoV of IMEP >2%) after 15% of EGR dilution using the STD ignition system. At this point, the EGR dilution no longer advanced the phasing enough to recover combustion speeds which affected stability. The cause may have been due to the shorter valve-overlap duration and increased loading, leading to much harsher in-cylinder conditions. Still, for this load, the HE ignition lowered the instability throughout the dilution range, which contributed to extended EGR tolerance of 13% (when considering stability limits).

Also, the CA90 position is shifted later which extended the CA50-CA90 burn durations because of the faster and earlier burn with the HE ignition. The faster earlier burn is suspected of bringing a slower tail end burn from rapid expansion effects of early burns.

4.3.2 Efficiency gains with external EGR dilution and HE ignition

The engines efficiency results with EGR dilution for the three engine loads tested is seen in Figure 4-10. Noticeable efficiency benefit can be seen in all loads tested with EGR dilution but to different extents. For all 16.4bar and 18.9bar Net_IMEP cases, a near-linear relation can be seen in BSFC/ISFC reduction. This is except for the final points where a sudden rise in BSFC and ISFC is seen which is due to combustion instability resulting in high THC emission. In comparison, at the 13.7bar Net_IMEP, the relation with EGR dilution is parabolic where the best efficiency is recorded between 15-20% EGR dilution rates, indicating a factor of optimisation in EGR dilution. The reasons for the different trends in BSFC at the lower load and higher loads can be explained by the fact that the ST is knock limited at the two higher load operations whereas knocking combustion is avoided by the introduction of EGR at the lower load. Therefore, the advanced ST and hence the improved combustion phasing near TDC lead to better engine efficiency and lower BSFC/ISFC with EGR. At the 13.7bar Net_IMEP, once the MBT has been reached at 15% EGR, the slower flame speed of more diluted mixture leads to lower energy conversion efficiency because of increased combustion duration and the negative work performed during the compression stroke with an early start of combustion.

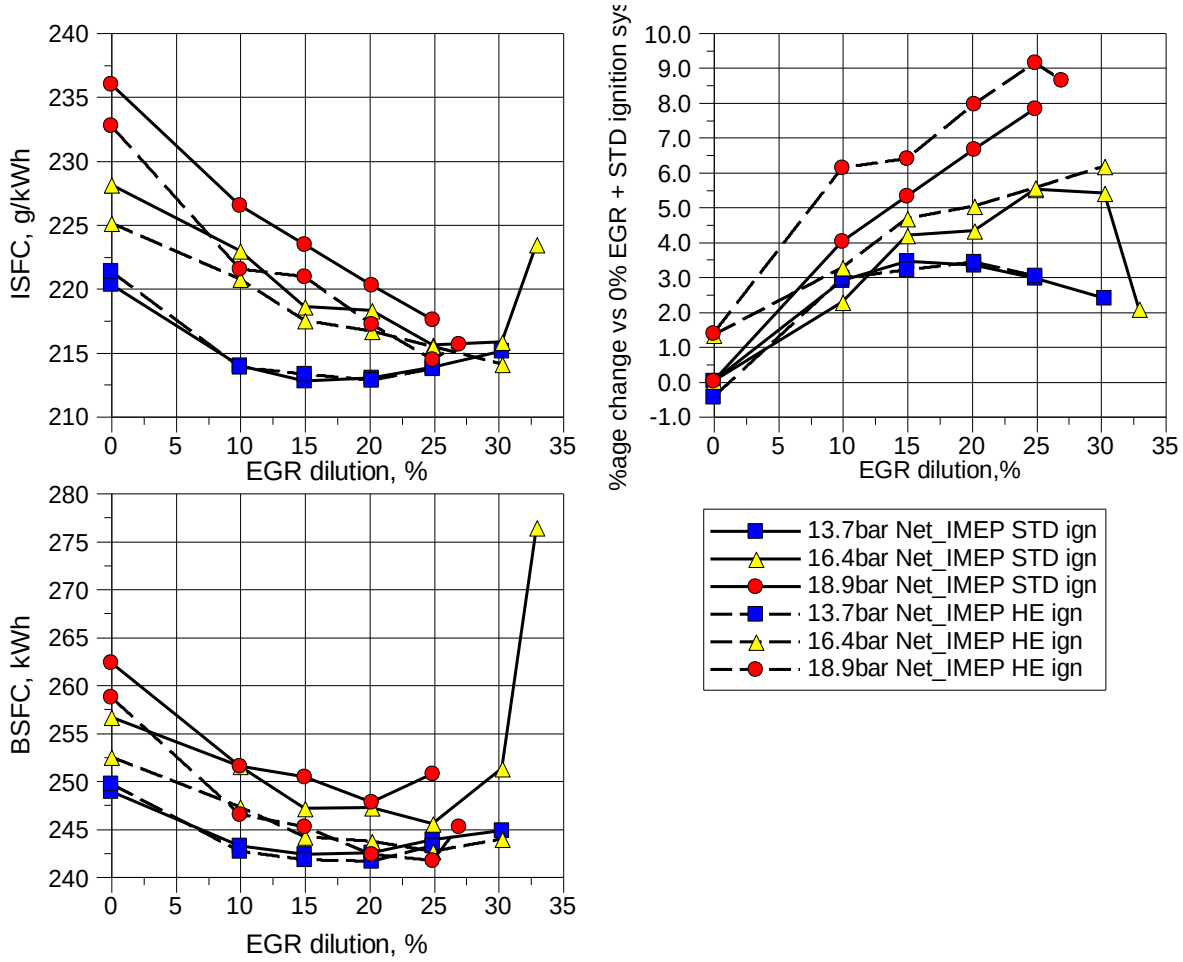

Figure 4-10 left, ISFC and BSFC vs EGR dilution % for 3 engines loads at 2000RPM. Right, ISFC percentage gain by EGR dilution

Use of HE ignition has further improved the engine efficiency at 16.4bar Net_IMEP and 18.9bar Net_IMEP because of the early and faster initial combustion as discussed previously. As shown by the bar graph in Figure 4-11, a maximum of 2.1% ISFC improvement is seen at 18.9bar Net_IMEP. The HE ignition has little or slightly negative effect on the engine's efficiency at 13.7bar Net_IMEP.

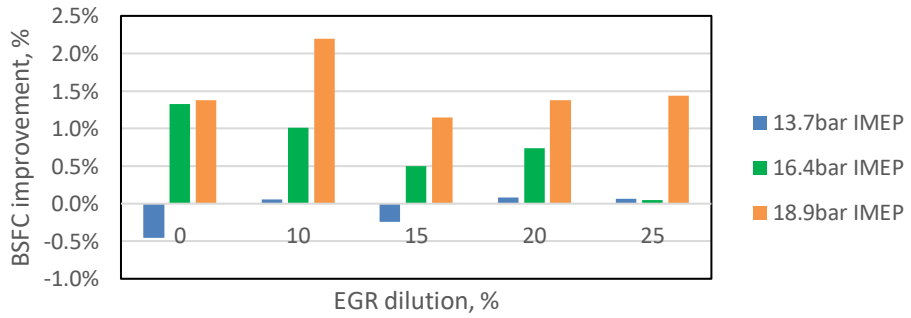

Figure 4-11 ISFC gain attributed to use of HE ignition. A positive value indicates ISFC gain

Figure 4-12 shows a scatter bubble plot of the friction mean effective pressure (FMEP) in an x-y plot where the position of the bubble is linked to the crank angle and value of the maximum pressure. The size of the bubble indicates the FMEP value in relative terms where larger bubble indicates a greater friction value. Observable is the increase in FMEP as EGR dilution is introduced to the mixture due to increased peak cylinder pressure. However, the impact is less than 0.4bar in IMEP increase at 18.9bar Net_IMEP case, as EGR is increased from 0 to 30%.

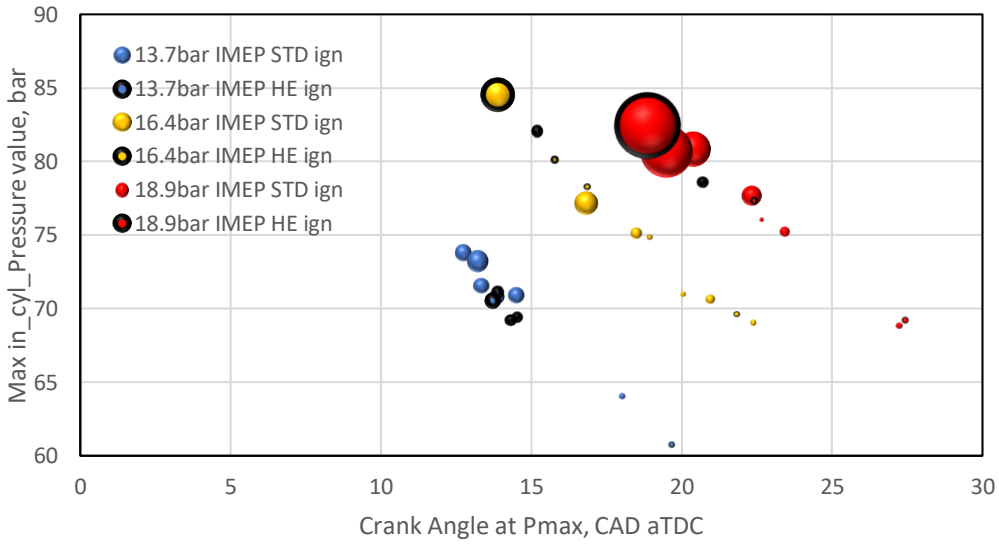

Figure 4-12 FMEP increase with EGR dilution due to higher and earlier P max occurrence

4.3.3 Emissions and other notable changes with cooled external EGR dilution at boosted loads

Figure 4-13 is a graph showing the average working gas pressure drop across the inlet and outlet ports. The larger value here will indicate a strong flow tendency during valve-overlap conditions. But it must be noted that larger durations of valve-overlap will reduce this value as flow settles the P_{drop} with increased flow mass of short-circuit air. The values taken is a cycle averaged pressure, and the instantaneous P_{drop} during valve-overlap is likely to be higher due to dynamic effects of 3-cylinder manifolds. 18.9bar Net_IMEP shows the highest figure of P_{drop} due to the narrower valve-overlap and highest boost demand. The 16.4bar Net_IMEP case came second which still had boosting pressures, but the wider overlap duration allowed a high volume of short-circuit air which lowered the P_{drop}. At 13.7bar Net_IMEP, there is no boost demand at 0%EGR which resulted in the lowest value. The use of EGR has clearly increased the P_{drop} for all load cases, which will increase the short-circuit air ratio as valve-overlap settings remain a constant for each load. This is an important measurement to note for wide overlap conditions with boosting due to the impact towards in-

cylinder ER. However, due to the decreased O_2 concentration of the fresh charge, the actual short-circuiting effects towards the in-cylinder ER is hard to estimate.

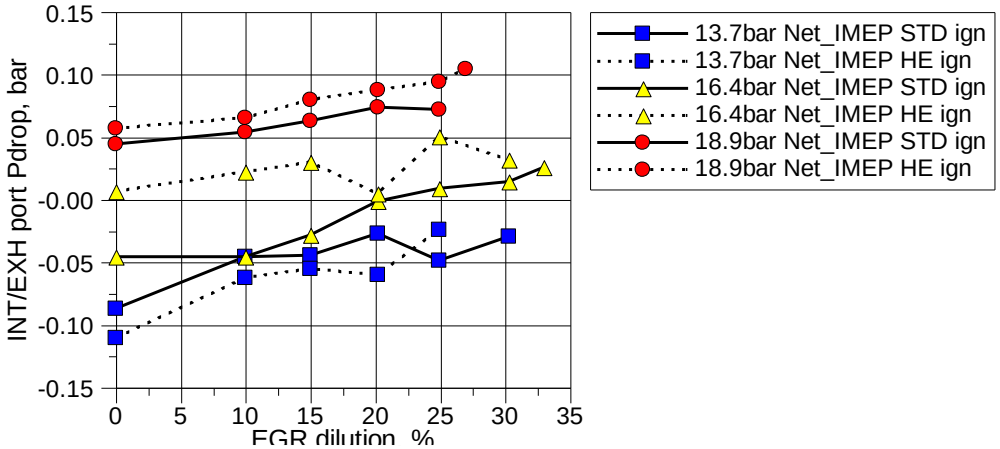

Figure 4-13 Int/Exh gas port P_{drop} average at boosted load using various levels of external EGR and ignition energy

Pre-TWC exhaust gas concentrations of major species are presented and discussed. The $ISNO_x$ output with EGR dilution is as seen in Figure 4-14. The $ISNO_x$ is reduced linearly with the increase in EGR by a factor of 10 with 25-30% EGR. While the differences are subtle, higher $ISNO_x$ emissions can be noticed with the use of the HE ignition system. The change can be attributed to hotter combustion that takes place with a faster and hotter burn.

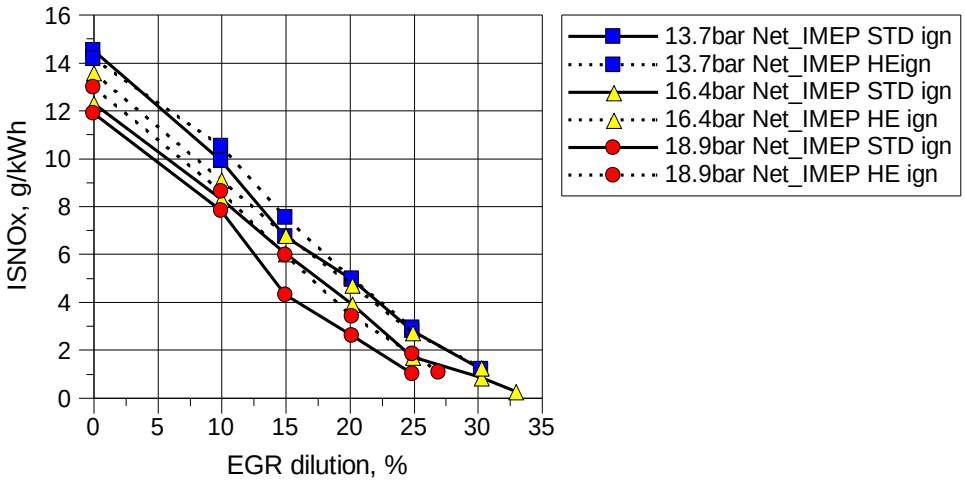

Figure 4-14 NO_x emissions characteristics with EGR dilution and HE ignition introduction

The emissions of ISTHC and ISCO are shown in Figure 12 in terms of specific output. The values in ISCO and ISTHC indicates some degree of in-cylinder ER condition, and this is also a trend indication of short-circuit air rate as EGR dilution is increased into boosted loads.

For all load cases and both ignition systems, the ISTHC emission shows a steady increasing trend with EGR dilution due to lower combustion temperature and hence lower oxidation of any THCs from crevices and quenching layer near the cylinder wall. In terms of ISCO emissions, both the 16.4bar and 18.9bar Net_IMEP cases had higher emissions due to the possible fuel-rich in-cylinder mixture. The ISCO emission values remain high throughout the EGR dilution range. However, a small decrease in the figures can be noticed at 18.9bar Net_IMEP, where the mixture ratio is suspected to improve with EGR dilution in the inlet air. At 13.7bat Net_IMEP, the use of greater boost with higher EGR ratio has caused for greater levels of short-circuiting, causing the ISCO levels to increase. HE ignition lowered the ISCO output at the higher loads at a very steady offset.

Another cause that may affect these emissions is the combustion phasing effects. In the 13.7bar Net_IMEP case, the CA50 target is reached just after 10% EGR dilution. This meant that any longer combustion resulted in very long combustion durations, starting as early as -40CAD aTDC. At higher loads, these phasing's are improved due to knock mitigation effects which in the 18.9bar Net_IMEP mean the combustion is optimised in terms of phasing, this may have contributed to the in-cylinder conditions for a cleaner burn leading to these changes in ISCO emissions.

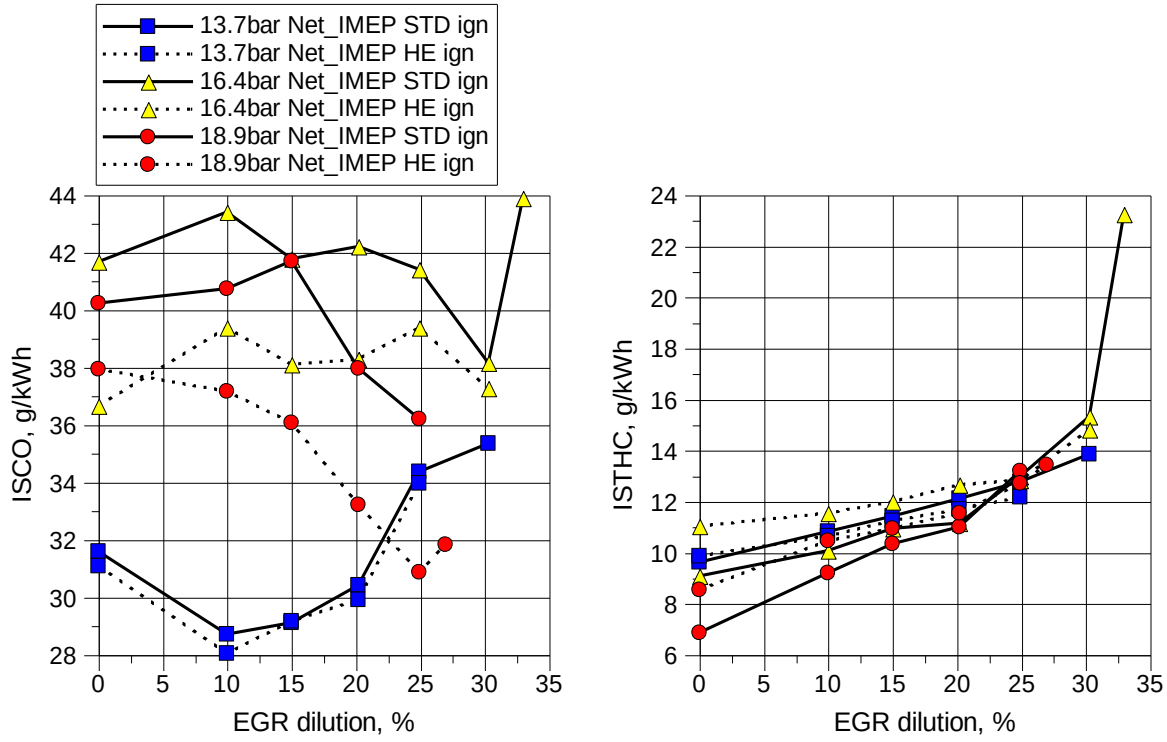

Figure 4-15 CO and THC emissions characteristics with EGR dilution and HE ignition introduction

In summary of the emissions results, the lower of combustion temperatures are confirmed by lower pre-TWC NO_x outputs. This is universal for all loads. The $ISNO_x$ decreased by a rate

of 4.5g/kWh for every 10% of EGR dilution introduced to the mixture. The lowest emission is 0.24g/kWh with 33% external EGR dilution. Thus, the maximum attainable effect of NO_x emissions is governed by the tolerated dilution percentage.

ISCO emissions fluctuated, and the characteristics due to EGR dilution differs between the loads. The sensitivity to load likely came from a change in trapped ER due to boost and wide valve-overlap. The highest ISCO is monitored at 16.4bar Net_IMEP with 51CAD of overlap, followed by the 18.9bar Net_IMEP case with 44CAD of overlap. Despite the higher boosting requirement for the 18.9bar Net_IMEP case, the shorter valve-overlap is restricting the short-circuiting and thus regulating the trapped ER towards stoichiometric than the 16.4bar Net_IMEP case. The fluctuation of ISCO values seen with EGR dilution comes from a combination of EGR effect towards combustion and changes to trapped ER. In the case of 13.7bar Net_IMEP, the highly lengthened combustion maybe combusting an underprepared mixture but the use of greater boost to accommodate the greater EGR dilution is also affecting the trapped mass ER.

THC emission increased with EGR dilution and trapped mass enrichment. Increased wall flame quenching effect from increased EGR dilution and O_2 deficiency is causing this increase.

4.4 Summary

The effectiveness of external EGR to lower the GTDi downsized engines fuel consumption at high load is presented and discussed. The successful combustion phase advancements prove the ability of external EGR to lower knock tendency. These effects are more pronounced at knock-limited combustion conditions, equating to advancements of CA50 by 4CAD with every 10% of external EGR dilution and worked with loads as high as 18.9bar Net_IMEP.

The EGR dilution results in slower combustion as seen by the analysed pressure traces and HRR trends. The slower combustion a combined effect of 1) increased inert gas concentration of air-fuel mixture and 2) combustion phased into the accelerated increase of cylinder volume stage (downstroke of the piston) where heat release rate tapers away. The latter decelerating effect can be mostly recovered by the advancement of combustion by keeping the combustion phasing closer to the TDC with lowered knock tendency, the bulk of combustion that takes place closer to piston TDC is accelerated due to the increased pressure conditions. This also leads to higher P_{max} values as EGR allowed more advanced ignition and combustion. Phasing advancements are limited to 16.4bar, and 18.9bar Net_IMEP cases as these are severely knock limited combustions. At 13.7bar Net_IMEP,

after 10% EGR dilution has phased the combustion optimally, the further elongated combustion due to slower flame propagation leads to advancements that began very early combustion into the compression stroke and finished very late into the power stroke. This has resulted in negative results.

The effectiveness of EGR to improve efficiency is highly dependent on the degree of deliberate combustion phasing delay due to knock mitigation. In such downsized engines, this has been found with higher loads (16.4 and 18.9 bar IMEP) at 2000rpm so that greater heat release required for the higher load does not lead to greater in-cylinder conditions (aggressive pressure/temperature climb) by using the greater expanding volume of lower piston position. Lowering the reactivity and temperature with external EGR diluted mixture during combustion permits earlier combustion and thus efficiency restores towards the optimal combustion phasing levels. This is accompanied by the slower combustion speed and ignitability, which prompts the need for even earlier ignition. At the load of 13.7bar Net_IMEP, the phasing is advanced to the optimal levels after 10% EGR dilution, but any further dilution requires earlier combustion (during the upstroke of the piston) and higher peak pressures with no real benefit.

The use of HE ignition system with expanded spark electrode gap has unlocked further phasing advances from stability improvement which allowed for further advancements and thus combustion speeds, and combustion speed improvements from a more powerful and large flame kernel production. The degree of improvements from each effect is not quantified, but theory and literature suggest the effectiveness of both effects.

The advanced phasing unlocked by the EGR dilution is considered as the primary reason for the efficiency gains. The gains are correlated with the phasing optimisations, and so the best results are seen with the highest load tested (18.9bar Net_IMEP) at 5.6% of BSFC improvement which extends to 7.9% with the use of HE ignition. The efficiency gains and phasing shifts observed due to EGR dilution are very comparable to similar studies using downsized engines.

Chapter 5 SFI EGR for downsized GTDI at boosted load operation

5.1 Introduction

The ability of EGR to lower knock tendency at boosted loads is evident from the results of chapter 4, this has also enabled greater efficiencies of the engine. However, two areas of concerns were reported 1) reduced combustion speeds due to inert gas fraction 2) increased instability due to difficulty of ignition with increased breakdown voltage and slower combustion speeds.

Reported in this chapter are the results of using stratified split injections with EGR dilution. Given the possibility to overcome the disadvantage of EGR dilution with split injection stratification, the two strategies are expected to be an effective engine strategy for optimised combustion phasing. The same engine and EGR system from the test used in chapter 4 are used for this investigation, some changes including fuel are present, but the use of an engine with proven positive EGR dilution response is important for this investigation.

The optimised stratified split injections are aimed at creating a stratified (and optimised) fuel/air mixture distribution near the spark electrode region and hence faster flame kernel development/propagation speeds than those of a homogeneous single injection strategy. Several advantages are expected, including -

1. A faster/weighted combustion towards the spray centre of the cylinder lowers knock tendency due to less time and energy availability on the end gas region.
2. A stable combustion condition: A rich region is easier for the early nascent flame kernel to propagate.
3. Lambda 1 operation can be sustained for TWC tailpipe emission control
4. Combustion mode can be switched from stratified lean-burn without the need for complicated control systems

The EcoBoost engine, amongst other modern downsized engines, has undergone many upgrades compared to the previous generations. This is because the degree of success of the downsizing ideology was dependent on the engine's tolerance to higher MEP operation and lowered knock tendencies. This has been achieved by implementing strategies which complement downsizing. Direct Injection is such a strategy that has lowered knock tendency by the introduction of charge cooling to the cylinder charge. It has also improved the fuel dosing accuracy compared to the previous PFI injection systems. The EcoBoost 1l engine has implemented the spray-guided multi-hole direct injection system. This injects a plume of fuel droplets at higher pressures pointing down towards the piston head from the engine head. Beyond this, the use of direct injection also unlocks the ability of injection events after

inlet valve closure, which is a limitation of port fuel injection. Due to this, multiple injection events with later injections are now possible for new mixture preparation strategies, without the need for any engine modifications. Split injection stratification is considered a suited strategy to such an engine set up.

Furthermore, with the combustion condition losses associated with EGR such as stability/ combustion speed/ ignitability, a well optimised stratified injection may unlock further EGR dilution benefits.

This chapter is focused on the study of the combustion phasing ability of such strategy named the SFI EGR combustion. It involves the analysis of combustion processes with and without EGR dilution and highlights differences in second injection effectiveness. The results are then linked to engine operating parameters such as combustion stability and efficiency to conclude the chapter.

5.2 Test condition

This is an experimental study designed to quantify the EcoBoost 1l engines ability to stratify the late injection for efficiency/performance benefits with and without external EGR dilution.

The timing and injection duration of the second injection must be optimised for such stratification to bring combustion benefits. This means a well-planned test of high-resolution sweep is vital to be able to identify the best combination of timings and quantities of split injections.

Two engine load points were chosen at 2000RPM to run the split injection sweeps. The details are as seen in Table 5-1, and global setting details also extends to Table 5-2.

Table 5-1 base static test condition set for second injection sweep

Net_IMEP, bar	13.7	16.4
ST, aTDC	-11.5	-6.6
IVO position, aTDC	-26	-27
EVC position, aTDC	27	24
Injection pressure, bar	120	128

Table 5-2 Global test condition set for investigation 2

Lambda setting	Exhaust UEGO setting=1 (stoichiometric)
Engine speed, RPM	2000
Start of first injection, aTDC	-299
Variable Oil Pressure	high
Inlet temperature, °C	30
EGR reintroduction temp, °C	60

The variables of the test are detailed in Table 5-3. With all the variables considered, eight sweep tests are required to investigate all cases. The injection ratio is a test parameter added as a key optimisation parameter identified by the literature review. A longer weighting for the first injection leads to a higher, more dispersed distribution of fuel within the cylinder, where a longer second injection leads to a greater concentration of fuel at the point and timing of injection. The dynamics of the in-cylinder condition and injection timing and duration are highly sensitive to each other, this promoted the need for such a parameter, despite a large addition to test points.

The two loads chosen were carried over from the tests performed in Chapter 4. 13.7bar Net_IMEP represents a WOT condition with minimum boost demand whereas 16.4bar Net_IMEP represents a mildly boosted condition, both conditions are significantly knock limited at reference condition. The two loads were chosen for their ample boost limit availability and greater engine safety margins when considering novel testing conditions, hence tests of highly boosted conditions were omitted from following tests.

Table 5-3 Controlled variables for stratified injection testing

Variable type	values	Factors
Load Net_IMEP, bar	13.7, 16.4	2
EGR dilution rate, %	0, 10	2
Injection ratio (by duration)	70:30, 80:20	2
second injection position, aTDC	-250- 50 (resolution 25CAD)	(up to) 9

5.3 Results and discussion

5.3.1 Combustion phasing with dual injection SFI and EGR

The results in this section will be presented in the form of graphs in Figure 5-1 in order to include a high number of variables to plot. Every line seen on a graph is a sweep of ‘end of second injection’ position (EOI2) in CAD aTDC. The EGR dilution and split ratio are fixed for each sweep. For every sweep, the first data point on the far left seen at EOI2= -299CAD aTDC is the single-injection result and is included as a reference for comparison. The test sweep progresses along the x-axis of the graph, indicating the result of the test points as

EOI2 is retarded. The two key variables are represented by the line properties as detailed in Table 5-4. Engine load in Net_IMEP is marked on the graph.

Table 5-4 chapter graph presentation explained

Variable	Distinguished by	Variable value	Representation
EGR dilution	Line type	0%	Solid line
		10%	Dotted line
Split ratio	Colour	70:30	Red
		80:20	Blue

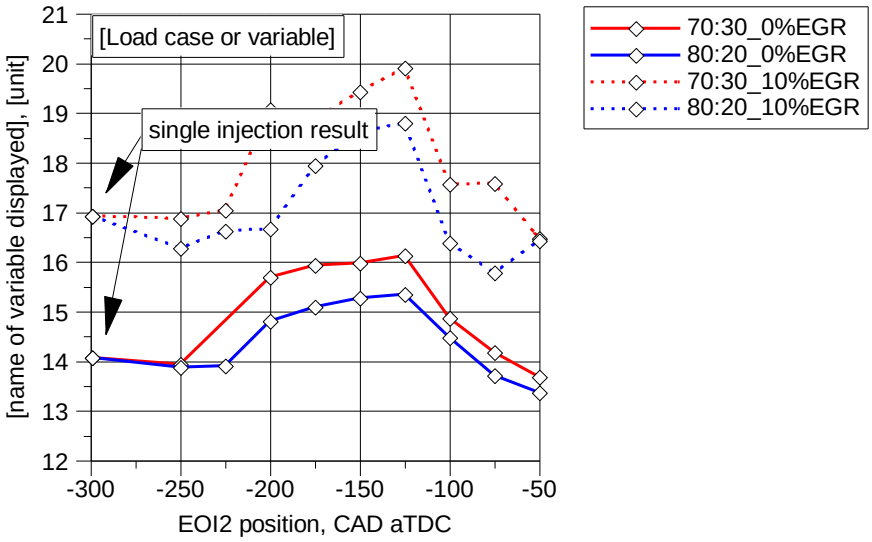

Figure 5-1 Example of a graph used for results presentation. Colour: Split ratio, Line time: EGR dilution %.

As all testing is performed at 2000RPM, the impact of split injection stratification to influence the combustion is quantified by CAD of set percentage burn positions. 'Initial burn' defined as the duration between ST to CA10, is an indicator of how the stratified second injection is able to create a faster burn region around the plug electrodes, indicated by a shorter burn duration than the single injection case. The resulting main burn duration (CA10 to CA90 CAD duration) is compared with the CA50 position for an overall effect analysis of the stratified second injection effectiveness.

Figure 5-2 is a graph of ST to CA10 (initial burn) duration. The dominant portion of the tested range results in a slower initial burn duration. In all cases, the longest initial burn is seen when EOI2 is positioned at -150CAD aTDC. The trend is almost symmetrical from this point, and the exception is the improved speeds seen at EOI2=-225CAD aTDC, especially at 16.4bar Net_IMEP with 80:20 split ratio and 0% external EGR dilution. The characteristic is very similar for all cases.

Use of external EGR has a negative effect on the initial burn duration. The deceleration of combustion has added around 3CAD to the initial burn stage duration.

In general, there is a steady favour towards an 80:20 split ratio where a few test cases have indicated a faster initial burn speed in comparison to the single injection case.

At 16.4bar Net_IMEP, 1 point has shown a clear result of an accelerated initial burn, this is seen with an 80:20 split ratio with no EGR dilution. It can be assumed that an ideally rich region has been successfully placed around and between the spark electrodes, creating a faster initial burn. Such quick successions in the split injection are associated with fuel penetration reduction, which might be improving the mixture [152].

Additionally, some cases of EOI2=50CAD aTDC show a great recovery of initial burn speed at 13.7bar Net IMEP.

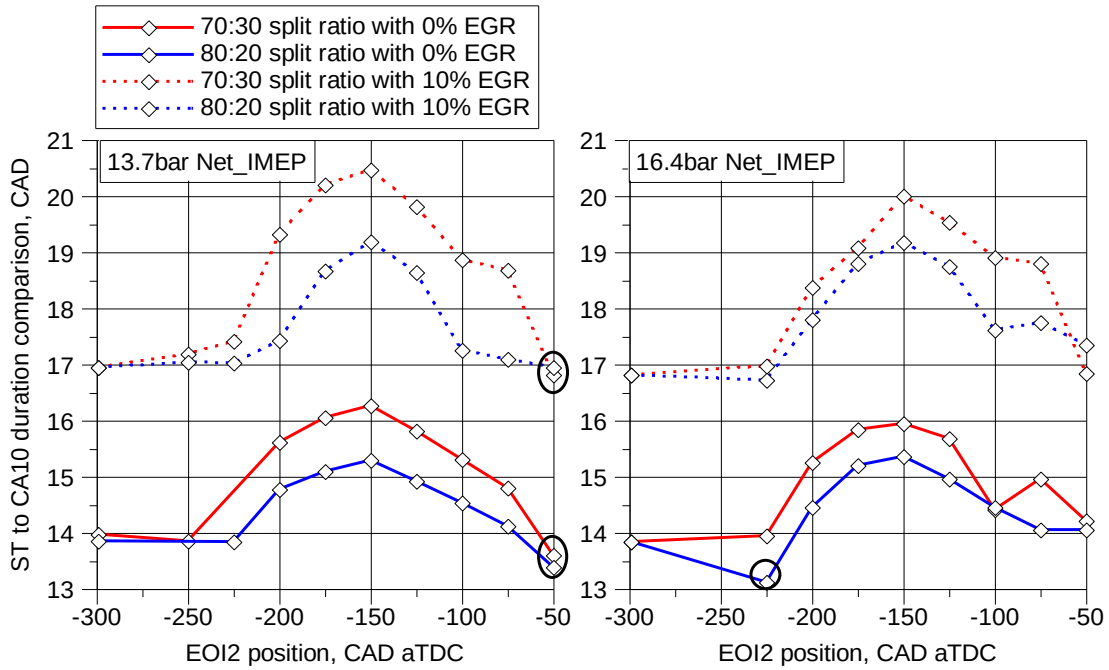

Figure 5-2 ST to CA10 crank angle duration, compared by second injection timing

Next, the combustion phasing and main combustion duration are analysed, and their relation to initial burn durations are discussed. Figure 5-3 plots the combustion phasing, as indicated by CA50 for both loads that were tested. For 13.7bar Net_IMEP, a very different characteristic is seen between the EGR dilutions. With 0% EGR dilution, the phasing is delayed until the second injection is positioned to EOI2=75CAD aTDC. This does, however, show the desired combustion phasing beyond this point, resulting in a maximum phasing advancement of 1.5CAD. With 10% EGR dilution, the CA50 acts erratically but around the 13CAD aTDC mark until EOI2 is positioned -100CAD aTDC, where the CA50 suddenly advances up to 3CAD beyond single injection levels. The overall combustion duration results

show a steady slowdown trend as EOI2 is delayed. After EOI2=-150CAD aTDC, the 80:20 split ratio cases show a favourable turn. These results indicate that split injection may have led to the adverse combustion flame propagation condition in the cylinder at many of the test points.

Figure 5-3 shows the corresponding results at 16.4bat Net_IMEP load. Combustion duration characteristic is very similar to the 13.7bar Net_IMEP case. There is a progressive slowdown of the combustion duration with a small advantage for the 80:20 split ratio for slightly faster combustions.

In terms of the CA50 positions, there is a unique trend. The mixture of EGR dilution and split injection has a drastic delay effect. Without EGR, the combustion process is mostly accelerated with a split injection limited to the 80:20 split injection case. At EOI2=-50CAD aTDC, the CA50 is advanced by more than 3CAD.

Despite the change in combustion phasing and peak heat release, the bulk combustion burn duration was similar between the two loads, the characteristic response to split injection were also shared which suggests that the KLSA condition is reflected closely to this parameter.

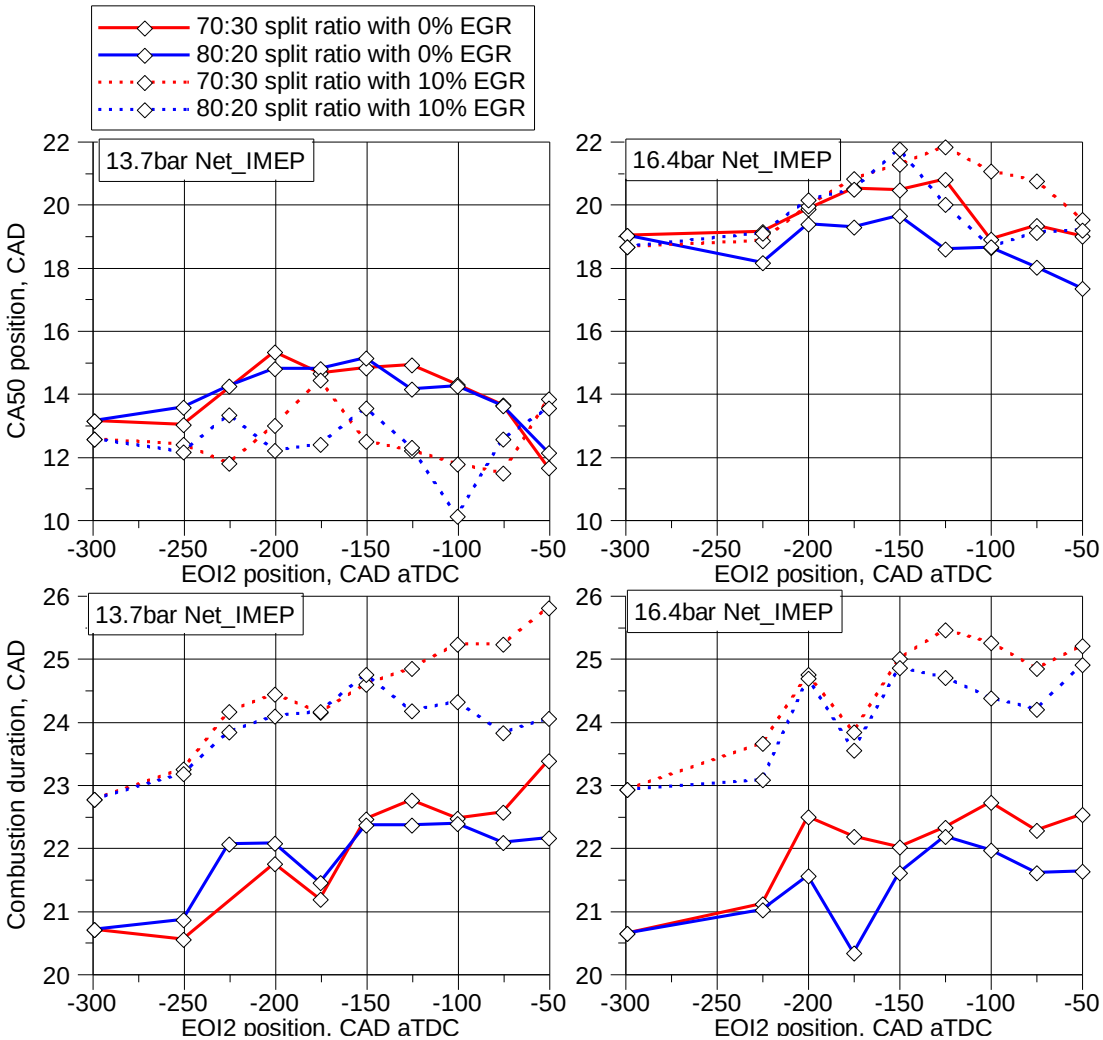

Figure 5-3 CA50 position and CA10-CA90 (bulk burn duration) with a sweep in EOI2 position

It should be noted that the advancements of the ST are knock limit for all test points. Figure 5-4 shows the changes in the KLSA with SFI EGR compared with the single injection case. Any positive number here indicates a delayed ST.

In the case of 16.4bar Net_IMEP, splitting the injection allows a 4-5 CAD advancement of KLSA in comparison to the single injection with no EGR dilution. However, these advancements do not lead to the advancement of combustion phasing, meaning the extra advancements made here are simply a recovery of combustion deceleration. The presence of EGR removes the advancement of KLSA with split injection at most EOI2 positions. At 13.7bar Net_IMEP, split injections have little effect on KLSA with the 80:20 split ratio while the 70:30 split ratio leads to KLSA retard. The introduction of EGR caused noticeable advancements of KLSA, peaking at EOI2=-150CAD aTDC.

Overall, the use of EGR had enabled a further 4.5CAD advancement from the single injection case, but further advancements were also made available with split injection.

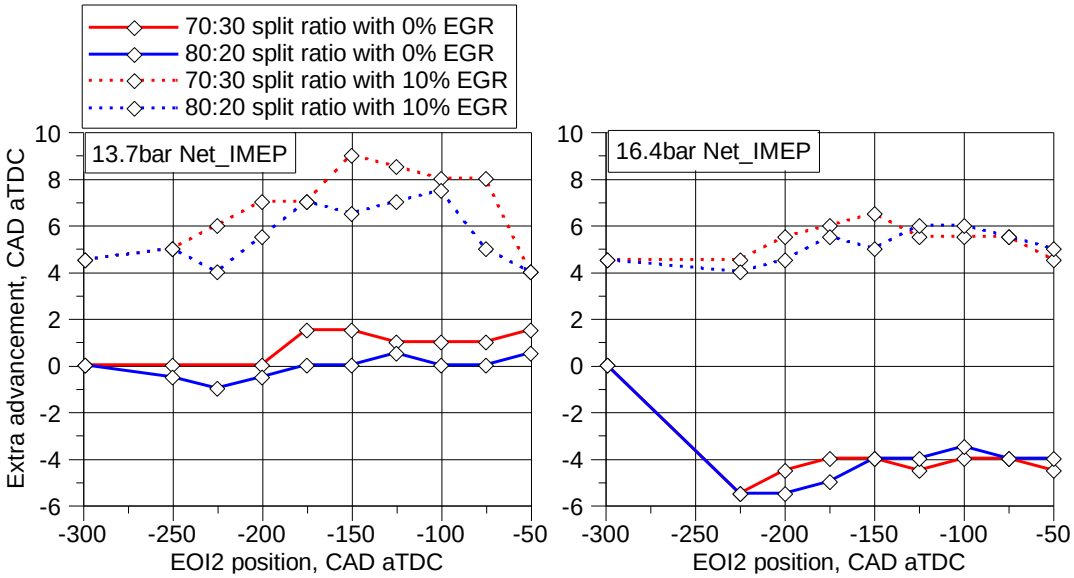

Figure 5-4 ST advancements through dual injection compared to a single injection case

5.3.2 Further analysis of heat release rates

Further analysis of HRR can be made by evaluation of the ribbon spectrum type plot seen in Figure 5-5 and Figure 5-6.

Every vertical ribbon is the HRR of a split injection operation, and the colour represents the value of HRR at a given crank. The warmer colour indicates a higher heat release and the deep red represents the highest value.

At 13.7bar Net_IMEP and 0% EGR, the delay of combustion phasing between EOI2=-200 to -100 CAD aTDC is most pronounced, this is more noticed at the 70:30 split ratio where the majority mixture will be leaner with a higher concentration factor. For the cases with 10% EGR dilution, the combustion phasing is arbitrary but can be seen to be earlier than the single injection case. It is hard to distinguish the degree of combustion phasing shift, but the most pronounced advancement is seen at the 70:30 split ratio at EOI2=-200CAD aTDC and 80:20 split ratio at EOI2=-100CAD aTDC (circled black on the chart). At EOI2=-50CAD aTDC, it is also seen that the use of EGR is less favourable for every second injection times (circled in green and red on the chart).

At 16.4bar Net_IMEP cases, a more certain combustion trait is seen at the split injection case of EOI=-225CAD aTDC. This indicates a minimal level of stratification occurring but combusting with a near homogeneous condition. This is also observed under EGR diluted condition and becomes more noticeable with the 80:20 split ratio. Otherwise, no noticeable trends are recognised by analysis of the HRR ribbon charts, indicating a very stable combustion phase that is not affected by stratification.

The combustion process is found to be phased very late for the 16.4bar Net_IMEP case with 10% EGR dilution with one case of burn still occurring at 40CAD aTDC, this slow and late combustion caused by knock mitigation may cause stability and combustion efficiency penalties.

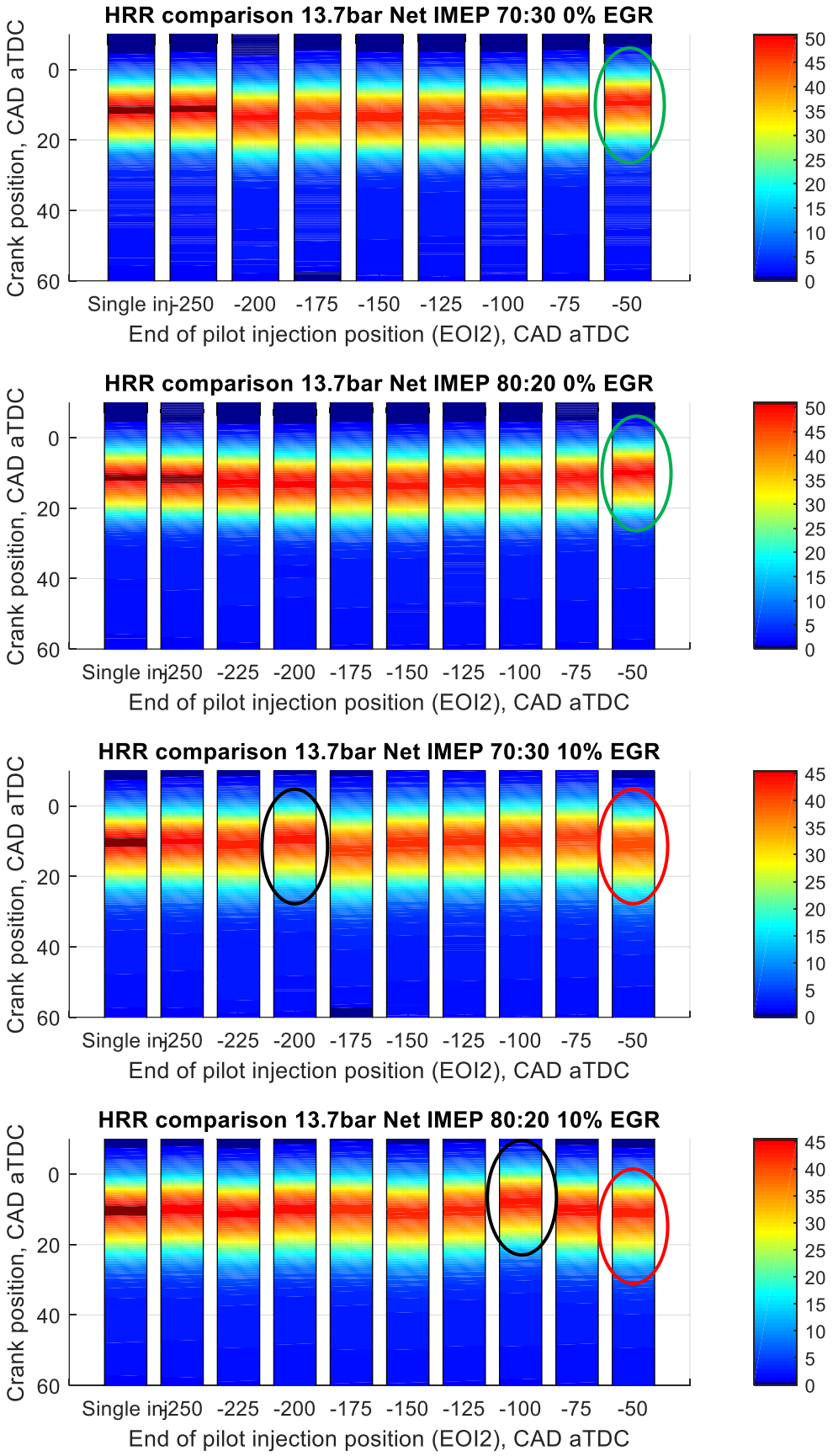

Figure 5-5 HRR profile by crank position for all cases of 13.7bar Net_IMEP. Comparison of the red and blue circle reveals the increased stratification opportunity at this load

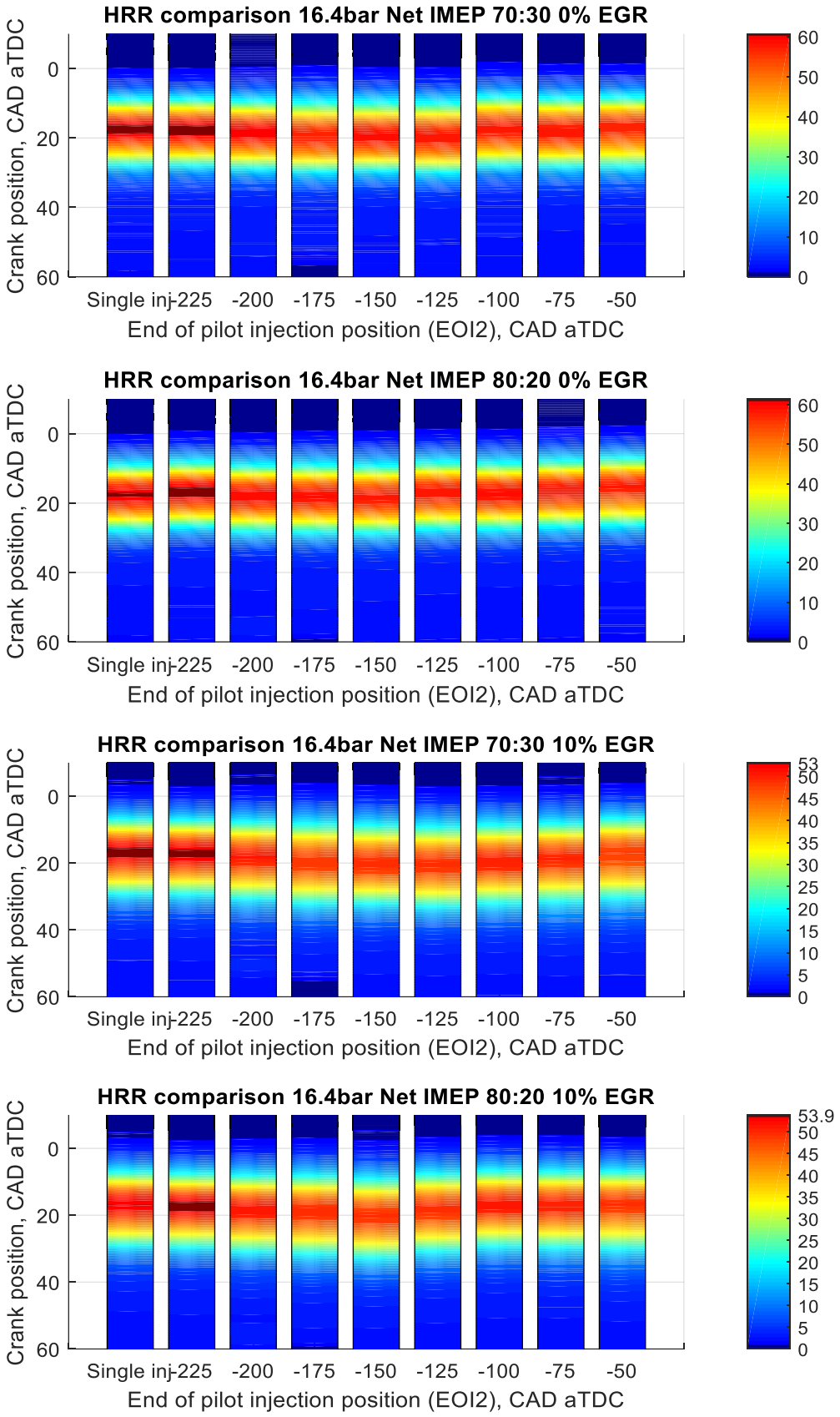

Figure 5-6 HRR profile by crank position for all cases of 16.4bar Net_IMEP.

5.3.3 Efficiency and other notable effects from SFI EGR

This sub-section will discuss the effect of split injections on engine efficiency and fuel consumption.

Figure 5-7 shows the results for ISFC and BSFC for all sweeps performed. At 13.7 bar Net_IMEP, the split injections led to increased fuel consumption as the second injection is introduced, and the phasing was retarded. When EGR is introduced, the ISFC and BSFC values decrease to a minimum with the second injection phased at -200CAD aTDC before the value rises and exceeds that of the single injection with the majority of the retarded second injection settings. The lowest ISFC and BSFC are seen at EOI2=-100CAD aTDC (80:20 with EGR) which can be attributed to successful phasing shift of split injection. Without EGR, the engine returned an overall negative effect on efficiency with split injection, the same can be said for the combustion phasing as seen in CA50 results. ISFC deteriorate rapidly after EOI2≥-75CAD aTDC, however, no apparent signs are seen in combustion phasing to explain this phenomenon, which suggests impingement or piston wetting from very late injection with high penetration which is a widely reported issue of near TDC injection [126].

The ISFC values fluctuate more at 16.4bar Net_IMEP with values below and above that of the single injection case, as the second injection is retarded. Minor efficiency gains are achieved at EOI2=-225CAD aTDC, except for 70:30 split ratio with EGR dilution (arrowed ‘1’ on the figure) due to ignition delay to mitigate knocking combustion. Further delay in EOI2 leads to high ISFC until EOI2 = -125CAD aTDC, when some degree of fuel stratification may have existed. Worst fuel economies are always seen with very late second injections.

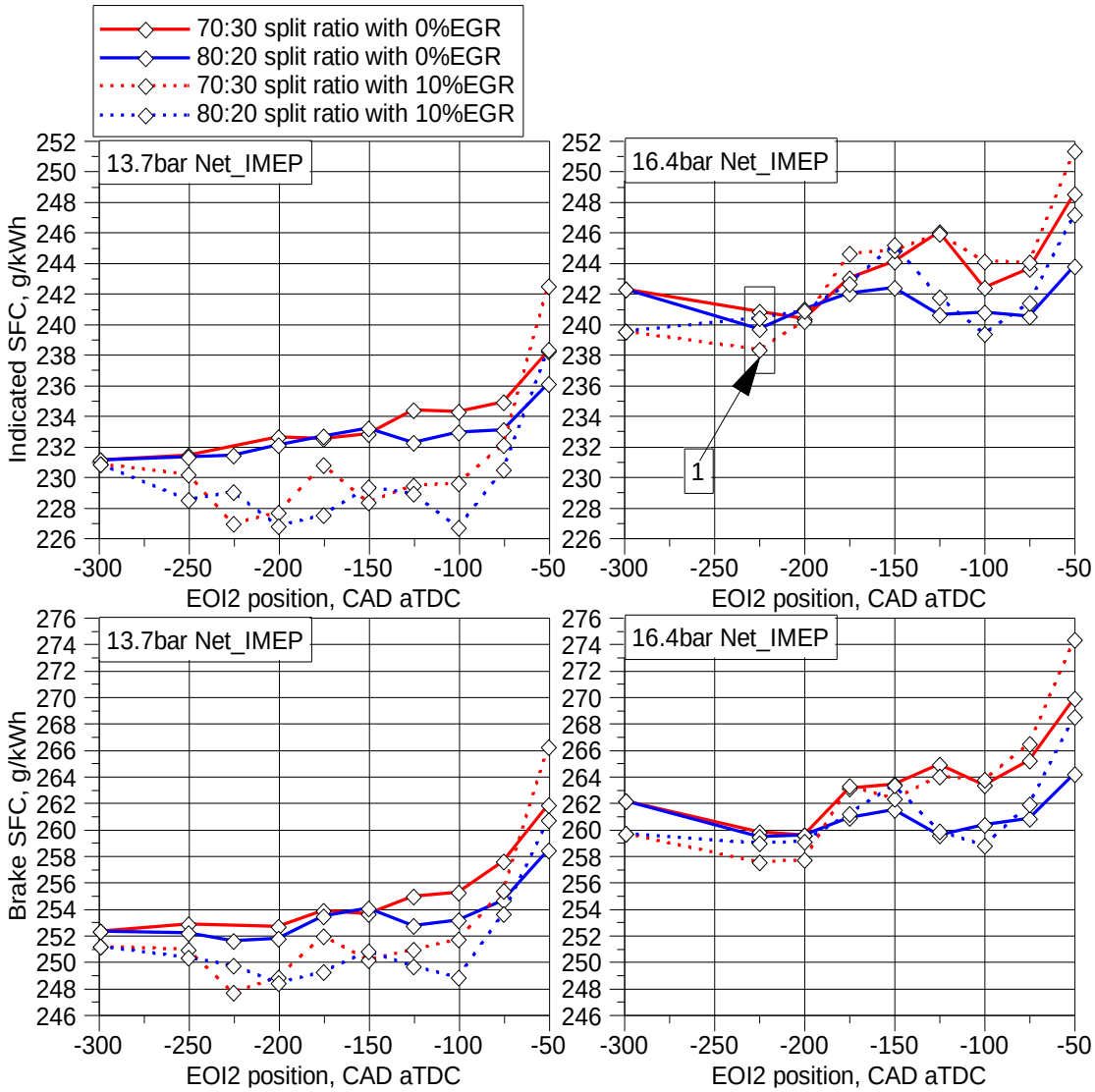

Figure 5-7 Indicated SFC and Brake SFC with the sweeps of EOI2 and single injection case

The combustion stability analysed over N=300 samples are shown in Figure 5-8. Very different characteristics are seen for the 16.4bar Net_IMEP case with EGR dilution; under these conditions, the combustion is less stable than the other cases. A degree of stratification benefit may have led to a small recovery of stability at EOI2=-100CAD aTDC. This stratification benefit is supported by combustion phasing results reported earlier in the chapter, and the overall instability can be attributed to the late phasing observed in the HRR charts of Figure 5-6. The combustion phasing for the higher load points are very late to avoid the onset of knock; this also promotes instabilities as the combustion takes place during the expansion stroke.

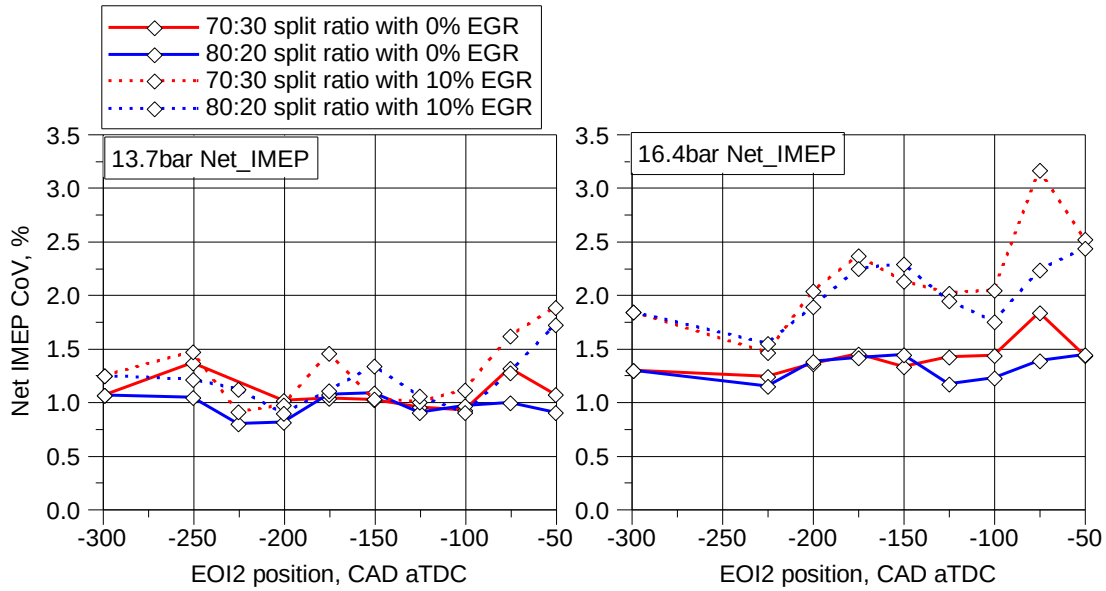

Figure 5-8 Combustion stability (CoV Net_IMEP) with a sweep of EOI2 and single injection case

The resulting inlet pressure (MAP) required to sustain the load is shown in Figure 5-9. MAP increases gradually as the EOI2 is retarded, this is a direct result of loss in engine and combustion efficiency. Inefficient combustion occurred from reduced mixture preparation time; as a result, more fuel and air is required to maintain the load. The gradual increasing trend suddenly diverts with the cases of EOI2=>-75CAD aTDC. This effect is larger with EGR dilution.

At 16.4bar Net_IMEP, the required MAP is noticeably lower for the 80:20 split ratio. From the ISFC results, it is evident that the 80:20 split ratio is favoured for efficiency and required less fuel.

The use of a higher MAP by increasing boost demand has also caused minor increments in P_{drop} across the inlet to exhaust manifold. The averaged pressure difference is also plotted in Figure 5-9 bottom chart. Due to the low requirement range of the boost at 13.7bar Net_IMEP, the P_{drop} characteristic is not found to be stable, but a subtle increasing trend can be noticed.

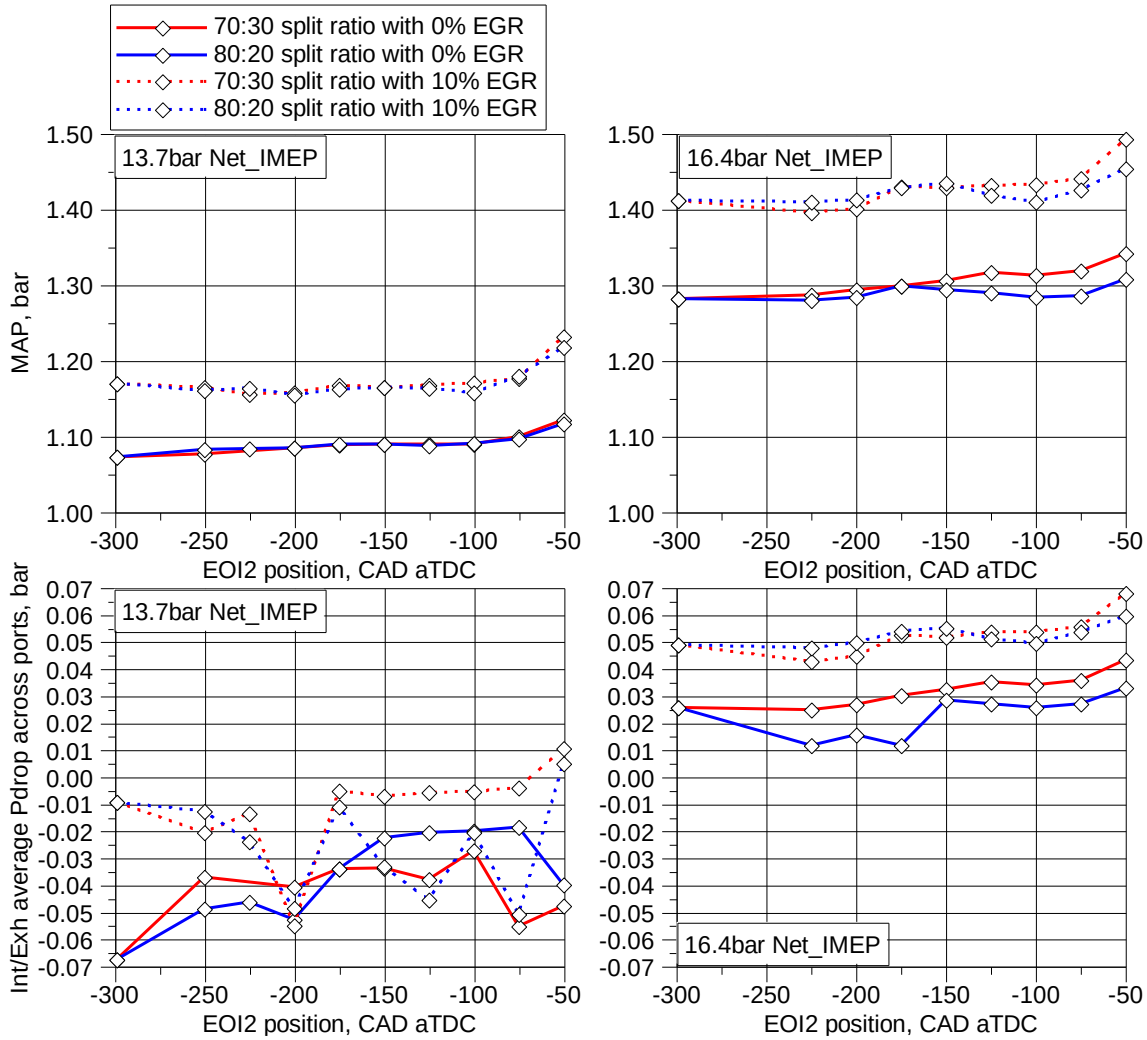

Figure 5-9 MAP with the EOI2 sweeps of and single injection case

The combustion efficiency comparison with split ratio and EGR dilution rates are as seen in Figure 5-10. Overall, there is a fluctuation of around 1% in combustion efficiency with all the split injection sweeps performed. A continuing trend that is noticed is the slightly lower combustion efficiency that persists with 70:30 split ratio. This can be seen for EOI2 after -175CAD aTDC repeatedly. Combustion efficiency is improved with the most retarded second injection timing at 16.4bar Net_IMEP, where the values rose to above 95% without EGR dilution.

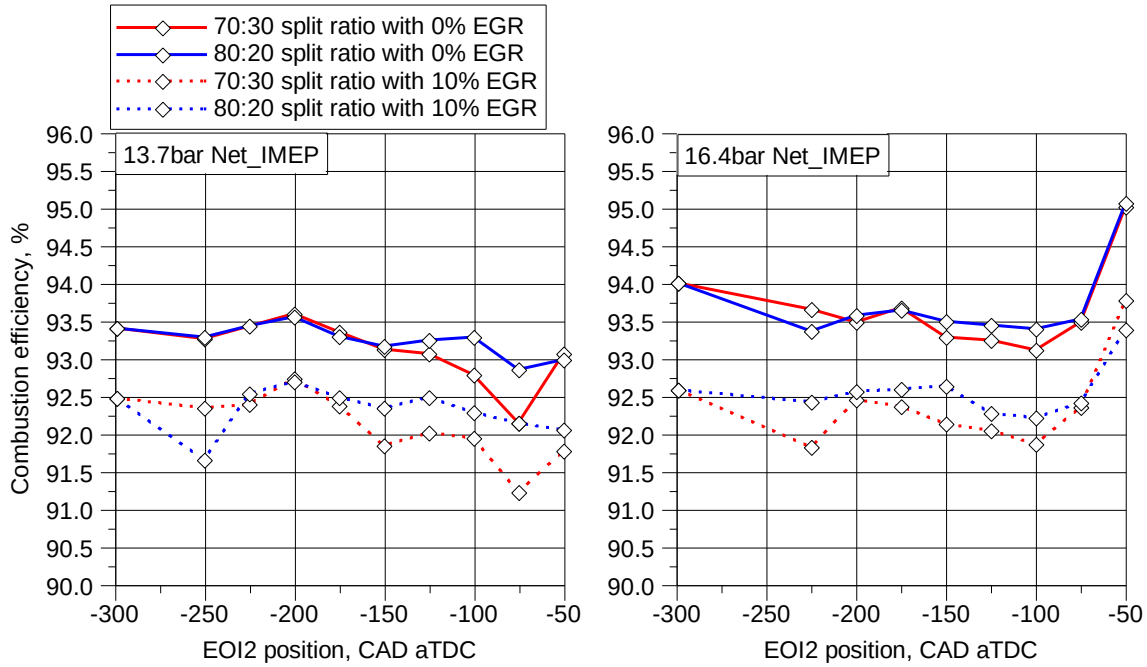

Figure 5-10 Combustion efficiency comparison at split injection using external EGR dilution

5.3.4 Effect of split injections and EGR on exhaust emissions

ISTHC and ISCO emission are as seen in Figure 5-11. For ISTHC emissions, all cases have a similar characteristic where specific emissions gradually rose before dropping to the lowest values at EOI2=-50CAD aTDC (the latest second injection). Throughout the sweep, higher THC emissions are observed with EGR dilution because of slower burn rate and lower combustion temperature. At both loads, 80:20 split ratio injections produce slightly fewer THCs than the 70:30 split ratios as the likelihood of producing undermixed fuel-rich mixture is reduced by the reduced amount of fuel in the late second injection.

Compared to the THC results, CO emission concentration differs significantly between the loads. Two factors are considered to contribute greatly to these results: 1) insufficient mixing from the retarded second injection 2) lower in-cylinder AFR with exhaust lambda=1. The insufficient mixing increases as the second injection is retarded towards TDC as shown by the results after EOI2>-100CAD aTDC. When the load is increased to 16.4bar Net_IMEP, positive air scavenging takes place during the valve-overlap period when the intake pressure

becomes greater than the exhaust pressure. By keeping the exhaust lambda sensor to 1, the short-circuited air/O_2 in the exhaust will lead to lower in-cylinder AFR mixture.

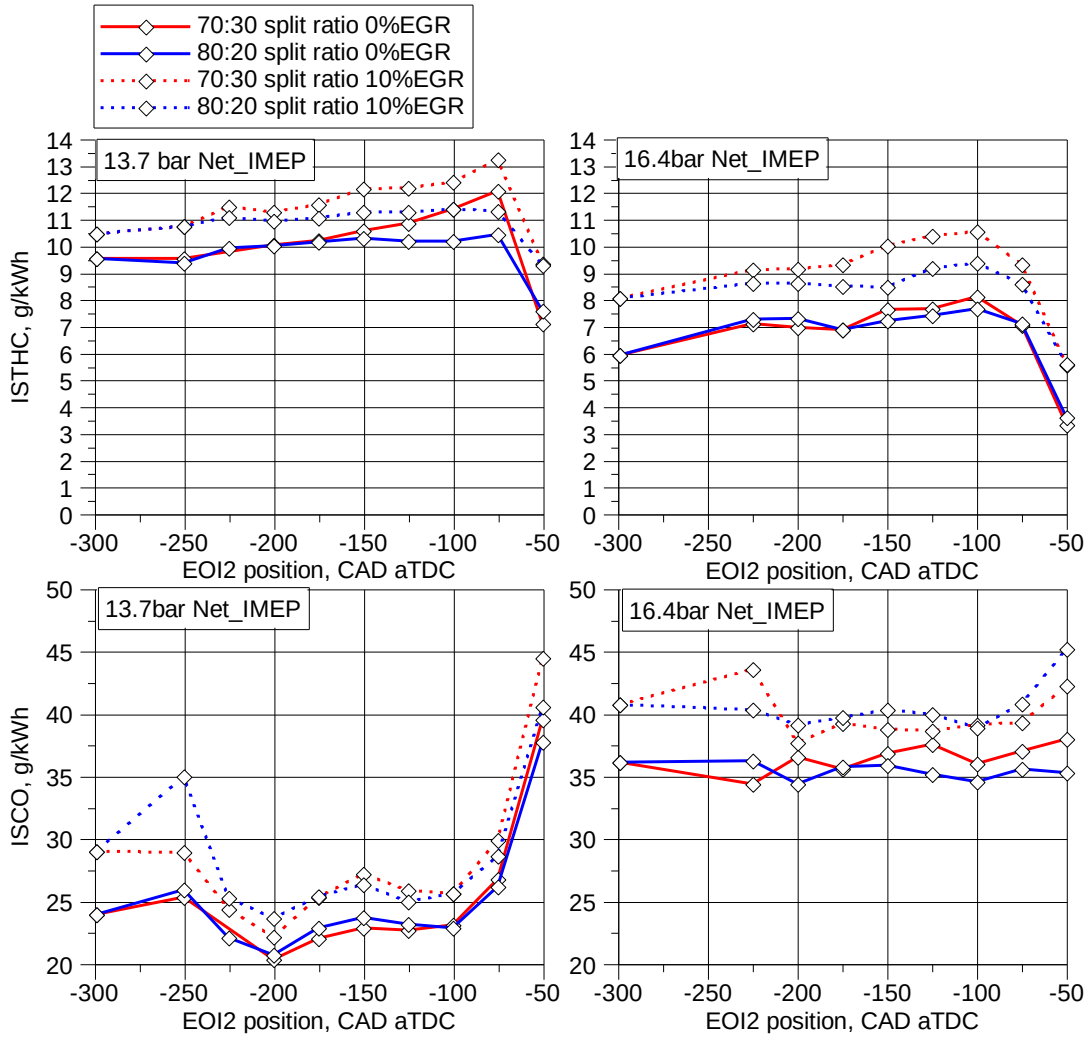

Figure 5-11 Specific emissions of THC and CO in comparison to single injection case with EGR at two different loads

The O2 emissions shown in Figure 5-12 reflect the THC and CO emissions for almost all cases. However, at the 16.4bar Net_IMEP, the O2 concentration remains almost constant and drops at EOI2=-50CAD aTDC. In comparison, at the 13.7bar Net_IMEP case, the O2 emissions increase significantly when the second injection is retarded beyond -100CAD aTDC in a similar way to the CO emissions, which indicates the occurrence of incomplete combustion caused by under distributed mixtures.

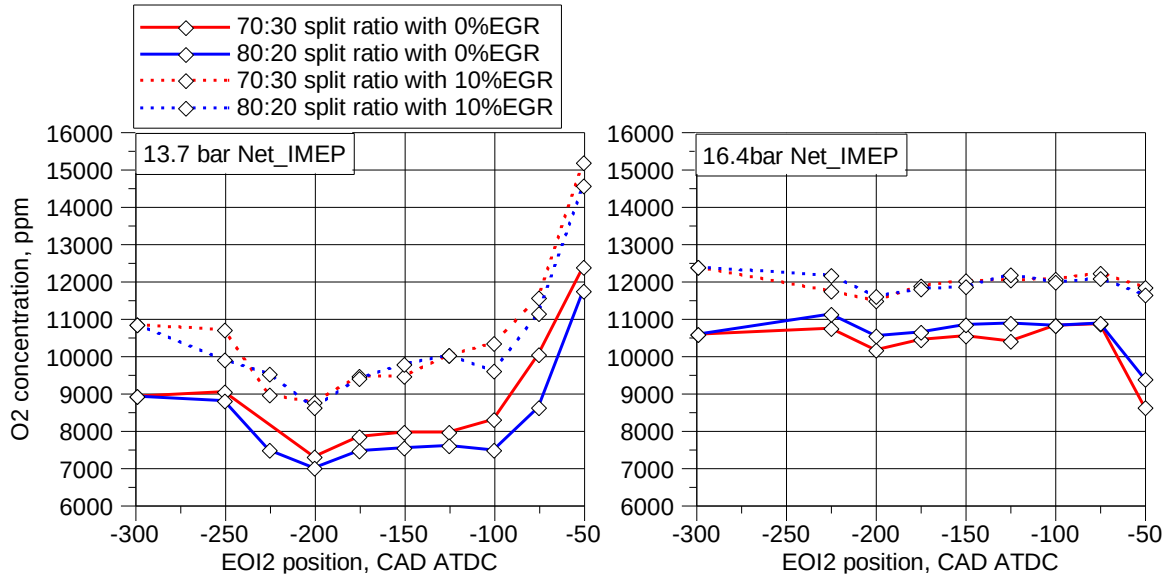

Figure 5-12 O2 emission concentration with sweeps in EOI2 timing

ISNO$_x$ results are shown in Figure 5-13. The addition of EGR reduced ISNO$_x$ emission by more than 50%. For all cases, a fall of ISNO$_x$ emissions value can be seen by a very similar factor at EOI2=-50CAD aTDC when fuel-rich combustion had taken place.

While the differences are subtle, points such as EOI2=-200CAD aTDC @13.7bar Net_IMEP and EOI2=-100~-75CAD aTDC, a small increase of ISNO$_x$ can be seen. This can be attributed to the increase in combustion temperatures due to a combination of earlier and thus faster burn of the mixture.

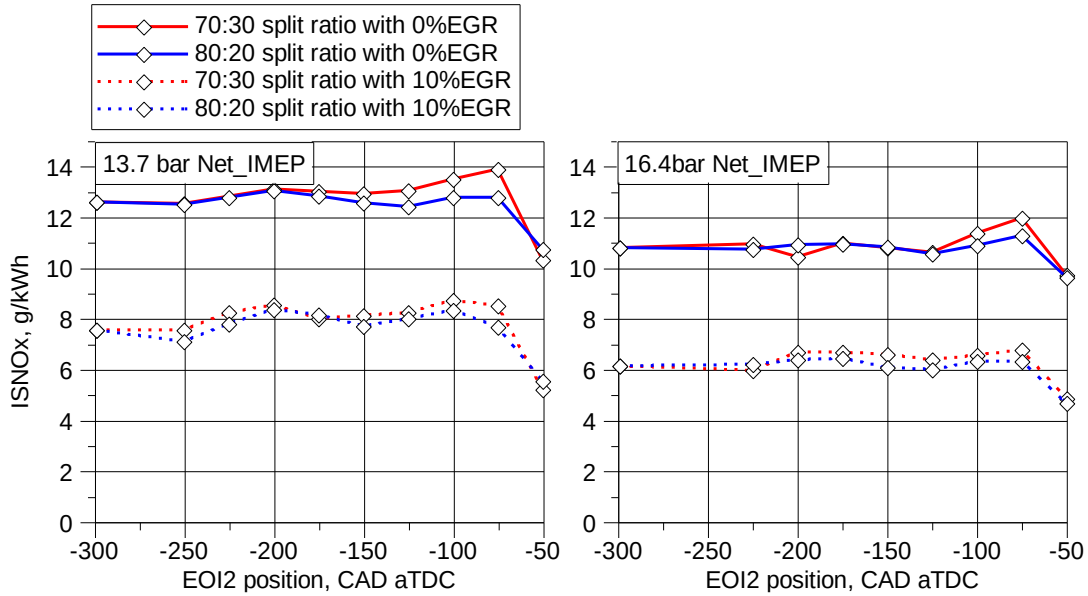

Figure 5-13 NO$_x$ emission concentration with sweeps in EOI2 timing

Finally, the exhaust temperatures as it enters the TC are seen in Figure 5-14. Such results are of interest when implementing new strategies due to the importance of TC component

temperature limitations. The use of EGR dilution has an averaged exhaust temperature reduction of 46C at 13.7bar Net_IMEP and 42C at 16.4bar Net_IMEP. The temperature fluctuations can be seen to be a direct effect of later combustion, where higher and later heat release leads to hotter exhaust gases. As a result, a peak of exhaust temperature can be seen at EOI2=-175CAD aTDC, where a higher peak can be seen through the HRR profile chart of Figure 5-6. At 16.4bar Net_IMEP case, a tendency was seen for the 70:30 split ratio to exhibit hotter exhaust temperatures with later EOI2 timings. Finally, overall temperatures rise after EOI2=-75CAD aTDC. The later combustion phasing at these loads may be forcing late heat additions that are undetectable by pressure rise due to the cylinder volume increase which explains the extremely low efficiencies.

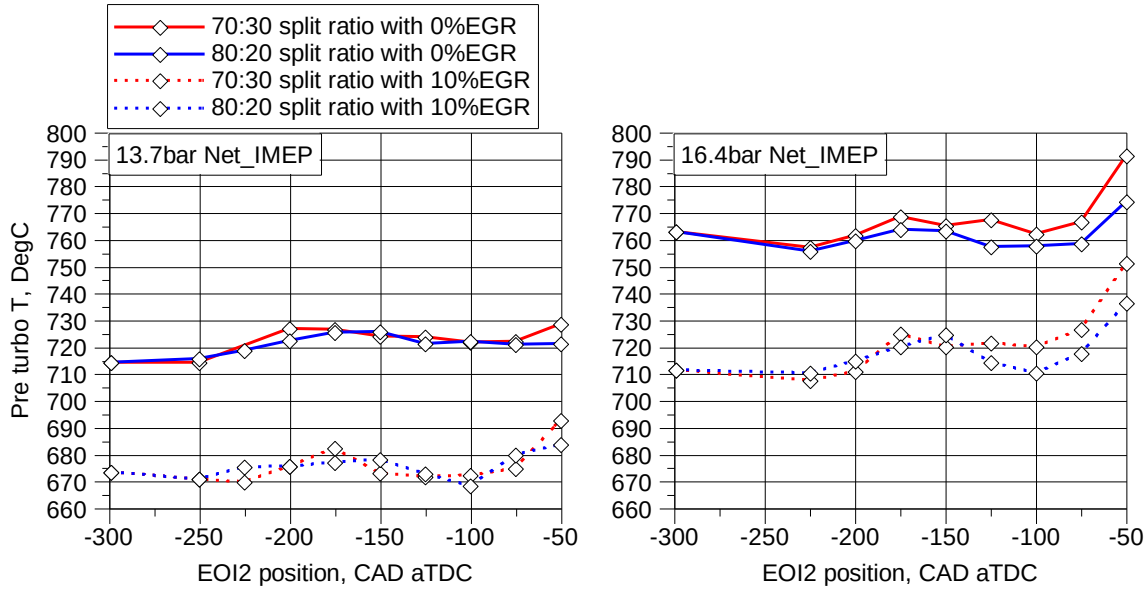

Figure 5-14 Pre-turbine exhaust temperature sweep of EOI2

5.3.5 3D CFD results for stratified condition analysis

3D CFD simulation was performed to understand the effects of EGR dilution and split injection. Comparison of fuel/air Equivalence Ratio (ER) distribution in the cylinder is made and further analysed with the processed combustion phasing and efficiency results. The analysis focuses on the distribution and concentration region within the cylinder as well as the equivalence ratio at the ignition source near TDC due to the importance of ER between the electrodes for a fast early flame propagation [29].

5.3.5.1 Effects of EGR dilution

Figure 5-15 shows the fuel enrichment distribution by equivalence ratio at the end of compression. Both cases are single early injection and compare the mixture distribution between 0% (reference) and 10% EGR dilution.

EGR dilution was found to affect the mixture distribution at ST. Single injection case had a significant stratification of fuel enrichment around the plug electrodes with defined lean regions. Combustion of such a mixture is associated with slower combustion due to over enrichment and lean pockets.

A more homogenous mixture that was seen with 10% EGR dilution and the lean pockets near the walls were reduced. The demand for extra boosting due to EGR dilution had enhanced the flow motion which resulted in the greater homogeneity mixture at ST.

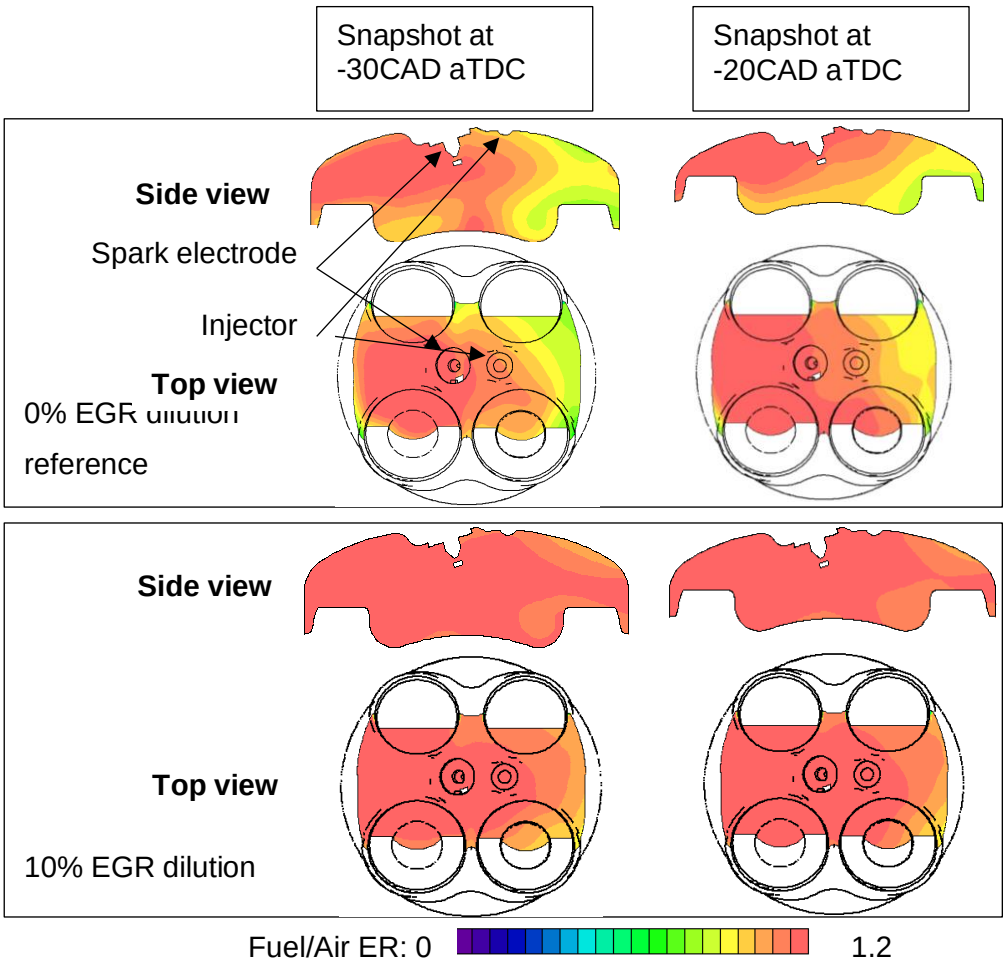

Figure 5-15 CFD simulation data, cross-sectional view of in-cylinder Fuel/Air ER during compression near TDC, comparison between 0% and 10% EGR dilution using single early injection at 13.7bar Net_IMEP.

5.3.5.2 Observations of late split injection effect

Figure 5-16 shows the fuel spray penetration within the cylinder, which is visualised by CFD simulation. The multi-hole injection is targeted for full cylinder coverage, and the spray formation is optimised for early injection with long penetration length, and late injection that occurs after intake BDC of the crankshaft is causing impingement that prevents effective evaporation and crevice loss. Thus, late wall wetting leads to crevice loss as the piston rings 'collected' the wet fuel from the wall during the upstroke, causing pool fire during combustion after the piston travels back down to reveal the fuel with some lost in the crevice as blow-by. A later second injection caused a full piston impingement as the piston would be at a higher position, leading to a reduction of crevice loss and increase of pool fire burn.

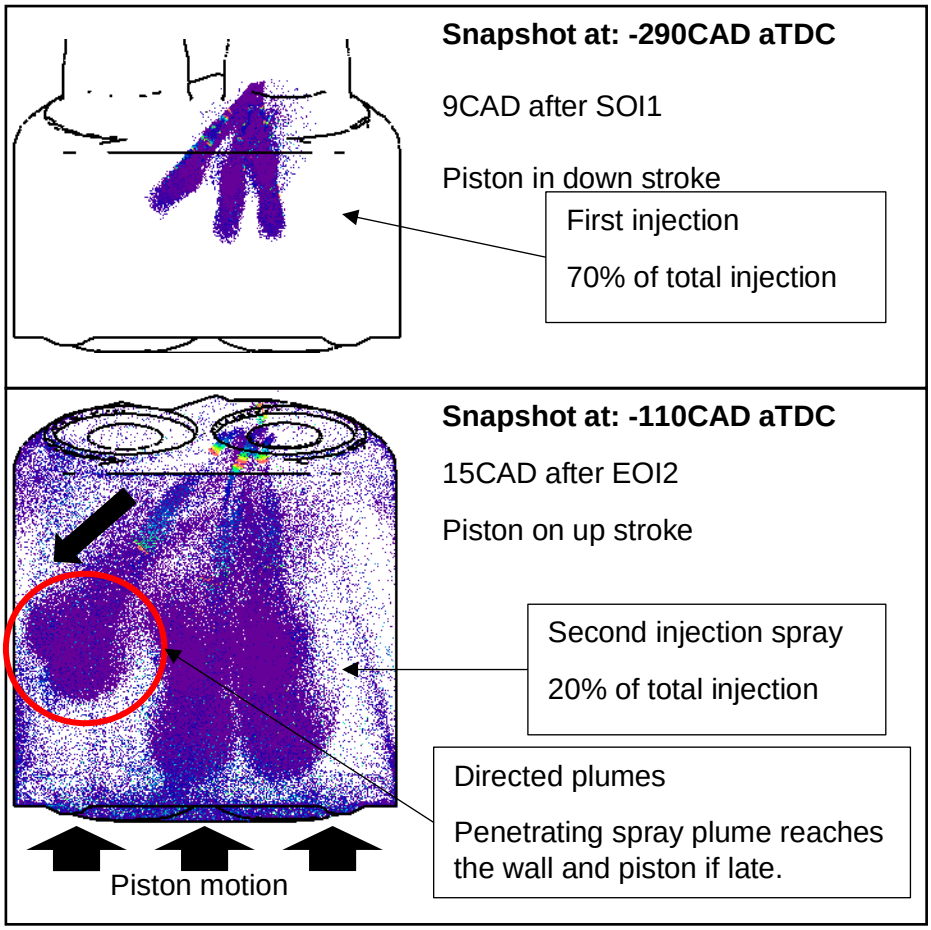

Figure 5-16 CFD spray trajectory visualisation, the late second injection has the potential to increase fuel loss to crevice due to high penetration of multi-hole direct injection. Example case with EOI2= -125CAD aTDC, 70:30 split ratio.

This is likely to cause very uneven enrichment and is thought to be the cause of very slow combustions with 70:30 injection ratio and late EOI2 timing. Increased inlet pressures from EGR dilution is likely improving the mixing to lower the negative effects of the late injection.

5.3.5.3 Effects of split injection at 13.7bar Net_IMEP

Mixture distribution created by a split injection strategy is shown in Figure 5-17. The split injection caused a slower combustion phasing compared to single injection according to the CA50 data. The split injection did not change the overall mixture distribution from a single injection case, the ratio of split injection is weighted towards the first injection, and thus the overall distribution is found to be the same. Subtle differences were seen, including the ER between the spark at ST. The ER is more fuel-rich with the single injection, which may have created a faster initial flame propagation; this finding agrees with the ST-CA10 combustion duration data in Figure 5-2. A more dispersed mixture is observed with a split injection. While this may lead to faster combustions by avoiding areas of over-enrichment and lean pockets, the shorter time avail for late injection droplets to evaporate may have resulted in the overall loss of combustion speed and efficiency.

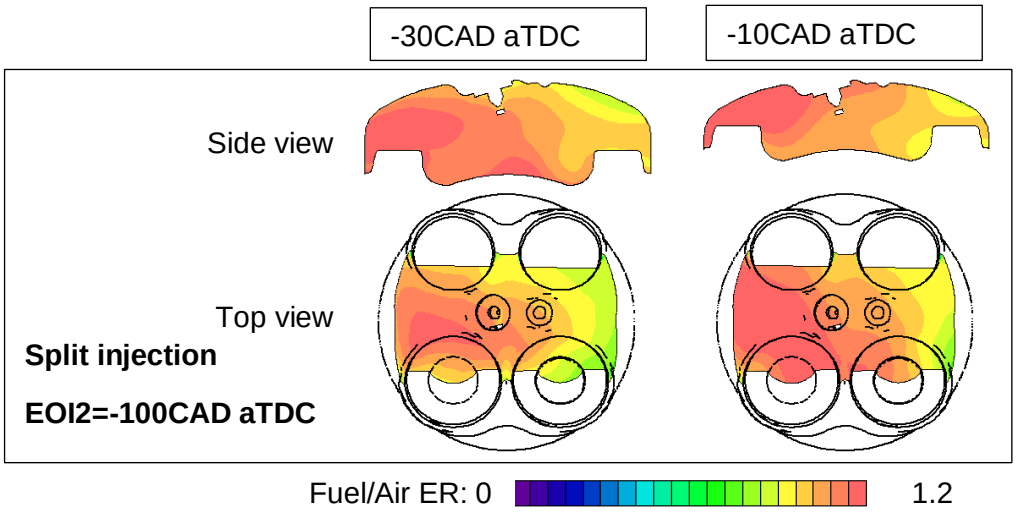

Figure 5-17 CFD simulation data, cross-sectional views of in-cylinder Fuel/Air ER during compression near TDC, comparison between single and split injection (80:20 split ratio) at 0% EGR 13.7bar Net_IMEP.

As was seen in the results of CA50 and ISFC graphs including Figure 5-5 (bottom chart, circled in black), the case at EOI2=-100CAD aTDC 80:20 ratio and 10% EGR was an isolated case with an earlier combustion phasing. The distribution of ER for this case is shown in Figure 5-18. The EGR dilution along with the well-timed split injection had made a homogenised mixture with lean regions around the piston walls, the area of concentration was concentric with the ignition location. Here it was demonstrated that some stratification phenomenon could create favourable combustion but at isolated cases.

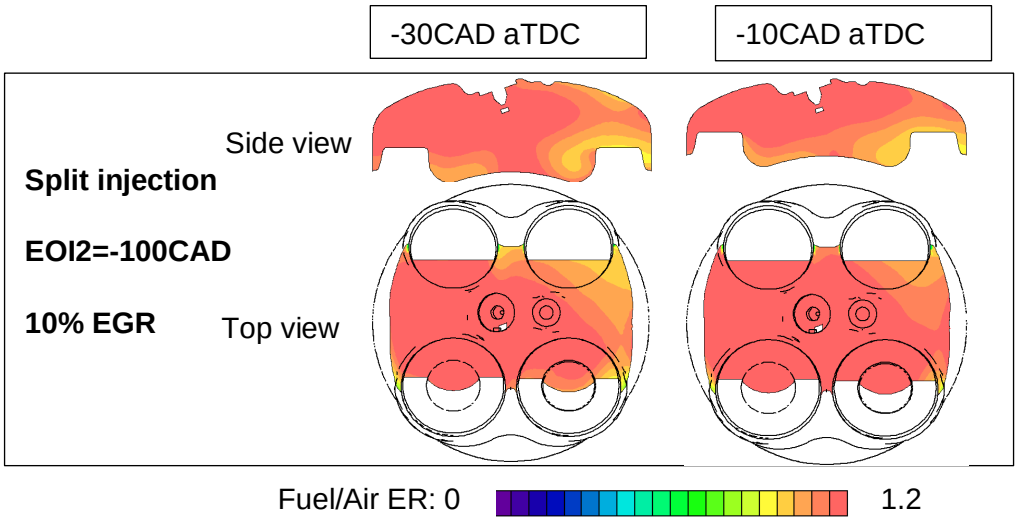

Figure 5-18 fuel distribution before TDC with EOI2=-100CAD aTDC 80:20 ratio and 10%EGR. This case had superior CA50 and efficiency benefits.

5.3.5.4 Effects of split injection with split ratio change at 16.4bar Net_IMEP

The distribution of fuel concentration for 16.4bar Net_IMEP is analysed for three split injection case and one single injection case, all without EGR dilution. A snapshot of the distribution at EOI2= -10CAD aTDC is laid out in Figure 5-19. The comparison of second injection timing and injection ratio can be made based on the distribution characteristics. As was the case with 13.7bar Net_IMEP, the split injection displayed a greater mixture potential but limited to the 80:20 split ratio. The use of 70:30 split ratio had exhibited a spatially focused enrichment to the left side of the cylinder. The increased late injection quantity had created a rich region that remained on the cylinder wall and piston crown until the tumble flow carried the fuel-rich mixture to the side of the cylinder near TDC, the resulting mixture at ST was of a lean mixture around the plug electrodes (arrowed) to retard the initial flame propagation and promote knock of the end-gas region, this resulted in the combustion of later phasing for most 70:30 injection ratio cases. Significant fuel is also thought to be trapped in the crevice volume, leading to losses. The two 80:20 cases shown here are cases with successful phasing effects as indicated by the CA50 figures. Both cases had created a slightly rich mixture around the plug electrodes with a superior homogeneity in the concentration distribution to promote faster combustion. The cases with 80:20 can be compared for the impact of injection timing at this load. EOI2=-225 CAD aTDC is a quick succession split injection, thus, has made a mixture distribution that is like the single injection case, but with less degree of concentration.

split ratio	Single injection	80:20	80:20	70:30
EOI2	N/A	-225	-125	-125
ER @ plug	1.12	1.13	1.13	0.87

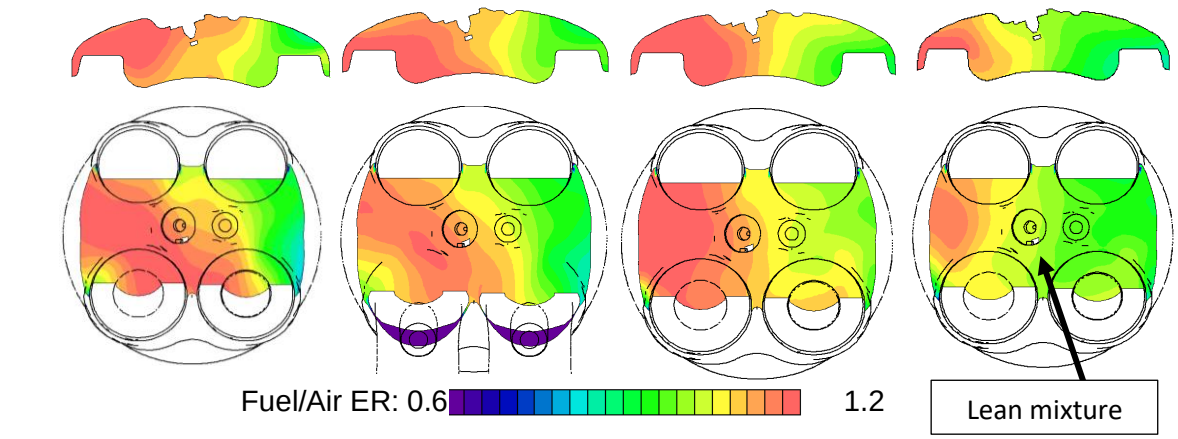

Figure 5-19 Comparison of fuel distribution at -10CAD aTDC for different second injection position and split ratio. Load at 16.4bar Net_IMEP with 0% EGR dilution.

In summary of the CFD simulation analysis, all variables had an impact on the distribution effects.

The engine was optimised for single injection operation and was found to have a positive stratification of fuel enrichment. But, EGR dilution had caused a mixing effect due to the need for more air compression, this has caused a more homogeneous mixture.

The split injection improves and worsens the fuel distribution with mixed results. Injecting the fuel in two parts had distributed the fuel in two plumes, the later injection had less time to evaporate which made the increased second injection amount less favourable, especially with late second injections. However, in some rare cases, a very dispersed but central mixture is realised, which complements the extra turbulence and internal flow due to the EGR dilution. 70:30 split ratio is found to produce a stronger fuel concentration region away from the ignition site, which lowered the combustion and encouraged knock.

Other effects such as injection induced Turbulent Kinetic Energy (TKE) and charge cooling is likely to have introduced significant changes to this mixture, but this has not been confirmed with the performed analysis.

5.4 Summary

The experiment was arranged to find the stratification optimisation point and quantify the gains or losses of such a strategy. The variables were load, EGR dilution, split ratio of injection, and crank angle position of the second injection, the fuelling was controlled by exhaust lambda =1. The boosted range of a downsized GTDi engine is found not to react positively to split injection. The split injection was expected to accelerate the combustion with optimised injections, especially with EGR dilution due to the favourable mixture conditions closer to the plug electrodes that creates a strong flame kernel. The overall effects showed that the split injection worsened the engine operation as the injector setup failed to create these favourable conditions.

There are two important facts to consider when analysing the data: -

1. Mixture preparation of the injector is not optimised for late injection
    a. Long penetration jets were not suited for local enrichment techniques, instead of leading to wall wetting and under-mixed conditions.
    b. Single-injection case operated with a level of optimised fuel stratification; however, improvement opportunities were noticed.
2. The high emission concentration of ISCO and ISTHC indicates a rich combustion from short-circuiting at 16.4bar Net_IMEP. This was lower for 13.7bar Net_IMEP. This is regarded as an intentional strategy to lower knock tendency.

This had meant that the split ratio and load had a large effect on the resulting mixture distribution. CFD analysis showed the second injection with larger quantity and later timing led to a region of fuel enrichment away from the ignition site due to unoptimized fuel spray formation. The ignition area was lean from the undermixed distribution, and this had slowed the combustion and increased knock tendency. Furthermore, the expected combustion stability improvements are not confirmed by the results, leading to overall instabilities in a certain range of second injection timing, which falls under the same region that led to decelerated combustion durations.

However, the conditions did improve under certain conditions. The maximum recorded efficiency improvement was 1.7% at 13.7bar Net_IMEP with EGR. It is a small efficiency benefit, but the CA50 figures suggest a mild (but erratic) improvement of combustion phasing with EGR dilution at this load. The extra boosting required for EGR dilution had dominated the cylinder flow which disrupted the stratification and resulted in a more homogeneous mixture with a single injection, in such a case, the split injection was able to reintroduce stratification to improve the combustion.

THC and NO_x are less affected by the split injection parameters for all the second injection sweeps, THC was found to increase gradually due to crevice loss from late wall impingement. But as the second injection approached EOI2=-50CAD aTDC, large combustion effects took place which decreased ISNOx/ISTHC emission to roughly 80% of the original value, also for 13.7bar Net_IMEP, and the ISCO increased to 28% at the same condition. This is due to large portions of very late second injection timing with the proximity of the piston crown that caused combustion of unprepared mixtures and pool fires.

Chapter 6 EGR SFI at high load operation of a downsized GTDI engine with valve-overlap duration reduction using dual-cam VVT

6.1 Introduction

Positive valve-overlap is widely adopted on downsized GTDI engines with the help of dual VVT setups to achieve higher loads at low speeds. This has been a trivial fact for emissions so far. However, it is to become an issue in the emissions targets with the more dynamic test cycles where LSHL operation ranges are becoming dominant. At these conditions, the reliance on boosting creates a positive pressure ratio, encouraging complete scavenging of residual gas by boosted air with the wide valve-overlap. The bursts of the O_2-rich mixture into the exhaust are known to cause two issues: -

1. Wideband zirconia lambda reading offset due to detection lag of sharp peak O_2 bursts
2. In-cylinder trapped mass tend to be fuel-rich with exhaust lambda sensor reading of 1.0

These issues lead to overall offending tailpipe NO_x emissions due to lower conversion efficiency of the TWC and combustion efficiency losses but with the gain of engine performance.

Documented in this chapter are the detailed experimental results of the tests performed to analyse the following: -

1. Varying degrees of valve-overlap and their effects on engine operation, particularly tailpipe NO_x emission and efficiency impacts.
2. Performance effects of valve-overlap reduction quantified for the tested loads with EGR operation
3. Investigation of EGR SFI combustion effects upon valve-overlap reduction at boosted SI operation

The above three investigations are performed at two load points. The first investigation explores the full valve setting combination, giving an insight into combinations of valve settings towards engine performance and combustion phasing with EGR. Once these are understood, the last investigation focuses on the effectivity of split injection on the combustion when symmetrical valve-overlap duration is shortened and how the split injection effects are affected when EGR dilution is present.

In this work, the remnants of combustion products trapped in the cylinder for the next cycle is termed the residual gas whereas the reintroduction of processed exhaust gas extracted after the TWC is termed external-EGR. The total fraction of combustion products that partake in the combustion cycle is thus the arithmetic sum of the two fractions. Both external-EGR gas

and residual gas affect the combustion process but in different ways due to the chemical and temperature conditions, it is important to note at this stage that while the external-EGR is quantified via a proven method, the fraction of residual gas remained unquantifiable in this work. However, it is known that residual fractions increase with reduction of valve overlap.

6.2 Experimental test condition and methodology

The investigations were carried out and results analysed in two sections:

1) Valve-overlap reduction with EGR at modified valve timing
2) Symmetrical valve-overlap reduction with SFI EGR combustion

The positive valve-overlap is achieved through the intake and exhaust VVT devices which allow the profiles of intake and exhaust camshaft to be altered independently.

Two key variables (EVC and IVO phasing) are introduced to the test. The valve timings are used to adjust the duration of the overlap event and the positioning bias towards the earlier (piston upwards exhaust stroke) or later (piston down intake stroke). For this investigation, due to the changes applied to the engine operation condition at these boosted loads, the optimisation process will start with a full exploration of valve-overlap mapping.

6.3 Part 1: Effect of mixed valve phaser timings on engine operation and efficiency

6.3.1 Test conditions

For this test, the valve event combinations indicated by Figure 6-1 are tested.

At a load of 13.7bar Net_IMEP, 12 points are tested starting at a reference valve profile equating to 53CAD to 5 CAD of valve-overlap.

At a load of 16.4bar Net_IMEP, 9 points are tested starting at a reference valve profile equating to 51CAD to 5 CAD of valve-overlap.

The reference valve timing is taken as the most extended positive valve-overlap (seen at right bottom), and 5 CAD of valve-overlap to be the shortest (seen at left top). The test points in between including full elimination of either early EVO or late EVO were chosen for their suitability and interest to study their effects in changes of valve timing.

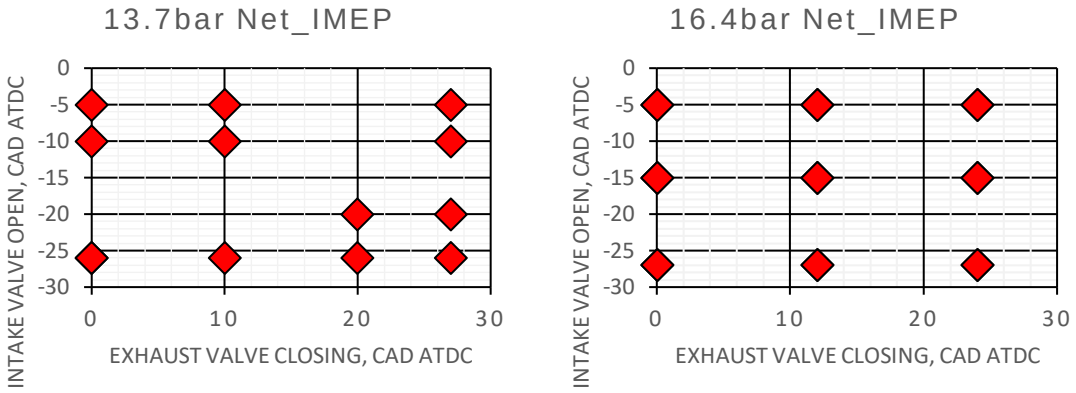

Figure 6-1 Valve event timing for tests. Left, 13.7bar Net_IMEP. Right, 16.4bar Net_IMEP

The remaining variables for the investigation of valve-overlap are as seen in Table 6-1. At both load points, tests were carried out with 0% and 10% EGR dilution.

Table 6-1 variables and values of EGR positive valve-overlap investigation

Variables	Values
Valve timing	As plotted in Figure 6-1
Load, bar Net_IMEP	13.7, 16.4
EGR dilution, %	0, 10

The 2D contour plot will present the results in this section with software-generated isolines—an example of the plot indicating that the valve-overlap period is presented in Figure 6-2. The x and y-axis are positions for the EVC and IVO; right bottom value is, therefore, the widest valve-overlap that is tested. The plot top left is the elimination of valve-overlap. The red dots are the location of data points, and the magenta dot shows the minimum value and green dot shows the highest value location in the respective plots. The plots will be labelled individually for the load point and EGR rate it represents. These plots are generated to visualise the characteristics of results through a range of valve configurations.

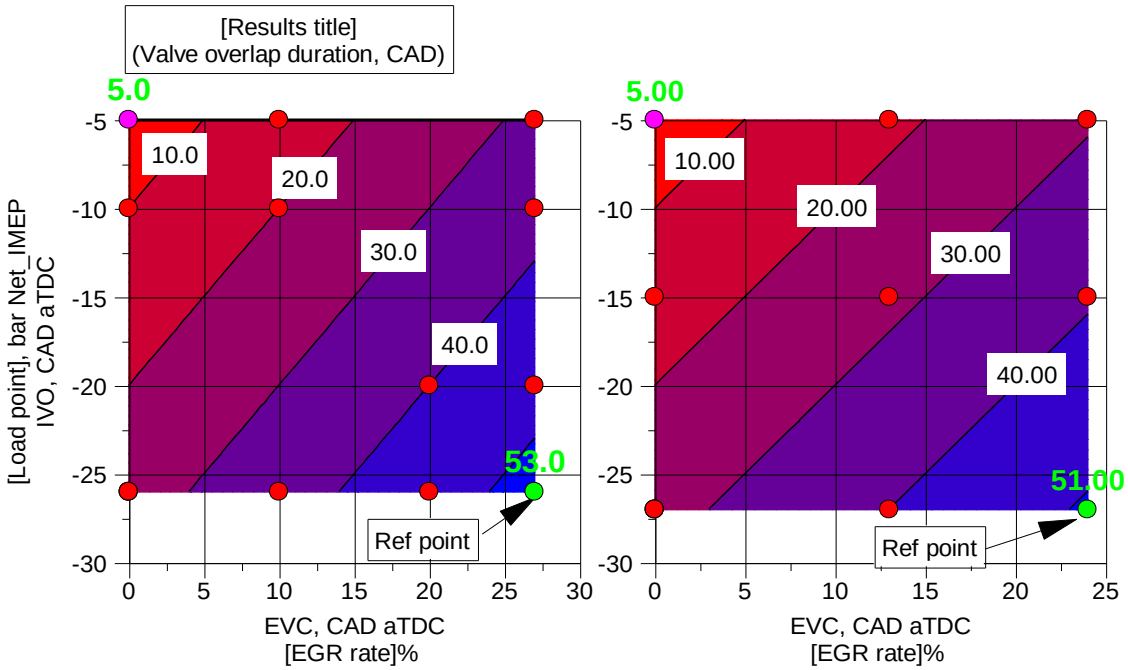

Figure 6-2 resulting valve-overlap from the setting of IVO and EVC, an example plot, with an indication of the reference valve set point at 13.7bar Net_IMEP (left) and 16.4bar Net_IMEP (right)

For this test, a fast particle analyser was connected to the exhaust passage and used to measure the particle emissions. The exhaust gas sample was taken after the TC and before the catalytic converter. The details of the particle analyser are as seen in Table 6-2. The particulate emissions data is recorded and processed by the built-in software. The data is further processed to have the first 5 seconds of recorded data removed and then averaged to reveal the final particle emissions data for the test point.

Table 6-2 Particle analyser settings for the test

Manufacturer	Cambustion
Product name	DMS500 MkII Fast engine particulate analyser
1st dilution factor setpoint	5.0
Sampling duration	30 sec (25sec average used in results)
Sampling frequency	2Hz

6.4 Part 1: Results and discussion of the investigation

6.4.1 Valve timing effects towards the in-cylinder pressure and combustion phasing

The four opposing valve phaser configurations are shown in Figure 6-3. The reference refers to the standard valve-overlap configuration used at the load and speed of the engine. The operating valve-overlap divided by the TDC piston position marker is minimised on the

exhaust stroke to make a retarded overlap condition, and vice versa for the advanced valve-overlap but phasing the IVO and EVC as seen in the visual reference.

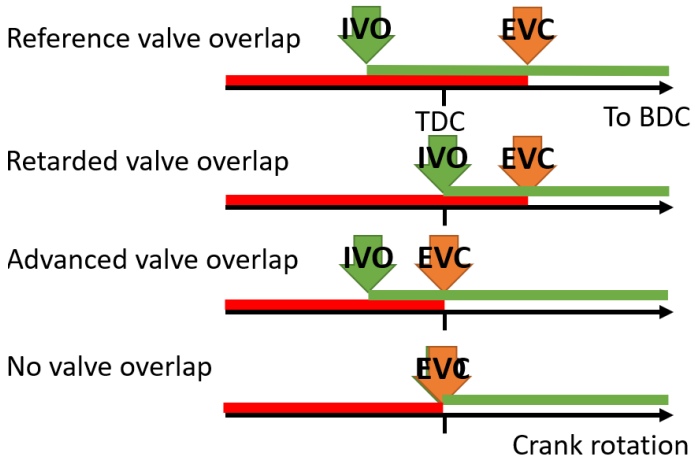

Figure 6-3 Visual representation of the types of valve-overlap configuration compared. The red line represents the exhaust valve open state, and the green line represents the intake valve open state.

The corresponding P-V diagrams are plotted in Figure 6-4. A zoomed plot shows the overlap period for better details.

In comparison to the reference overlap case, the advanced overlap case has a higher peak at TDC overlap, and the retarded configuration results in lower pressure. Advanced valve-overlap introduces the air sooner with a possible higher trap rate of residual exhaust gas, potentially leading to overall most extended dwell in fresh charge in the cylinders. The effect is intensified with a higher load, and the use of 10% EGR dilution shifts the pressure to higher positions.

In the cases of retarded and no-overlap, the late IVO causes a rush of inlet air to cause a dynamic momentary high-pressure state which later settles as the valve opens further and piston scavenges air.

With regards to the EVO timing impact (near BDC), higher pressure retention is seen with retarded and reference overlap where EVC timing remains after TDC. The effect is further increased for the 16.4bar Net_IMEP load where more significant fractions of the exhaust gas are directed to the turbine due to increased load demands. The lowest recorded pressures are usually seen with later IVO on the overlap TDC, the lower pressures created by the inertial fluid draw of the turbine is thought to provide to this phenomenon.

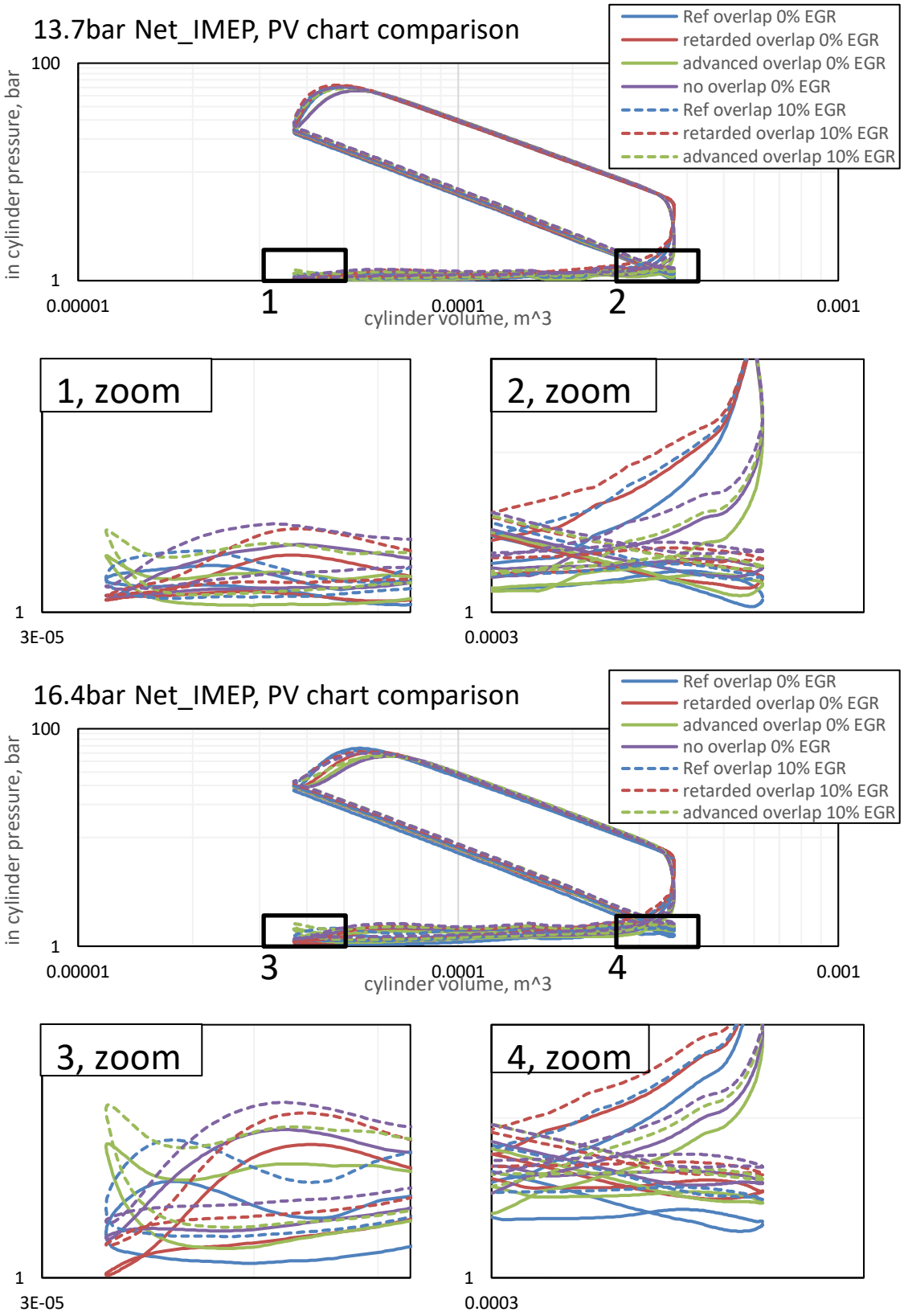

Figure 6-4 PV plot comparison of 4 valve-overlap configurations with 10% EGR dilution at boosted loads. Every combination of valve parameter has an output to unique cylinder pressure effects at either the overlap position, start of compression (IVC), peak pressure points or exhaust blowdown (EVO)

The pressure difference between the exhaust and inlet manifolds are visualised in Figure 6-5. The MAP and exhaust pre-turbo pressure values are averaged; this means that the values here do not represent the instantaneous pressure difference during valve-overlap periods which are dynamically greater. However, the averaged pressure values can be used to illustrate the changing trend of these pressures with different valve timings and overlaps.

At 13.7bar Net_IMEP without EGR, the engine operates at near WOT condition with no boosting. However, due to the shifts of valve timings (such that overlap is reduced), the boosting increases with all valve phasing change, this has increased pressure difference as valve-overlap is reduced. The early EVC results in mild pressure differences and the maximum pressure difference are seen at the latest IVO with 15CAD of overlap duration. With 10% EGR dilution, higher pressure differences are observed as the valve-overlap is shortened; this also includes some cases of late IVO settings.

At 16.4bar Net_IMEP, the extra boost required is further amplified as an increasing pressure difference with the shortened valve-overlap. Like the lower load, operations with EGR mandate even greater pressure difference across the intake and exhaust ports.

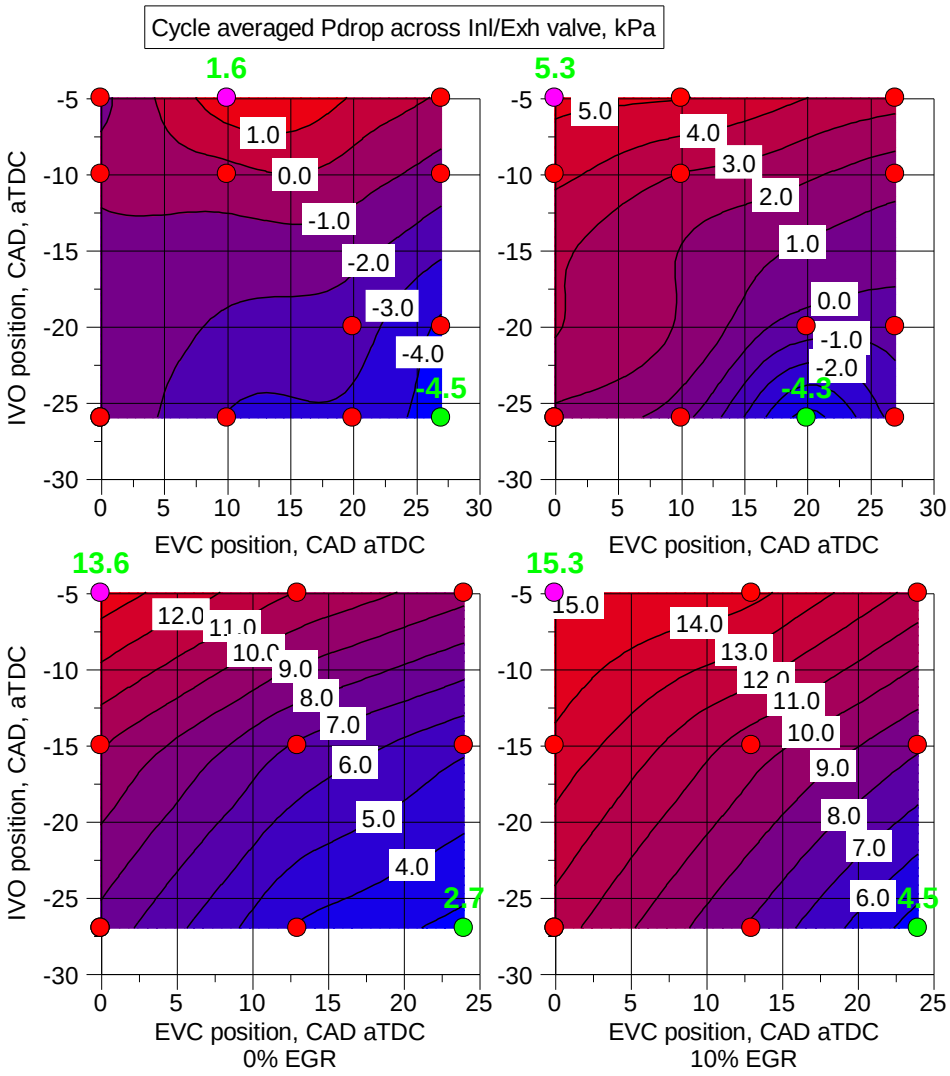

Figure 6-5 averaged P_{drop} between the inlet and exhaust manifold with varying valve phase setting

Figure 6-6 shows the MAP for all the valve setting tested. The required MAP to maintain the same load increases with the reduction of valve-overlap, this implies the reduction of volumetric efficiency, and the need to further compress the inlet air at these reduced overlap points. The rate of required compression increases at the higher load of 16.4bar Net IMEP.

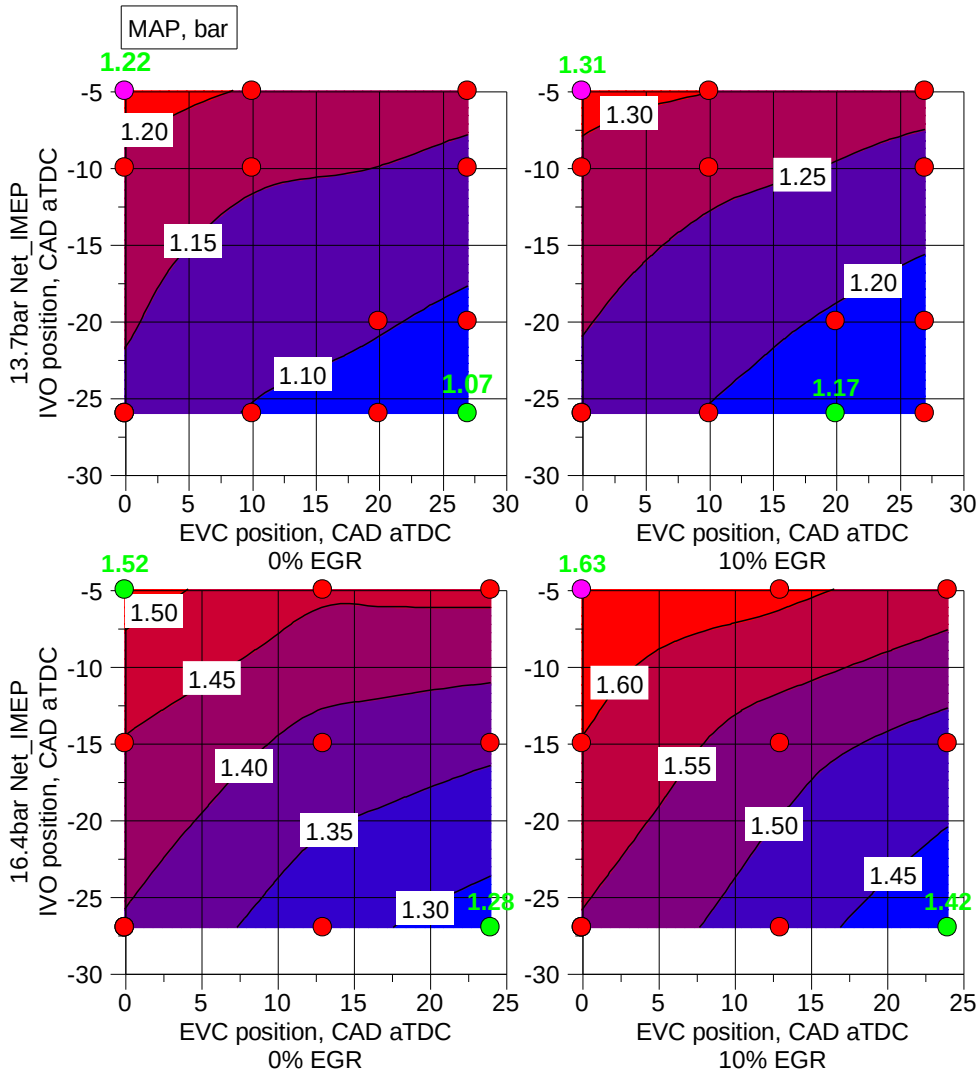

Figure 6-6 MAP with varying valve phase setting

Another effect of valve timing is the ECR which is calculated from the in-cylinder pressure, and averaged MAP. The results are as plotted in Figure 6-7. Here the ECR is defined as the ratio of the cylinder volume between $IVC_{effective}$ to TDC, where $IVC_{effective}$ is the crank angle of MAP=in-cylinder pressure during compression. As the IVO is advanced (and IVC is moved closer towards BDC), and the effective compression starts earlier, resulting in higher ECR. Also, the in-cylinder gas pressure at IVC is affected by the intake pressure, which varies with the EVC and the amount of valve-overlap. Between the EGR dilution cases, the required MAP may have varied because of gas composition $P_{ivc}V_{ivc}^{n}= P_{TDC}V_{TDC}^{n}$, where n will depend on the gas composition and heat transfer.

This means there is an increased reliance on the turbo-compressor, thus charge cooling rate is also increased as the higher pressures of the inlet is subjected at the intercooler. This decreases the heat energy of the charge at the beginning of second compression (piston compression) leading to decreased knock mitigation. Thus, possibly leading to effective

combustion phasing advancements [101]. However, it is important to note that the increased charge temperature is also influenced by the ratios of residual gas which may have resulted in an overall hotter charge.

Also noticed is the sudden drop in TC/MAP demand at 10% EGR dilution with specifically IVO=-26, EVC=10, it is assumed that some flow field created at this point was favourable to the mixture preparation that led to such a unique case.

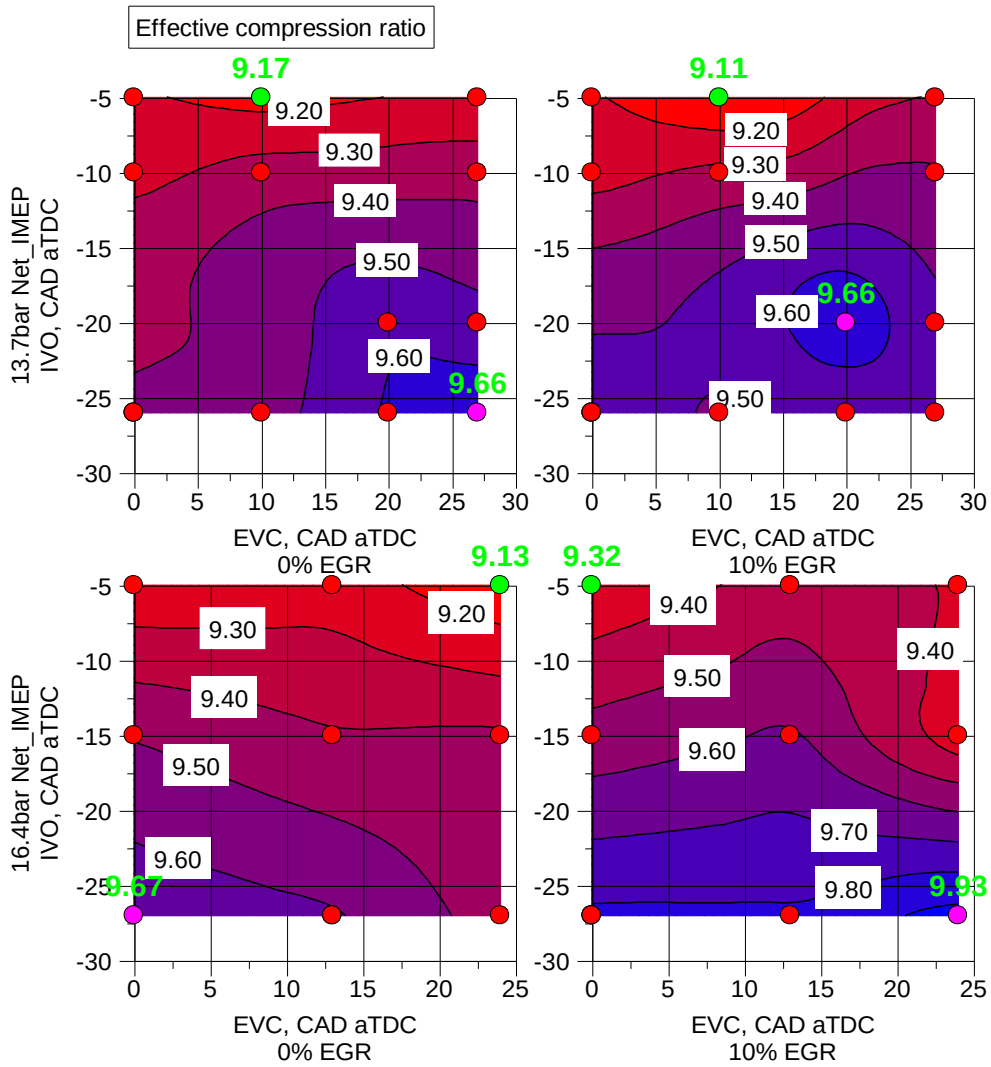

Figure 6-7 ECR with varying valve phase setting

Figure 6-8 shows the ignition advancement trends. It should be noted that the ST is KLSA and the increase in the ST advance would indicate better tolerance to knocking combustion. At 13.7bar Net_IMEP without EGR, the KLSA timing is advanced from -5.5 to -7.5 CAD aTDC when the EVC is retarded from TDC to 25CAD aTDC. With EGR, the KLSA is advanced to -13CAD aTDC independent of valve timings and overlaps. At 16.4bar Net_IMEP without EGR, the KLSA is advanced from 0.5 to -4.5 CAD aTDC as the valve-overlap period is increased towards the bottom right corner in the graph. The stronger

correlation between the valve-overlap period and the KLSA can be explained by the increased effect of positive scavenging at the higher load. This is also reflected in the CA50 results with the valve-overlap in the results with 10% EGR dilution, where KLSA is advanced by several CADs due to EGR effects.

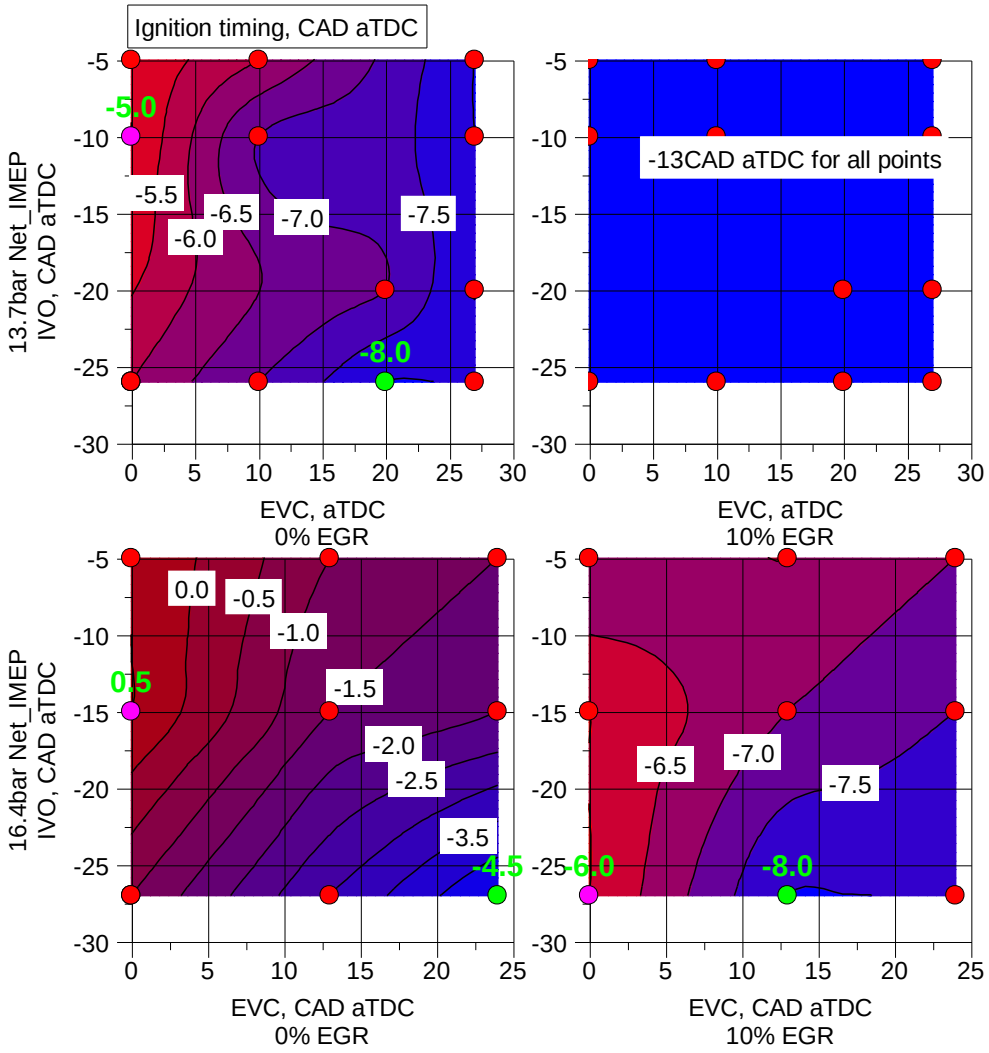

Figure 6-8 Knock limited Ignition advance with varying valve phase setting

The combustion phasing, as indicated by the CA50 position for every valve timing is seen in Figure 6-9. The results follow the same trend as those of the KLSA. At 13.7bar Net_IMEP, the position of CA50 is advanced from 17CAD aTDC to 13CAD aTDC as the EVC is shifted from TDC to 25CAD aTDC, almost independent of the IVO. At 16.4bar Net_IMEP, overlap positioning has less effect on the CA50 position and more influence from the overlap duration. With EGR dilution, the CA50 is affected by the EVC position only, which is likely caused by the increased levels of boosting by EGR having a negative influence on the residual gas fraction.

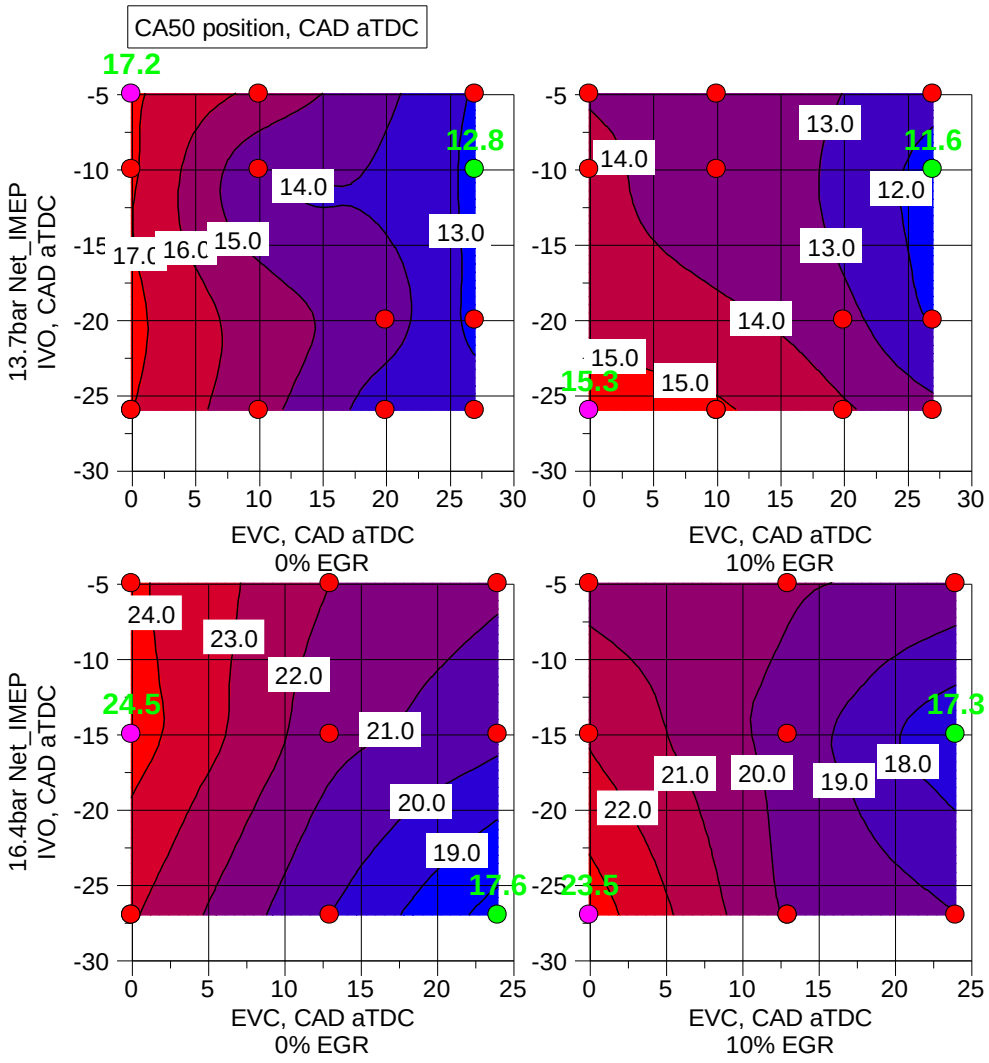

Figure 6-9 CA50 position at KLSA combustion with varying valve phase setting

The results for combustion duration are as seen in Figure 6-10. At 13.7bar Net_IMEP, the combustion duration is reduced slightly from 20CADs aTDC to 17.5CADs as the EVC is retarded from TDC to 25CAD aTDC. At 16.4bar Net_IMEP, the combustion duration remains mostly constant and then is reduced by 2CADs with the most retarded EVCs in the bottom right of the graph. With EGR dilution, the combustion duration tends to increase with earlier EVCs when there is more trapped residual gas.

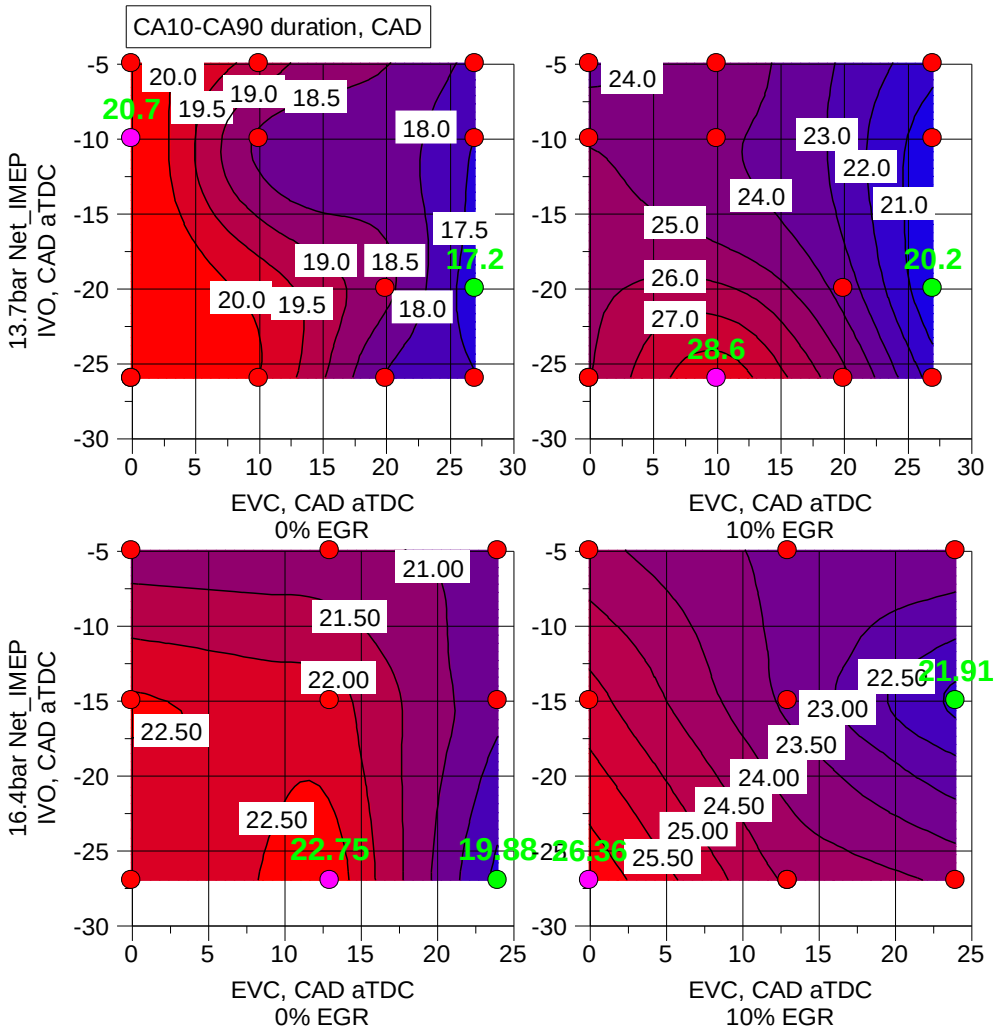

Figure 6-10 Combustion duration at KLSA with varying valve phase setting

With no EGR dilution, the stability of the combustion as seen on the graphs on Figure 6-11 increases a little with the earlier EVC when the combustion takes place later and longer in the expansion stroke. With EGR, at 13.7bar net IMEP, the highest CoV Net_IMEP of 1.6 is located at the shortest valve-overlap location. At 16.4bar Net_IMEP case, the max value is 2.5 seen at the advanced overlap point. The higher CoV values observed with EGR operations are directly related to the increased combustion duration.

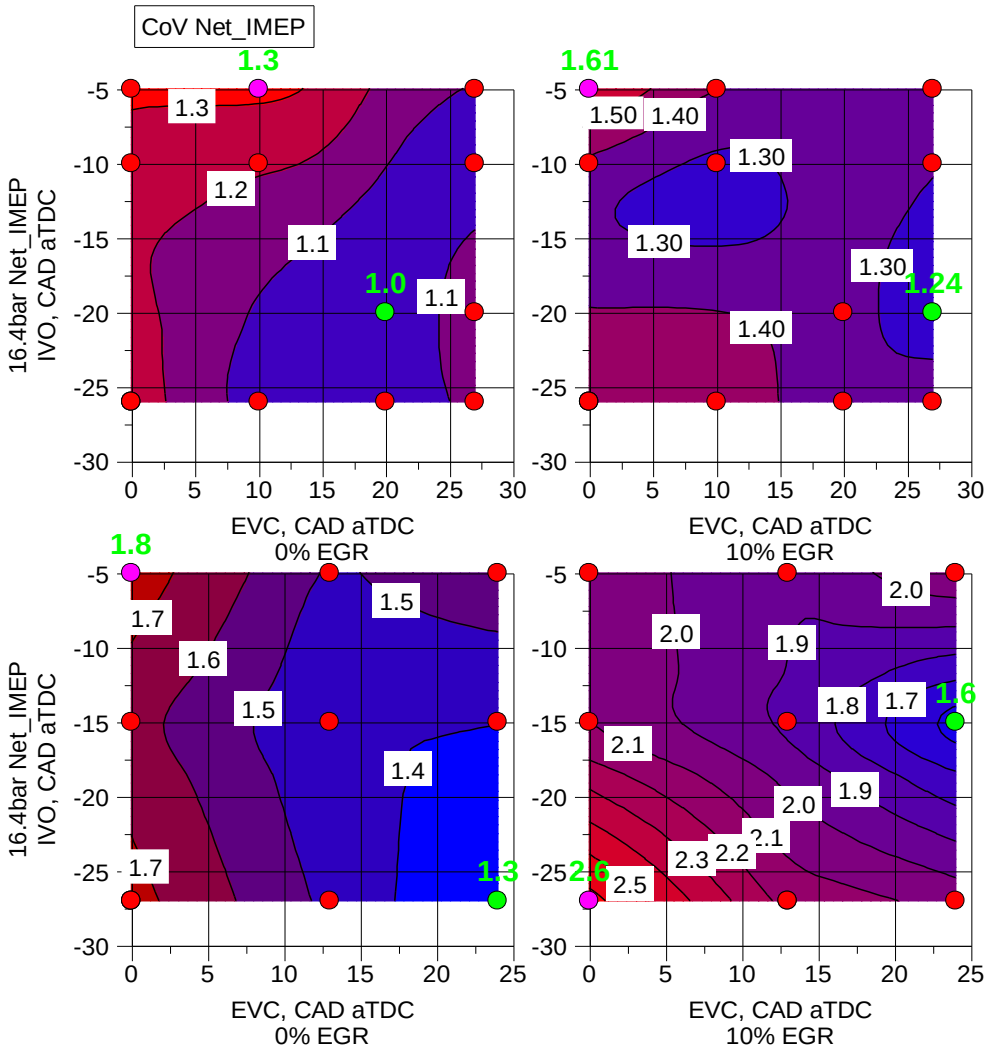

Figure 6-11 Combustion stability (CoV of N_IMEP) n=300cycles with varying valve phase setting

6.4.2 Valve timing phasing for engine and TC efficiency

The valve-overlap influenced the engine's overall efficiency with distinctive characteristics, as seen in the BSFC results in Figure 6-12, ISFC results in Figure 6-13, and the comparison in Figure 6-14. The trend for engine operating efficiency due to IVO and EVC position is different for each load and EGR dilution case. However, the most notable observation is the ability of external-EGR dilution to improve the efficiency of the engine at all non-reference valve settings.

At 13.7bar Net_IMEP without EGR, a maximum efficiency (252.8g/kWh) is seen at a point with 20CAD of valve-overlap duration which improves (246.9g/kWh) with 10% EGR dilution but at only 10CAD of overlap duration. Similarly, at 16.4bar Net_IMEP, the best efficiency improves from 266.2g/kWh to 253.4g/kWh, where the best efficiency was seen at minimum overlap duration with the EGR dilution present.

The effect of 10% EGR increases the effectivity of reducing valve-overlap for both loads, the gap in BSFC gain jumps from 4.2 to 7.1g/kWh at 13.7bar Net_IMEP and 7 to 8.1kWh for 16.4bar Net_IMEP loading. The increased residual fraction due to reduced valve-overlap /early EVC valve timings and the reactivity of the residual gas determines the knock tendency and thus the overall efficiency, the use of 10% EGR has lowered the reactivity of the residual gas to allow for advancements at these high residual conditions, leading to an overall efficiency gain.

At 16.4bar Net_IMEP with no external EGR dilution, the increase in boost demand has increased the fraction of very hot and reactive residual gas, leading to the worst phasing delay with late EVC condition. The negative effect of overly rich trapped ER was also seen at longer overlap regions, especially with the external EGR dilutions where more short-circuiting takes place.

The heavier use of boosting from increased demand and EGR has made the characteristics of SFC charts very different from one to another, due to the fraction and properties of the residual gas and response of wide valve-overlap condition.

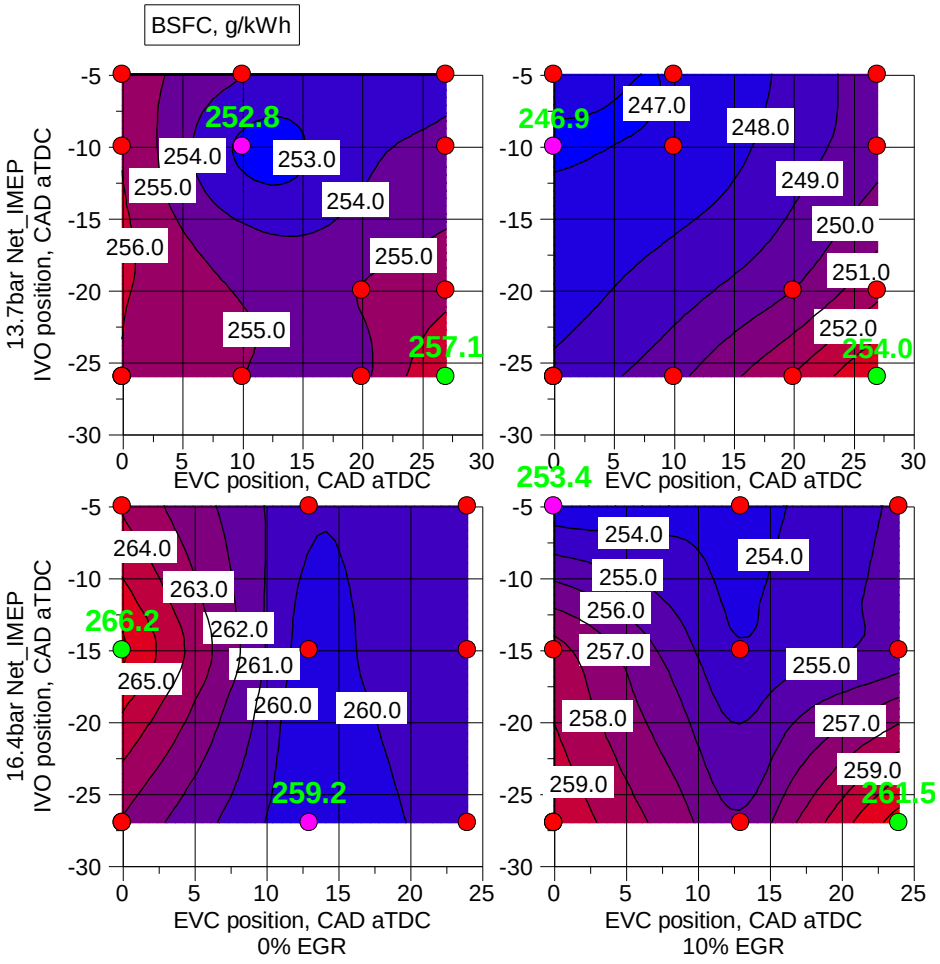

Figure 6-12 BSFC with varying valve phase setting

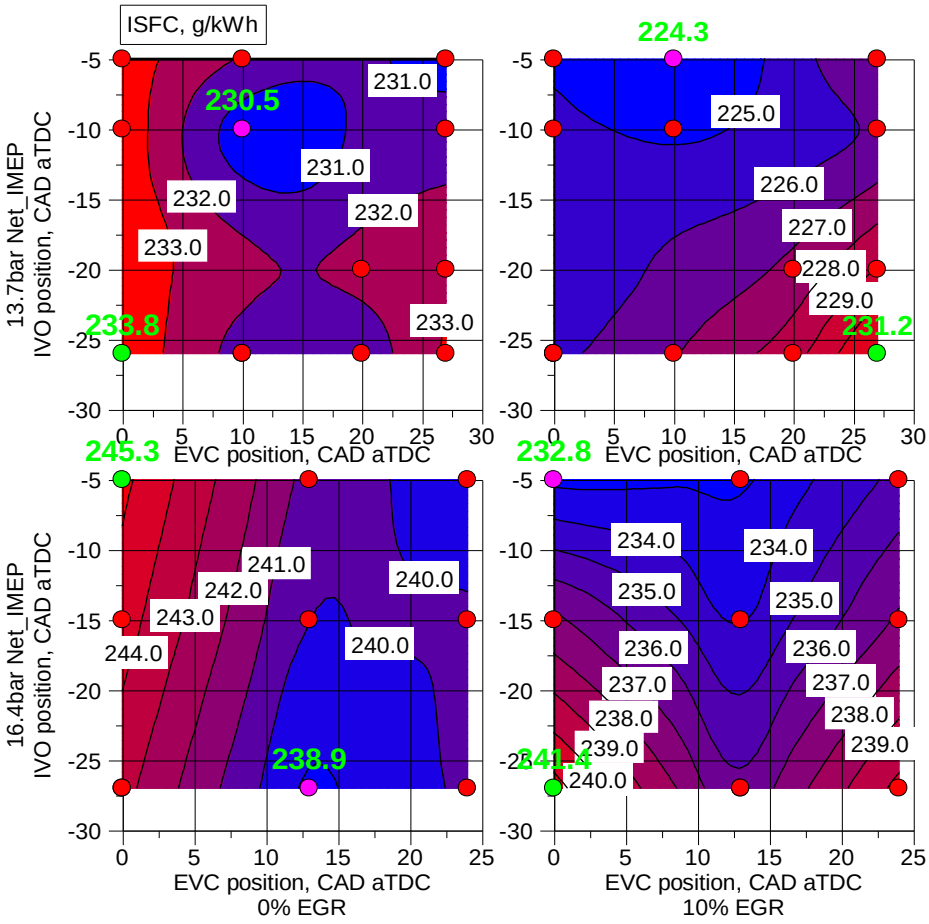

Figure 6-13 ISFC with varying valve phase setting

The difference between the two indicates the 'frictional' SFC which contains pumping, rubbing friction and accessory mean fuel loss, and these can be assumed to be a constant due to the fixed speed and load of operation. Thus, the lower numbers can indicate a case of higher TC efficiency. The frictional SFC is as plotted in Figure 6-14.

At the 13.7bar Net_IMEP load, a distinctive improvement of TC efficiency can be noticed as the valve-overlap is reduced, or as the overlap region is advanced. With wide overlap and increased volumetric efficiency, very little turbo demand is required which operates the engine with higher turbo related losses that result in this characteristic. At 16.4bar Net_IMEP, A slightly more chaotic characteristic is seen with no clear regression. It can, however, be seen that with EGR dilution, the efficient region lies at either advanced or retarded valve-overlap configurations.

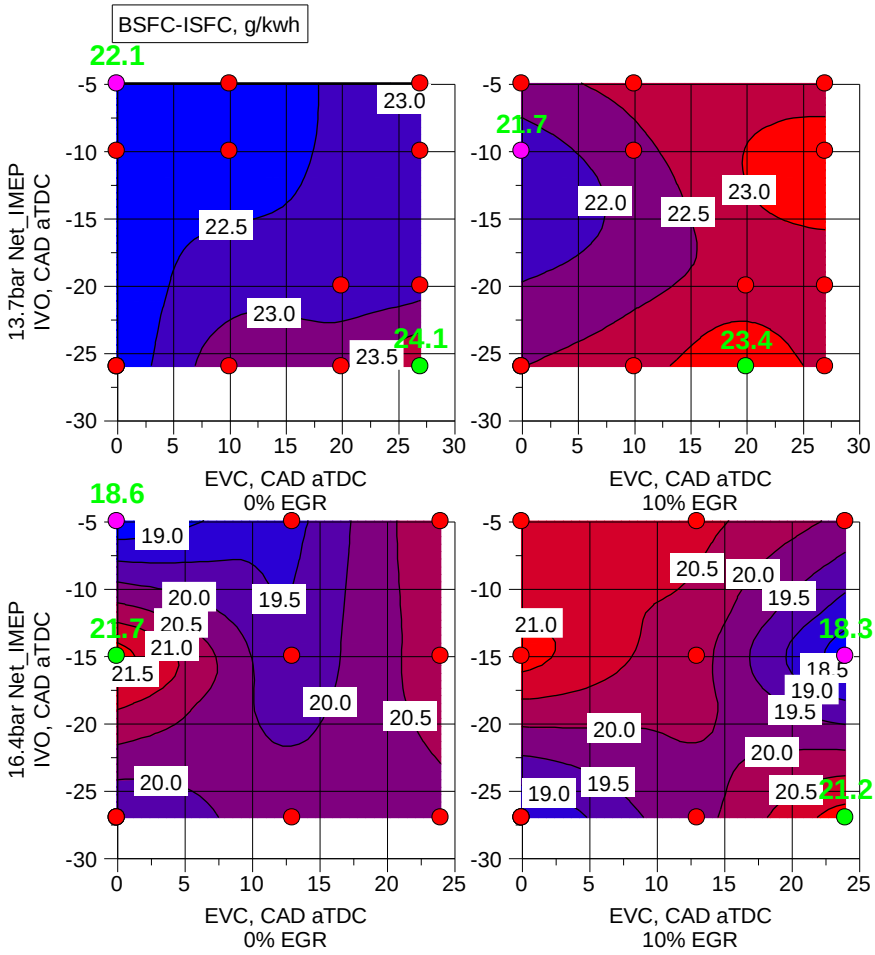

Figure 6-14 difference between BSFC and ISFC as an indication of turbocharger loss comparison with varying valve phase setting

The effects of TC operation condition and the resulting efficiency changes are identified by the changes of TC speed and turbine inlet pressures plotted in Figure 6-15, and further correlating the values to the turbine and compressor maps in Figure 6-16. The TC maps show the operation region at 13.7bar Net_IMEP at reference condition which is on the lower edge of the operation capacity with poor conversion efficiencies (noted by the colder colours). Reduction of valve-overlap and EGR dilution can be seen to increase the TC operation speed and higher-pressure ratios due to the increased boost demand. The resulting shift of the operation point is in the direction of the black arrow of the TC map, which is closer towards the higher efficiency island, resulting in an overall efficiency gain in the waste heat recovery process.

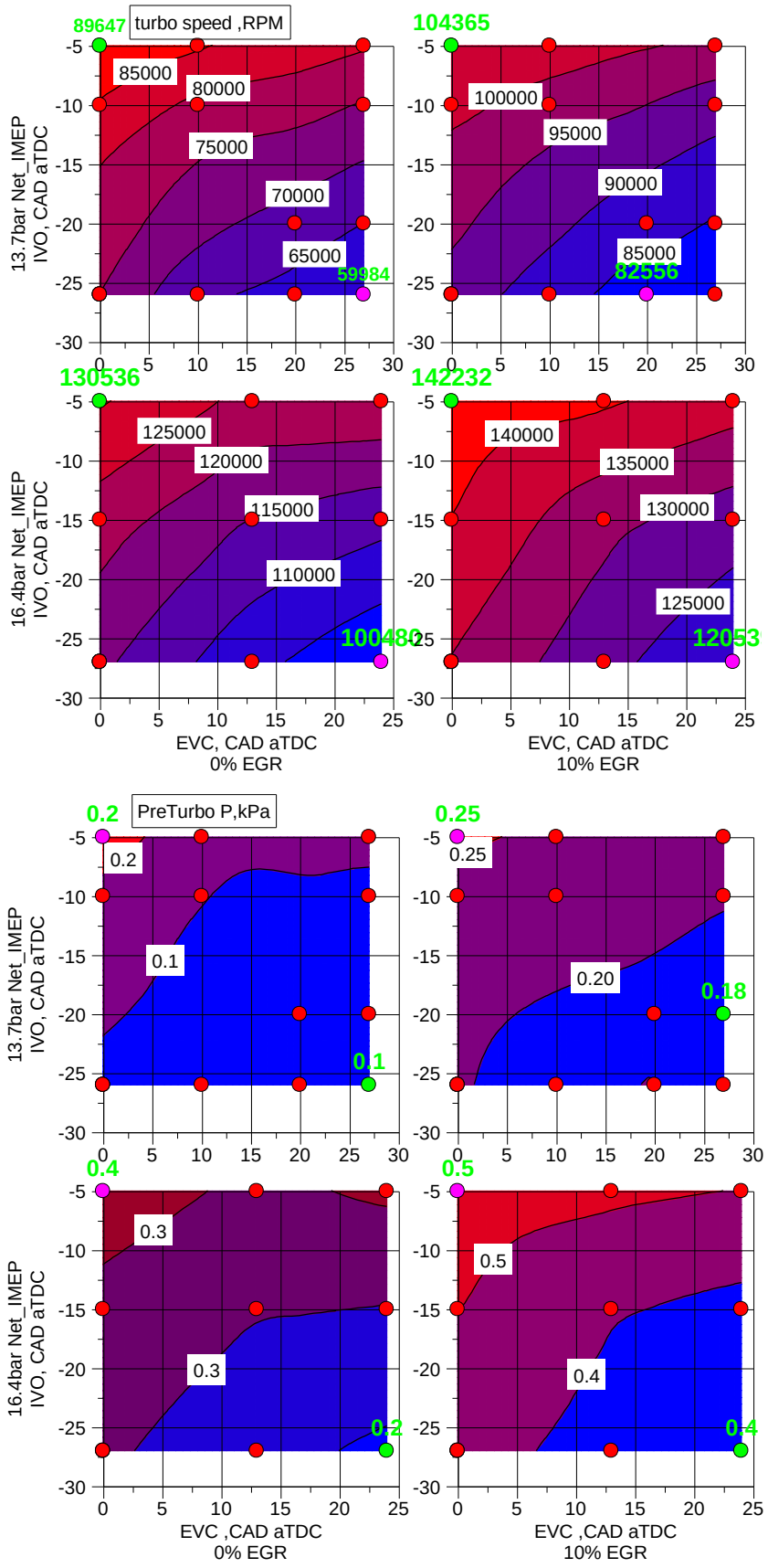

Figure 6-15 Turbo rotational speed and pre-turbo exhaust pressure comparison with varying valve phase setting

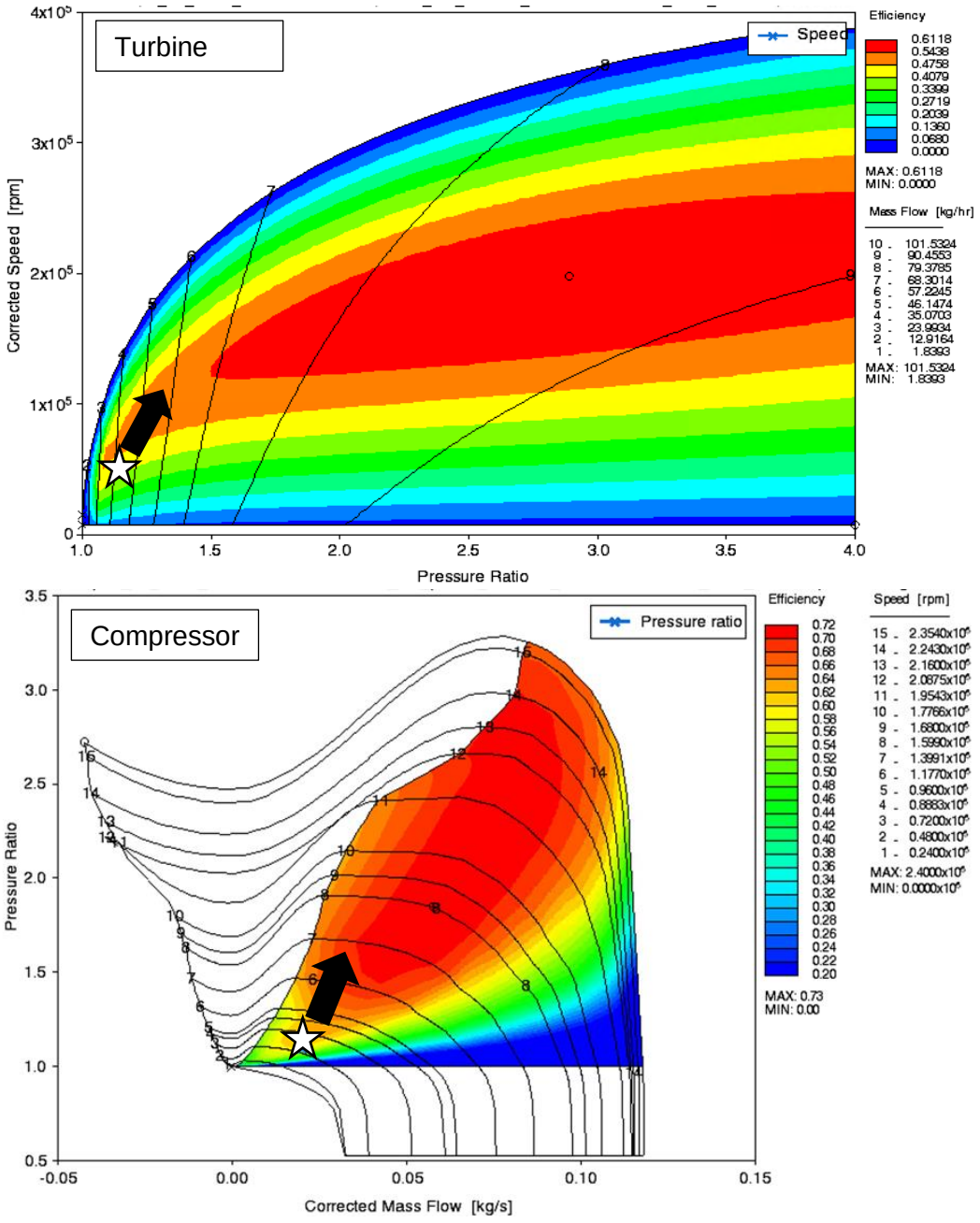

Figure 6-16 Turbine and compressor map for efficiency region. Star mark notes the turbo operation point of 13.7bar Net_IMEP, 0%EGR, and Reference Valve phasing. Arrow notes the turbine and compressor operation shift as the valve is closed or EGR dilution is introduced.

The boosting demand to achieve the respective loads with the various valve setting and EGR dilution is plotted in Figure 6-17. The plotted value shows the TC wastegate setpoint where 100% indicates a full exhaust gas diversion to the turbine and 0% would retain zero pressure for TC spooling. The results show a significant rise in boost demand from the reduction of valve-overlap, load and EGR. The reduced volumetric efficiency and the diluted mixture of less O_2 content prompt the need for these higher TC use. At 13.7bar Net_IMEP, the combination of strategies adds an extra 38.5% of wastegate closure, and at 16.4bar

Net_IMEP this was at 21% increase. The wastegate setpoint does not equate directly to pressure diversion ratio, so these numbers do not compare, but the large increase in TC usage will prompt issues with the proposed strategies limited load range owed to the heavy demand it puts on the exhaust energy recovery.

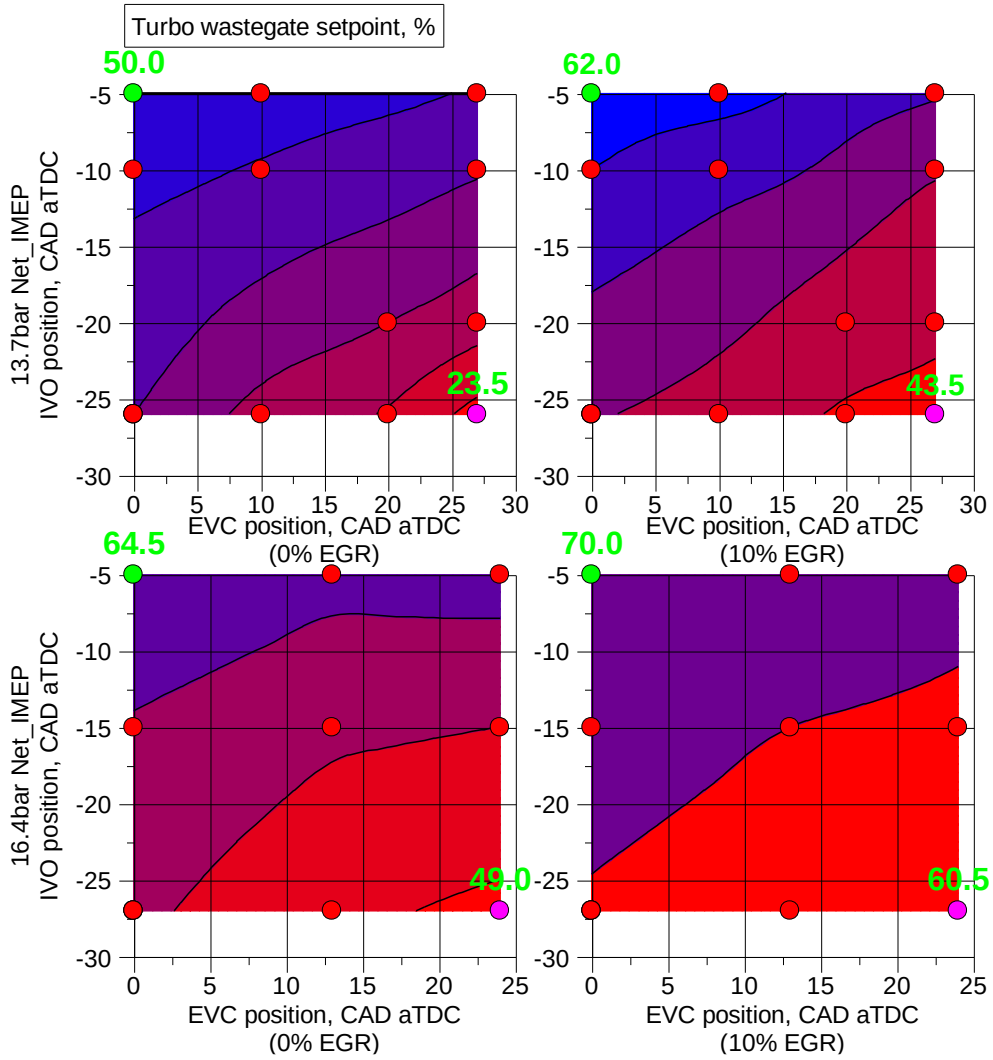

Figure 6-17 Turbo wastegate setpoint, the higher setpoint for tighter closure of wastegate, 0% for fully open and no boost demand with varying valve phase setting

6.4.3 Valve timing effects on pre-TWC emissions and exhaust conditions

Valve timing and EGR dilution have dynamic effects on pre-TWC emissions. Changes to the mixture preparation and combustion conditions have taken effect on the combustion products.

$ISNO_x$ was affected because of the valve phase change; the results are as plotted in Figure 6-18. The same characteristic was observed between the two loads, and in both cases, the significant differences were seen between the two EGR dilution cases. At the 0% EGR

dilution cases the highest $ISNO_x$ emissions are seen with early IVO phasing, this is with contrast to the 10% EGR where the late EVC led to the highest observed $ISNO_x$ emissions.

In both load cases with 10% EGR dilution, the lowest $ISNO_x$ emissions were seen at shorter valve-overlap durations, especially for the 13.7bar Net_IMEP case. From these data obtained, it is seen that the presence of EGR makes an effect on the engine running condition when valve-overlap is reduced. It can be concluded that the use of EGR has lowered the residual gas reactivity from reduced $ISNO_x$ and temperatures, which has enabled further combustion phasing advancements as seen by the CA50 plot in Figure 6-9. Additionally, the lowest $ISNO_x$ emissions observed for the 16.4bar Net_IMEP was at the widest valve-overlap, which goes against the trend (arrowed 1). The suspected combustion of rich trapped ER maybe lowering the combustion temperatures to have a similar effect to that of EGRs, however at the expense of combustion efficiency.

Furthermore, the high $ISNO_x$ emissions at early IVO and EVC is linked to the increased levels of trapped residual gases.

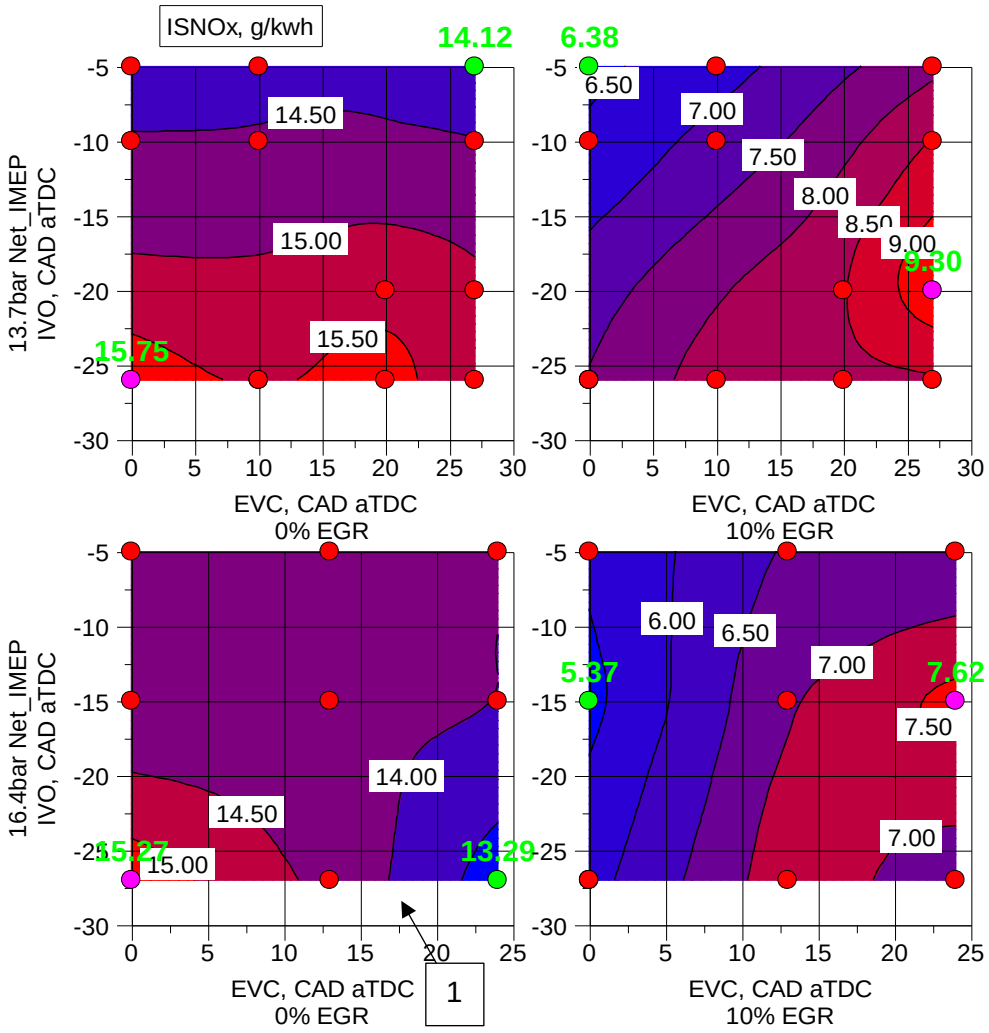

Figure 6-18 $ISNO_x$ for different valve timing

Pre-TWC ISCO emissions are as seen in Figure 6-19, as the injection timing and strategy are the same for all conditions. This can be assumed to reflect the trapped mass ER and thus the short-circuiting equivalence, which focuses on areas of wide valve-overlap.

At 13.7bar Net_IMEP case, this is more sensitive to the EVC phasing than IVO phasing. This would indicate a higher short-circuit flow at this condition when the exhaust valve is phased earlier, even with the inlet valve is phased late. At the higher load of 16.4bar Net_IMEP, greater levels of CO concentration can be seen with longer valve-overlap duration. However, this time its trend for lowered concentration is sensitive to both EVC and IVO phasing.

The use of 10%EGR has some effect on the ISCO value, and the elimination of valve-overlap quickly lowers the emissions. It appears that complete elimination of valve-overlap is not required to revert trapped mass ER to near stoichiometric. Comparison of the two loads can conclude that boosting contributes significantly to the trapped mass effects when valve timings are changed.

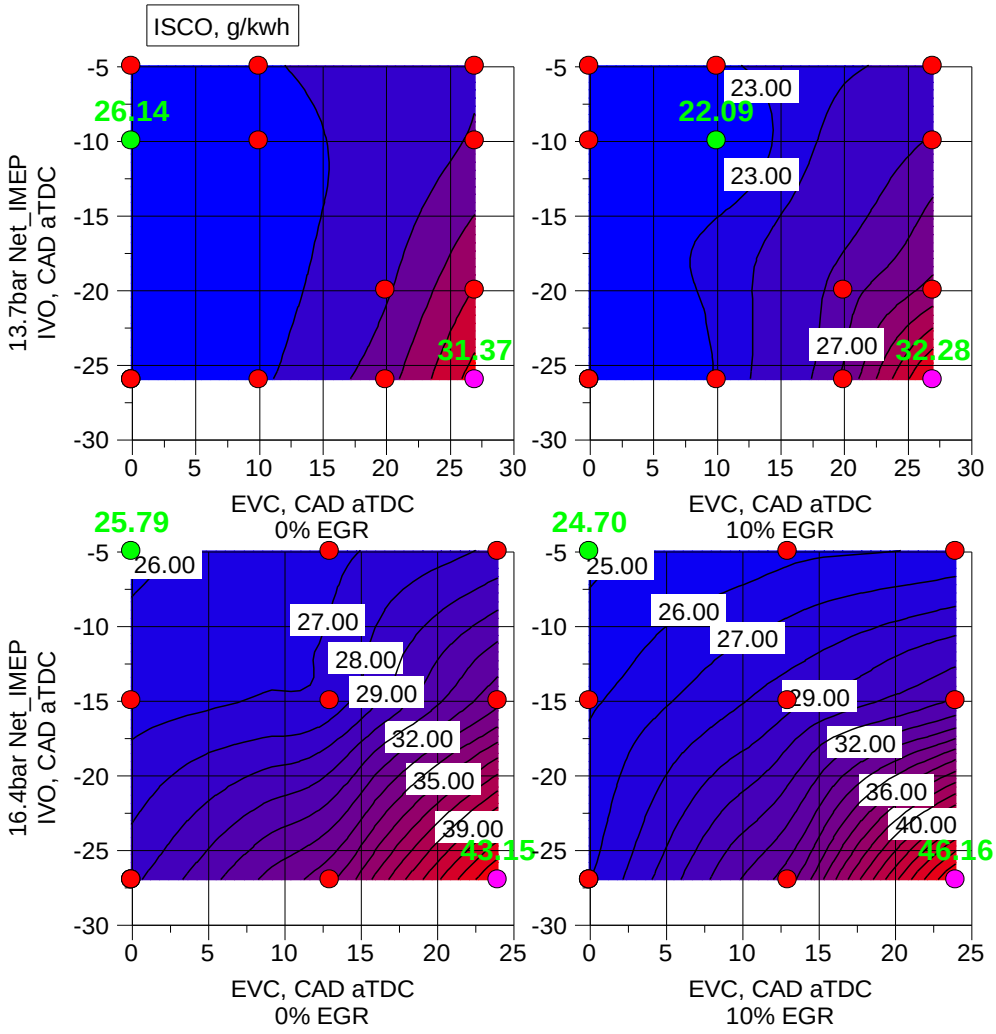

Figure 6-19 ISCO with varying valve phase setting

The ISTHC emissions are plotted in Figure 6-20. The trends are clear and in alignment with the ISCO figures, and it appears that two effects are dominating the results. 1) Trapped ER towards stoichiometric (as valve-overlap is eliminated) leads to lower ISTHC emissions 2) EGR dilution leads to longer and later burns which leads to higher end-gas ejection at time of EVO. In the early EVC regions where higher RGF is expected, a tendency for slightly lower ISTHC concentrations is observed, this further supports the reduced amounts of short-circuiting at these valve event timings.

Comparing the eliminated overlap cases, the use of EGR has increased the ISTHC readings, as no short-circuiting takes place at this point, the high values at this point indicates an increased effect of end-gas quenching due to EGR dilution.

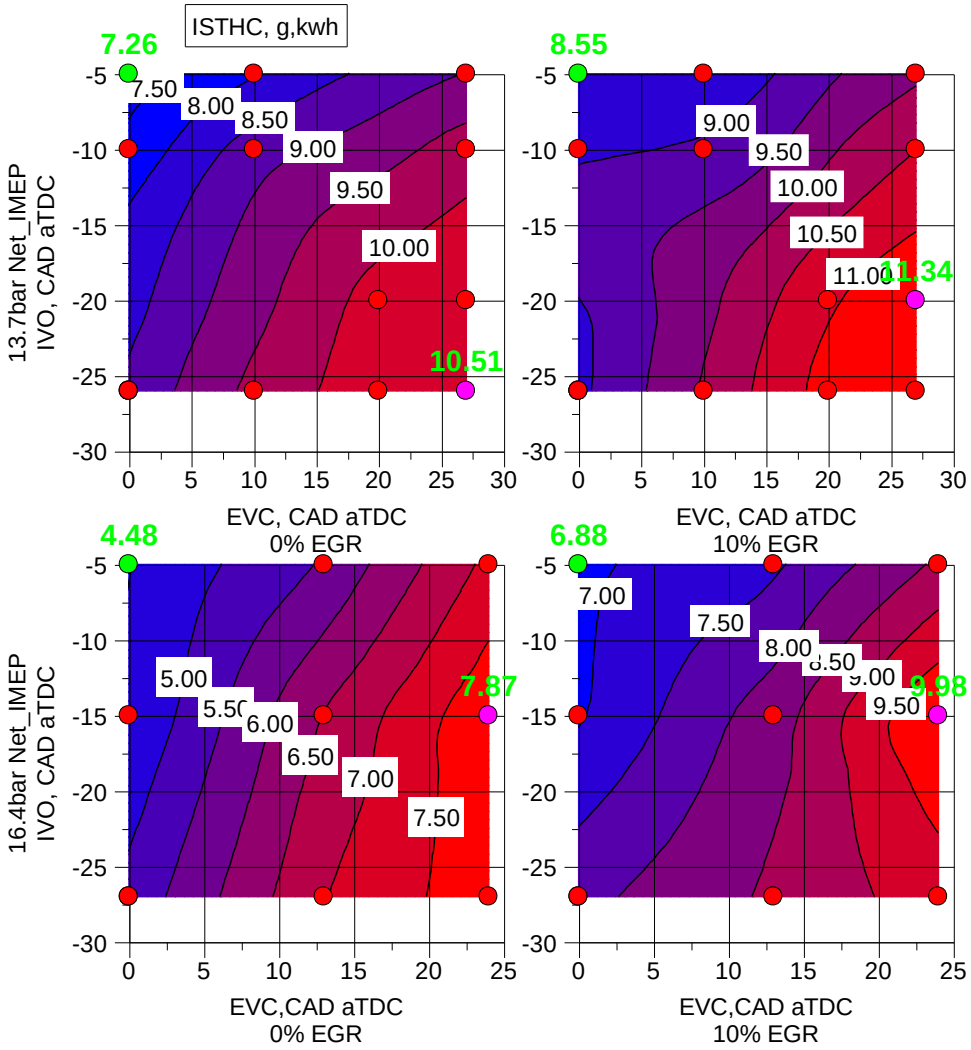

Figure 6-20 ISTHC with varying valve phase setting

The resulting calculated combustion efficiency is plotted in Figure 6-21. The effect of valve-overlap on combustion efficiency is relative to the valve-overlap duration, improving as the positive valve-overlap duration is reduced for all cases. The recovery scope is roughly 2%,

spanning to 3 % in the case of 16.4bar Net_IMEP with EGR. It also appears that the use of EGR decreases the efficiency globally by ~1%, due to the increased ISTHC emissions.

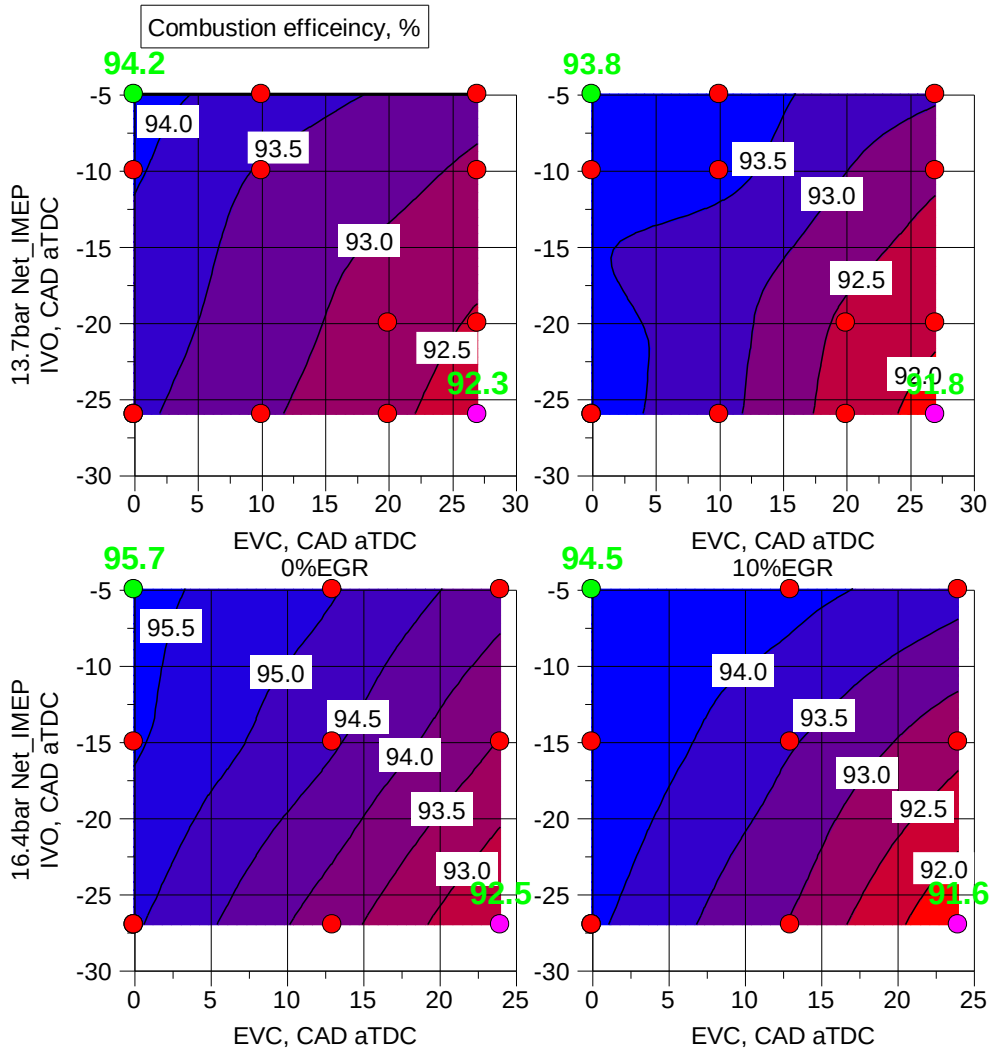

Figure 6-21 Combustion efficiency with varying valve phase setting

6.5 Part 2: Symmetrical valve-overlap reduction with SFI EGR combustion

6.5.1 Test variables

The elimination of positive valve-overlap with EGR dilution was found to be able to improve engine operation efficiency. The improvement was concluded to be a combined effect of 1) trapped ER towards stoichiometric and 2) external-EGR to lower the reactivity of RGF, which allowed for better combustion phasing ability.

However, the use of increased EGR dilution rate at high loads lowered the combustion speeds, which also affected the combustion stability.

Tested in this section is the ability of split injection to recover and improve the combustion issues caused by external EGR dilution and valve-overlap elimination. Furthermore, this section aims to understand any new interactions between split injections with valve-overlap reduced operation with EGR. An experiment with four variables (valve-overlap, EGR, load, second injection position) was performed to investigate the topics. The details of the variables are as noted in this subsection.

The details of all the variables and their values are summarised in Table 6-3. Asymmetrical valve-overlap settings were not tested as they did not yield characteristic properties of specific interest. The number of valve-overlap points is reduced to three; the largest valve-overlap at reference, smallest at 0CAD valve-overlap and the final point in the middle, which will yield a characteristically significant conclusion to the planned test. The tested valve settings are as plotted in Figure 6-22.

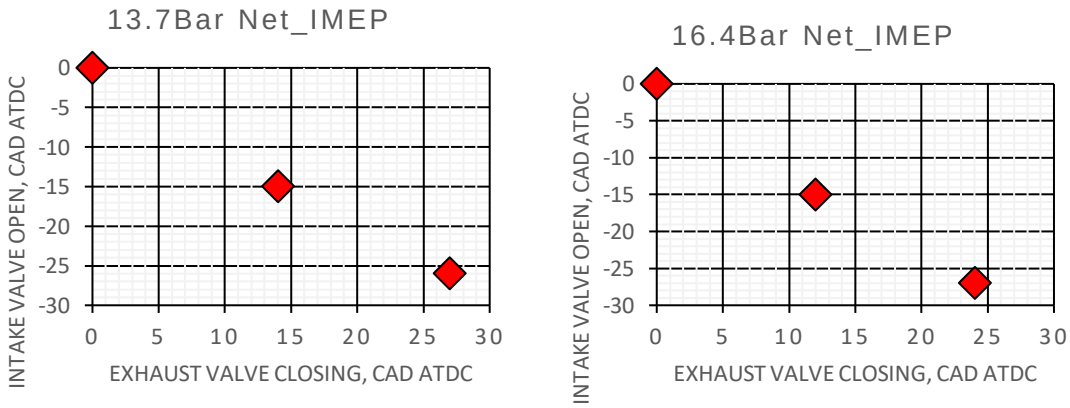

Figure 6-22 Valve event timing for tests. Left, 13.7bar Net_IMEP. Right, 16.4bar Net_IMEP

The two same loads (13.7, 16.4bar Net_IMEP) were used to maintain consistent test regime across the chapters of this thesis.

The split ratio was limited to one setting with an 80:20 result as the 70:30 split ratio yielded results of similar characteristic with more prominent combustion delay effects. Thus, the effect of variance in the split ratio will not contribute significantly to the conclusion of the studies performed here.

Table 6-3 Variables and values of test 3.2

Variables	13.7bar Net_IMEP	for 16.4bar Net_IMEP
Symmetrical valve-overlap duration	53, 29, 0 (3 points)	51, 27, 0 (3 points)
EGR dilution, %	0, 10 (2 points)	0, 10 (2 points)
EOI2 position, CAD aTDC	Single, 250-50(10 points)	Single, 225-50(9 points)

At 16.4bar Net_IMEP, second injection position of EOI2=-250CAD aTDC was omitted from testing due to the immediate timing between the end of the first injection and the start of the second injection. Such events are best avoided to lessen chances of injection failures or ECU crashes.

With all the variables considered, the investigation consists of 114 test points across 12 EOI2 sweeps.

6.6 Part 2: Results and discussion of the investigation

6.6.1 Symmetrical valve-overlap effects on in-cylinder pressure results

Changes are seen to almost all aspects of the engine operation performance with the introduction of valve-overlap duration change to the split injections sweep.

A log-log PV plot with the changes in valve-overlap is seen in Figure 6-24 (for 13.7bar Net_IMEP) and Figure 6-24 (for 16.4bar Net_IMEP). With a VVT system, it is essential to note that the valve timings are phased with the same valve-lift profile, and as the valve-overlap duration is shortened the EVO is advanced, and IVC is delayed.

The following changes can be observed from the P-V plots; -

- The lessened scavenging effect leads to the need for higher boosting to maintain the same load. The compression curve indicates higher polytrophic compression pressure as the overlap is eliminated. (arrowed 1)
- As overlap is shortened later combustion phasing is seen from later timing of peak pressure. Leading to lower peak pressure. It is a possible effect of higher pressure or higher fraction of residual gas at high load.
- Earlier EVO from shortening the valve-overlap duration causes an earlier drop of pressure. (arrowed 2)

- Higher pressures are seen with exhausting and inlet pressure with shortened valve-overlap, lower pressure seen at TDC due to decompression effects of earlier EVC.

Significant changes to the in-cylinder pressure are observed because of changing the valve-overlap duration. It is noted that the peak pressures are lower with shorter retention of in-cylinder pressure due to the earlier EVO.

The same characteristic changes are seen between the two loads. Minor changes to note are: -

- 13.7bar Net IMEP, the mid and no overlap timings show a very similar pressure trace
- 16.4bar Net IMEP, the no overlap valve timing shows even lower peak pressures at later phasing in comparison to the mid overlap timing.

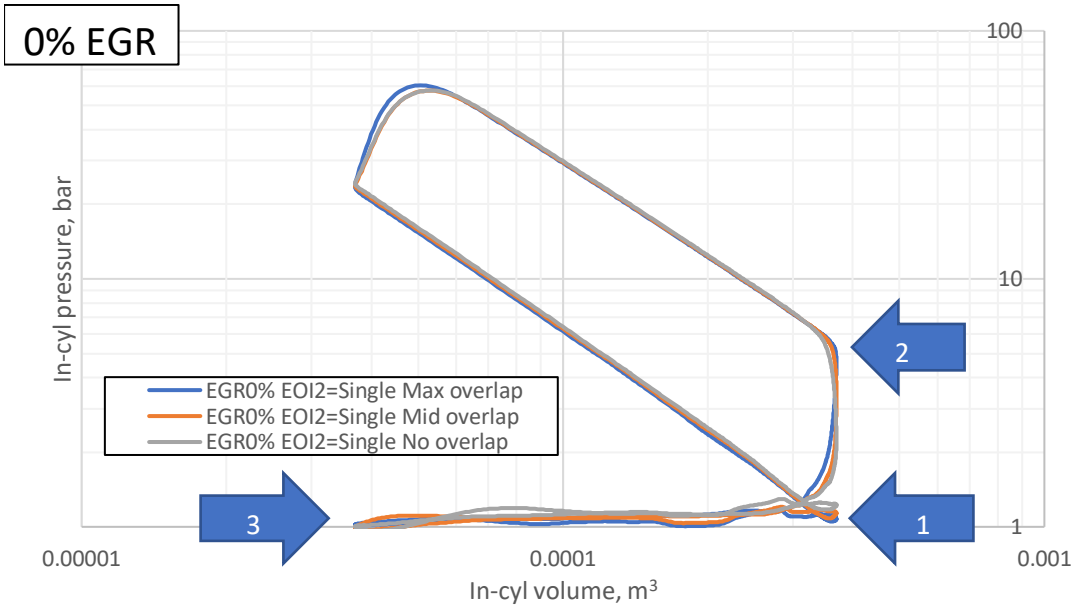

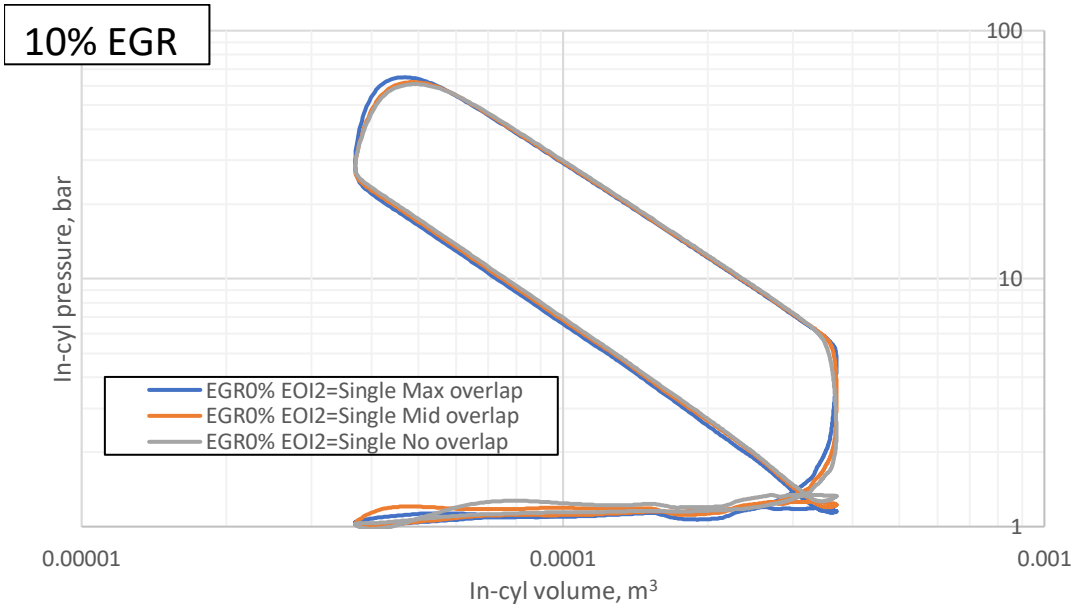

Figure 6-23 comparisons of in PV plot between different valve-overlap durations at 13.7bar Net_IMEP. Top=0% EGR case, bottom=10%EGR case.

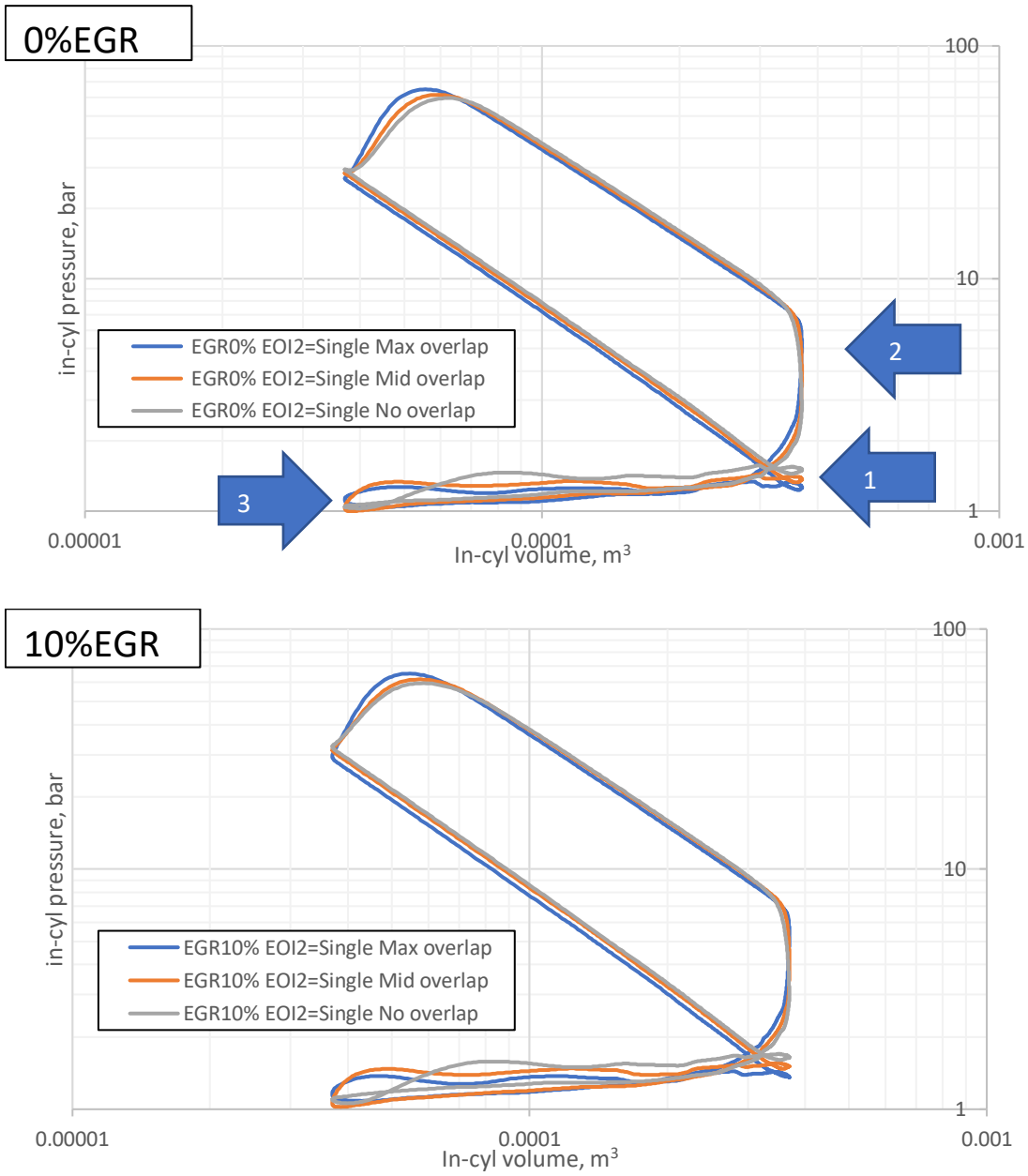

Figure 6-24 comparisons of in PV plot between different valve-overlap durations at 16.4bar Net_IMEP. Top=0% EGR case, bottom=10%EGR case.

6.6.2 Combustion phasing

The initial burn duration (ST-CA10) in CAD is plotted on the upper graph of Figure 6-25. All 'second injection position' test sweeps have the same characteristics, and the only effects seen are due to EGR and use of reduced valve-overlap duration, which results in a global offset of the same characteristic. The split injection has little effect on the early stage combustion. This combustion delay effect peaks at around EOI2=-150CAD aTDC.

The CA50 and CA90 results are shown in Figure 6-25, on the middle and lower chart. Here very different effects are shown at the two loads tested. At 13.7bar Net_IMEP. The addition of EGR causes a clear shift in combustion phasing for all valve-overlap cases, and the degree of shift remains similar. In contrast, at 16.4bar Net_IMEP case, the positive effect of EGR is noticeably larger when the valve-overlap is fully eliminated.

CA90 position plot shows the same characteristics as the CA50 position plot but with more pronounced characteristics. The sudden advancement of CA90 position is noticed once again specifically at max valve-overlap duration with EGR when EOI2 =-100, -75 CAD aTDC before a big delay is noticed for later second injection timing. As the same can be seen in both 13.7bar Net_IMEP and 16.4bar Net_IMEP, it can be said that the effects of the second injection are near-universal and regardless of inlet pressure and overall phasing of combustion.

To summarise, three traits can be noticed regarding the combustion phasing by studying the three plots: 1) regardless of the valve-overlap duration, the combustion speed is sensitive to split injection timing when EGR is present 2) combustion phasing is principally determined by the EGR presence or load, where at 13.7bar Net_IMEP- the presence of EGR increases the effectivity of split injection strategy, and at 16.4bar Net_IMEP- shortening the valve-overlap duration delays the CA50. Split injections have little impact on the phasing and knock tendency 3) for combustion duration, EGR slows down the combustion speed as shown by the increased combustion duration results. The split injection is also seen to have little effect on the combustion process with EGR. It is however noticed that the use of EGR and reduced valve-overlap duration lead to a more visible effect of combustion delay that closely resembles the initial burn speed effects. One area of interest shows a sporadic speed up and a slowdown of the combustion speeds seen at 13.7bar Net_IMEP without EGR when second injection timing is between EOI2=-250 to -175 CAD aTDC.

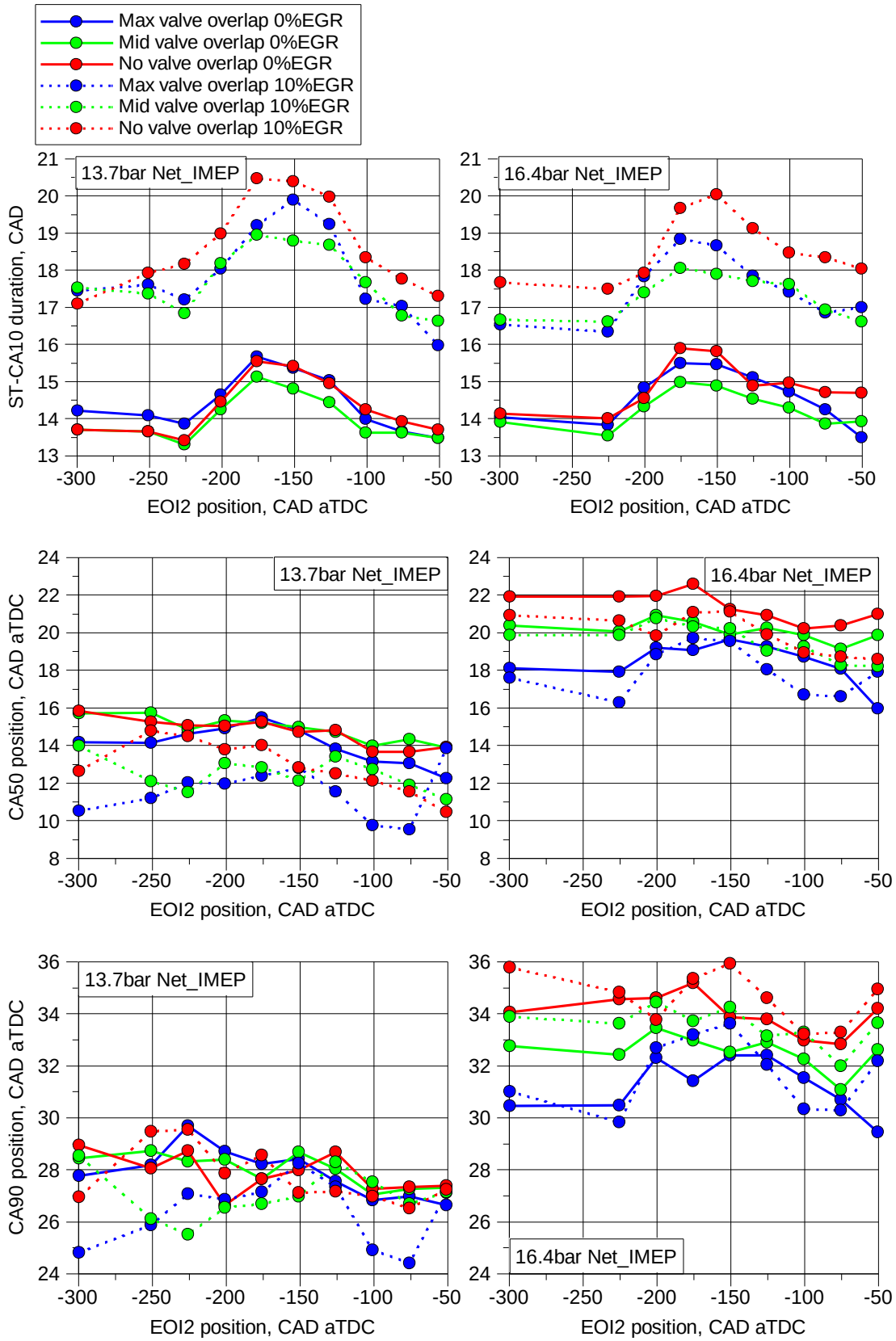

Figure 6-25 Combustion phasing data with valve-overlap reduction and split injection timing a. Early flame propagation ST-CA10 b. CA50 position c. CA90 position

The HRR average of n=300 consecutive cycle is plotted in a ribbon type graph in Figure 6-26, Figure 6-27, Figure 6-28, and Figure 6-29. The plots are bundled by load and EGR

dilution cases, the far-left ribbon shows the single injection case for comparison, and each ribbon to the right shows the next EOI2 timing corresponding HRR. The test details are given by the labels in the Figures. The colour represents the HRR, where hotter colours indicate a higher HRR at that crank angle point. By observing the hotter colour positions for every chart, the level of combustion phasing for higher heat release can be studied for every sweep.

In general, the use of shortened valve-overlap has lowered the HRR. However, the use of split injections with shortened valve-overlap has recovered the HRR, in some cases, phased the HRR_{max} position earlier than the single injection case. This suggests a synergy between split injections with the valve-overlap elimination.

At the of 13.7bar Net_IMEP with 0%EGR and the maximum valve-overlap, the highest HRR is observed in the single injection case. As split injections are introduced with later EOI2 timing, the combustion becomes less intense. From EOI=-75CAD aTDC the split injections produce more advanced combustion as seen circled in red. As the valve-overlap is shortened, the HRR phasing is shifted earlier with split injections. This indicates a minor level of optimizable second injection position with shortened valve-overlap.

With the introduction of EGR, the combustion is lengthened with an increased knock tolerance. HRR_{max} values are reduced by around 10J/CAD. But noticed is the effect of split injections on both advancing and retarding the combustion phasing as seen by the HRR plots. The lengthened combustion appears to have amplified the split injection effects to cause a more chaotic response in these figures.

At 16.4bar Net_IMEP, the overall late phasing of the combustion appears to have amplified the stratification effects of split injections even further at the maximum valve-overlap. However, the same effect is not seen with the other overlap cases or with EGR.

While no conclusive trend is observed, the visual appearance observed in these plots has helped to understand the mixed effects of split injections, EGR, and load. Amongst them, there is a clear pattern showing that the second injection timing (EOI2) can be used to advance the HRR phasing.

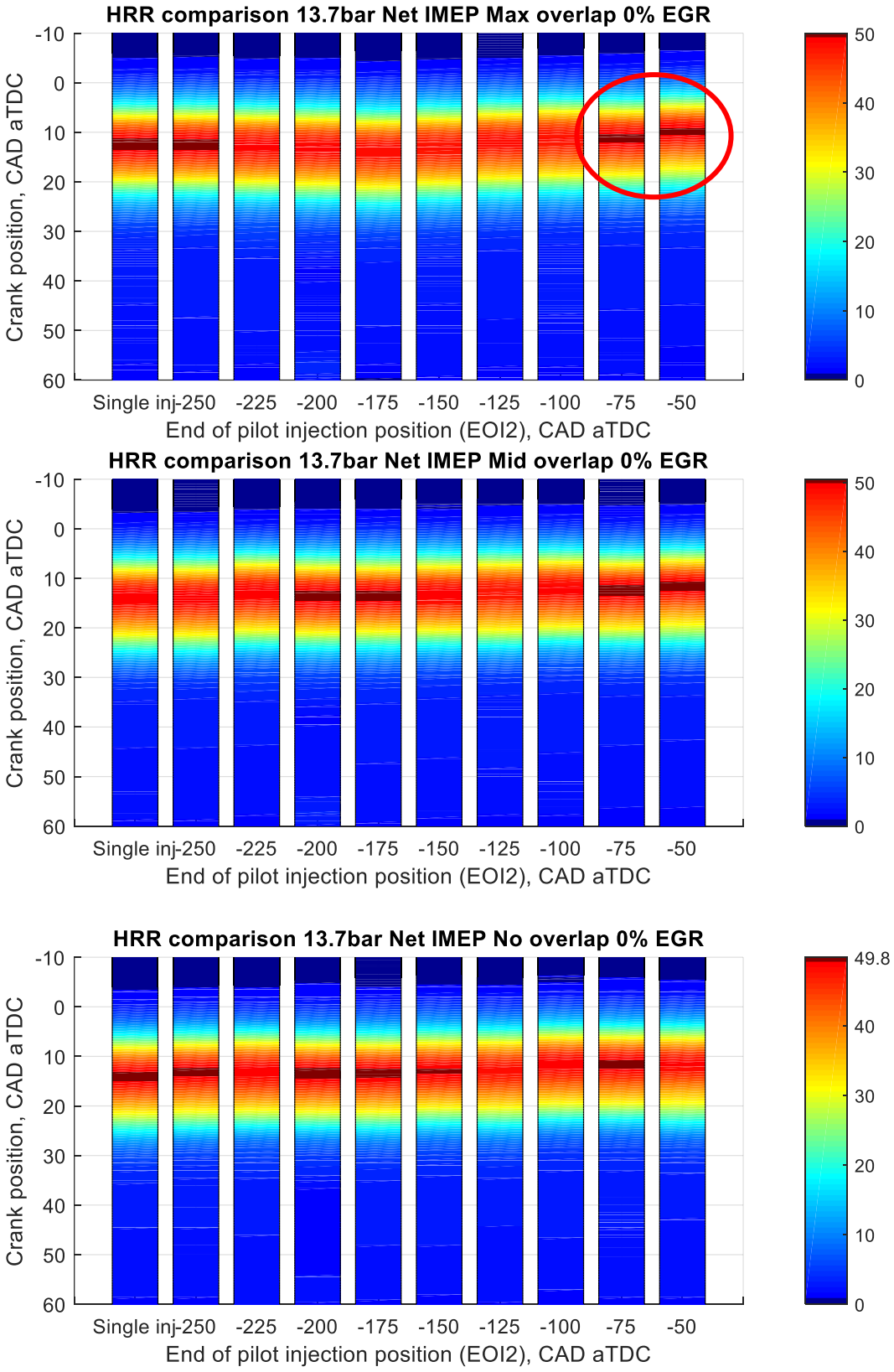

Figure 6-26 HRR comparison 13.7bar Net_IMEP without EGR dilution

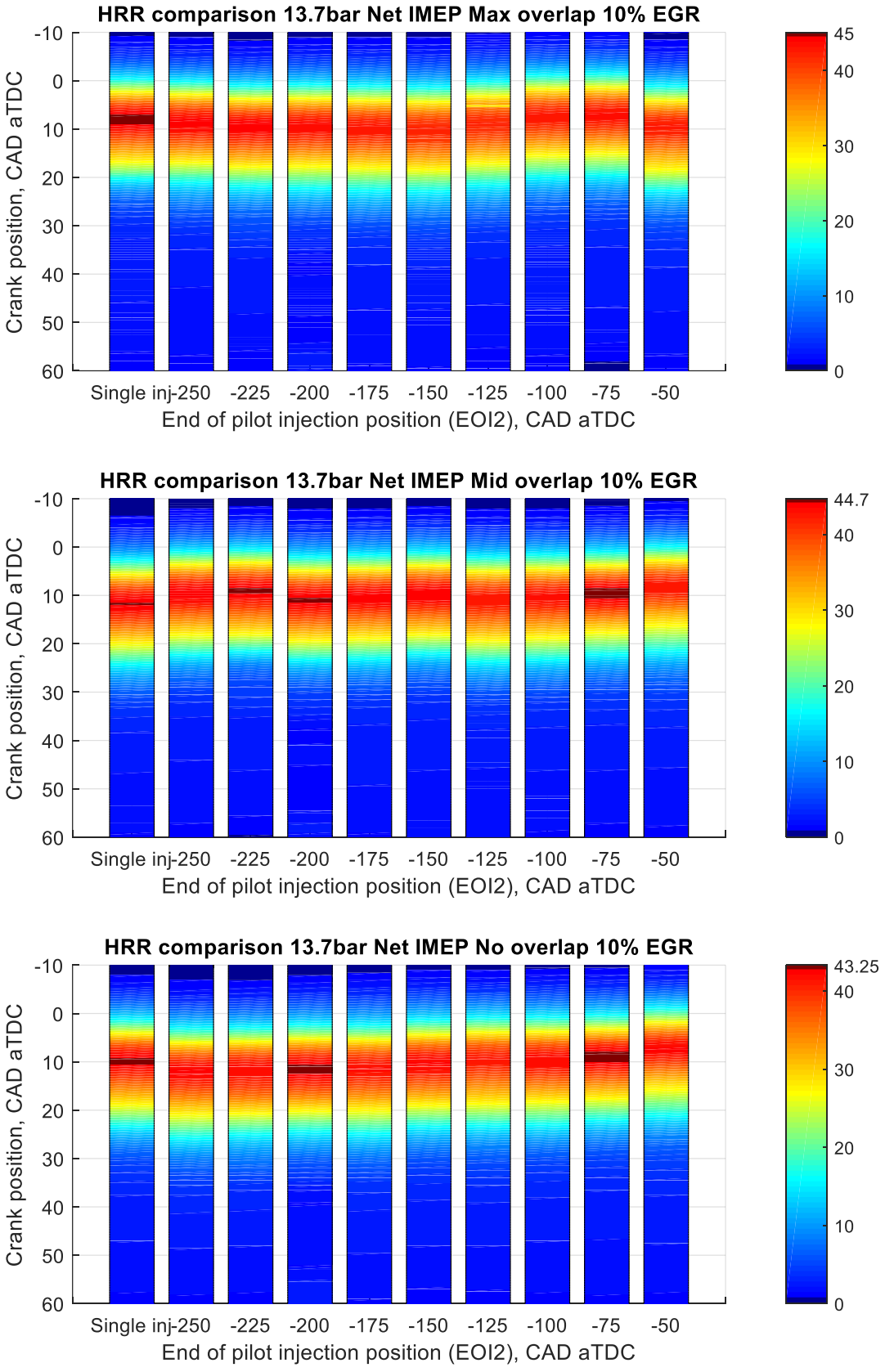

Figure 6-27 HRR comparison 13.7bar Net_IMEP with 10% EGR dilution

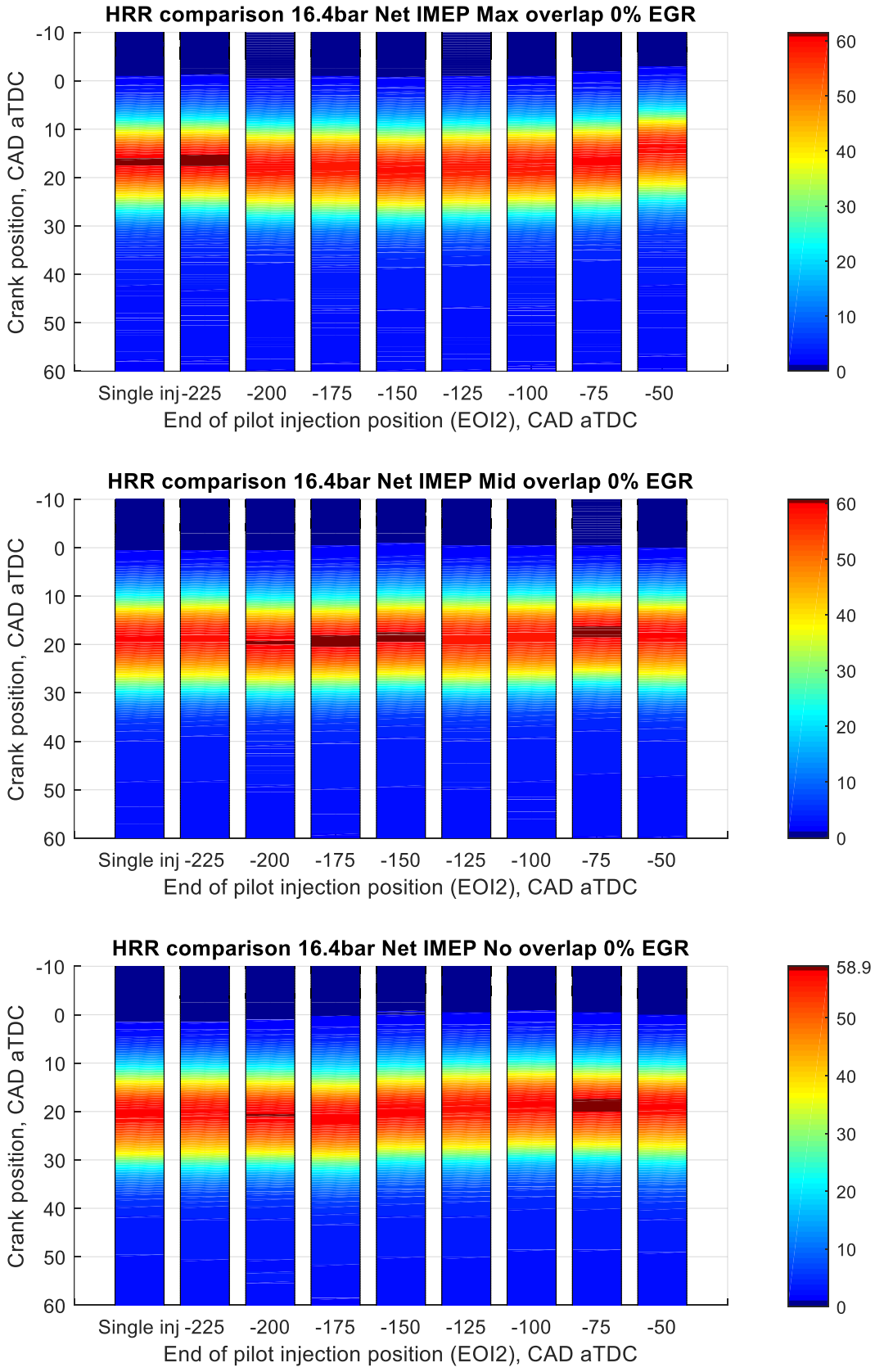

Figure 6-28 HRR comparison 16.4bar Net_IMEP without EGR dilution

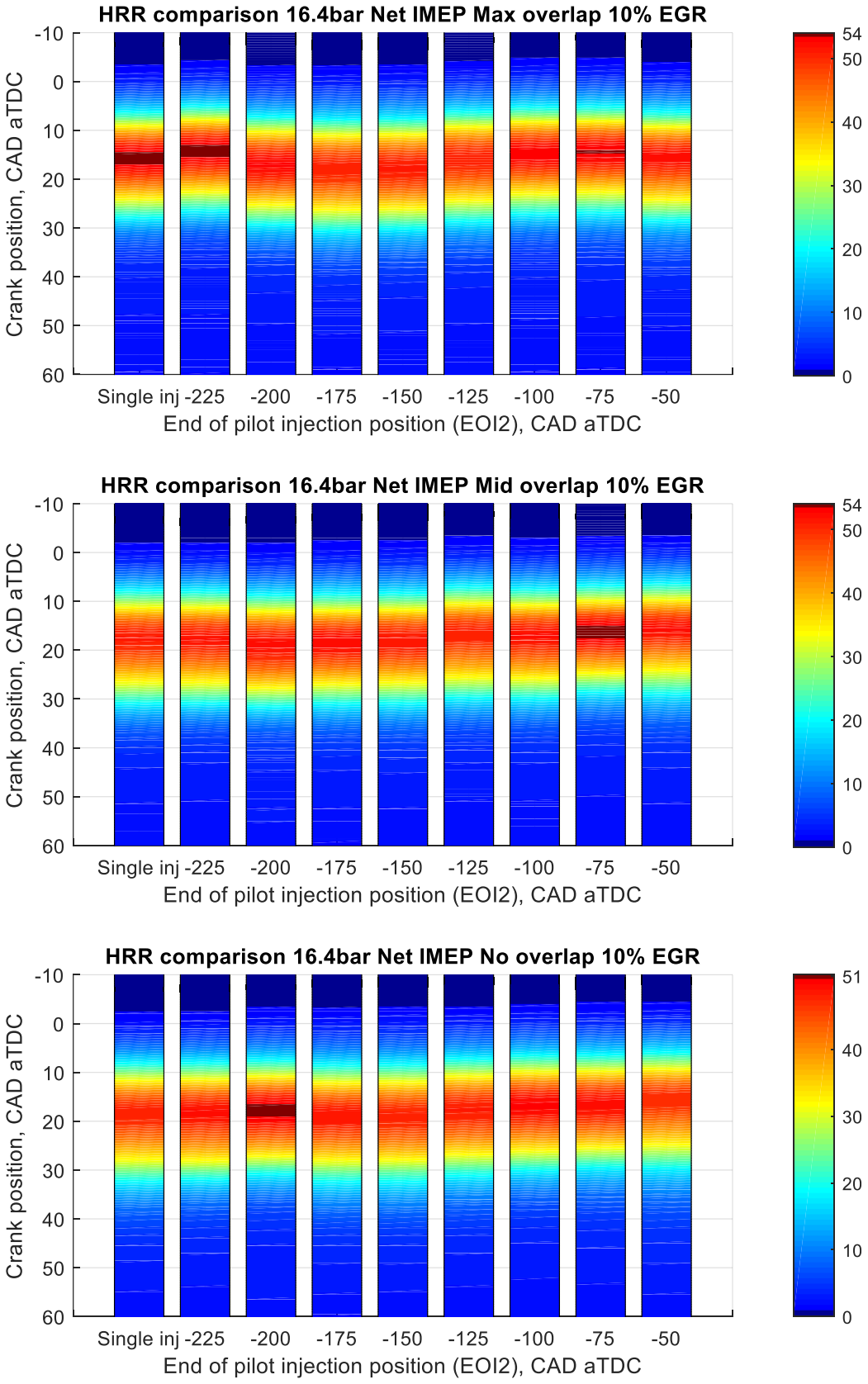

Figure 6-29 HRR comparison 16.4bar Net_IMEP with EGR dilution

6.6.3 Effects of split Injections on combustion stability

The effect of split injections and timings on combustion stability is displayed in Figure 6-30 with changes in the valve-overlap duration change and EGR.

In all cases, better stability values are seen at around EOI2=-225 and -100CAD aTDC. Instabilities are found at EOI2=-150 and -50CAD aTDC. Both single injection and split injections with EOI2=-250CAD aTDC cases (exclusively for 13.7bar Net_IMEP tests) have higher levels of cyclic variation than other split injection cases. The trend is highly correlated to the combustion phase defined by CA50 and the HRR profile. The slower initial combustion after TDC is worsened by the increasing cylinder volume and EGR with no valve-overlap. The combination of 10% EGR dilution and valve-overlap elimination takes the cyclic variation above 2.0% at 16.4bar Net_IMEP.

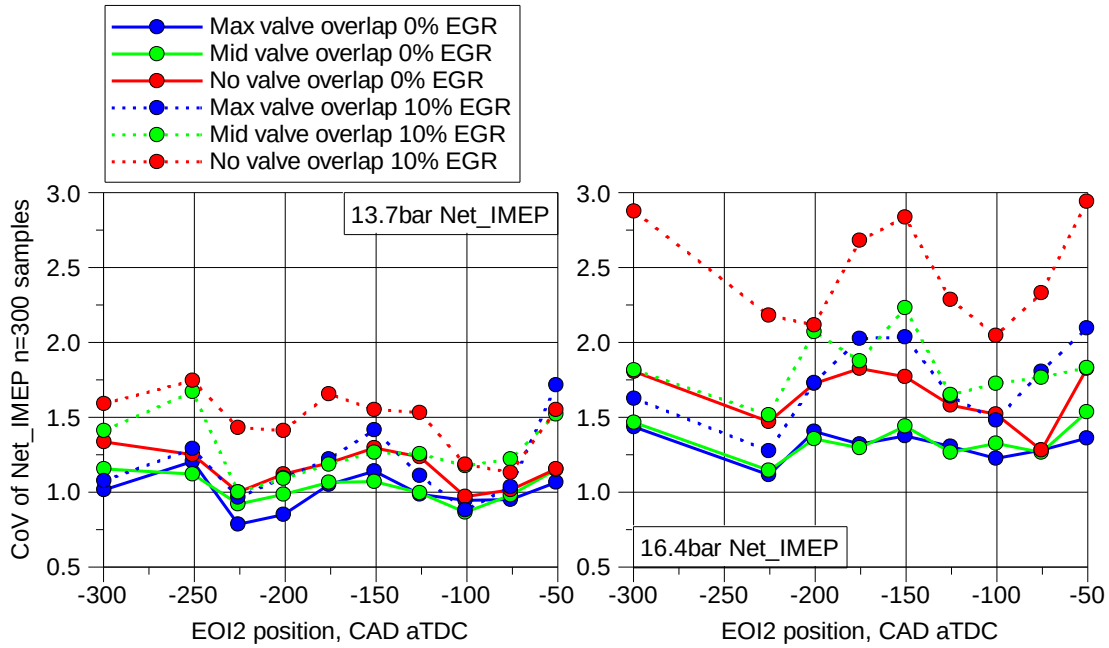

Figure 6-30 CoV of Net_IMEP across n=300cycles, indicating the stability of combustion for all sweep cases with EGR introduction and valve-overlap elimination.

6.6.4 The resulting efficiency of the EGR and reducing valve-overlap duration

Figure 6-31 to Figure 6-32 show the BSFC and ISFC values from the SFI EGR operation with valve-overlap reduction.

The characteristic response of BSFC and ISFC values to the split injection is similar for all cases. Both the valve-overlap duration and EGR have a large effect on the efficiencies. The impact of the second injection position is slightly more pronounced at engine operations with a shorter overlap and EGR.

For a better comparison of efficiency effects, the plot in Figure 6-32 shows the %age improvement of ISFC with regards to EOI2 timing. A positive number indicates an efficiency benefit and the comparison is made between the corresponding EOI2 time to the single injection case of every sweep. Split injection brought fuel efficiency benefits when the valve-overlap was reduced. At 13.7bar Net_IMEP, this effect is flat and stayed around the 1-2% improvement mark. EGR dilution further improves the ISFC/BSFC, especially when the valve-overlap is reduced. In contrast, at 16.4bar Net_IMEP case, ISFC shows a high sensitivity to EOI2 timing, albeit depending on the valve-overlap and EGR dilution settings. At EGR diluted conditions where the combustion speed is further reduced, the split injection appears to have a greater effect. In contrast, the split injection has almost no effect in the wide-overlap cases.

Finally, as a repeated trend, the case of latest second injection led to unfavourable efficiency condition due to suspected fuel impingement and insufficient mixing of fuel and air.

In summary, the efficiency gains are thought to have come from several areas: -

- Stoichiometric combustion from reduced valve-overlap to improve combustion efficiency
- Successful stratification increases combustion speed and stability for phasing recovery (at stoichiometric combustion condition with higher EGR fraction)
- External EGR to lower reactivity which increases mixture phasing ability
- External EGR to lower residual gas reactivity at reduced overlap conditions for even more phasing ability

The combination of above is true for the high load condition with EGR and no valve-overlap, which explains the biggest gains seen in the results (above 5% at ISFC improvement).

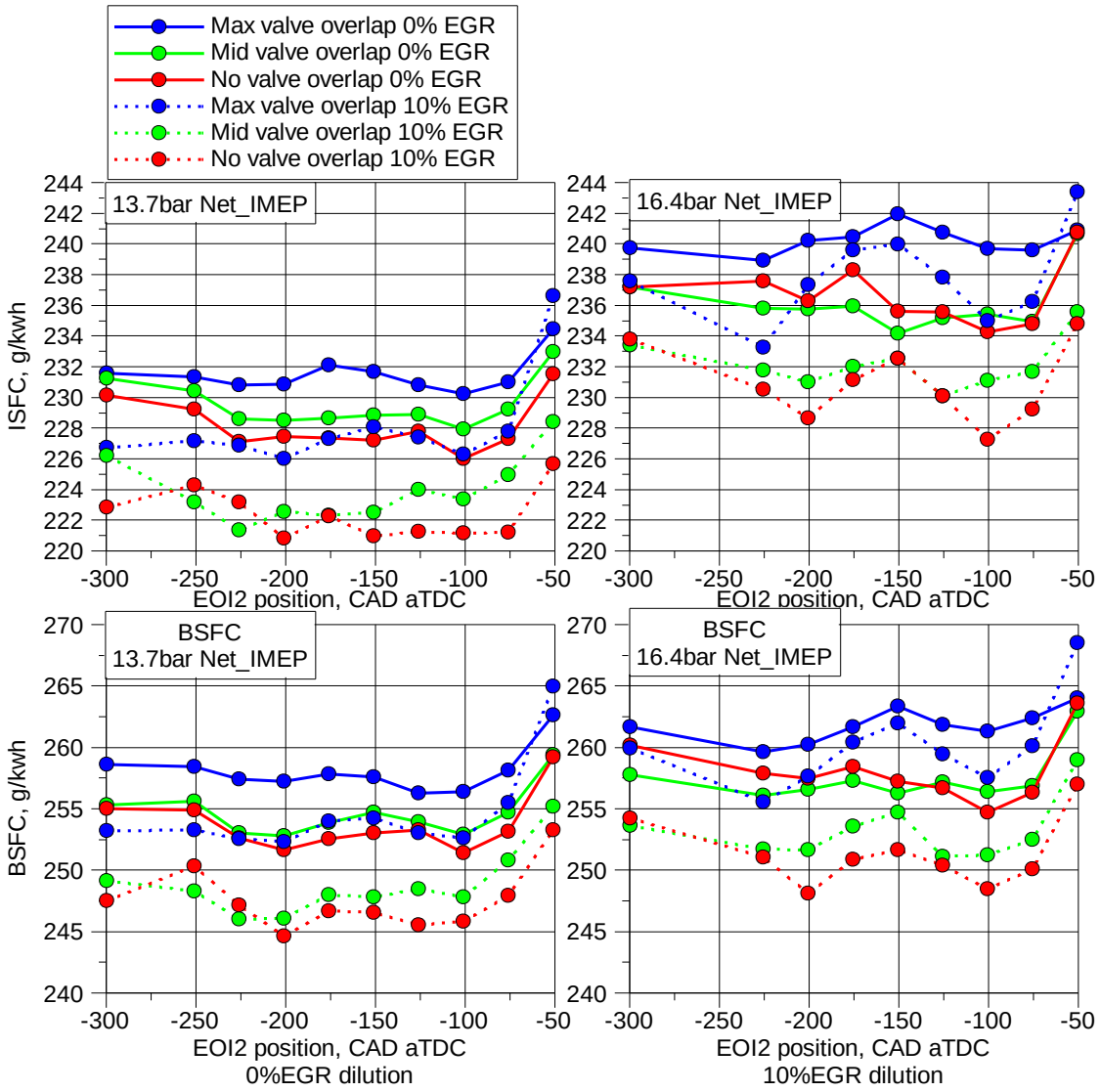

Figure 6-31 BSFC and ISFC of all results; with variance in valve-overlap duration, EGR dilution and second injection position

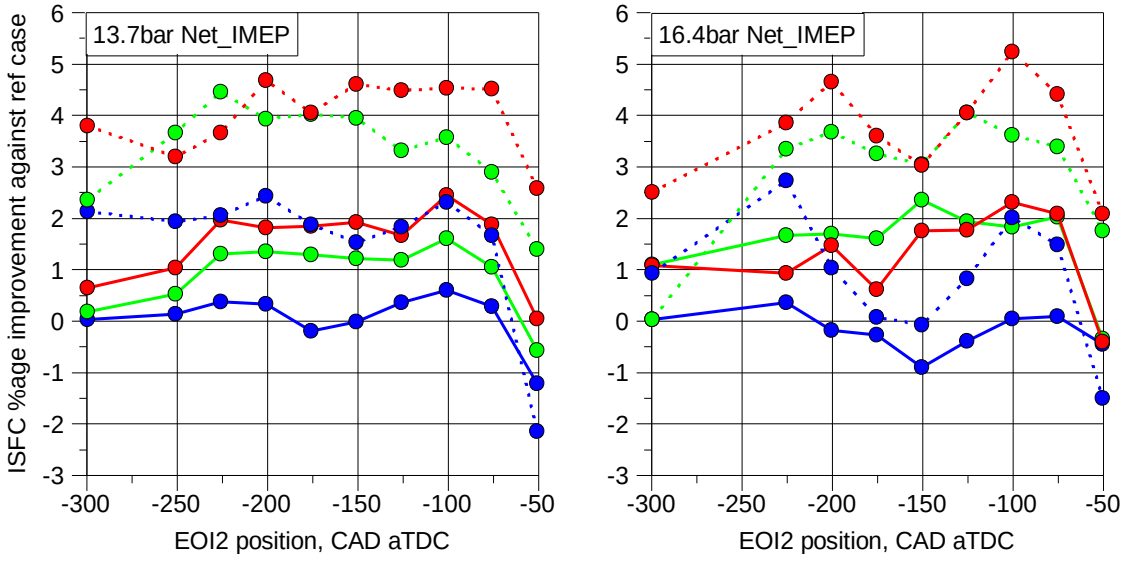

Figure 6-32 Engine ISFC change percentage against single injection case

The frictional SFC that is calculated by direct comparison of BSFC and ISFC is as plotted in Figure 6-33. Due to the fixed load and speed, the comparison of these figures is assumed to be a direct effect of the TC efficiency. A similar analysis is made in Section 5.3.3.

Second injection timing had an impact on TC efficiency, the effect comes from a mixture of exhaust gas condition change and boost demand differences, but how either of those effects comes to these results is not conclusive with the result available here.

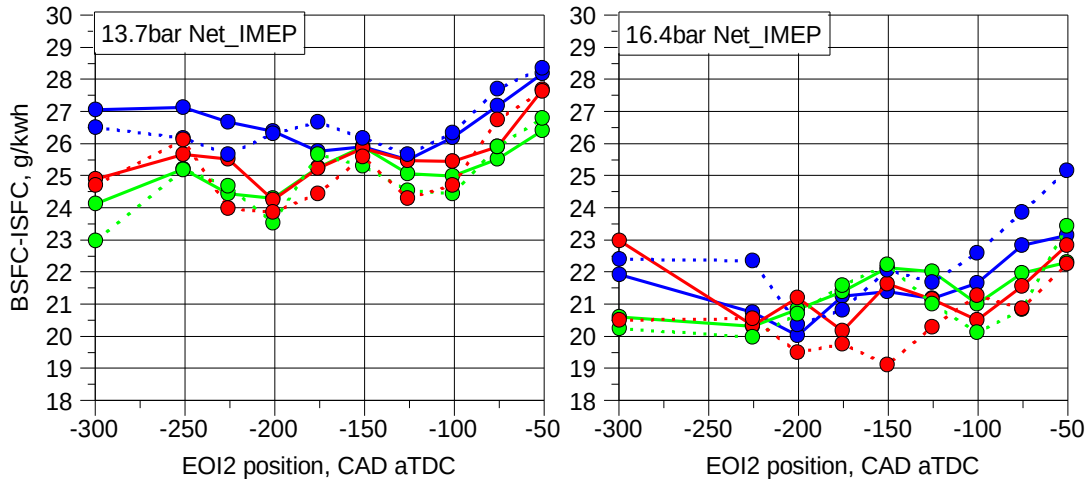

Figure 6-33 BSFC-ISFC figures against a single injection case

6.6.5 Symmetrical valve-overlap with SFI EGR on emissions

NO_x emissions were measured both before and after the TWC in the exhaust. The engine-out $ISNO_x$ results are plotted in Figure 6-34, and they are identical between the two tested loads.

As stated previously, EGR is effective in reducing the in-cylinder NO_x formation and exhaust NO_x emission. Without EGR, the NO_x emission is lower with the maximum overlap duration, but with EGR, the NO_x emission becomes higher with increased overlap duration. In general, as the valve-overlap is increased, the better scavenging charge cooling effect of fresh charge short-circuiting lead to lower charge temperature but it also leads to more advanced combustion phasing and hence higher combustion temperature. It seems that the charge cooling effect is more dominant in reducing the combustion gas temperature and hence lower NO_x formation, whilst when there is no EGR, the more advanced combustion phasing has a more pronounced effect on combustion temperature and NO_x formation due to earlier combustion near piston TDC.

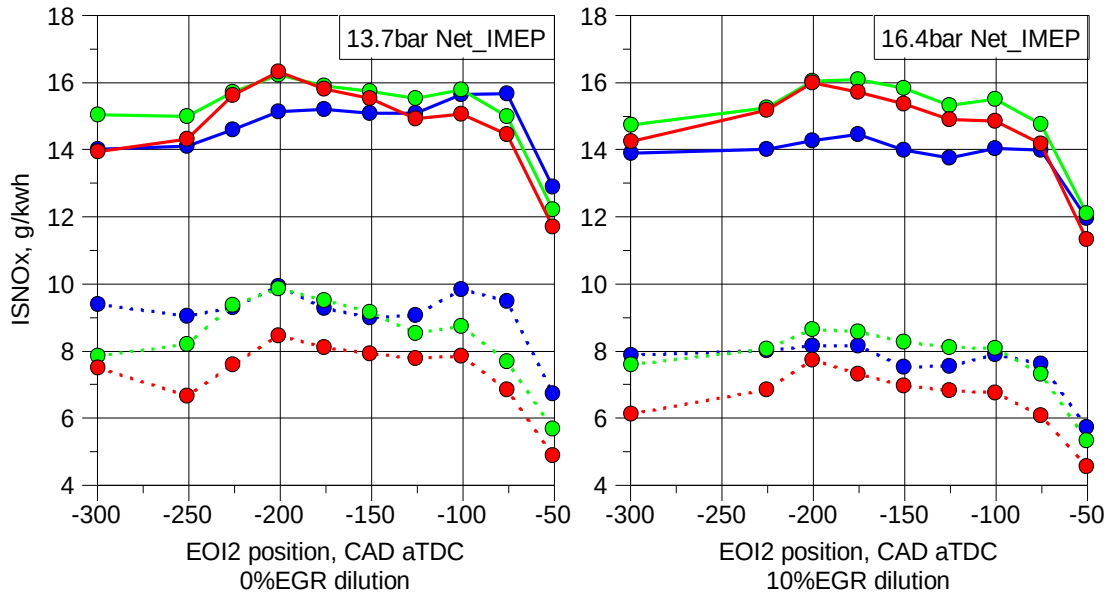

Figure 6-34 Pre-TWC ISNO$_x$ emission with variance in valve-overlap duration, EGR dilution and second injection position

NO_x presence in the tailpipe gas is plotted in Figure 6-35 by ISNO$_x$ figures. The emissions of NO_x are found to be very high in 3 conditions, 1) 16.4bar Net_IMEP max valve-overlap 0% EGR 2) 16.4bar Net_IMEP max valve-overlap 10% EGR, 3) 13.7bar Net_IMEP max valve-overlap 0% EGR at EOI2=-50CAD aTDC. For cases 1 and 2, the fresh air short-circuiting becomes larger at higher loads due to the greater inlet/exhaust pressure difference and wide valve-overlap. The NO_x conversion efficiency of the TWC drops with increasing O_2 concentration from the short-circuited air. In addition, the short-circuited fresh charge with EGR contains less O_2 and hence would have a lower impact on the conversion efficiency of the TWC.

A minor increase of ISNO$_x$ emissions is also noticed at 13.7bar Net_IMEP with max valve-overlap and 16.4bar Net_IMEP with mid valve-overlap when the EOI2 is retarded to -50CAD aTDC. This can be explained by the leaner mixture, as shown by the exhaust lambda results.

The engine-out ISCO emissions in Figure 6-37 indicates the combustion of the fuel-rich mixture in the cylinder because of the air short-circuiting. The larger the overlap and higher the boost, the richer the in-cylinder mixture becomes for higher ISCO emissions. The rise in ISCO emission with the most retarded injection is caused by the incomplete combustion of a locally fuel-rich mixture from the second injection.

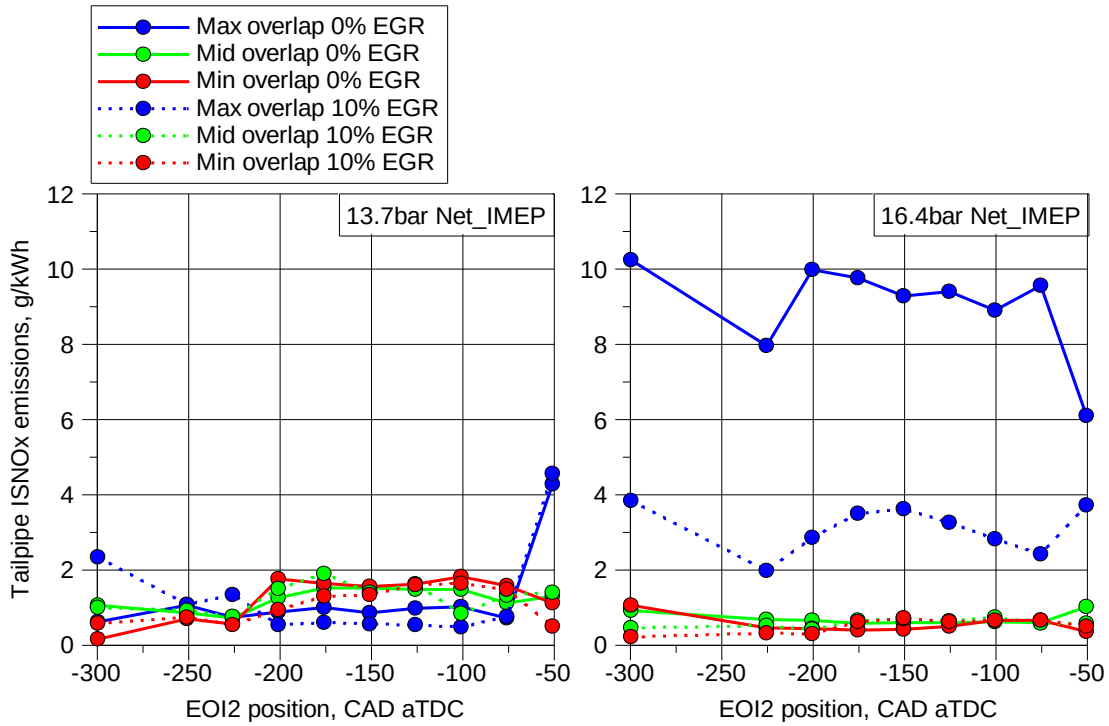

Figure 6-35 Tailpipe indicated specific NO_x emissions with variance in valve-overlap duration, EGR dilution and second injection position

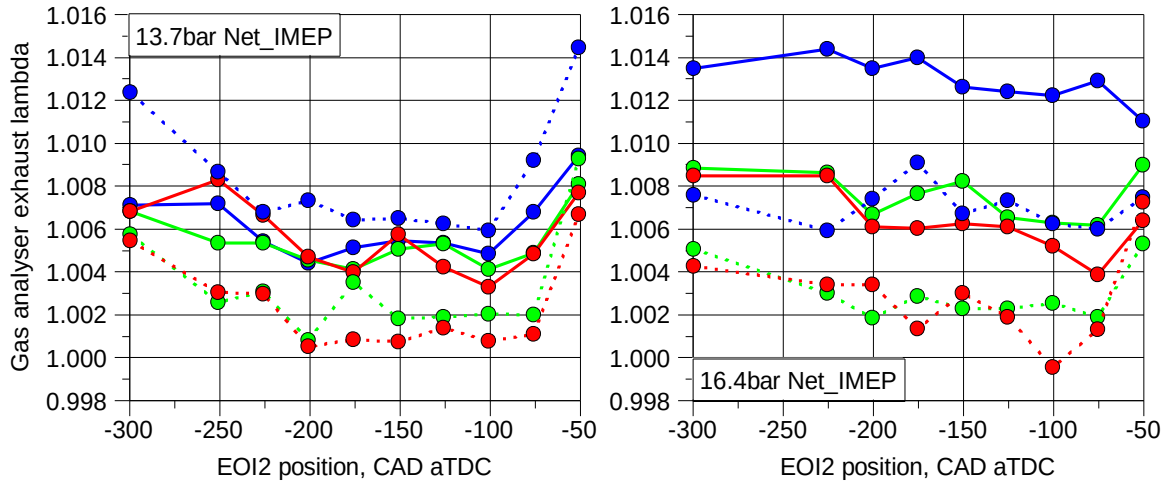

Figure 6-36 Horiba exhaust gas analyser result for true engine operating lambda with variance in valve-overlap duration, EGR dilution and second injection position

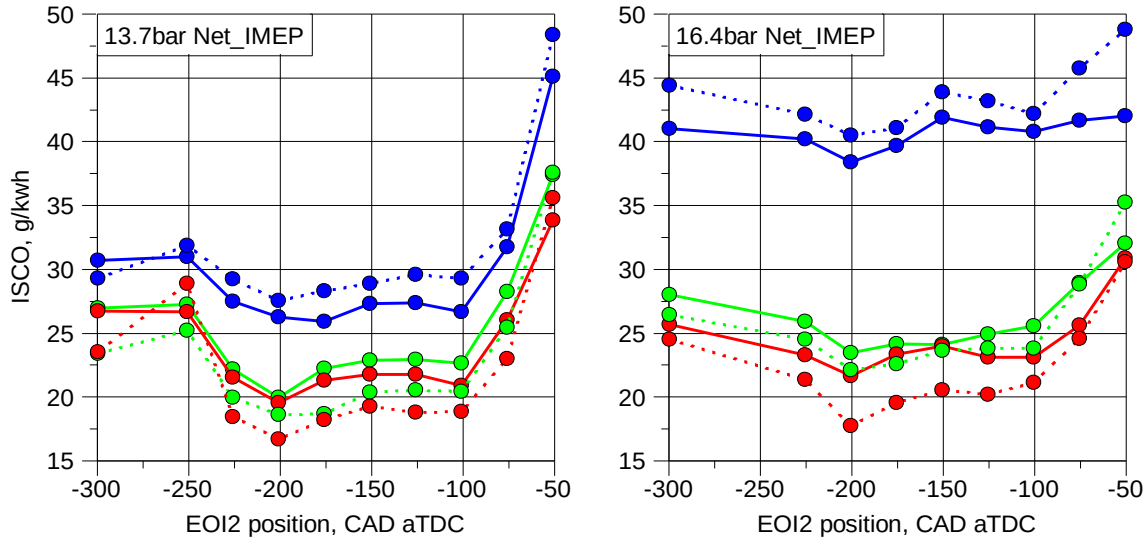

Figure 6-37 Pre-TWC ISCO emission with variance in valve-overlap duration, EGR dilution and second injection position

For the same reasons, THC emissions increases as the valve-overlap is widened. There is a gradual increase then a sudden drop in THC emission as the second injection is retarded; the same results are seen in Chapter 5. Crevice volume losses were increased from wall spray impingement from the late second injection. The sudden drop at EOI2=-50CAD aTDC was associated with the full impingement of the second injection at the piston crown (as opposed to the cylinder wall) which suggest promoted post-combustion oxidation of fuel as indicated by the slightly higher exhaust gas temperature shown in Figure 6-39.

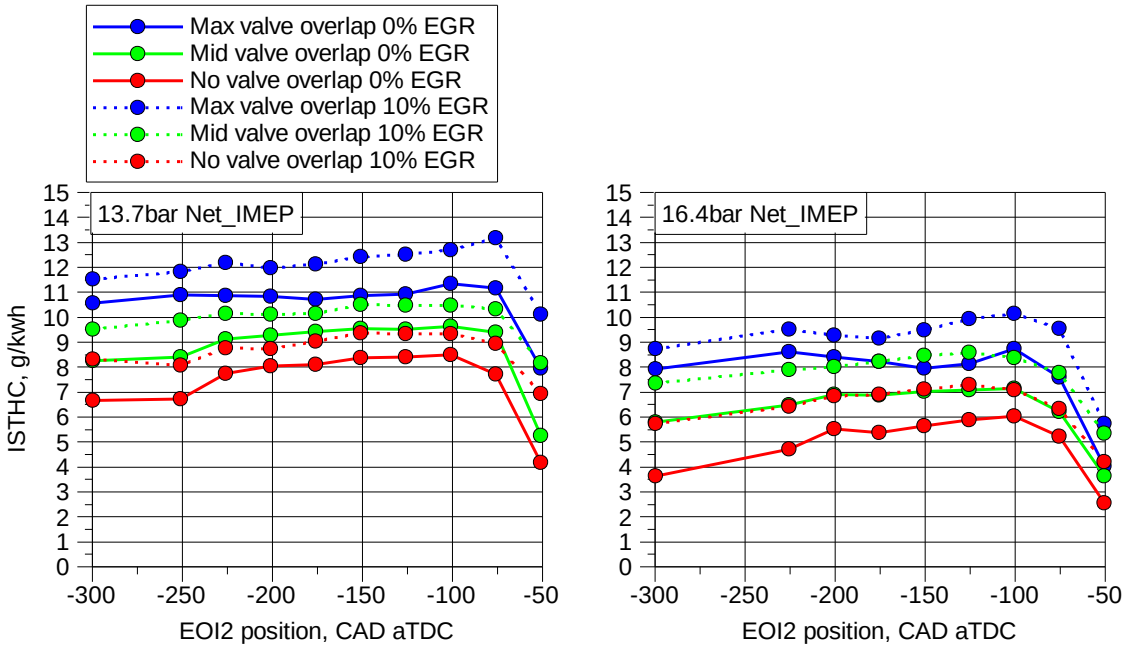

Figure 6-38 Pre-TWC ISTHC emission with variance in valve-overlap duration, EGR dilution and second injection position

Finally, another notable result of the test is the pre-turbo exhaust temperature as plotted in Figure 6-39. The hottest temperature is seen with reduced valve-overlap with no EGR dilution using late second injection position (T_{exh}=822DegC). The earlier opening and increased boost demand at this point have caused these conditions. Second injection position has affected the exhaust temperature where a peak was seen at EOI2=-175 and -50 CAD aTDC all conditions. Thus, the effect of combustion phasing has also affected the exhaust temperatures. External EGR dilution lowers the exhaust temperatures globally, which can be an effect of the increased heat capacity as well as the ability to advance the combustion. Valve-overlap duration had a very big effect due to a combination of two effects, the shift of combustion towards stoichiometric combustion and earlier opening of exhaust valves, thus increasing the temperature of combustion and exhaust gas that is ejected by the engine.

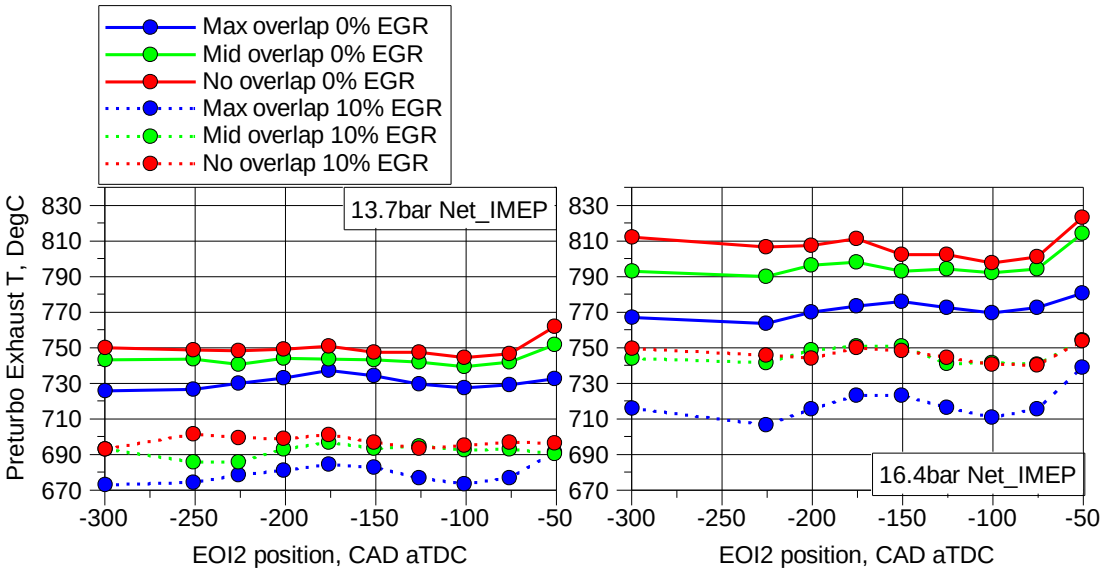

Figure 6-39 Pre-turbo exhaust temperature with variance in valve-overlap duration, EGR dilution and second injection position

6.6.6 Symmetrical valve-overlap with SFI EGR on particulate emissions

Figure 6-40 shows the effect of second injection timing on the particulate emission before at the TWC. The nucleation mode particles are defined as the particles of size less than 35 µm, and accumulation cells are any particles larger than 35 µm of size.

The variation in the particle concentration of both nucleation and accumulation modes exhibits similar trends at both loads. The accumulation mode particle count rises as EOI2 is retarded to -75CAD aTDC followed by a reduction of value on EOI=-50CAD aTDC. With the retarded second injection cases, the closer proximity of the piston is allowing the injection to reach the crown surface, causing a pool fire that leads to an incandescent burn with higher levels of accumulation mode particles forming. The reduction of these particles seen at

EOI=-50CAD aTDC can be associated with the earlier phasing of burn achieved from the stratification, causing a hotter burn with more time available to oxidize the carbon particles.

For cases of second injection earlier than EOI2=-100CAD aTDC, the accumulation particulate count at 13.7bar Net_IMEP the is higher, mainly when the valve-overlap duration is wider. Use of reduced valve-overlap is thought to have reduced the particulates due to a hotter in-cylinder condition from increased internal EGR rates. At the higher load of 16.4bar Net_IMEP, the higher-pressure conditions may have caused a similar effect leading to an overall lower count.

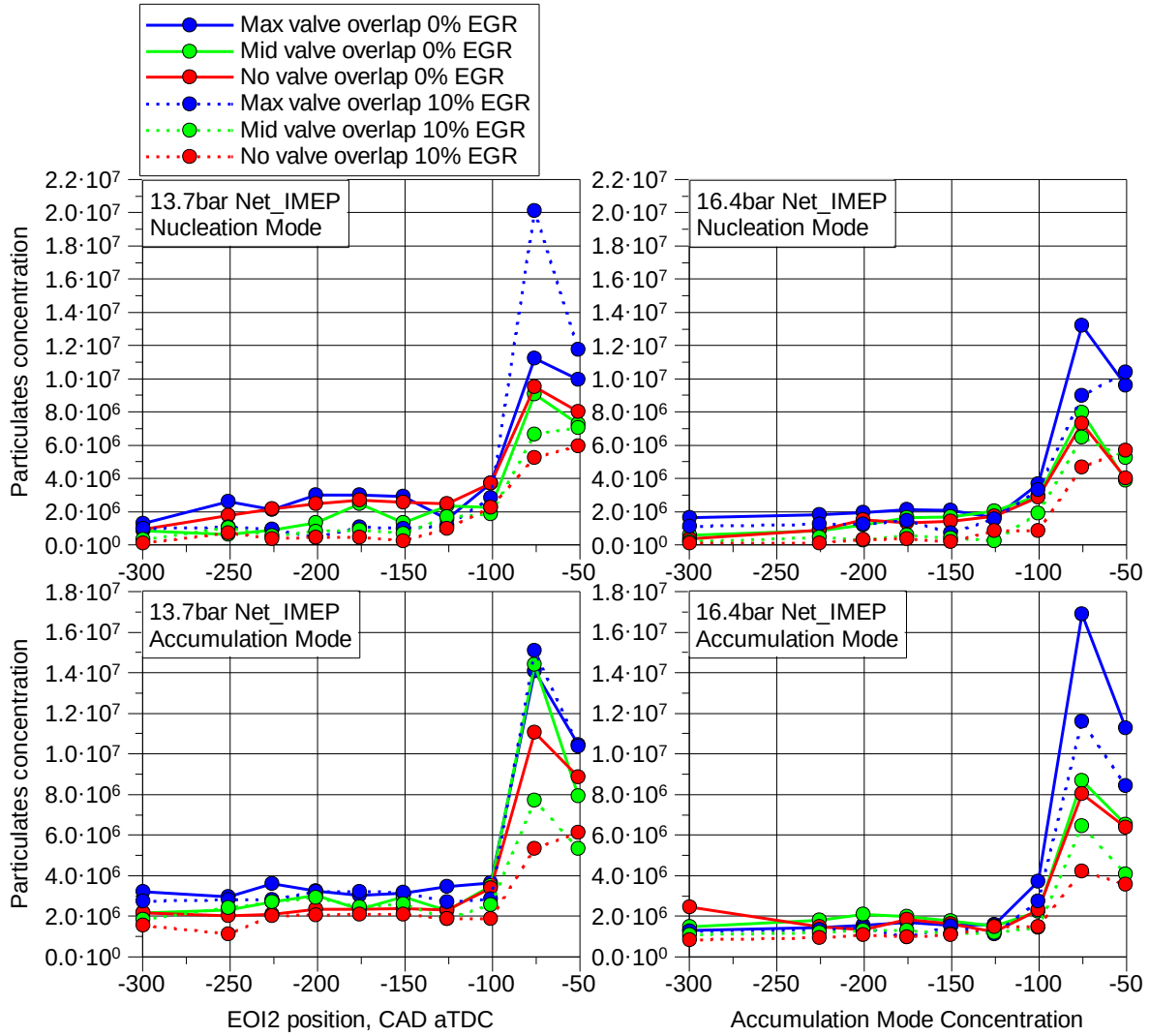

Figure 6-40 Accumulation mode particulates concentration by EOI2 position sweep

The particle size distributions are plotted in Figure 6-41 at different valve-overlap and EGR levels. The reduction of valve-overlap duration and the use of EGR has led to an overall drop in particle count.

At 16.4bar Net_IMEP with 0% EGR, the particle count seems to be insensitive to the valve-overlap duration. The addition of 10% EGR reduces the number of particles of >50nm in the nucleation mode.

For most of the cases seen here, the biggest changes in the particulate count are seen around the size< 40nm regions. The increase in the finest measured particles (size<7nm) is most pronounced in the cases with EGR and reduced valve-overlap period.

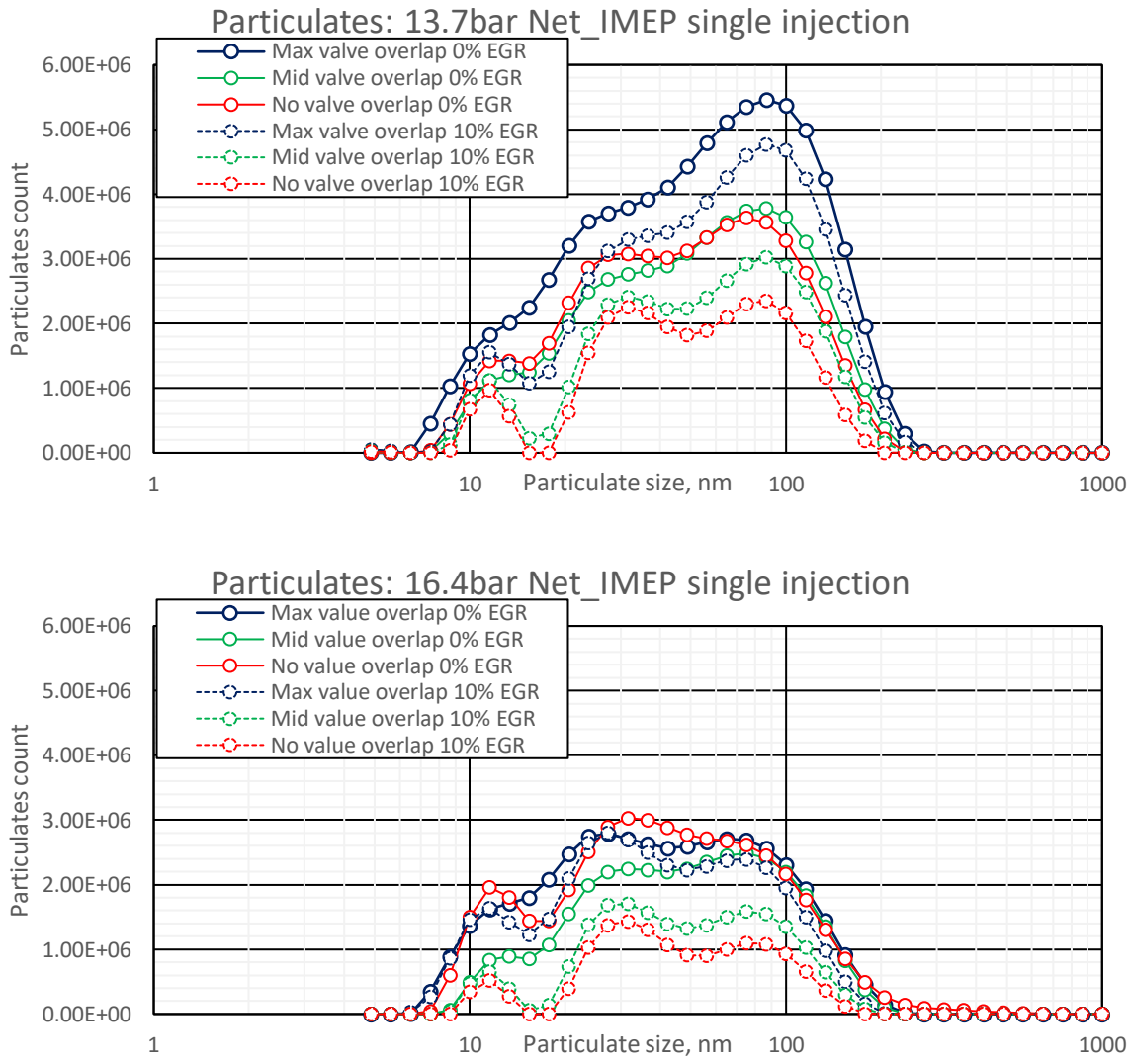

Figure 6-41 Particulates emission characteristic for single injection case with reduced valve-overlap and EGR

The particulates emission with the second injection at EOI2=-200CAD aTDC is plotted Figure 6-42 for comparison. With an early second injection, there is a small overall increase

of particulates emission for the 13.7bar Net_IMEP case but no considerable change at 16.4bar Net_IMEP.

Like the single injection case, 10% EGR reduces the particle count by different factors depending on the valve-overlap and load case.

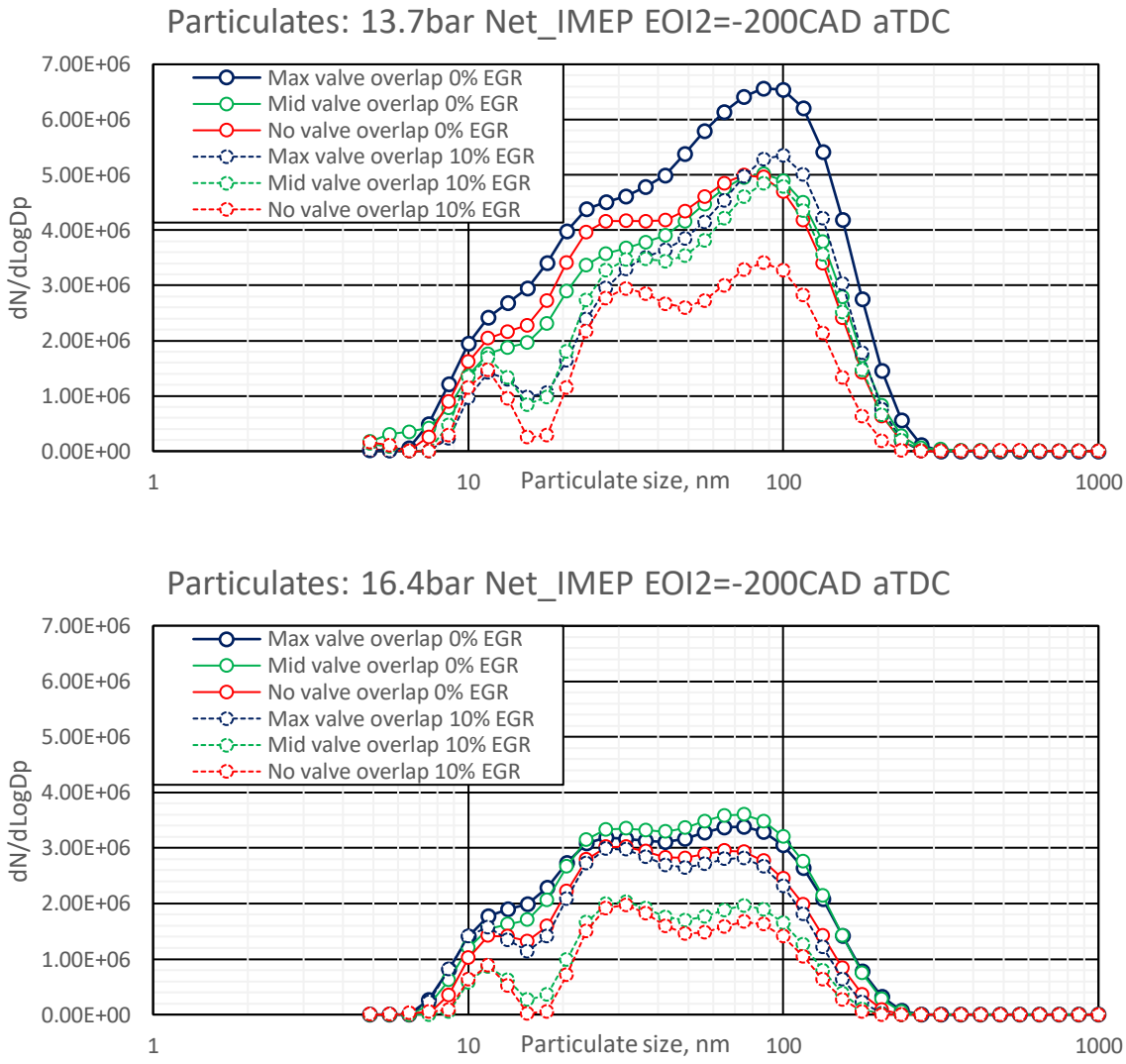

Figure 6-42 Particulates emission comparison with split injection (EOI2=-200CAD aTDC), reduced valve-overlap, and EGR

A detailed look at the two latest second injection timings (EOI2=-75, -50CAD aTDC) are compared and displayed on Figure 6-43, these retarded second injection timings are found to emit the highest particulates as highlighted in the particle concentration charts. First, it is important to note that the order of power has increased to 7 on the particulate count (y-axis), which highlights the dramatic increase of particulate count for this load.

With the split injections, the valve-overlap has the biggest impact on the particle count where the highest concentration is observed with the max valve-overlap. While the same trend is seen in other loads, the emissions seen here far surpasses the others.

At EOI2=-75CAD aTDC, the highest observed count is in the nucleation particulate size range, a peak is seen at 5.6nm particle. The same is seen in both loads, and the presence of EGR made no difference to these figures. The shortening of valve-overlap reduces the particulate counts drastically to around 66% of the original value at 13.7bar Net_IMEP and a 10% at 16.4bar Net_IMEP, which contrasts greatly. These very small particles are thought to be THC (VOC) that atomised and reformed after leaving the cylinders, hence the greater value at richer trapped conditions.

The EGR dilution appears to lower the particle concentration of all sizes only when the valve-overlap is shortened. The level is reduction is significant for both loads and second injection timings.

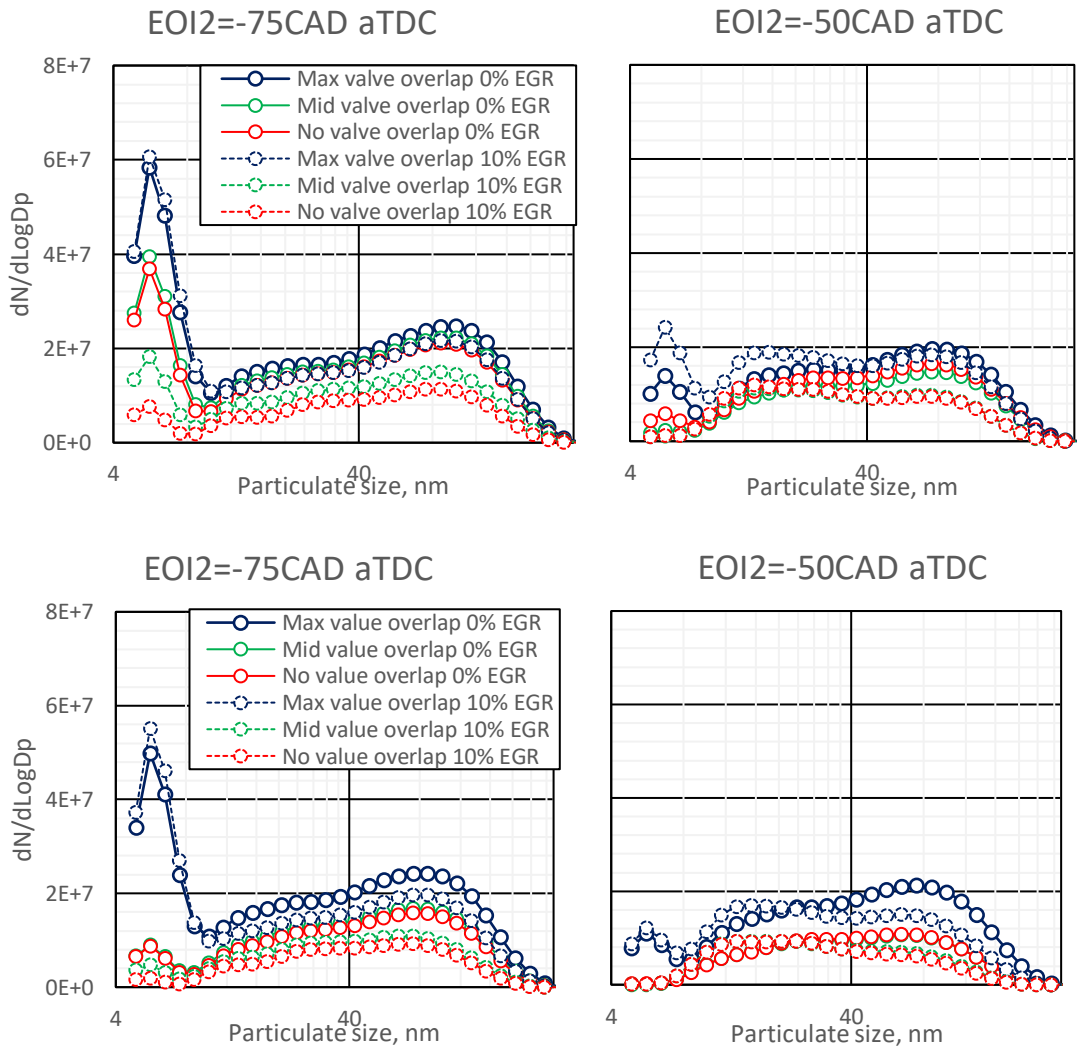

Figure 6-43 Particulates emission comparison with split injection (EOI2=-75CAD aTDC), reduced valve-overlap, and EGR

The highest particulates are seen at the second most retarded second injection timings (EOI2=-75CAD aTDC) where the 13.7bar Net_IMEP case is roughly twice higher than the 16.4bar Net_IMEP case. At this point, most of the particle size is determined by the presence of external EGR. In almost all cases, the particulate count of size>10nm is reduced with no valve-overlap, but also increased the smaller particulates for cases with EGR dilution. The characteristics of this increase are dependent on the EOI2 position.

6.7 CFD investigation of valve timing effects

The effects of flow interaction and short-circuiting had dominated the results when the valve timings were changed at boosted loads. This section investigates these changes in flow and quantifies the effects by analysing the 3D CFD data.

A 3D CFD simulation is run with inlet/exhaust ports and valve, the full scavenging to compression process was simulated. The short-circuiting was thus monitored for flow ratio and analysis of occurrence mechanics.

6.7.1 Short-circuiting comparison due to boosting, EGR dilution and wide valve-overlap

Three cases were simulated to compare the short-circuiting effects of the valve-timing

- 16.4bar Net_IMEP 51CAD overlap 0% EGR (Baseline)
- 16.4bar Net_IMEP 27CAD overlap 0% EGR
- 16.4bar Net_IMEP 51CAD overlap 10% EGR

The higher load and thus greater boosting are suspected to increase the short-circuiting, the reduced overlap of the second case is expected to lower this short-circuit ratio as shorter time is avail for the flow to make it across from the inlet to exhaust ports.

The short-circuit flow indication is visualised by the distribution of RGF as shown in Figure 6-44. The figures show the baseline case with the highest short-circuit ratio, and development of flow can be observed with signs of unmixed fresh air travelling straight to the exhaust port at TDC.

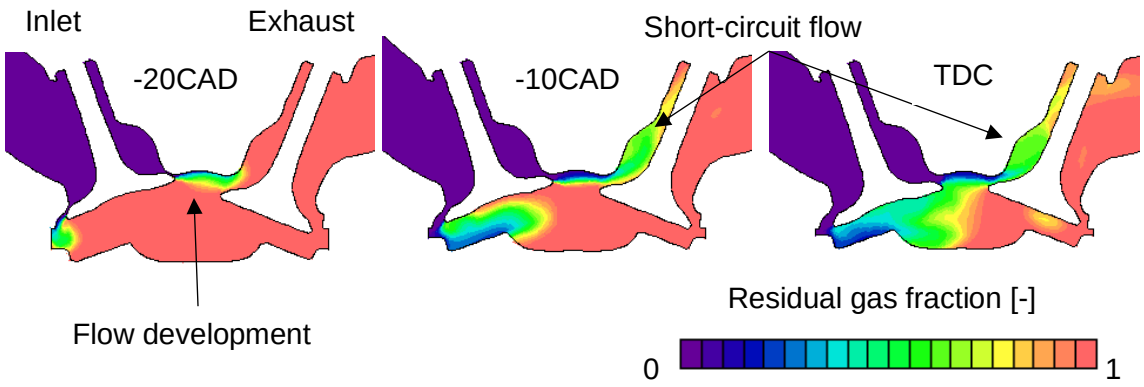

Figure 6-44 Short-circuit flow seen in cross-section visualisation of the residual gas fraction. 16.4bar Net_IMEP, 51CAD valve-overlap

The CFD based visualisation for the mid valve-overlap case is shown in Figure 6-45. When the overlap duration was shortened to 27CAD, the exhaust port was closed before the flow channel was established. However, some short-circuiting is observed.

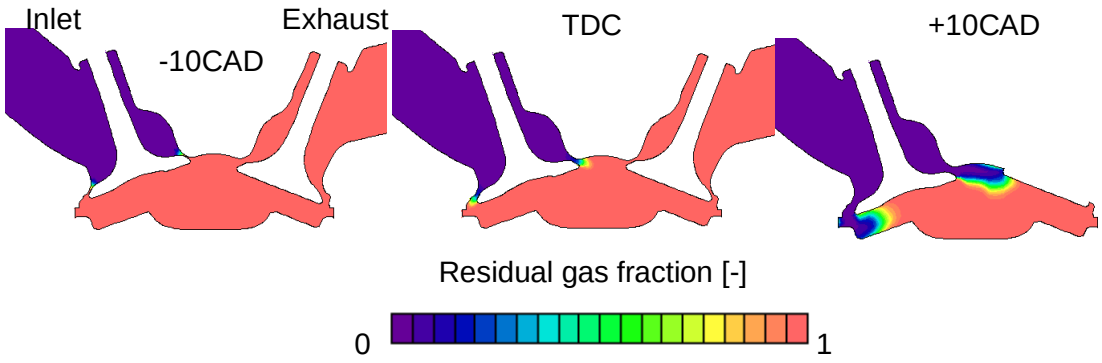

Figure 6-45 Short-circuit flow seen in cross-section visualisation of the residual gas fraction. 16.4bar Net_IMEP, 27CAD valve-overlap

The flow velocity is visualised and is shown in Figure 6-46; the differences between the EGR dilutions are compared. Analysis of the flow velocity during the overlap duration shows the high-speed flows, and thus inertia of the exhaust flow, the proximity of the inlet port is also found to contribute to the flow that causes the short-circuiting. In the case with 10% EGR dilution, the flow contour difference between the ports, the inlet flow appears to be directed by the flow inertia and thus less flow is directed towards the exhaust ports.

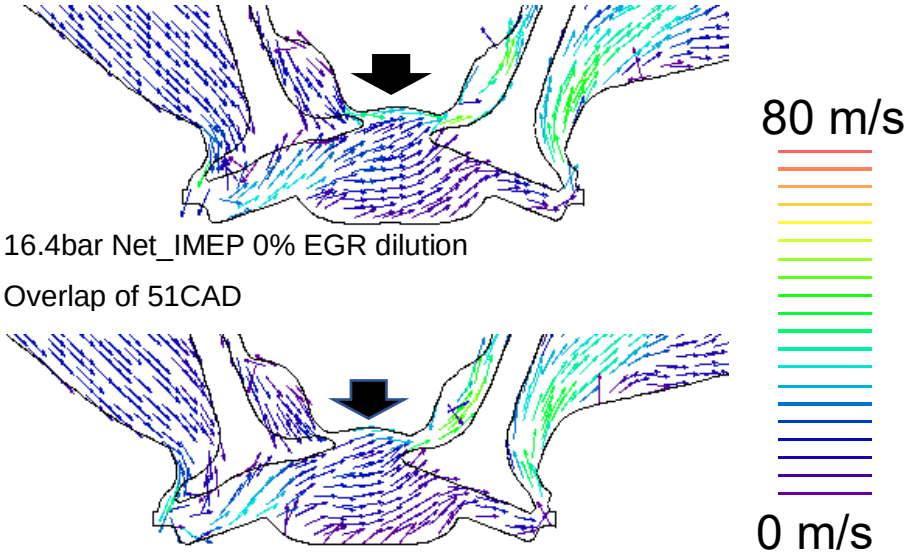

16.4bar Net_IMEP 0% EGR dilution

Overlap of 51CAD

16.4bar Net_IMEP 10% EGR dilution

Overlap of 51CAD

Figure 6-46 Internal flow field during the valve-overlap period. Cross-section across valve centres.

The total mass of O_2 in the exhaust port is traced in a graph as seen in Figure 6-47; Table 6-4 is the relative ratio of short-circuited mass in comparison to the total trapped obtained by processing the CFD data. This is an indication of short-circuit air comparison with EGR dilution and valve-overlap reduction. The baseline case results in the highest short-circuit mass. 10% EGR dilution reduces short-circuiting to 83% of reference condition, the greater demand for boosting has changed the flow fields, which reduces short-circuit flow with the same load as seen from the vector imaging. The short-circuit air is reduced to less than $1/10^{th}$ when the valve overlap was reduced to 27CAD, a very effective strategy to reduce short-circuit flow.

The short-circuit ratio estimated via CFD analysis is found to be an underestimate as the simulation does not consider the dynamic inlet and exhaust pressures caused by cyclic pumping of the 3 cylinders.

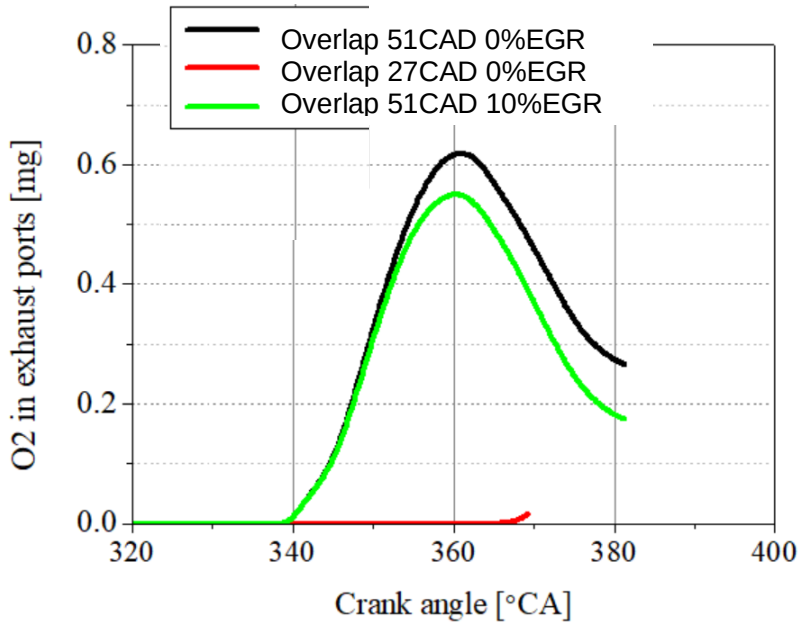

Figure 6-47 CFD output data, O2 mass in exhaust port during overlap duration, the plot ends when the exhaust port closes.

Table 6-4 Short-circuit ratio comparison (by mass) as estimated by the CFD simulation

Case	Relative Short-circuit ratio, %
Overlap of 51CAD 0% EGR	100% (ref)
Overlap of 51CAD 10% EGR	83%
Overlap of 27CAD 0% EGR	8%

6.7.2 The contributing effects of EGR dilution and valve-overlap reduction

The effects of valve timing and EGR dilution upon the in-cylinder mixing effects are evaluated in this section. The same three cases are utilised to understand the effects of valve overlap reduction and EGR dilution effects.

Figure 6-48 shows four graphs that plot the common mixing metrics. These are 1) tumble ratio 2) cross tumble ratio 3) swirl ratio 4) total kinetic energy. The graphs x-axis is the crank angle and starts at 180CAD (exhaust stroke BDC).

In terms of tumble ratio, neither EGR dilution or overlap reduction had a big effect on the characteristic, but a small increase in tumble intensity was seen at 420CA which is when the first injection takes place, this may encourage a more vigorous mixing (arrowed). The reduction of valve-overlap had a big impact on the CTR and SR, and the flow characteristics were varied from the exhaust stroke, which had a knock-on effect on the intake stroke. EGR dilution showed small changes despite the increased mass flow rate. The TKE is increased

with valve-overlap reduction, but majorly in the exhaust stroke due to the earlier EVO, the rest of the flow remains like the other cases due to the similar load range. Here EGR dilution had a greater intensity which could promote mixing during compression.

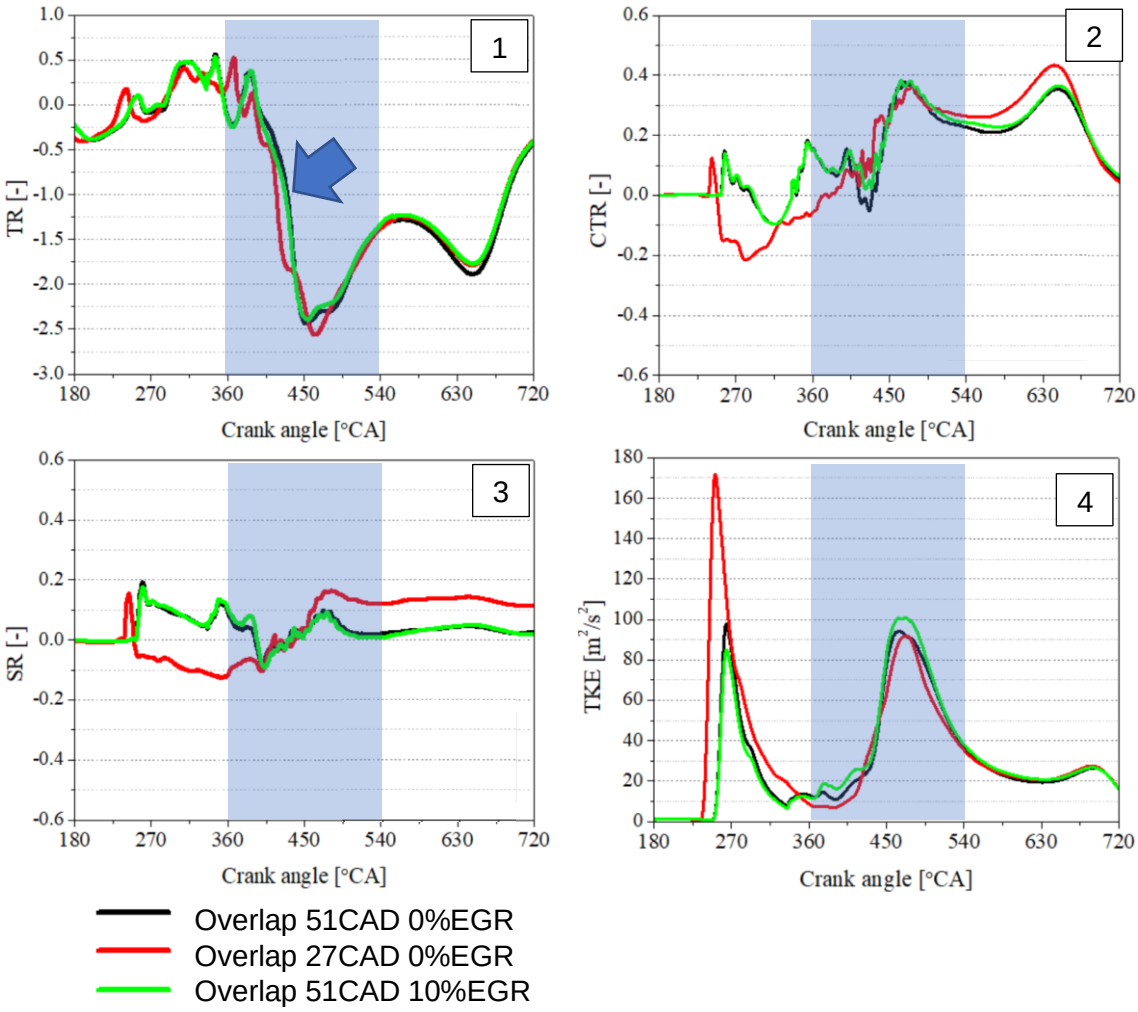

Figure 6-48 Comparison of EGR dilution and valve overlap reduction towards intake mixing for 1) tumble ratio 2) cross tumble ratio 3) swirl ratio 4) total kinetic energy. The shaded region represents intake stroke (TDC to BDC)

6.8 Summary

In this chapter, the effect of removing positive valve-overlap at two high load operation points is presented and discussed. The combined use of SFI with EGR is another major output included in the study.

The results from the first investigation are shown for different valve-overlap settings with and without EGR dilution. The changes in the valve-overlap period and timing directly affect the RGF and the fresh air short-circuit.

The RGF is found to be the highest at advanced valve-overlap and least at maximum (default overlap duration) valve-overlap when the most scavenging takes place. The hot residual gas at the tested loads affects the combustion negatively. The use of 10% external EGR lowers the reactivity of the in-cylinder charge, and this is found to be helpful in valve settings where higher amounts of residual gas fractions are present. But a higher ratio of RGF to external EGR affected the higher load conditions negatively.

The degree of the short-circuiting air affects the in-cylinder AFR when the exhaust lambda is set to one, and it is indicated by the CO emissions results. Thus, the highest CO is measured at max-overlap conditions, reaching the lowest at the no-overlap condition. EGR dilution and higher load operation are shown to have a greater occurrence of short-circuit air for a given overlap condition.

With the study performed to investigate different valve-overlap combinations, it is found that the use of reduced valve-overlap has a good synergy effect with EGR. The efficiency is seen to improve as follows: -

- 13.7bar Net_IMEP 1.7% → **2.8%** BSFC gain with 10% EGR dilution
- 16.4bar Net_IMEP 0.5% → **3.1%** BSFC gain with 10% EGR dilution

The reasons for the improvement can be explained by the combination of improved combustion efficiency from minimised overlap and better combustion phasing ability from EGR dilution.

Additionally, significant reductions in both engine-out and vehicle-out ISCO and $ISNO_x$ emissions are also achieved at both loads with reduced overlap and external EGR dilution. Due to the later slower combustion, the ISTHC emissions suffer a small increase. But the overall combustion efficiency was improved.

Performance of the engine is negatively affected as the valve-overlap is reduced and can be recovered by further boosting but with a higher fraction of residual gas. While this was not an issue in the tests performed, this may lower the maximum torque obtainable using this strategy. And the combustion instability was worsened with EGR dilution rate, which is especially the case at advanced valve-overlap.

The results in the second part of the chapter are analysed for three settings of symmetrical valve-overlap with SFI and EGR, and the main findings can be summarised as follows:

- Shortened valve-overlap increases the combustion duration and phasing as the air/fuel ratio of the in-cylinder charge is increased towards stoichiometric
- Split injections are found to have some effect in shortened valve-overlap conditions due to the stoichiometric in-cylinder conditions and hotter mixture temperatures during mixing

- Split injections can improve the combustion stability and engine efficiency from very late combustion with EGR dilution.
- Tailpipe NO_x emissions with reduced valve-overlaps are much lower due to better conversion efficiency of the TWC as the O_2 level is reduced with less air short-circuiting.
- Particulates concentration falls with the use of both external EGR and residual gas but increases with split injections. However, the combined use of EGRs and split injections produces lower particulates concentration than the reference case of single injection with wide valve-overlap.

Due to the combined effects of EGR and SFI with eliminated valve-overlap, the ISFC is improved by around 5% for both boosted loads tested. At the higher load (16.4bar Net_IMEP); however, the very late combustion phasing causes some combustion instability which lowers the overall efficiency when the split injection has little effect.

In terms of the emissions data, the tailpipe NO_x is found to be reduced drastically by valve-overlap reduction, but some early and late EOI2 timings tend to increase these emissions because of the unknown effects towards the exhaust lambda readings. ISCO is also sensitive to the second injection timing as well as the overlap duration. Lower ISCO figures are seen with the majority of the second injection timing due to favourable in-cylinder mixing conditions. Finally, very late second injection timings led to high ISCO lowered NO_x and lowered THC combustions due to pool fire conditions. This required extra fuel and air to cover for the lost combustion efficiency.

The particulate emission measured before the TWC shows that the split injections lead to higher levels of both nucleation and accumulation mode particles due to localised fuel-rich combustion and reduced mixture preparation time. The highest count is seen at a very retarded second injection of EOI2=-75CAD aTDC. However, EGR and reduced valve-overlap lowered the particulates count drastically, because of the higher mixture preparation temperature of earlier combustion by EGR and increased air/fuel ratio with small valve overlap.

Chapter 7 Conclusion and future work

7.1 Introduction

There is a seemingly never-ending demand for transport, but there are concerns with energy resources, and the transport sector contributes to the on-going environmental crisis with GHG and harmful emissions. This has made the need for transport technology advancements to lower emissions and increase the efficiency of road transport vehicles. The need for IC engine advancements is identified to be important due to the continuous demand forecast.

This project caters for such demand by developing a strategy to improve efficiency and minimise harmful emissions of a downsized GTDI engine. The challenge for these engines comes from the inefficiencies that exist due to the current knock prevention engine control strategies. They are late combustion phasing and wide valve-overlap for more complete scavenging efficiency of hot residual gas. In addition, these strategies were also found to cause harmful tailpipe emissions of NO_x.

Thus, alternative strategies were researched and applied to lower knock tendency, recover combustion speeds and lower tailpipe NO_x emission. The effects of the following alternative strategies and their combinations were investigated: -

- EGR dilution at high load operation
    - To lower knock tendency during high load conditions
- High energy ignition / Split late injection
    - Recovery of combustion speeds and ignitability of diluted mixtures
- Valve-overlap reduction to reduce fresh air short-circuiting
    - restore trapped gas equivalence ratio
    - reduce tailpipe NO_x

Many studies highlighted the shortfalls of engine downsizing at LSHL conditions, knocking is the inherent issue that is often overcome by fuel-intensive strategies (late phasing, trapped mass enrichment, short-circuit for cylinder cooling). EGR dilution is a known method for knock tendency reduction where significant efficiency gains are possible by deviating away from the need for fuel enrichment.

High energy ignition systems were reported to stabilise ignition of diluted mixtures. Extended dilution limits from improved ignition performance also unlocked further dilution for improved gains. Similarly, split/late injection can improve ignition and combustion speeds which suits EGR diluted mixtures. But the success of this strategy relies on intricate optimisation of flow and injection. The goal is to achieve a mixture of superior ignitability. Literature showed

success cases with lean or dilution limit extension, further improvements in efficiency were seen.

Wide valve-overlaps with boosted operations lead to exhaust lambda sensor measurement errors, as a result, the engine can operate slightly lean and cause NO_x tailpipe emissions with regular TWC after treatment. But reducing the valve-overlap at boosted loads is expected to reduce fuel efficiency and limit performance from increased residual gas fraction and occurrence of knocking combustion. There are no benefits reported by reducing valve-overlap at boosted loads.

Systematic engine experiments were carried out to evaluate the above strategies and their synergies. A Ford EcoBoost 1litre engine was fitted with a custom LP cooled external-EGR system. The engine supplied was fitted with a low inertia TC, multi-hole GDI injectors and dual VVT system, and was controlled using a fully programmable ECU system. In addition to the engine experiments, further analysis with 3D CFD simulation was carried out to assist the understanding of the experimental results.

7.2 Conclusions

The following four tests were performed to investigate the interaction of the strategies reviewed, all at LSHL, where the ST is knock limited: -

- Test1 - EGR sweep with high energy ignition impact towards dilution limit
    a. Determine EGR dilution limit and performance effects
    b. Unlocked efficiency improvements from HE ignition
- Test 2 - Split late injection with different external-EGR dilution and split ratios
    a. Second injection position sweep for stratification effects
    b. Response to EGR dilution and combustion recovery effects
- Test 3 - Valve profile timing with EGR
    a. Effect of different configurations of inlet and exhaust timing
    b. Changes to above with EGR dilution
- Test 4 - Valve-overlap reduction with EGR and split injection strategy
    a. Second injection position sweep for stratification effects with overlap reduction
    b. Changes to response with EGR reduction

7.2.1 Effect of EGR and HE ignition

Chapter 4 detailed the results of test 1 at three boosted loads of 13.7bar Net_IMEP, 16.4bar Net_IMEP and 18.9bar Net_IMEP all at 2000RPM.

Firstly, the results have clearly demonstrated the effectiveness of EGR to lower knock tendency and improve operating efficiency at the LSHL operations. A maximum ISFC improvement of 7.8% (at 25% EGR dilution) was obtained at 18.9bar Net_IMEP, this was reduced to 5.3% (at 25% EGR dilution) and 3.2% (15% EGR dilution) at 16.4 and 13.7bar Net_IMEP, respectively.

Secondly, the high energy ignition was found to have a positive impact on improving combustion stability due to faster combustions, with a CoV of IMEP drop of around 0.4% throughout the sweep. The use of HE ignition had also improved the results at 16.4bar and 18.9bar Net_IMEP by 1-2% owed to the higher EGR tolerance.

Furthermore, EGR dilution significantly lowered the engine-out NO_x emissions which were near-linear with EGR dilution. At 30% EGR, the NO_x emission was reduced by a factor of 10.

7.2.2 Effect of split injections

The results of tests with the split injections are detailed in Chapter 5. Tests were performed with the start of the first injection fixed at -299CAD ATDC whilst the end of the second injection (EOI2) ranged from -250 to -50CAD ATDC, with and without 10% EGR dilution, at two boosted loads (13.7bar, 16.4bar Net_IMEP) and two split ratios (70:30, 80:20). Splitting the injection resulted in worsening ISFC in most cases. The limited cases with ISFC improvements were seen at: -

- 16.4bar Net_IMEP with EOI2= -225CAD ATDC with and without EGR with a typical ISFC improvement of around 0.5%, due to reduced spray penetration length.
- 13.7bar Net_IMEP with 10% EGR dilution, EOI2=-250 to -50CAD aTDC due to the reduction in the trapped mass enrichment and effective SFI condition. The best improvement of ISFC was 1.7% at EOI2=-100CAD aTDC.

Combustion and heat analysis results showed that most cases had a slower initial burn because of split injections, especially with the 70:30 ratio. The loss in combustion speed was found to be due to over enrichment of the mixture away from the plug electrodes. The in-cylinder mixture was rich due to the air short-circuiting of the large valve overlap, but the introduction of split injection caused the relative air/fuel ratio of the stratified mixture mostly away from the plug electrodes, resulting in the combustion of lean and over enriched mixture. In the most retarded second injection of EOI2=-75CAD aTDC, there was evidence of pool fire as shown by the rapid rise in fuel consumption and combustion instability.

Pre-TWC engine exhaust emission results were largely unaffected by the split injections until pool fire effects of very retarded second injection started to dominate. In most cases, THC emissions fell by 20% from the reduced crevice and wall loss when the split injections were used.

7.2.3 Effects of valve overlap and valve timings

The results for tests 3 and 4 are presented in Chapter 6. The effects of valve phasing change, EGR dilution and split injection are investigated at boosted loads. The first test investigates the full range of valve phasing for both inlet and exhaust valve, whereas the

second test focuses on a limited setting to investigate the stratification effects with reduced valve-overlap.

7.2.3.1 Single injection operations

The change in all variables (valve phasing of inlet and exhaust, external EGR, load) had a very big impact on the performance of the engine. The variables had a major effect on the following key parameters: -

- Residual gas fraction
    - The combination of wide valve-overlap and positive pressure gradient leads to greater short-circuit air and thus fuel enriched trapped mass
    - Shorter valve-overlap duration (and or exhaust valve closure timing) trapped more residual gas in the premixed mixture
    - A greater pressure gradient between inlet and exhaust encourages gas exchange for less trapped residuals
- Reactivity of the residual gas
    - Higher load leads to residuals of greater temperatures and reactant concentration
    - External EGR dilution lowers the residual gas reactivity, leading to knock onset reduction from mixtures with higher residual fraction

The above changes further influenced the three following engine operating parameters which ultimately affected the engine efficiency: -

- Combustion phasing based on knock onset due to reactivity of the trapped mixture
- Combustion efficiency due to trapped ratio of residual gas
- TC efficiency (heat recovery) from the change in the operating region of greater efficiency
- Increased charge cooling effect from LIVC due to less compression from piston

Without the use of EGR dilution, the reduction in ISFC (between reference valve setting and minimum ISFC figure) with a change in inlet and exhaust valve phasing was 1.3% at 13.7bar Net_IMEP and 0.5% gain for 16.4bar Net_IMEP. Highest ISFC values were typically seen at earlier EVCs which has higher residuals. Thus, combustion phasing suffered as the valve-overlap was reduced (and early EVC), knock limited CA50 figures were delayed by 4.4 and 7CAD at 13.7bar and 16.4bar Net_IMEP respectably between earliest and latest EVC. But combustion efficiency was increased by around 2% by minimising the overlap and TC efficiency (as indicated by friction SFC) improved by up to 2g/kWh from recovered trapped ER and increased boost demand due to decreased volumetric efficiency.

When EGR was introduced to the same test, the ISFC gains due to valve phasing had changed dramatically. ISFC improvements of 2.8% and 3% were seen at 13.7bar and 16.4bar Net_IMEP, respectively. In both cases, the best efficiency was seen at (or near) the minimum valve overlap region. The knock limited CA50 positions now show delays of 0.7

and 1.8 CAD for the two loads due to reduced knock onset from increased residual fractions. This allowed the increased combustion efficiency to take positive efficiency effect.

Knock mitigation due to external EGR dilution was also present, but the biggest impact came from improving the quality of residual gas and combustion of the stoichiometric mixture.

In terms of other effects that were universal between the cases, it is important to note the lowered volumetric efficiency had increased the TC wastegate setpoint from 23.5% to 62% at 13.7bar Net_IMEP and 49% to 70% at 16.4bar Net_IMEP, the rise in MAP was between 0.14 to 0.29bar due to valve overlap reduction and 0.1 to 0.19bar from EGR dilution. This is expected to lower the maximum load limit of the engine. Combustion instabilities were also increased as more combustion products constituted the total trapped mass, the differences were much larger on EGR diluted cases and higher loads where combustion duration was longer and phased later, the maximum observed difference of CoV was an increase from 1.6% to 2.6%.

Thus, limitations of such a strategy exist in the boosting capability and combustion stability limits from the increased ratios of burned gases (EGR and residual gas).

7.2.3.2 Reduced valve-overlap with split injections

The second test further explored the use of split injections with shortened valve-overlap at boosted conditions (13.7, 16.4bar Net_IMEP) with EGR dilution. Here, the valve-overlap cases were reduced to three durations for each load tested, these were the original wide valve-overlap, eliminated overlap with an addition in between.

With the reduced valve overlap, the removal of air short-circuiting restored the overall mixture towards stoichiometric. The stoichiometric air mixture and high ratios of burned gases (external EGR and residual gas fraction) had allowed the split injection to improve the combustion. The maximum ISFC improvements achieved were 4.8% for 13.7bar Net_IMEP and 5.2% at 16.4bar Net_IMEP, achieved with the reduced valve overlap, split injection and external EGR dilution. Similarly, the BSFC improvements were seen at 5.1% for 13.7bar Net_IMEP and 5.0% at 16.4bar Net_IMEP.

The maximum ISFC benefit due to split injections increased as EGR dilution increased and valve-overlap duration was shortened, such that EGR dilution and reduced valve-overlap brought an extra 1% improvement on average for each strategy.

The improvements from reduced valve-overlap and EGR dilution made were put down to 2 reasons. 1) CFD simulation showed internal flow changes to increase turbulence and flow characteristics, this had made changes to the interaction of the second injection for better mixing properties. 2) Increased in-cylinder temperatures from higher residual fractions have

increased the evaporation speeds, which prepared the late injection mixture sooner, prior to combustion. This was also monitored as a 10 - 20% reduction in both nucleation and accumulation mode particle concentration.

Another trend that was observed was the occurrence of piston crown impingement as the end of second injection approached -100CAD aTDC, this caused the efficiency to drop due to deteriorated combustion conditions, with a sharp rise in particulate emissions.

In terms of particulate emissions, EGR dilution was found to lower the particulate counts as combustion oxidation times were increased from better phasing. The number of nucleation particles was reduced by more than 10% and accumulation mode particle were reduced by around 80% of the original value. Reduction of valve overlap was also found to lower particulates.

And finally, the tailpipe emission of NO_x was 10g/kWh at 16.4bar Net_IMEP with wide valve overlap due to the lower conversion efficiency of the TWC caused by the short-circuit air in the exhaust stream. The NO_x emission was successfully reduced to sub 1g/kWh by reducing the valve-overlap duration to restore the lambda sensor accuracy. Use of EGR dilution lowered NO_x emission by around 50%.

7.2.4 Summary

In summary of the project, the effects of EGR dilution, HE ignition, valve-overlap elimination, and split injection were investigated on a GTDI downsized engine at boosted loads. A very effective synergy effect was found that lowered fuel consumption and tailpipe NO_x. There was an underlying inefficiency and issue at LSHL of a downsized GTDi engine which was alleviated by removing the need for traditional knock mitigation techniques. The EGR dilution lowered the temperature of combustion and reactivity of the residual gas which allowed for valve-overlap to be eliminated, thus split injection made effective SFI condition, the stoichiometric mixture increased the combustion efficiency, and the conversion efficiency of the TWC improved. Thus, the eliminated valve-overlap successfully controlled the tailpipe NO_x and further lowered particulate emissions without the onset of knock.

An opportunity for knowledge contribution was identified in the literature review. The concluding synergy of the combined effects has not been previously reported due to the scarcity of work involving reduced valve-overlap strategies at high-load. Further positive effects were seen in reduced emissions. Thus, the contribution of this work is justified.

The strategy, when implemented, is expected to help future downsized GTDi engines to meet the stringent emission limits by eliminating harmful tailpipe emissions and reducing GHG emissions at LSHL regions of the engine map.

7.3 Suggestions for future works

The project presented the initial findings of synergy effects when EGR dilution was used with valve-overlap elimination and split injections. For a better understanding of the effects, further improvement of the synergy and considerations for implementation, studies in the following areas are recommended: -

- Full valve profile impact for external EGR at boosted loads of a downsized GTDI engine. For this test, a dual VVT system was used with fixed valve profiles, this means the change of valve-overlap had changed the EVO and IVC timing, inevitably altering the effective expansion and CR. Further works to re-perform these tests once again by changing the overlap duration alone will, therefore, be a valuable output to understand the isolated impact of overlap effects.
- In-cylinder flow optimisation for stratification. The engine used here was optimised for single early injection, thus, the second injection characteristics were not performed with the best internal flows. Different levels of swirl and tumble or a modified piston for stratification could bring considerable early combustion benefits and interact positively with EGR diluted boosted operation.
- Effect of injector optimisation and use of piezo type injector. All injections in this project were performed with a direct injection multi-hole system. The use of piezo injectors which are known for shorter penetration and atomisation performance may yield valuable results for strategy improvements. These differences with multi-hole injector will forward the optimisation study.
- The full effects of EGR dilution upon SFI and valve overlap elimination should be explored by further increasing the tested range of EGR dilution. The preliminary studies were performed in this project by testing the effects of 10% external EGR dilution, but due to the limited test points the full trend effect is not concluded. Further exploration of this variable will yield valuable information of the effect.
- Lean operation with the suggested strategy instead of EGR dilution will be of interest. Literature has much to offer on the efficiency gains of highly diluted mixtures and lean boost strategy. The use of lean boost with valve overlap elimination effects may be interesting as this too can lower combustion temperature combined with residual gas fractions, meaning that the reactivity of the residuals may be low enough for knock mitigation effects. Furthermore, split injection and novel ignition systems have been reported to enable combustion of very lean mixtures. It may, however, re-introduce harmful emissions that can be dealt via special after treatments, or very low-temperature combustions may be realised with high EGR dilution which can bypass such needs.

- EOI2 timing effects towards global lambda. Tests in Chapter 6 showed that very late EOI2 events led to a small underestimation of O_2 in the exhaust by the UEGO sensor. During this project, the mechanism for such underestimation was not established, however, such knowledge would be useful to increase the accuracy of engine operating lambda with the proposed strategy.
- Novel ignition systems or high energy ignition systems such as distributed coronal discharge and turbulent jet ignition with the proposed strategy is expected to bring further efficiency benefits from faster combustion speeds. A study of efficiency gains through such a system would be very beneficial. As literature and the results of Chapter 4 uncovered, ignition system can accelerate the combustion and advance the combustion phasing at boosted loads, but the interaction with stratified mixtures, EGR dilution and residual gases may bring further synergy benefits to the strategy.
- Impact and improvement of EGR dilution transient delay. This is a universal issue for all engines looking to employ external low-pressure EGR dilution. The longer path is taken and the valve operated system results in a delay of EGR dilution from the moment of demand, this is expected to bring losses to the efficiency gain potential and drivability. A study into a system that can lower the impacts of these dynamic losses, either by optimising the EGR system or improving the control may be vital for safe and successful implementation of this strategy.

Reference

1. OICA: Sales Statistics | OICA, http://www.oica.net/category/sales-statistics/
2. Macdonald, J.: ELECTRIC VEHICLES TO BE 35% OF GLOBAL NEW CAR SALES BY 2040. (2016)
3. WHO: Who Health and Climate Change Survey Report Tracking Global Progress. 1–32 (2019)
4. Church, J.A., White, N.J., Aarup, T., Wilson, W.S., Philip, L., Domingues, C.M., Hunter, J.R., Lambeck, K.: Understanding global sea levels : past , present and future Address for correspondence : Sustain. Sci. 3, 1–48 (2007)
5. European Environmental Agency: EEA Report No 12/2018. (2018)
6. Anenberg, S., Miller, J., Minjares, R., Du, L., Henze, D., Lacey, F., Malley, C., Emberson, L., Franco, V., Klimont, Z., Heyes, C.: FACT SHEET : GLOBAL IMPACTS AND MITIGATION OF EXCESS DIESEL NO X EMISSIONS IN 11 MAJOR VEHICLE MARKETS A NEW STUDY PUBLISHED IN NATURE OFFERS THE FIRST QUANTITATIVE ANALYSIS OF THE GLOBAL IMPACTS OF REAL-WORLD ON-ROAD DIESEL. (2017)
7. Hooftman, N., Messagie, M., Van Mierlo, J., Coosemans, T.: A review of the European passenger car regulations – Real driving emissions vs local air quality. Renew. Sustain. Energy Rev. 86, 1–21 (2018). https://doi.org/10.1016/j.rser.2018.01.012
8. Tietge, U., Mock, P., Dornoff, J.: CO2 emissions from new passenger cars in the European Union: Car manufacturers' performance in 2018. (2018)
9. ICCT, I.C. on C.T., Mock, P.: Real-Driving Emissions Test Procedure for Exhaust Gas Pollutant Emissions of Cars and Light Commercial Vehicles in Europe. nternational Counc. Clean Transp. 1–10 (2017)
10. Automotive, D., Technology, C.: Effect of Fuel Pressure on GDi Multi-Hole Injector Particulate Emissions and Tip Coking Robustness. 1–12 (2016)
11. Roland, W.: New requirements and solutions for LD and HD vehicles. (2016)
12. Williams, M., Minjares, R.: A technical summary of Euro 6 / VI vehicle emission standards. (2016)
13. Joshi, A.: Review of vehicle engine efficiency and emissions. SAE Tech. Pap. 2019-

April, 734–761 (2019). https://doi.org/10.4271/2019-01-0314

14. Vilchez, J.J.G., Thiel, C.: The effect of reducing electric car purchase incentives in the European Union. World Electr. Veh. J. 10, (2019). https://doi.org/10.3390/wevj10040064

15. Zhang, R., Fujimori, S.: The role of transport electrification in global climate change mitigation scenarios. Environ. Res. Lett. (2019). https://doi.org/10.1088/1748-9326/ab6658

16. Kalghatgi, G.: Is it really the end of internal combustion engines and petroleum in transport?, (2018)

17. Liu, C., Lin, Z.: How uncertain is the future of electric vehicle market : Results from Monte Carlo simulations using a nested logit model. 8318, (2017). https://doi.org/10.1080/15568318.2016.1248583

18. Bryant, L.: The Origin of the Four-Stroke Cycle. Technol. Cult. (1967). https://doi.org/10.2307/3101967

19. Heywood, J.B.: Internal Combustion Engine Fundementals. (1988)

20. Lee, K., Bae, C., Kang, K.: The effects of tumble and swirl flows on flame propagation in a four-valve S.I. engine. Appl. Therm. Eng. 27, 2122–2130 (2007). https://doi.org/10.1016/j.applthermaleng.2006.11.011

21. Hill, P.G., Zhang, D.: The effects of swirl and tumble on combustion in spark-ignition engines, (1994)

22. Wu, Y., Modica, V., Rossow, B., Grisch, F.: Effects of pressure and preheating temperature on the laminar flame speed of methane/air and acetone/air mixtures. Fuel. 185, 577–588 (2016). https://doi.org/10.1016/j.fuel.2016.07.110

23. Briggs, T., Alger, T., Mangold, B.: Advanced Ignition Systems Evaluations for High-Dilution SI Engines. SAE Int. J. Engines. 7, 2014-01–2625 (2014). https://doi.org/10.4271/2014-01-2625

24. Ratnak, S., Kusaka, J., Daisho, Y., Yoshimura, K., Nakama, K.: Experiments and Simulations of a Lean-Boost Spark Ignition Engine for Thermal Efficiency Improvement. SAE Int. J. Engines. 9, 379–396 (2015)

25. Hann, S., Grill, M., Bargende, M.: Laminar Flame Speed Engine Simulation of Lean Combustion and Exhaust Gas Recirculation at High Load. MTZ Worldw. 79, 26–33 (2018). https://doi.org/10.1007/s38313-018-0002-z

26. Stone, R., Stone, R.: Combustion and Fuels. In: Introduction to Internal Combustion Engines (1992)

27. Zhao, J.: Research and application of over-expansion cycle (Atkinson and Miller) engines – A review, (2017)

28. Guardiola, C., Pla, B., Real, M., Travaillard, C., Dambricourt, F.: Short-circuit effects on spark ignition engine after-treatment and fuel-to-air ratio control. Int. J. Engine Res. (2018). https://doi.org/10.1177/1468087418796705

29. Fansler, T.D., Reuss, D.L., Sick, V., Dahms, R.N.: Invited Review: Combustion instability in spray-guided stratified-charge engines: A review. Int. J. Engine Res. 16, 260–305 (2015). https://doi.org/10.1177/1468087414565675

30. Ma, F., Wang, Y., Wang, J., Ding, S., Wang, Y., Zhao, S.: Effects of Combustion Phasing , Combustion Duration , and Their Cyclic Variations on Spark-Ignition (SI) Engine Efficiency. 3022–3028 (2008). https://doi.org/10.1021/ef8003027

31. NissanMotorCorporation: Reducing CO2 Emissions From Internal Combustion Engines, https://www.nissan-global.com/EN/TECHNOLOGY/OVERVIEW/ice.html

32. Kutlar, O.A., Arslan, H., Calik, A.T.: Methods to improve efficiency of four stroke, spark ignition engines at part load. Energy Convers. Manag. 46, 3202–3220 (2005). https://doi.org/10.1016/j.enconman.2005.03.008

33. Doornbos, G., Hemdal, S., Dahl, D.: Reduction of Fuel Consumption and Engine-out NOx Emissions in a Lean Homogeneous GDI Combustion System, Utilizing Valve Timing and an Advanced Ignition System. SAE Tech. Pap. 2015-April, (2015). https://doi.org/10.4271/2015-01-0776

34. Mayer, A., Wolf, D., Günther, M., Medicke, M.: Fully Variable Valve Train to Apply Miller/Atkinson Strategies for Future Downsizing Concepts. MTZ Worldw. 79, 56–63 (2018). https://doi.org/10.1007/s38313-018-0046-0

35. Kulzer, A., Christ, A., Rauscher, M., Sauer, C., Würfel, G., Blank, T.: Thermodynamic analysis and benchmark of various gasoline combustion concepts. SAE Tech. Pap. (2006). https://doi.org/10.4271/2006-01-0231

36. He, X., Ratcliff, M.A., Zigler, B.T.: Effects of gasoline direct injection engine operating parameters on particle number emissions. Energy and Fuels. 26, 2014–2027 (2012). https://doi.org/10.1021/ef201917p

37. Raza, M., Chen, L., Leach, F., Ding, S.: A Review of particulate number (PN)

emissions from gasoline direct injection (gdi) engines and their control techniques. Energies. 11, (2018). https://doi.org/10.3390/en11061417

38. Wang, Z., Liu, H., Reitz, R.D.: Knocking combustion in spark-ignition engines. Prog. Energy Combust. Sci. 61, 78–112 (2017). https://doi.org/10.1016/j.pecs.2017.03.004

39. Baek, H.K., Lee, S.W., Han, D., Kim, J., Lee, J., Aino, H.: Development of valvetrain system to improve knock characteristics for gasoline engine fuel economy. SAE Tech. Pap. 1, (2014). https://doi.org/10.4271/2014-01-1639

40. Westin, F., Grandin, B., Ångström, H.E.: The influence of residual gases on knock in turbocharged SI-engines. SAE Tech. Pap. (2000). https://doi.org/10.4271/2000-01-2840

41. Dahnz, C., Han, K.M., Spicher, U., Magar, M., Schiessl, R., Maas, U.: Investigations on pre-ignition in highly supercharged SI engines. SAE Tech. Pap. 3, 214–224 (2010). https://doi.org/10.4271/2010-01-0355

42. Kalghatgi, G.: Knock onset, knock intensity, superknock and preignition in spark ignition engines. Int. J. Engine Res. 19, 7–20 (2018). https://doi.org/10.1177/1468087417736430

43. Winklhofer, E., Hirsch, A., Kapus, P., Kortschak, M., Philipp, H.: TC GDI engines at very high power density irregular combustion and thermal risk. SAE Tech. Pap. 4970, (2009). https://doi.org/10.4271/2009-24-0056

44. Inoue, T., Inoue, Y., Ishikawa, M.: Abnormal combustion in a highly boosted SI engine-the occurrence of super knock. SAE Tech. Pap. (2012). https://doi.org/10.4271/2012-01-1141

45. Okada, Y., Miyashita, S., Izumi, Y., Hayakawa, Y.: Study of Low-Speed Pre-Ignition in Boosted Spark Ignition Engine. SAE Int. J. Engines. 7, 2014-01–1218 (2014). https://doi.org/10.4271/2014-01-1218

46. Attard, W.P., Toulson, E., Watson, H., Hamori, F.: Abnormal combustion including mega knock in a 60% downsized highly turbocharged PFI engine. SAE Tech. Pap. (2010). https://doi.org/10.4271/2010-01-1456

47. Zahdeh, A., Rothenberger, P., Nguyen, W., Anbarasu, M., Schmuck-Soldan, S., Schaefer, J., Goebel, T.: Fundamental Approach to Investigate Pre-Ignition in Boosted SI Engines. SAE Int. J. Engines. 4, 246–273 (2011). https://doi.org/10.4271/2011-01-0340

48. Haenel, P., Seyfried, P., Kleeberg, H., Tomazic, D.: Systematic approach to analyze and characterize pre-ignition events in turbocharged direct-injected gasoline engines. SAE 2011 World Congr. Exhib. (2011). https://doi.org/10.4271/2011-01-0343

49. Lee, S., Bae, C., Lee, Y., Han, T.: Effects of engine operating conditions on catalytic converter temperature in an SI engine. SAE Tech. Pap. (2002). https://doi.org/10.4271/2002-01-1677

50. Nakata, K., Nogawa, S., Takahashi, D., Yoshihara, Y., Kumagai, A., Suzuki, T.: Engine Technologies for Achieving 45% Thermal Efficiency of S.I. Engine. SAE Int. J. Engines. 9, 179–192 (2015). https://doi.org/10.4271/2015-01-1896

51. Ogata, K.: A High Energy Ignition System for EGR Combustion Engine. (2017). https://doi.org/10.4271/2017-01-0675

52. Cairns, A., Blaxill, H., Irlam, G.: Exhaust Gas Recirculation for Improved Part and Full Load Fuel Economy in a Turbocharged Gasoline Engine. SAE Tech. Pap. (2006). https://doi.org/10.4271/2006-01-0047

53. Ellinger, R., Meitz, K., Prenninger, P., Salchenegger, S., Brandstätter, W.: Comparison of CO2 emission levels for internal combustion engine and fuel cell automotive propulsion systems. SAE Tech. Pap. (2001). https://doi.org/10.4271/2001-01-3751

54. Zhao, F.Q., Lai, M.C., Harrington, D.L.: A review of mixture preparation and combustion control strategies for spark-ignited direct-injection gasoline engines. SAE Tech. Pap. 106, 861–904 (1997). https://doi.org/10.4271/970627

55. Shin, J.Y., Park, C., Jung, J., Bae, C.: The Fuel Economy Improvement through the Knock Margin Expansion in a Turbocharged Gasoline Direct Injection Engine. SAE Tech. Pap. Ser. 1, 1–19 (2018). https://doi.org/10.4271/2018-01-1671

56. H. Zhao, H.: Overview of gasoline direct injection engines. In: Advanced Direct Injection Combustion Engine Technologies and Development. pp. 1–18. Woodhead Publishing (2009)

57. Storey, J.M., Lewis, S., Szybist, J., Thomas, J., Barone, T., Eibl, M., Nafziger, E., Kaul, B.: Novel Characterization of GDI Engine Exhaust for Gasoline and Mid-Level Gasoline-Alcohol Blends. SAE Int. J. Fuels Lubr. 7, 2014-01–1606 (2014). https://doi.org/10.4271/2014-01-1606

58. Shuai, S., Ma, X., Li, Y., Qi, Y., Xu, H.: Recent Progress in Automotive Gasoline

Direct Injection Engine Technology. Automot. Innov. 1, 95–113 (2018). https://doi.org/10.1007/s42154-018-0020-1

59. Bandel, W., Fraidl, G.K., Cowland, C.N., Sikinger, H., Kapus, P.E.: The Turbocharged GDI Engine: Boosted Synergies for High Fuel Economy Plus Ultra-low Emission. In: SAE Technical Paper Series (2010)

60. Hoffmann, G., Befrui, B., Berndorfer, A., Piock, W.F., Varble, D.L.: Fuel System Pressure Increase for Enhanced Performance of GDi Multi-Hole Injection Systems. SAE Int. J. Engines. 7, 2014-01–1209 (2014). https://doi.org/10.4271/2014-01-1209

61. Kasseris, E., Heywood, J.B.: Charge Cooling Effects on Knock Limits in SI DI Engines Using Gasoline/Ethanol Blends: Part 2-Effective Octane Numbers. SAE Int. J. Fuels Lubr. 5, 844–854 (2012). https://doi.org/10.4271/2012-01-1284

62. Lecointe, B., Monnier, G.: Downsizing a Gasoline Engine Using Turbocharging with Direct Injection. SAE Tech. Pap. Ser. 1. 2003-01–05, (2003). https://doi.org/10.4271/2003-01-0542

63. Chambon, P., Huff, S., Norman, K., Edwards, K.D., Thomas, J., Prikhodko, V.: European lean gasoline direct injection vehicle benchmark. SAE 2011 World Congr. Exhib. (2011). https://doi.org/10.4271/2011-01-1218

64. Noguchi, M., Sanda, S., Nakamura, N.: Development of Toyota Lean Burn Engine. In: 1976 Automobile Engineering Meeting. SAE International (1976)

65. Stokes, J., Lake, T.H., Osborne, R.J.: A gasoline engine concept for improved fuel economy -The lean boost system. SAE Tech. Pap. (2000). https://doi.org/10.4271/2000-01-2902

66. Shen, K., Li, F., Zhang, Z., Sun, Y., Yin, C.: Effects of LP and HP cooled EGR on performance and emissions in turbocharged GDI engine. Appl. Therm. Eng. 125, 746–755 (2017). https://doi.org/10.1016/j.applthermaleng.2017.07.064

67. Szybist, J.P., Wagnon, S.W., Splitter, D., Pitz, W.J., Mehl, M.: The Reduced Effectiveness of EGR to Mitigate Knock at High Loads in Boosted SI Engines. SAE Int. J. Engines. 10, 2017-24–0061 (2017). https://doi.org/10.4271/2017-24-0061

68. H., W., T., Z., G., S., L., T., Y., W.: Gasoline engine exhaust gas recirculation - A review. Appl. Energy. 99, 534–544 (2012). https://doi.org/10.1016/j.apenergy.2012.05.011

69. Rodriguez, J.F., Cheng, W.: Potential of Negative Valve Overlap for Part-Load

Efficiency Improvement in Gasoline Engines. SAE Int. J. Engines. 11, 657–668 (2018). https://doi.org/10.4271/2018-01-0377

70. Shutty, J.: Control strategy optimization for hybrid EGR engines. SAE Tech. Pap. (2009). https://doi.org/10.4271/2009-01-1451

71. Fischer, M., Kreutziger, P., Sun, Y., Kotrba, A.: Clean EGR for Gasoline Engines - Innovative Approach to Efficiency Improvement and Emissions Reduction Simultaneously. SAE Tech. Pap. 2017-March, (2017). https://doi.org/10.4271/2017-01-0683

72. Bourhis, G., Chauvin, J., Gautrot, X., de Francqueville, L.: LP EGR and IGR Compromise on a GDI Engine at Middle Load. SAE Int. J. Engines. 6, 2013-01–0256 (2013). https://doi.org/10.4271/2013-01-0256

73. Francqueville, L., Michel, J.-B.: On the Effects of EGR on Spark-Ignited Gasoline Combustion at High Load. SAE Int. J. Engines. 7, 2014-01–2628 (2014). https://doi.org/10.4271/2014-01-2628

74. Parsons, D., Akehurst, S., Brace, C.: The potential of catalysed exhaust gas recirculation to improve high-load operation in spark ignition engines. Int. J. Engine Res. 16, 592–605 (2015). https://doi.org/10.1177/1468087414554628

75. Alger, T., Chauvet, T., Dimitrova, Z.: Synergies between High EGR Operation and GDI Systems. SAE Int. J. Engines. 1, 2008-01–0134 (2008). https://doi.org/10.4271/2008-01-0134

76. Szybist, J.P., Wagnon, S.W., Splitter, D., Pitz, W.J., Mehl, M.: The Reduced Effectiveness of EGR to Mitigate Knock at High Loads in Boosted SI Engines. SAE Int. J. Engines. 10, 2305–2318 (2017). https://doi.org/10.4271/2017-24-0061

77. Alger, T., Chauvet, T., Dimitrova, Z.: Synergies between High EGR Operation and GDI Systems. SAE Int. J. Engines. 1, 101–114 (2008). https://doi.org/10.4271/2008-01-0134

78. Luján, J.M., Climent, H., Novella, R., Rivas-Perea, M.E.: Influence of a low pressure EGR loop on a gasoline turbocharged direct injection engine. Appl. Therm. Eng. 89, 432–443 (2015). https://doi.org/10.1016/j.applthermaleng.2015.06.039

79. Alger, T., Gingrich, J., Roberts, C., Mangold, B.: Cooled exhaust-gas recirculation for fuel economy and emissions improvement in gasoline engines. Int. J. Engine Res. 12, 252–264 (2011). https://doi.org/10.1177/1468087411402442

80. Bureshaid, K., Shimura, R., Zhao, H., Feng, D., Bunce, M.: Investigation on Knock Resistance with Turbulent Jet Ignition at Different Engine Load in an Optical Engine. SAE Tech. Pap. Ser. 1, (2019). https://doi.org/10.4271/2019-01-2151

81. Tsuboi, S., Miyokawa, S., Matsuda, M., Yokomori, T., Iida, N.: Influence of spark discharge characteristics on ignition and combustion process and the lean operation limit in a spark ignition engine. Appl. Energy. 250, 617–632 (2019). https://doi.org/10.1016/j.apenergy.2019.05.036

82. Paschen, F.: Ueber die zum Funkenübergang in Luft, Wasserstoff und Kohlensäure bei verschiedenen Drucken erforderliche Potentialdifferenz. Ann. Phys. (1889). https://doi.org/10.1002/andp.18892730505

83. Piock, W.F., Weyand, P., Wolf, E., Heise, V.: Ignition Systems for Spray-Guided Stratified Combustion. SAE Int. J. Engines. 3, 2010-01–0598 (2010). https://doi.org/10.4271/2010-01-0598

84. Dale, J., Checkel, M.D., Smy, P.R.: Application of high energy ignition systems to engines. Prog. Energy Combust. Sci. 23, 379–398 (1997). https://doi.org/10.1016/S0360-1285(97)00011-7

85. Yu, S., Yu, X., Yang, Z., Wang, M., Han, X., Tjong, J., Zheng, M.: Ignition Improvement for Ultra-Lean Dilute Gasoline Combustion. SAE Tech. Pap. 2017-Octob, (2017). https://doi.org/10.4271/2017-01-2244

86. Sevik, J., Wallner, T., Pamminger, M., Scarcelli, R., Singleton, D., Sanders, J.: Extending Lean and Exhaust Gas Recirculation-Dilute Operating Limits of a Modern Gasoline Direct-Injection Engine Using a Low-Energy Transient Plasma Ignition System. J. Eng. Gas Turbines Power. 138, 112807 (2016). https://doi.org/10.1115/1.4033470

87. Naiki, T., Obata, K., Watanabe, M., Yokomori, T., Iida, N.: Research of Fuel Components to Expand lean-limit in Super lean-burn condition. SAE Tech. Pap. Ser. 1, (2019). https://doi.org/10.4271/2019-01-2257

88. Jung, D., Sasaki, K., Sugata, K., Matsuda, M., Yokomori, T., Iida, N.: Combined Effects of Spark Discharge Pattern and Tumble Level on Cycle-to-Cycle Variations of Combustion at Lean Limits of SI Engine Operation. In: SAE Technical Papers. SAE International (2017)

89. Martin, S., Beidl, C., Mueller, R.: Responsiveness of a 30 Bar BMEP 3-Cylinder Engine: Opportunities and Limits of Turbocharged Downsizing. SAE Tech. Pap. Ser.

1, (2014). https://doi.org/10.4271/2014-01-1646

90. Brandt, M., Rauscher, M., Lejsek, D., Nau, M., Baeuerle, M.: Scavenging to improve Low-End Torque of a Direct Injected Turbocharged SI-Engine GT-Suite User Conference 2005 Scavenging to Improve Low-End Torque of Turbocharged SI-Engines Outline Motivation. GT-Suite user Conf. 2005. 1–24 (2005)

91. Martensson, J., Flardh, O.: Modeling the Effect of Variable Cam Phasing on Volumetric Efficiency , Scavenging and Torque Generation. (2010)

92. Hu, B., Akehurst, S., Brace, C.: Novel approaches to improve the gas exchange process of downsized turbocharged spark-ignition engines: A review. Int. J. Engine Res. 17, 595–618 (2016). https://doi.org/10.1177/1468087415599866

93. Kirwan, J.E., Shost, M., Roth, G., Zizelman, J.: 3-Cylinder Turbocharged Gasoline Direct Injection : A High Value Solution for Low CO2 and NOx Emissions. 3, (2010)

94. Bandel, W., Fraidl, G.K., Kapus, P.E., Sikinger, H., Cowland, C.N.: The Turbocharged GDI Engine: Boosted Synergies for High Fuel Economy Plus Ultra-low Emission. SAE Tech. Pap. Ser. 1. (2006). https://doi.org/10.4271/2006-01-1266

95. Yang, C., Cheng, H., Fan, Z., Yin, J., Shen, Y., Haubner, F., Slotman, J., Seibel, J., Baer, S.: Development of Combustion System for a 1-Liter Advanced Turbocharged Gasoline Direct Injection 3-Cylinder Engine. In: SAE Technical Papers. SAE International (2016)

96. Asif, M., Giles, K., Lewis, A., Akehurst, S., Turner, N.: Influence of Coolant Temperature and Flow Rate, and Air Flow on Knock Performance of a Downsized, Highly Boosted, Direct-Injection Spark Ignition Engine. SAE Tech. Pap. 2017-March, (2017). https://doi.org/10.4271/2017-01-0664

97. Zhuang, Y., Zhao, P., Wang, C., Qian, Y., Gong, Z.: Mechanism study of scavenging process and its effect on combustion characteristics in a boosted GDI engine. Energy. 165, 246–266 (2018). https://doi.org/10.1016/j.energy.2018.09.077

98. FRIEDFELDT, R., ZENNER, T., ERNST, R., FRASER, A.: THREE-CYLINDER GASOLINE ENGINE ENGINE TARGETS AND CONCEPT DEFINITION. 32–37 (2013)

99. Ndir, A.N., Ndir, T.: GDI blow-through during scavenging at high load. 1–2

100. Cld, A.N., Downsized, I.: GDI vehicle NOx breakthrough due to scavenging (blow-through). 3–5 (2014)

101. Taylor, J., Fraser, N., Dingelstadt, R., Hoffmann, H.: Benefits of late inlet valve timing strategies afforded through the use of intake cam in cam applied to a gasoline turbocharged downsized Engine. In: SAE 2011 World Congress and Exhibition (2011)

102. Wang, Y., Conway, G.: Combined Benefits of Variable Valve Actuation and Low-Pressure EGR on SI Engine Efficiency Part 2: High Load. SAE Int. 1–9 (2019). https://doi.org/10.4271/2019-01-0237.Abstract

103. Luisi, S., Doria, V., Stroppiana, A., Millo, F., Mirzaeian, M.: Experimental Investigation on Early and Late Intake Valve Closures for Knock Mitigation through Miller Cycle in a Downsized Turbocharged Engine. SAE Tech. Pap. 2015-April, (2015). https://doi.org/10.4271/2015-01-0760

104. Dieterich, C., Ye, Y., Wang, J., Yao, K., Morcinkowski, B., Xu, L., Zhao, M., Souren, M.: Development of a New 1.8L Down-Speeding Turbocharged Gasoline Engine with Miller Cycle. SAE Tech. Pap. Ser. 1, 1–11 (2018). https://doi.org/10.4271/2018-01-1712

105. Hakariya, M., Toda, T., Sakai, M.: The New Toyota Inline 4-Cylinder 2.5L Gasoline Engine. SAE Tech. Pap. 2017-March, (2017). https://doi.org/10.4271/2017-01-1021

106. Hadded, O., Denbratt, I.: Turbulence characteristics of tumbling air motion in four-valve S.I. Engines and their correlation with combustion parameters. SAE Tech. Pap. (1991). https://doi.org/10.4271/910478

107. Endres, H.F.M.G.& C.K., NeuRer, H.-J.F.M.G.& C.K., Wurms, R.F.M.G.& C.K.: Influence of Swirl and Tumble on Economy and Emissions of Multi Valve SI Engines. SA E Tech. PA PER Ser. 920516, (1992)

108. Brusiani, F., Falfari, S., Cazzoli, G.: Tumble motion generation in small gasoline engines: A new methodological approach for the analysis of the influence of the intake duct geometrical parameters. Energy Procedia. 45, 997–1006 (2014). https://doi.org/10.1016/j.egypro.2014.01.105

109. Wheeler, J., Polovina, D., Ramanathan, S., Roth, K., Manning, D., Stein, J.: Increasing EGR Tolerance using High Tumble in a Modern GTDI Engine for Improved Low-Speed Performance. (2013). https://doi.org/10.4271/2013-01-1123

110. Wang, T., Liu, D., Tan, B., Wang, G., Peng, Z.: An investigation into in-cylinder tumble flow characteristics with variable valve lift in a gasoline engine. Flow, Turbul. Combust. 94, 285–304 (2015). https://doi.org/10.1007/s10494-014-9562-4

111. C. L. MYUNG1), K. H. CHOI1), I. G. HWANG1), K.H.L. and S.P.: EFFECTS OF VALVE TIMING AND INTAKE FLOW MOTION CONTROL ON COMBUSTION AND TIME-RESOLVED HC & NOx FORMATION CHARACTERISTICS. Int. J. Automot. Technol. 10, 161–166 (2009). https://doi.org/10.1007/s12239

112. Chang, Y., Wooldridge, M., Bohac, S. V.: Extending the Dilution Limit of Spark Ignition Combustion via Fuel Injection during Negative Valve Overlap. SAE Tech. Pap. 2016-April, (2016). https://doi.org/10.4271/2016-01-0671

113. Cairns, A., Blaxill, H.: The Effects of Combined Internal and External Exhaust Gas Recirculation on Gasoline Controlled Auto-Ignition. 2005, (2005). https://doi.org/10.4271/2005-01-0133

114. Smith, J., Szekely, G., Solomon, A., Parrish, S.: A Comparison of Spray-Guided Stratified-Charge Combustion Performance with Outwardly-Opening Piezo and Multi-Hole Solenoid Injectors. SAE Int. J. Engines. 4, 1481–1497 (2011). https://doi.org/10.4271/2011-01-1217

115. Goodger, E.M.: Fuels and combustion. Mech. Eng. Ref. B. 11/1-11/20 (1994). https://doi.org/10.1016/b978-0-08-052398-9.50015-9

116. Drake, M.C., Fansler, T.D., Lippert, A.M.: Stratified-charge combustion: Modeling and imaging of a spray-guided direct-injection spark-ignition engine. Proc. Combust. Inst. 30 II, 2683–2691 (2005). https://doi.org/10.1016/j.proci.2004.07.028

117. Park, C., Kim, S., Kim, H., Moriyoshi, Y.: Stratified lean combustion characteristics of a spray-guided combustion system in a gasoline direct injection engine. Energy. 41, 401–407 (2012). https://doi.org/10.1016/j.energy.2012.02.060

118. Oh, H., Bae, C.: Effects of the injection timing on spray and combustion characteristics in a spray-guided DISI engine under lean-stratified operation. Fuel. 107, 225–235 (2013). https://doi.org/10.1016/j.fuel.2013.01.019

119. Park, C., Kim, S., Kim, H., Lee, S., Kim, C., Moriyoshi, Y.: Effect of a split-injection strategy on the performance of stratified lean combustion for a gasoline direct-injection engine. Proc. Inst. Mech. Eng. Part D J. Automob. Eng. 225, 1415–1426 (2011). https://doi.org/10.1177/0954407011406469

120. Oh, H., Bae, C.: Effects of a split injection in a spray-guided direct-injection spark ignition engine under lean stratified operation. Proc. Inst. Mech. Eng. Part D J. Automob. Eng. 228, 1232–1244 (2014). https://doi.org/10.1177/0954407013502781

121. Feng, S., Hong, W., Xie, F., Yang, Y., Su, Y., Li, X.: Influence of stratified charge organized by double injection strategy on combustion and emissions on an EGR diluted GDI engine. Appl. Therm. Eng. 158, 113803 (2019). https://doi.org/10.1016/j.applthermaleng.2019.113803

122. Costa, M., Sorge, U., Allocca, L.: Increasing energy efficiency of a gasoline direct injection engine through optimal synchronization of single or double injection strategies. Energy Convers. Manag. 60, 77–86 (2012). https://doi.org/10.1016/j.enconman.2011.12.025

123. Costa, M., Sorge, U., Merola, S., Irimescu, A., La Villetta, M., Rocco, V.: Split injection in a homogeneous stratified gasoline direct injection engine for high combustion efficiency and low pollutants emission. Energy. 117, 405–415 (2016). https://doi.org/10.1016/j.energy.2016.03.065

124. Merola, S.S., Irimescu, A., Tornatore, C., Valentini, S., Kruczek, G., Szlek, A., Adamczyk, W.: UV-visible digital imaging of split injection in a gasoline direct injection engine. Therm. Sci. 19, 1873–1886 (2015). https://doi.org/10.2298/TSCI141121071M

125. Bai, Y., Wang, Z., Wang, J.: Knocking suppression using stratified stoichiometric mixture in a DISI engine. SAE Tech. Pap. (2010). https://doi.org/10.4271/2010-01-0597

126. Costa, M., Sementa, P., Sorge, U., Catapano, F., Marseglia, G., Vaglieco, B.M.: Split Injection in a GDI Engine Under Knock Conditions: An Experimental and Numerical Investigation. Presented at the September 6 (2015)

127. Lv, M., Li, Y., Hu, X., Liu, Y., Chang, L.: Super-knock Suppression Using Split Injection in a Turbo-Charged GDI Engine. MATEC Web Conf. 40, 02011 (2016). https://doi.org/10.1051/matecconf/20164002011

128. Serras-Pereira, J., Aleiferis, P.G., Richardson, D.: An experimental database on the effects of single- and split injection strategies on spray formation and spark discharge in an optical direct-injection spark-ignition engine fuelled with gasoline, iso -octane and alcohols. Int. J. Engine Res. 16, 851–896 (2015). https://doi.org/10.1177/1468087414554936

129. Fushimi, A., Kondo, Y., Kobayashi, S., Fujitani, Y., Saitoh, K., Takami, A., Tanabe, K.: Chemical composition and source of fine and nanoparticles from recent direct injection gasoline passenger cars: Effects of fuel and ambient temperature. Atmos. Environ. 124, 77–84 (2016). https://doi.org/10.1016/j.atmosenv.2015.11.017

130. Lee, D., Miller, A., Kittelson, D., Zachariah, M.R.: Characterization of metal-bearing diesel nanoparticles using single-particle mass spectrometry. 37, 88–110 (2006). https://doi.org/10.1016/j.jaerosci.2005.04.006

131. Zhao, L., Yu, X., Qian, D., Dong, W., Sun, P., He, L., Yang, S.: The effects of EGR and ignition timing on emissions of GDI engine. Sci. China Technol. Sci. 56, 3144–3150 (2013). https://doi.org/10.1007/s11431-013-5379-y

132. Price, P., Twiney, B., Stone, R., Kar, K., Walmsley, H.: Particulate and hydrocarbon emissions from a spray guided direct injection spark ignition engine with oxygenate fuel blends. SAE Tech. Pap. 776–790 (2007). https://doi.org/10.4271/2007-01-0472

133. Qin, J., Li, X., Pei, Y.: Effects of Combustion Parameters and Lubricating Oil on Particulate Matter Emissions from a Turbo-Charged GDI Engine Fueled with Methanol/Gasoline Blends. SAE Tech. Pap. 2014-Octob, (2014). https://doi.org/10.4271/2014-01-2841

134. Leach, F., Stone, R., Richardson, D., Lewis, A., Akehurst, S., Turner, J., Remmert, S., Campbell, S., Cracknell, R.F.: Particulate emissions from a highly boosted gasoline direct injection engine. Int. J. Engine Res. 19, 347–359 (2018). https://doi.org/10.1177/1468087417710583

135. Li, T., Yin, T., Wang, B.: Anatomy of the cooled EGR effects on soot emission reduction in boosted spark-ignited direct-injection engines. Appl. Energy. (2017). https://doi.org/10.1016/j.apenergy.2016.12.105

136. Leach, F.C.P., Stone, R., Richardson, D., Turner, J.W.G., Lewis, A., Akehurst, S., Remmert, S., Campbell, S., Cracknell, R.: The effect of oxygenate fuels on PN emissions from a highly boosted GDI engine. Fuel. 225, 277–286 (2018). https://doi.org/10.1016/j.fuel.2018.03.148

137. Xie, F., Hong, W., Su, Y., Zhang, M., Jiang, B.: Effect of external hot EGR dilution on combustion, performance and particulate emissions of a GDI engine. Energy Convers. Manag. 142, 69–81 (2017). https://doi.org/10.1016/j.enconman.2017.03.045

138. Chen, L., Stone, R., Richardson, D.: Effect of the valve timing and the coolant temperature on particulate emissions from a gasoline direct-injection engine fuelled with gasoline and with a gasoline-ethanol blend. Proc. Inst. Mech. Eng. Part D J. Automob. Eng. 226, 1419–1430 (2012). https://doi.org/10.1177/0954407012444966

139. Sun, Y., Dong, W., Yu, X.: Effects of coolant temperature coupled with controlling strategies on particulate number emissions in GDI engine under idle stage. Fuel. 225,

1–9 (2018). https://doi.org/10.1016/j.fuel.2018.03.075

140. De Francqueville, L.: Effects of ethanol addition in ron 95 gasoline on GDI stratified combustion. SAE Tech. Pap. (2011). https://doi.org/10.4271/2011-24-0055

141. Su, J., Xu, M., Yin, P., Gao, Y., Hung, D.: Particle Number Emissions Reduction Using Multiple Injection Strategies in a Boosted Spark-Ignition Direct-Injection (SIDI) Gasoline Engine. SAE Int. J. Engines. 8, 20–29 (2014). https://doi.org/10.4271/2014-01-2845

142. Merola, S.S., Irimescu, A., Tornatore, C., Valentini, S., Kruczek, G., Szlek, A., Adamczyk, W.: UV-visible digital imaging of split injection in a gasoline direct injection engine. Therm. Sci. 19, 1873–1886 (2015). https://doi.org/10.2298/TSCI141121071M

143. BSI Standards Publication Automotive fuels — Unleaded petrol — Requirements and test methods. (2012)

144. Burke, J., Salow, J.D., Stocki, a J.: COOLANT, ORGANIC ADDITIVE TECHNOLOGY (OAT), CONCENTRATE, FOR PASSENGER CAR AND LIGHT TRUCK, (2006)

145. Cambustion: Fast response aerosol size measurements with the DMS500, https://www.cambustion.com/products/dms500/aerosol

146. Official Journal of the European Union EN: Regulation No 49 of the Economic Commission for Europe of the United Nations (UN/ECE) — Uniform provisions concerning the measures to be taken against the emission of gaseous and particulate pollutants from compression-ignition engines for use in vehicles. Off. J. Eur. Union. 44–47 (2012)

147. Fernando, M., Brito, M.D.E.: PROCEDURE FOR UNCERTAINTY OF MEASUREMENT DETERMINATION OF SPARK IGNITION ENGINE EMISSION TESTS. (2020)

148. Silvis, W.M.: HORIBA AFR calc doc R015-04-017_01.pdf, (1997)

149. Wang, X., Ma, J., Zhao, H.: Analysis of mixture formation process in a two-stroke boosted uniflow scavenged direct injection gasoline engine. Int. J. Engine Res. (2018). https://doi.org/10.1177/1468087417736451

150. Wang, X., Xie, H., Xie, L., Zhang, L., Li, L., Chen, T., Zhao, H.: Numerical simulation and validation of SI-CAI hybrid combustion in a CAI/HCCI gasoline engine. Combust. Theory Model. (2013). https://doi.org/10.1080/13647830.2012.730627

151. Jung, D., Sasaki, K., Iida, N.: Effects of increased spark discharge energy and

enhanced in-cylinder turbulence level on lean limits and cycle-to-cycle variations of combustion for SI engine operation. Appl. Energy. 205, 1467–1477 (2017). https://doi.org/10.1016/j.apenergy.2017.08.043

152. Husted, H.L., Piock, W., Ramsay, G.: Fuel efficiency improvements from lean, stratified combustion with a solenoid injector. SAE Tech. Pap. 2, 1359–1366 (2009). https://doi.org/10.4271/2009-01-1485

Appendix

Section 1: Fuel specification for E10 Fuel with respective test method

FUEL SPECIFICATION					
Batch No :	W18/20275				
Fuel Type :	95 Ron Gasoline			Delivery :15/2/18	
Supplier:	Haltermann Carle				
Specification :	XE-M4CX424-C				
Fuel Certified Date:	14-Feb-18				
PROPERTY	**UNIT**	**MIN**	**RESULTS**	**MAX**	**Test method**
Research Octane Number		94	**95.1**	96	ASTM D2699
Motor Octane Number		84	**85.8**	86	ASTM D2700
Reid Vapour Pressure	kPa	52	**56**	58	ASTM D5191
Distillation					
Initial Boiling Point	° C		**38.6**		ASTM D86
10% Vol Point	° C	54	**57.5**	60	ASTM D86
50% Vol Point	° C	96	**98.1**	102	ASTM D87
90% Vol Point	° C	158	**162.5**	164	ASTM D88
Final Boiling Point	° C		**190**		ASTM D89
Residue	% vol		**1.1**	2	ASTM D90
Hydrocarbon Contents					
Aromatics	% vol		**25.9**	31	ASTM D1319
Olefins	% vol	3	**3.4**	15	ASTM D1319
Saturates	% vol		**60.8**		ASTM D1319
Existent Gum	mg/100ml		**<0.5**	4	ASTM D381
Existent Gum (Unwashed)	mg/100ml				
Oxidation Stability	minutes	600	**>600**		ASTM D525
Lead Content	mg/L		**<2.5**	2.5	EN237
Sulpher Content	mg/Kg		**3.6**	10	IP 490
Benzene Content	% wt				
Ethanol Content	% vol	9.8	**9.8**	10.2	EN 13132
Ethanol Purity	%				
Additional Data					
Density @ 15° C	kg/l		**0.7461**		ASTM D4052
Carbon Content	%		**83.16**		ASTM D5291
Hydrogen Content	%		**13.18**		ASTM D5291
Oxygen Content	%		**3.66**		ELEMENTAL
Carbon Weight Fraction			**0.8316**		
H/C Ratio			**1.889**		
O/C Ratio			**0.033**		
Calorific Value - Gross	KJ/kg		**44220**		IP 12
Calorific Value - Gross	Btu/lb		**19011**		
Calorific Value - Nett	KJ/kg		**41420**		IP 12
Calorific Value - Nett	Btu/lb		**17807**		
Stoichiometric			**13.92**		
	Values to be entered in Puma Cell Configuration window, Emission Analyser & Horiba AFR meter				

Section 2: Full list of measured parameters and respective instrumentation installed on the test rig

Measurement	Units	Device	Logged DAQ	Sensor model	Measured range	Remarks
Engine torque	Nm	Load cell	Dynamometer	U4000		For cross-check validation
Engine torque	Nm	Load cell	Slow CH/LabVIEW	U4000		
Engine speed	RPM	dyno rotor/hall sensor	Dynamometer	Froude		For cross-check validation
Engine speed	RPM	Variable reluctant	ECU/Vision 5.1	-		
Crank position	-	Crank angle encoder	Fast CH/Yantec	AVL 365-Series	-	
Reference position	-	Crank angle encoder	Fast CH/Yantec	AVL 365-Series	-	
Dyno cooling water MFR	Kg/hr	Pressure diff sensor	Slow CH/LabVIEW	PMP50G6-TA-A1-CA-HO-PB	0-2bar ±0.2% FS BSL	Orifice plate $P_{difference}$
Fuel flow rate	Kg/hr	Coriolis sensor	Slow CH/LabVIEW	Promass 83A02, DN2 1/12	up to ±0.1%	
Turbo rotation Speed	RPM	Speed sensor	Slow CH/LabVIEW	Acam picoturn PT1G	-	Component protection
In-Cylinder Pressure	bar	Pressure sensor	Fast CH/Yantec	Kistler 6041B	0-250bar ≤±0.3%FSO	Type 5011 charge amp
Inlet dynamic P	bar abs	Pressure sensor	Fast CH/Yantec	4007D005RDS1-2,0	0-5bar ≤±1FSO	Piezo-Resistive Miniature Absolute Pressure
Low-Pressure Fuel P	bar	Pressure sensor	Slow CH/LabVIEW	PXM319-010G10V	0-10bar ±0.25%	
High-Pressure Fuel P	Mpa	Pressure sensor	ECU/Vision 5.1	-	engine OEM	ECU feedback signal
Oil gallery P	bar	Pressure sensor	Slow CH/LabVIEW	PXM319-010G10V	0-10bar ±0.25%	
Exh Pre turbo P	bar	Pressure sensor	Slow CH/LabVIEW	PMP50G6-TC-A2-CA-H0-PT	0-0.7bar ±0.1%	

Exh Pre-TWC P	bar	Pressure sensor	Slow CH/LabVIEW	PXM319-001G10V	0-0.07 bar ±0.25%	
MAP average	bar abs	Pressure sensor	Slow CH/LabVIEW	PX419-050A5V	0-3.4 bar ±0.08%	Absolute pressure sensor
Crankcase P	bar	Pressure sensor	Slow CH/LabVIEW	PXM319-0.14G10V	0-0.14bar ±0.25%	
Engine coolant in temperature	DegC	temperature sensor	Slow CH 2/LabVIEW	Type K TC	−270 to 800°C	
Engine coolant out temperature	DegC	temperature sensor	Slow CH 2/LabVIEW	Type K TC	−270 to 800°C	
Throttle air temperature	DegC	temperature sensor	Slow CH 2/LabVIEW	Type K TC	−270 to 800°C	
MAT	DegC	temperature sensor	Slow CH 2/LabVIEW	Type K TC	−270 to 800°C	
Sump oil temperature	DegC	temperature sensor	Slow CH 2/LabVIEW	Type K TC	−270 to 800°C	
Oil gallery temperature	DegC	temperature sensor	Slow CH 2/LabVIEW	Type K TC	−270 to 800°C	
Exhaust after CAT temperature	DegC	temperature sensor	Slow CH 2/LabVIEW	Type K TC	−270 to 800°C	
Exhaust before CAT temperature	DegC	temperature sensor	Slow CH 2/LabVIEW	Type K TC	−270 to 800°C	all Type K TC read via 16bit isolated DAC
Exhaust before turbo temperature	DegC	temperature sensor	Slow CH 2/LabVIEW	Type K TC	−270 to 1150°C	Inconel for higher temp
EGR temperature	DegC	temperature sensor	Slow CH 2/LabVIEW	Type K TC	−270 to 800°C	16bit isolated DAC
actual EVC timing	CAD	cam/hall sensor	ECU/Vision 5.1	-	-	
actual IVO timing	CAD	cam/hall sensor	ECU/Vision 5.1	-	-	
First injection timing	CAD	-	ECU/Vision 5.1	-	-	
First injection duration	ms	-	ECU/Vision 5.1	-	-	
Second injection timing	CAD	-	ECU/Vision 5.1	-	-	
Second injection duration	ms	-	ECU/Vision 5.1	-	-	Validation possible with current clamp
lambda cor I val	-	-	ECU/Vision 5.1	-	-	

inlet air flow meter	Kg/hr	LFM	Slow CH/LabVIEW	LFE with 1500DP transmitter		For cross-check validation
Inlet_rel_hum	%	Humidity sensor	Slow CH/LabVIEW		-	
tailpipe NO_x	ppm	Gas analyser Signal	Slow CH/LabVIEW	Signal 4000VM	-	Tailpipe NOx emission
pre-cat CO	ppm	Horiba gas analyser	Yantech	MEXA7170D-EGR	-	details found in the thesis
pre cat CO2	ppm	Horiba gas analyser	Yantech	MEXA7170D-EGR	-	
pre cat HC	ppm	Horiba gas analyser	Yantech	MEXA7170D-EGR	-	
pre cat NOx	ppm	Horiba gas analyser	Yantech	MEXA7170D-EGR	-	
pre cat O2	ppm	Horiba gas analyser	Yantech	MEXA7170D-EGR	-	
EGR dilution	%	Horiba gas analyser	Yantech	MEXA7170D-EGR	-	
Horiba Lambda	-	Horiba gas analyser	Yantech	MEXA7170D-EGR	-	true lambda measurement
ECU Lambda	-	Lambda sensor	ECU/Vision 5.1	-	-	For engine control
Pre-TWC particulate	-	particulate fast analyser	Cambustion software	Cambustion DMS500 MKII	-	details found in the thesis